NASA Tech Briefs

National
Aeronautics and
Space
Administration

A lightweight fireman's air tank and breathing system are based on technology developed for astronauts' equipment.

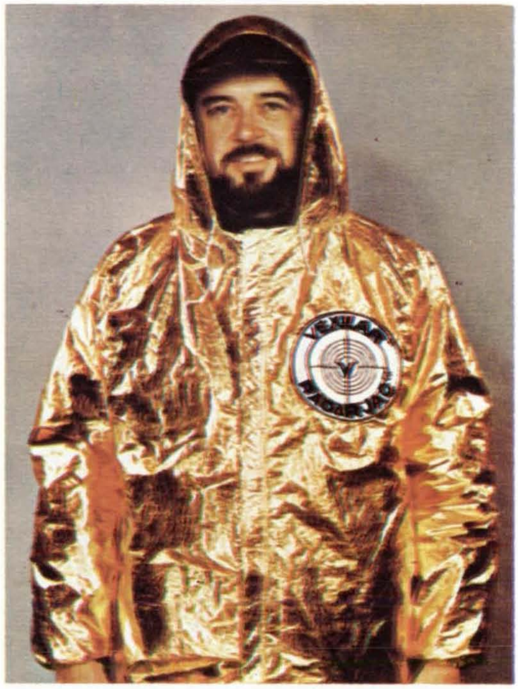

Aluminized Mylar, developed originally as reflectors for satellites, is used for jackets, parkas, blankets, sleeping bags, and other consumer products.

Heat pipes, similar to those used to cool equipment in spacecraft, keep the permafrost frozen around sections of the Alaskan pipeline to prevent frost-heaving damage.

Vol. 1, No. 2

SUMMER 1976

About the NASA Technology Utilization Program

The National Aeronautics and Space Act of 1958, which established NASA and the United States civilian space program, requires that "The Administration shall provide for the widest practicable and appropriate dissemination of information concerning its activities and the results thereof."

To help carry out this objective the NASA Technology Utilization (TU) Program was established in 1962. It offers a variety of valuable services to facilitate the transfer of aerospace technology to nonaerospace applications, thus assuring American taxpayers maximum return on their investment in space research; thousands of spinoffs of NASA research have already occurred in virtually every area of our economy.

The TU Program has worked for engineers, scientists, technicians, and businessmen. And it can work for you.

NASA Tech Briefs

Tech Briefs is published quarterly and is free to any U.S. citizen or organization. It is both a current-awareness medium and a problem-solving tool. Potential products ... industrial processes ... basic and applied research ... shop and lab techniques ... computer software ... new sources of technical data ... concepts ... you will find them all in NASA Tech Briefs. The first section highlights a few of the potential new products contained in Tech Briefs. The remainder of the volume is organized by technical category to help you quickly review new developments in your areas of interest. Finally, a subject index makes each issue a convenient permanent reference file.

Further Information on Innovations

Although many articles are complete in themselves, others are backed up by Technical Support Packages (TSP's). TSP's are available without charge and may be ordered by simply completing the enclosed TSP Request Card. Further information on some innovations is available for a nominal fee from other sources, as indicated at the ends of the articles. In addition, Technology Utilization Officers at NASA Field Centers will assist you directly when necessary. (See page A4.)

Patent Licenses

Many of the inventions described are under consideration for patents or have been patented by NASA. Unless NASA has decided not to apply for a patent, the patent status is described at the end of each article. For further information about the Patent Program see page A8.

Other Technology Utilization Services

To assist engineers, industrial researchers, business executives, city officials, and other potential users in applying space technology to their problems, NASA sponsors six Industrial Applications Centers. Their services are described on page A6. In addition, an extensive library of computer programs is available through COSMIC, the Technology Utilization Program's outlet for NASA-developed software. (See page A5.)

Applications Program

To help solve public-sector problems in such areas as safety, health, transportation, and environmental protection, NASA TU Applications Teams, staffed by professionals from a variety of disciplines, work with Federal agencies, local governments, and health organizations to identify critical problems amenable to technical solutions. Among their many significant contributions are a rechargeable heart pacemaker, a lightweight fireman's breathing apparatus, aids for the handicapped, and safer highways.

Reader Feedback

We hope you find the information in NASA Tech Briefs useful. A reader feedback card has been included because we want your comments and suggestions on how we can further help you apply NASA innovations and technology to your needs. Please use it, or if you need more space, write us a letter.

NASA Tech Briefs

SUMMER 1976
Volume 1, Number 2

National
Aeronautics and
Space
Administration

COVERS: The photographs on the front and back covers illustrate recent developments by NASA and its contractors that have resulted in commercial and nonaerospace spinoffs.

About This NASA Publication

NASA Tech Briefs, a quarterly publication, is distributed free to U.S. citizens to encourage commercial application of U.S. space technology. For information on publications and services available through the NASA Technology Utilization Program, write to the Director, Technology Utilization Office, P. O. Box 8756, Baltimore/Washington International Airport, Maryland 21240.

Change of Address

Change of Address: If you wish to have NASA Tech Briefs forwarded to your new address, use one of the Subscriptions cards enclosed in the back of this volume of NASA Tech Briefs. Be sure to check the appropriate box indicating change of address.

Communication Concerning Editorial Matter

For editorial comments or general communications about NASA Tech Briefs, you may use the self-addressed Feedback card in the back of NASA Tech Briefs, or write to: The Publications Manager, Technology Utilization Office (Code KT), NASA Headquarters, Washington, DC 20546. Technical questions concening specific articles should be directed to the Technology Utilization Officer of the sponsoring NASA Center (addresses listed on page A4.)

NASA
TU SERVICES

THE NASA TECHNOLOGY UTILIZATION OFFICERS

They will help you apply the innovations described in Tech Briefs.

The Technology Utilization Officer (TUO)

Each NASA Center has a Technology Utilization Officer — An applications engineer whose job is to help you make use of new technology developed at his center. He brings you the NASA Tech Briefs and other special publications, sponsors conferences, and arranges contacts with NASA technical experts.

Technical Assistance

Working together with NASA Scientists and Engineers and the Industrial Applications Centers, the center TUO's can answer specific questions about innovations and related NASA technology.

Technical Support Package (TSP's)

For many of the innovations described in Tech Briefs, the center TUO has prepared additional material that will help you in detailed evaluation and actual use or construction of the new technology. You may get TSP's free of cost by using the TSP Request Card or writing the center TUO.

Who to Contact. Of course, many technical questions about Tech Briefs are answered in the TSP's, but when no TSP is available, or you have further questions, write the Technology Utilization Officer at the center that sponsored the research at the address listed below.

Charles K. Kubokawa
Ames Research Center
Code AU: 230-2
Moffett Field, CA 94035
(415) 965-5554

Clinton T. Johnson
Hugh L. Dryden Flight Research Center
P. O. Box 273
Edwards, CA 93523
(805) 258-3311, Ext. 568

Donald S. Friedman
Goddard Space Flight Center
Code 704.1
Greenbelt, MD 20771
(301) 982-6242

John T. Wheeler
Johnson Space Center
Code AT3
Houston, TX 77058
(713) 483-3809

Raymond J. Cerrato
John F. Kennedy Space Center
Code SA-RTP
Kennedy Space Center, FL 32899
(305) 867-2780

John Samos
Langley Research Center
Mail Stop 139A
Hampton, VA 23665
(804) 827-3281

Paul Foster
Lewis Research Center
21000 Brookpark Rd.
Cleveland, OH 44135
(216) 433-4000, Ext. 6832

Aubrey D. Smith
Marshall Space Flight Center
Code AT01
Marshall Space Flight Center, AL 35812
(205) 453-2224

John C. Drane
NASA Resident Legal Office-JPL
4800 Oak Grove Drive
Pasadena, CA 91103
(213) 354-6420

Gilmore H. Trafford
Wallops Flight Center
Wallops Island, VA 23337
(804) 824-3411, Ext 201

Louis Mogavero, Director
Technology Utilization Office
Code KT
NASA Headquarters
Washington, DC 20546
(202) 755-3103

COSMIC

(Computer Software Management & Information Center)

AN ECONOMICAL SOURCE OF COMPUTER PROGRAMS DEVELOPED BY THE GOVERNMENT.

COSMIC is sponsored by NASA to give you access to over 1400 computer programs developed by NASA and the Department of Defense, and selected programs from other government agencies. It is one of the Nation's largest software libraries.

COSMIC charges very reasonable fees for programs to help cover part of their expenses—and NASA pays for the remainder. Programs generally cost from $500 to $1000, but a few are more expensive and many are less. Documentation is available separately and very inexpensively.

COSMIC collects and stores software packages, insures that they are complete, prepares special announcements (such as Tech Briefs), publishes an indexed software catalog, and reproduces programs for distribution. COSMIC helps customers to identify their software needs, follows up to determine the successes and problems, and provides updates and error corrections. In some cases, NASA engineers can offer guidance to users in installing or running a program.

COSMIC programs range from management (pert scheduling) to information science (retrieval systems) and computer operations (hardware and software). Hundreds of engineering programs perform such tasks as structural analysis, electronic circuit design, chemical analysis, and design of fluid systems. Others determine building energy requirements, optimize mineral exploration, and draw maps of water-covered areas using NASA satellite data. In fact, the chances are, if you use a computer, you can use COSMIC.

COSMIC is eager to help you get the programs you need. For more information about services or software available from COSMIC, fill out and mail the COSMIC Request Card in this issue.

COSMIC: Computer Software and Management Information Center

Suite 112, Barrow Hall, Athens, Georgia 30602 Phone: (404) 542-3265

The IAC's are one of the most economical ways of staying competitive in today's world of exploding technology. The help available from the network ranges from literature searches through expert technical assistance.

Literature Searches
Help in designing your search, typically from 30 to 300 abstracts in as narrow or broad an area as you need, and complete reports when you need them. The most complete "search before research" available!

Current Awareness
Consult with our applications engineers to design your personal program — selected monthly or quarterly abstracts on new developments in your speciality. It's like having your own journal!

Technical Assistance
Our applications engineers will help you evaluate and apply your literature-search results. They can help find answers to your technical problems and put you in touch with scientists and engineers at NASA Field Centers.

To obtain more information about how NASA's IAC's can help you —
Check the IAC box on the TSP Request Card in this issue,
Or write or call the IAC nearest you.

APPLICATIONS CENTERS

How to get reports and other documents discussed in this issue of Tech Briefs

Many of the innovations in Tech Briefs are described in detail in reports available at a reasonable cost through one or more of the IAC's. To order a report, call or write the IAC referenced at the end of the Tech Brief article at the address below. Be sure to list the titles and accession numbers (N76-..., N75-..., etc.) of those you wish to purchase.

Aerospace Research Applications Center (ARAC)
Indiana University
400 E. 7th St.
Bloomington, IN 47401
Dr. Robert D. Shriner, Director
(812) 337-7833

Knowledge Availability Systems Center (KASC)
University of Pittsburgh
Pittsburgh, PA 15260
Edmond Howie, Director
(412) 624-5211

New England Research Application Center (NERAC)
Mansfield Professional Park
Storrs, CT 06268
Dr. Daniel U. Wilde, Director
(203) 486-4533

North Carolina Science & Technology
Research Center (NC/STRC)
P. O. Box 12235
Research Triangle Park, NC 27709
Peter J. Chenery, Director
(919) 549-0671

Technology Application Center (TAC)
University of New Mexico
Albuquerque, NM 87131
Dr. Carey O'Bryan, Director
(505) 277-4000

Western Research Application Center (WESRAC)
University of Southern California
University Park
Los Angeles, CA 90007
Radford King, Director
(213) 746-6132

NASA INVENTIONS AVAILABLE FOR LICENSING

Over 3,500 NASA inventions are available for licensing in the United States - both exclusive and nonexclusive.

Nonexclusive Licenses

Nonexclusive licenses for commercial use are encouraged to promote competition and to achieve the widest use of inventions. They must be used by a negotiated target date but are usually royalty free.

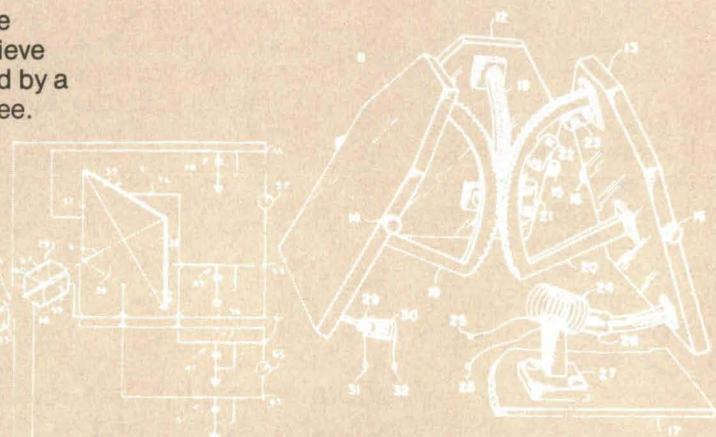

Exclusive Licenses

An exclusive license may be granted to encourage early commercial development of NASA inventions, especially when considerable private investment is required. These are generally for 5 to 10 years and usually require royalties based on sales or use.

The NASA patent licensing program also provides for licensing of NASA-owned foreign patents. In addition to inventions described in Tech Briefs, "NASA Patent Abstract Bibliography," containing abstracts of all NASA inventions, can be purchased from: National Technical Information Service, Springfield, Va., 22151. This document is updated semi-annually.

Patent Licenses and the NASA Tech Brief

Many of the inventions reported in Tech Briefs are patented or are under consideration for a patent at the time they are published. When this is the case, the current patent status is described at the end of the article; otherwise, there is no statement about patents. **If you want to know more about the patent program or are interested in license for a particular invention, write the Patent Counsel at the NASA Field Center** that sponsored the research. Be sure to refer to the NASA reference number at the end of the Tech Brief.

Robert F. Kempf
NASA Headquarters, Code GP
400 Maryland Ave., S.W.
Washington, DC 20546
(202) 755-3932

Darrell G. Brekke
Ames Research Center
Mail Code: 200-11A
Moffett Field, CA 94035
(415) 965-5104

John O. Tresansky
Goddard Space Flight Center
Mail Code: 204
Greenbelt, MD 20771
(301) 982-2351

Marvin F. Matthews
Lyndon B. Johnson Space Center
Mail Code: AM
Houston, TX 77058
(713) 483-4871

James O. Harrell
John F. Kennedy Space Center
Mail Code: SA-PAT
Kennedy Space Center, FL 32899
(305) 867-2544

Howard J. Osborn
Langley Research Center
Mail Code: 313
Hampton, VA 23665
(804) 827-3725

Norman T. Musial
Lewis Research Center
Mail Code: 500-113
21000 Brookpark Road
Cleveland, OH 44135
(216) 433-4000 Ext. 346

Leon D. Wofford, Jr.
Marshall Space Flight Center
Mail Code: CC01
Marshall Space Flight Center, AL 35812
(205) 453-0020

Monte F. Mott
NASA Resident Legal Office-JPL
4800 Oak Grove Drive
Pasadena, CA 91103
(213) 354-2700

NEW PRODUCT IDEAS

NEW PRODUCT IDEAS are just a few of the many innovations described in this issue of NASA Tech Briefs and having promising commercial applications. Each is discussed further on the referenced page in the appropriate section in this issue. If you are interested in developing a product from these or other NASA innovations, you can receive further technical information by requesting the TSP referenced at the end of the full-length article or by writing the Technology Utilization Office of the sponsoring NASA center (see page A4). NASA's patent-licensing program to encourage commercial development is described on page A8.

Electrical-Conduit Sizing Gage

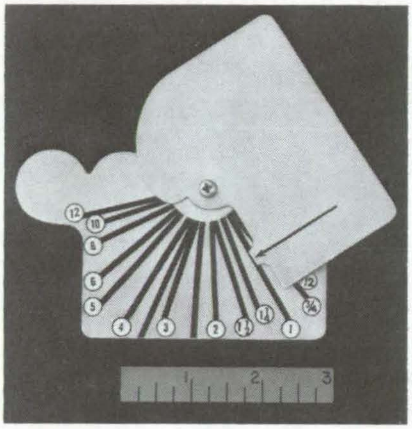

An electrical-conduit sizing gage could be used by electricians, communication technicians, and engineers. It indicates the trade-size number, which is not the same as the conduit diameter, without the use of tables or references. The small tool is easily carried in a pocket or toolbox. Simple in design and construction, it could be manufactured with little or no capital investment and at a very reasonable cost.
(See page 163.)

Fluorescent-Lamp Power Supply

A new power supply for fluorescent lamps reduces energy costs and improves running efficiency by using separate modes for starting and operating the lamp. With some redesign for 12-V battery operation, the supply would be ideal for use with mobile homes, campers, boats, and other applications where energy availability is limited. The transistorized supply consists of a dc-driven 25-kHz oscillator and the associated voltage/current regulatory circuitry.
(See page 154.)

DC-to-DC Conversion With Voltage Multipliers

A new dc-to-dc converter uses voltage multipliers to convert from low to high voltage dc. It does not require the bulky transformers and inductor/capacitor filters used in conventional converters. Simplicity and small size should make this converter economical to produce and adaptable to modular or integrated-circuit systems. Further advantages include efficiency at high power levels, increased reliability due to the elimination of magnetics and associated electrical transients, and no requirement for magnetic shielding. A 100-watt, 1,000-volt version has been operated at an efficiency of 94 percent.
(See page 152.)

Large-Diameter Fasteners of CRES Alloy

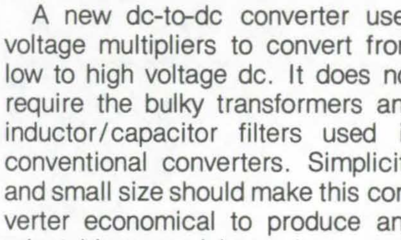

A specially-designed double-hex bolthead allows bolts of high-strength corrosion-resistant steel (CRES) to be made in larger diameters than previously possible. The high-strength fasteners, previously limited to 3/4 in. in diameter, can now be made in sizes up to 1-1/4 in. The new design allows the 12-point tension heads to be cold formed to retain a required minimum tensile strength of 220,000 psi and to retain a high fracture strength. Fabrication is essentially the same as for conventional CRES alloy fasteners.
(See page 259.)

Coating for Solar Panels

A new energy-absorbent coating with a high absorptivity (0.95) can be used with thermal solar-energy systems. The coating is economical to manufacture, being made from readily available materials, including carbon black, ethyl alcohol, and polyvinyl butyral. It is both simple and economical to use as no primer is required for application to aluminum, copper, or stainless steel.
(See page 205.)

Power-Control Switch

An improved power-control switch reduces power dissipation and has a consistent rise time over its input voltage range. It operates with inputs from 60 to 90 V, with transients as high as 120 V. In a previous switch, large variations in the input voltage caused excess power dissipation in a resistive divider that supplied base current to a driving transistor. By replacing the resistive divider with a constant-current source, drive current is independent of input-voltage variations and power loss in the base drive circuitry is cut in half.
(see page 161.)

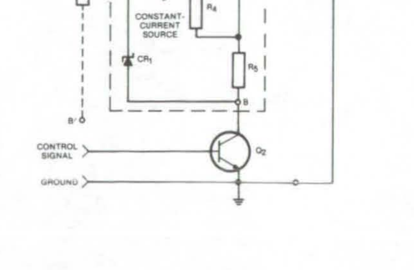

Combined GaAs Laser Diodes

A new technique for combining the outputs of an array of small semiconductor lasers increases the total output power while relaxing fabrication tolerances to make manufacture potentially less costly. By using a free-running mode, the power of one array was raised from 2 to 5 watts, making the compact semiconductor laser array suitable for many of the recent applications and products requiring a lightweight rugged coherent light source. A primary advantage of the free-running mode is that the spacing between the junction-diode lasers is less critical than for conventional, phase-coherently coupled arrays.
(See page 183.)

CMOS-Compatible Tristate Driver

A CMOS-compatible tristate driver has good noise immunity and low power consumption. It can improve performance where the same bus is used to connect several pieces of CMOS equipment, such as computers, communications equipment, process control modules, and other devices employing the increasingly-used CMOS logic devices. Unlike the more common TTL-family cable drivers, power consumption is low and comparable to CMOS. The circuitry is relatively simple, yet it provides noise immunity similar to CMOS.
(See page 162.)

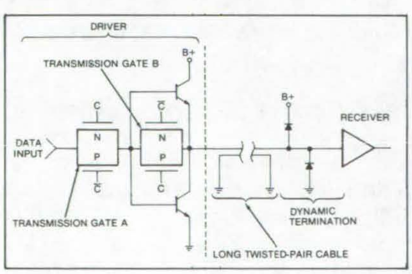

Aseptic Fluid-Transfer System

An inexpensive and easily-used transfer terminal can be used to move fluids from one container to another without the risk of contamination. The transfer device, which could be manufactured as a section of plastic tubing with a special terminal clamp, would be useful in hospitals, research labs, and certain manufacturing processes. It is used by inserting separate tubes into the two containers and heat sealing the "clamps" at the ends of the tubes. The heat forms a sterile airtight connection. The special design of the clamps allows them to be heat-sealed without blocking the fluid passageway.
(See page 220.)

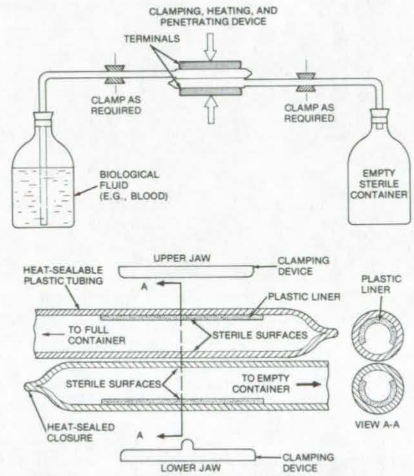

"Thermal-Diode" Heat Pipe

A new heat pipe transfers heat in one direction only. With equipment subjected to varying temperatures, it could cool when overheating occurs yet inhibit heat absorption when the environment gets hot. Conversely, it could be used to absorb heat during warm periods (e.g., daylight) and to inhibit heat loss during cooler hours (evening). The one-way heat transfer can be achieved by using mechanical valves or a passive working fluid such as ammonia. Fabrication requires spiral arteries made from stainless screen and tubing to provide adequate film coefficients and vapor cross sections.
(See page 237.)

Improved Soldering-Iron Tip

A specially-designed soldering-iron tip speeds up the soldering of multipin electronic modules. The tip could be useful in assembly-line and repair work. Requiring no special tools for manufacture, this nickel-plated tip applies an even heat simultaneously to all the pins ofa module, thus reducing the chance of damage to adjacent components.
(See page 158.)

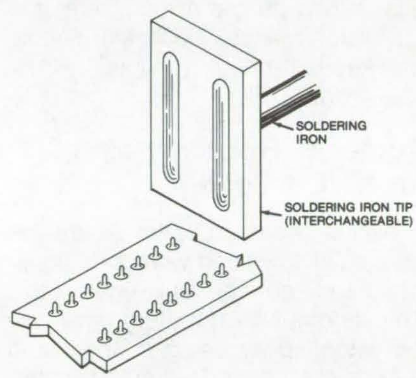

ROUS System

The ROUS, which stands for "reflection-oscillator ultrasonic spectrometer" extends the possible application of ultrasonics as a nondestructive testing technique. The ROUS is an ultrasonic generator and a monitor, including a specially designed transducer, that could be used to detect contaminants in lubricants, measure stresses in metals, determine bolt tension, and be applied to the detection of bubbles and clots in blood or other liquids. The ROUS is sensitive, economical, and requires contact with only one side of the sample being measured. The system has high-frequency stability, no duty cycle effects, and is relatively simple to construct and use.
(See page 228.)

(continued next page)

Method of Removing Drilling Chips

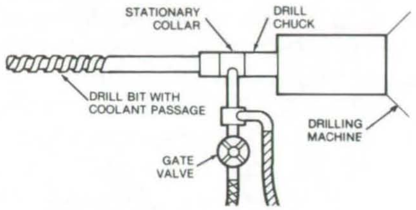

A special drill chuck is designed to direct a mixture of pressurized air and water through a drill bit during use. When drilling a long hole, the air/water mixture flushes the hole and keeps it clear of chips.
(See page 275.)

Compact Reconditioner for Ni/Cd Cells

Nickel-cadmium batteries are becoming widely used with both industrial and commercial equipment. The life of a Ni/Cd battery pack can be extended by using a small and lightweight reconditioner. It maintains a minimal cell voltage during reconditioning discharge to prevent voltage-reversal damage to the battery, a problem common to conventional reconditioners. The device uses a dc-to-dc converter to replace relays and sensors previously used, which makes it more compact and simpler to manufacture.
(See page 155.)

Tool Removes Brazed Fittings

A new tool for removing brazed fittings from thin-walled tubing has several advantages over conventional techniques. It will not accidentally bond to the fitting, nor will it cause the tube wall to melt. The tool design is uncomplicated, and use is straightforward. A key feature is the use of an expendable split-ring heat-sink insert.
(See page 253.)

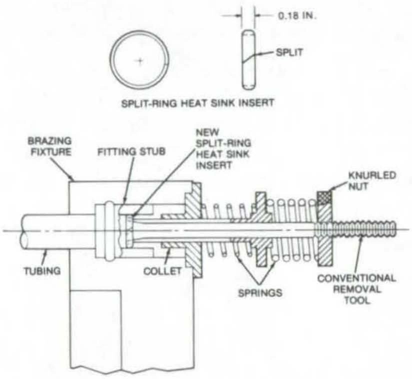

Contrast Enhancement of Transparency

A relatively inexpensive system can be used to solve a problem faced by most graphics and photography shops and many offices and laboratories. It can enhance (or reduce) the contrast of transparencies or films and thus be used to convert poor slides, viewgraphs, or photographs into ones of improved clarity. The system is potentially less expensive than electronic CRT methods and is more accurate than trial-and-error manual techniques. Unlike either of these, it also allows one to accurately observe and to adjust for the desired contrast while making the new transparency. The system is an optical arrangement that employs a collimated coherent light source to adjust contrast by constructive or destructive interference of the light.
(See page 190.)

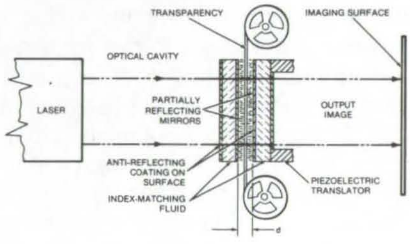

PATENT LICENSES RECENTLY GRANTED BY NASA FOR COMMERCIAL USE OF NASA-OWNED INVENTIONS

The patent licenses listed below have been recently awarded by NASA as part of its program to encourage the commercial application of its new technology. For information on how you may obtain nonexclusive or exclusive license for the commercial use of NASA inventions, see page A8 of this issue.

A nonexclusive license to Tomar Electronics Company for U.S. Patent No. 3,526,845 covering an invention entitled "Apparatus for Overcurrent Protection of a Push-Pull Amplifier"

A nonexclusive license to Del Manufacturing Company for U.S. pending patent application No. 617,202 covering an invention entitled "Lightweight Reflector Assembly and Method"

A nonexclusive license to Willard S. Blanchard, Jr., for U.S. Patent No. 3,884,432 covering an invention entitled "High Lift Aircraft"

A nonexclusive license to A. D. Weiss Lithograph Company for U.S. pending patent application No. 630,582 covering an invention entitled "Smokestack Mounted Airfoil"

A nonexclusive license to Plasma Technology, Incorporated, for U.S. pending patent application No. 513,611 covering an invention entitled "Bearing Material"

A nonexclusive license to Donald E. Barthlome for U.S. pending patent application No. 583,487 covering an invention entitled "Therapeutic Hand Exerciser"

An exclusive license to Joe Gillerman for U.S. Patent No. 3,547,801 covering an invention entitled "Water Management System and an Electrolytic Cell Therefor"

Electronic Components and Circuits

Transistor-to-Substrate Bond Quality

Bond-void area is determined from X-ray photographs using a light meter.

Marshall Space Flight Center, Alabama

The attachment of power-transistor chip devices to a heat sink is a critical operation. A complete bond, void free and with a uniform wetting of chip and substrate, is required in order for the transistor to handle maximum power. Unfortunately, the quality of this bond cannot be determined visually. Other methods of evaluating bond quality with the exception of the electrical power-burst test are destructive. Even the power-burst test may be destructive, and it can be performed only after the device has been wired. X-ray examination can be used to evaluate bond quality, but its effectiveness depends upon the accuracy of the interpretation of the X-ray photograph.

A new method of interpreting the X-ray images of bonded power-transistor chips has been developed. A light meter is used to examine the X-ray images to determine the percentage of voids in the bond. Normally these voids take the form of small independent areas scattered throughout the face of the bond. The light meter provides a quantitative percentage measurement of void area as opposed to a visual estimate. It has been found empirically that void areas approaching 20 percent of the chip area can be tolerated if they are scattered. To obtain repeatable results, X-rays of identical assemblies must be taken at identical machine settings.

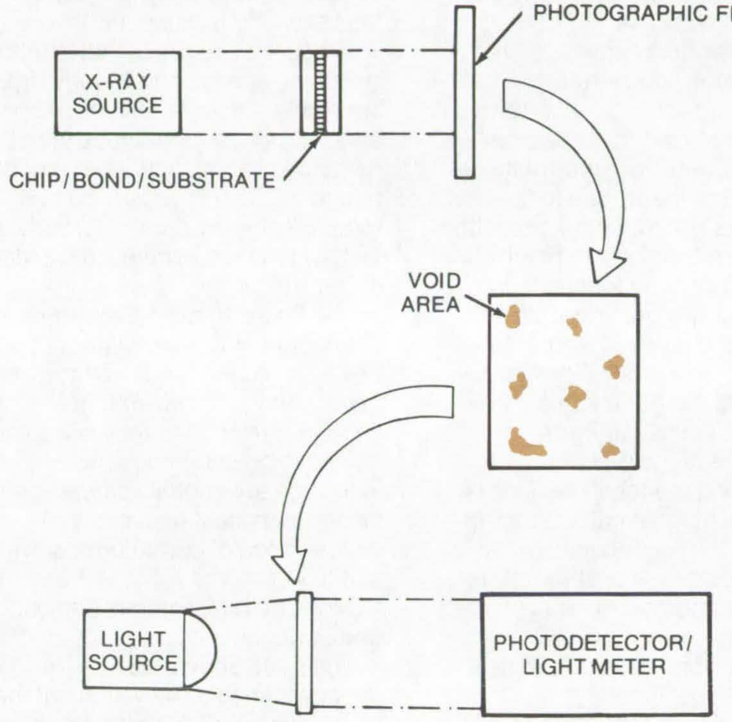

The **Apparatus for Bond Evaluation** includes a combination photodetector and light meter that is used to measure the exposure area of an X-ray photograph.

This work was done by Thomas A. Telfer of General Electric Co. for **Marshall Space Flight Center.** *For further information, Circle 1 on the TSP Request Card.*

Inquiries concerning rights for the commercial use of this invention should be addressed to the Patent Counsel, Marshall Space Flight Center [see page A8]. Refer to MFS-21931.

DC-to-DC Conversion With Voltage Multipliers

A high-frequency chopper and a capacitor/diode voltage multiplier are used in a high-performance converter.

Lewis Research Center, Cleveland, Ohio

Methods now available for low to high voltage dc conversion include the series inverter/converter, the parallel inverter/converter, the inductor energy pump converter, and the bridge-type inverter/converters. The disadvantages of these systems are primarily due to the transformers and inductor/capacitor filters required, which are much heavier than desired for spacecraft and other lightweight applications. Also, the inductance in the circuit may cause transients which destroy transistors and other electrical components and cause failure. A third disadvantage of the present methods using magnetic devices is that leakage magnetic fields may interfere with the operation of particular experiments on a spacecraft. In addition, transformer/inductor systems are complex.

A new converter design consists of a specially-designed high-frequency chopper, matched to a high-frequency, lightweight capacitor/diode voltage multiplier. The multiplier is constructed of high energy density capacitors, chosen to have appropriately low losses at the operating frequencies involved. The diodes used are selected with switching speeds and voltage drops appropriate to high-efficiency operation. Other chopper types than that described can also be used, such as bridge choppers. Silicon-controlled rectifiers, or any other appropriate fast switches, can be used in place of transistors.

The figure shows the dc-to-dc converter using a transistor chopper and a capacitor/diode voltage multiplier. Although two voltages, V_{1i} and V_{2i}, are shown, they will be assumed to be equal for simplicity. The extension to unequal voltages can easily be made if necessary. A typical mode of operation, equivalent to $V_{1i} = V_{2i} = V_i$, is the use of a bridge of four switches and only one power supply.

The switch operates at a frequency f, so that the voltage at the left terminal of C_N is alternately at $-V_i$ and $+V_i$, f times per second. Since C_N charges to V_i volts, the voltage at the junction of the capacitors C_{N-2} and C_{N-4} alternates between $2V_i$ and $4V_i$. In general, the voltage at the junction between C_{2j+2} and C_{2j} varies over a $2V_i$ range.

Thus the voltages at the junction points in the upper (even-numbered) string of capacitors are square waves of voltage of amplitude V_i riding on top of a dc voltage which depends on the location in the chain. For the lower, or load string of capacitor (odd-numbered values C_1 . . . C_{N-1}), the voltage across each capacitor is $2V_i$, and across the entire ladder is NV_i, where N is the number of capacitors or diodes in the multiplier chain. Thus this converter may be thought of as a dc voltage transformer.

Advantages

- Very lightweight.
- Makes possible transformerless, high-efficiency dc-to-dc conversion at high power levels.
- Due to simplicity and small size, should be less expensive than present systems using transformers.
- More reliable operation due to elimination of magnetic devices,

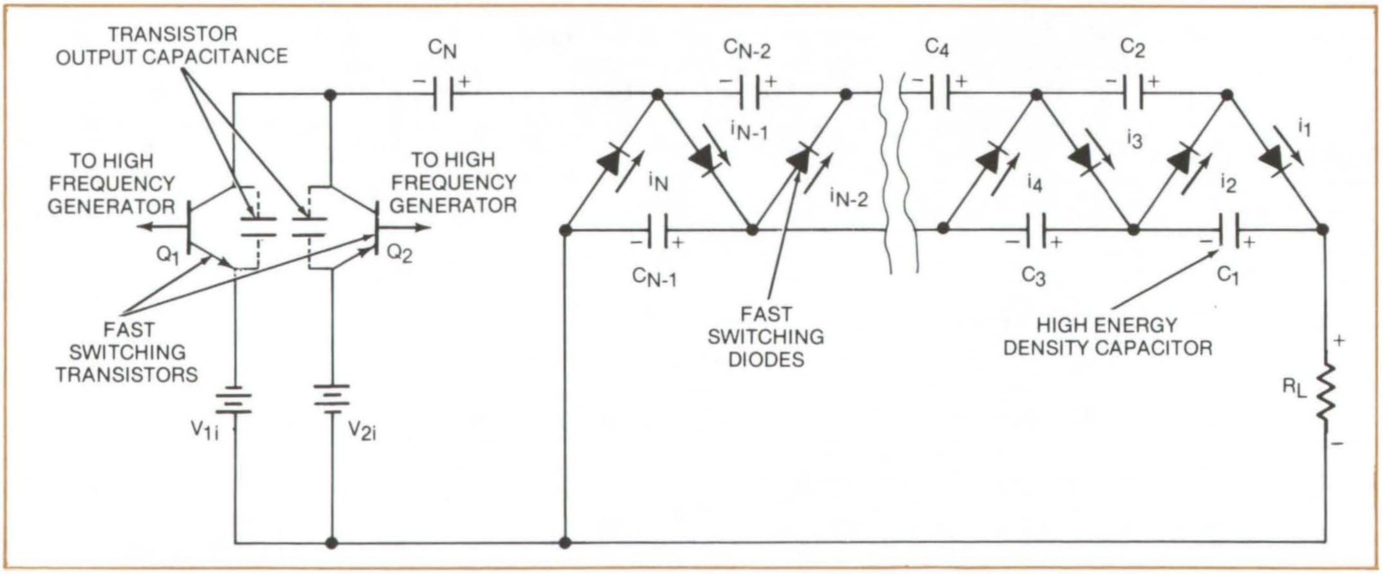

The **High-Performance DC-to-DC Converter** is a transformerless capacitor/diode voltage multiplier. Either V_{1i} or V_{2i} can be zero, or they may be chosen arbitrarily within component ratings.

such as transformers and inductors, with consequent electrical transients reduction.

- Elimination of stray magnetic fields.
- Elimination of core loss and reduction of weight by eliminating magnetic materials, including magnetic shielding.
- Simplifies dc-to-dc converter electrical design.
- Simplifies dc-to-dc converter weight analysis and weight-vs.-efficiency tradeoff calculations.
- Lends itself well to modular or integrated-circuit type of construction for low-cost, high-volume construction.

A 100-watt, 1,000-volt dc-to-dc converter of this type has been operated at an efficiency of 94 percent. The new converter offers a better combination of efficiency and weight, compared to conventional converters, and also has the capability of a wide range of weight and efficiency to fit a wide range of applications.

This work was done by W. T. Harrigill, Jr., and I. T. Myers of **Lewis Research Center.** *Further information may be found in:*

NASA TM-X-71566 (N74-26737) "High Performance DC-DC Conversion with Voltage Multipliers" and

NASA TM-X-71735 [N75-23851] "Efficiency and Weight of Voltage Multiplier Type Ultra Lightweight DC-DC Converters."

Copies of these reports may be obtained at cost from Aerospace Research Applications Center, Indiana University *[see page A7].*

LEW-12297

Modular Design of High Frequency Analog Circuits

Standardized input/output impedances and stock components simplify the design of amplifiers, mixers, and filters.

Marshall Space Flight Center, Alabama

A simple, systematic method of rapidly designing analog signal-processing circuitry for experimental (breadboard) or prototype equipment is useful up to at least 400 MHz. The electrical and mechanical design procedures are identical for wideband amplifiers, band-pass filters, and frequency-mixer circuits. The design and fabrication guides were originally intended for a system requiring custom-built circuits built to better-quality commercial standards, but they may also be used for less precise systems.

In circuit-development projects where interdependent combinations of amplifiers, mixers, and filters are designed simultaneously, changes in design details may impose new electrical design requirements. The new method simplifies the circuit development by separating the electrical functions (gain, frequency mixing, and signal filtering) into non-interdependent elements. Procedures are also simplified by two other factors: (1) the selection of standard, commercially-available circuit elements and (2) the establishment of a unified circuit-packaging arrangement. The packaging scheme is cost effective, does not compromise electrical circuit performance from video to uhf frequencies, and leaves circuits accessible for modification and adjustment.

A 50-ohm input/output interface is used for all circuit functions. The various functions may therefore be cascade connected or interconnected without circuit modification. The 50-ohm interconnections also simplify printed-wiring board fabrication.

Wideband amplifiers and mixer stages are coupled via passive, multiple-pole filters. Each broadband amplifier has a nominal gain of 35 dB, and is packaged in a TO-5 case. More or fewer of these amplifiers can be connected to provide required gain. A typical circuit built using these amplifiers has a maximum output power capability of + 15 dBm. Commercially-available double-balanced mixer assemblies using hot-carrier (Schottky) diodes implement frequency conversion. These passive devices have a uniform 6-dB conversion loss. Typical band-pass filters, usually connected immediately following the mixer stage, are wired to 50-ohm attenuator pads. Although pad loss is added to the mixer conversion loss, the total loss is not normally significant, because the amplifiers are low-noise types.

Multiple-pole Chebyschev band-pass filters are used to define amplifier bandwidth and to reject undesired mixer output frequencies. The mechanical layout of components on the printed-wiring boards directly affects filter bandwidth, which is a practical method for bandwidths up to 30 percent.

An inexpensive, RF-tight mounting enclosure uses die-cast aluminum boxes which are commercially available. The boards are mounted within the box, using square aluminum bar stock. Type BNC connectors couple signals, and circuit power is brought in via standoff capacitors.

This work was done by John T. Zimmer of Raytheon, Inc. for **Marshall Space Flight Center.** *For further information, including design data on a prototype signal processor built using these methods, Circle 2 on the TSP Request Card.*

Inquiries concerning rights for the commercial use of this invention should be addressed to the Patent Counsel, Marshall Space Flight Center *[see page A8].* *Refer to MFS-23408.*

Fluorescent-Lamp Power Supply

Separate modes for starting and running improve efficiency.

Lyndon B. Johnson Space Center, Houston, Texas

A new high-efficiency fluorescent-lamp power supply operates over an input range of 16 to 32 Vdc. Similar to other light supplies in which a dc to ac inversion is employed, the operational frequency of the new supply is above 15 kHz to insure maximum light efficiency. However, unlike other supplies that drop the high voltage required for the lamp across a ballast, this supply employs a resonant circuit to change modes when passing from the starting to the run condition. Present efficiencies are 84 percent for a 25-watt load and 95 percent for a 65-watt load.

The operation of a fluorescent lamp requires a sequence of three steps: (1) ionization, followed by (2) arc turn-on (starting the lamp, and (3) the application of a controlled current to sustain operation. This power supply, as shown in the illustration, provides the power to both start the lamp and sustain operation. The mode shift from starting to sustaining power occurs because of the arrangement of the

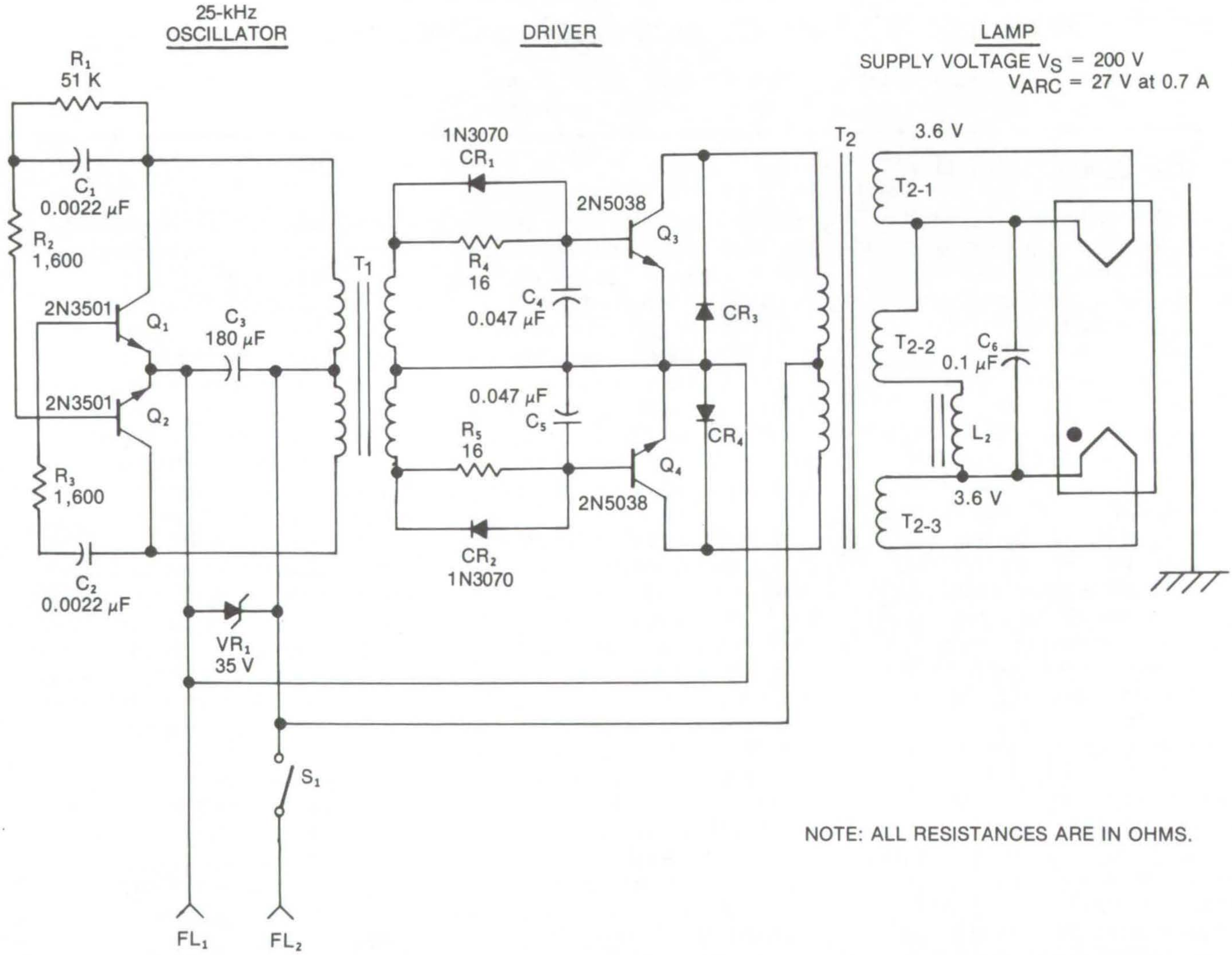

In the **Lamp Power Supply,** an oscillator consisting of transistors Q_1 and Q_2 provides the base drive to Q_3 and Q_4. The resistor, capacitor, and diode arrangement in the base circuit of Q_3 and Q_4 is chosen to prevent reverse base-emitter breakdown and to optimize the drive. Diodes CR_3 and CR_4 recover energy contained in the leakage inductance of transformer T_2 and the stored charge on inductor L_2. The driver stage provides 3.6 V rms across filament windings $T_{2\text{-}1}$ and $T_{2\text{-}3}$ of transformer T_2, and the nominal lamp voltage appearing across winding $T_{2\text{-}2}$ is 48 V.

series resonant circuit consisting of inductor L_2 and capacitor C_6. During startup, this 25-kHz tank circuit (with a composite Q factor of somewhat less than 5) multiplies the voltage from T_2 to provide the power and the 200 V required for ionization and for arc turn-on in the lamp. (This starting voltage appears across C_6 which bridges the lamp.)

Once the lamp is turned on, the ionization arc across the lamp acts as a shunt on the tank circuit, reducing the Q factor to unity. Thus the current formerly flowing through the tank capacitor flows through the lamp.

Since mercury-vapor lamps present an extremely low impedance at the arc voltage set, a ballast is necessary to limit the arc current. This function is assumed by inductor L_2. The ground starting aid serves to provide an electrostatic plane which enhances the ionization of the lamp, thus permitting a lower starting voltage for an increased operational safety margin.

This work was done by W.E. Milberger of Westinghouse Electric Corp. for **Johnson Space Center.** *No further documentation is available.*

Inquiries concerning rights for the commercial use of this invention should be addressed to the Patent Counsel, Johnson Space Center [see page A8]. Refer to MSC-14900.

Compact Reconditioner for Ni/Cd Cells

A dc-dc converter maintains a minimal cell voltage during discharge to prevent voltage-reversal damage.

Marshall Space Flight Center, Alabama

The life of multiple-cell nickel-cadmium battery packs can be extended by a reconditioning method requiring discharge of each of the battery cells. Conventionally the discharge of each cell is controlled individually by relays and separate cell sensors. A dc-dc converter replaces the system of relays and sensors. It is more compact and lighter, and it protects against voltage reversal. The converter can additionally be used to detect the presence of a low-voltage cell.

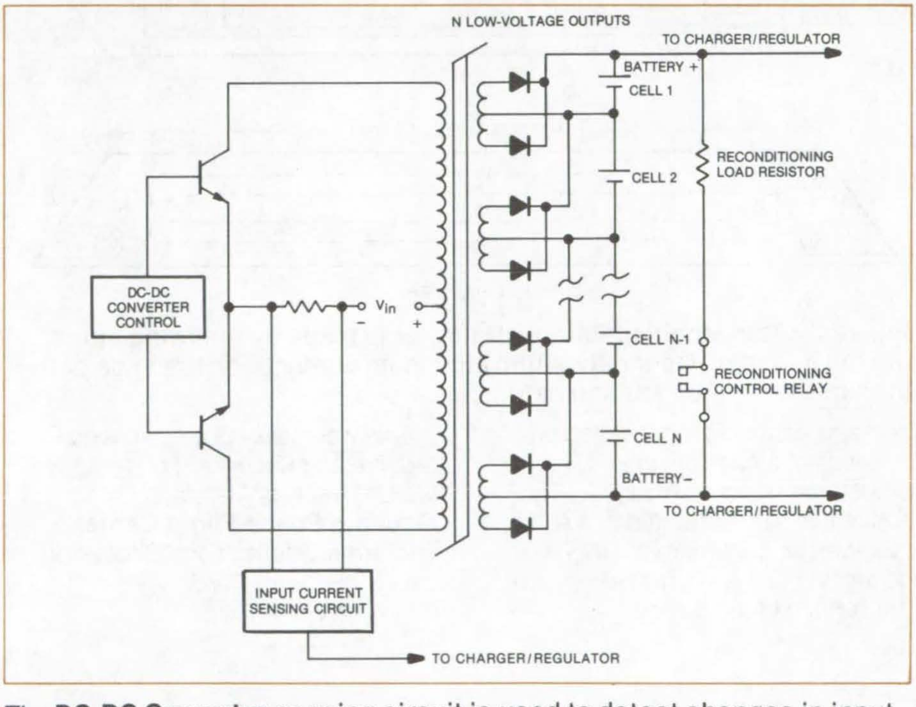

The **DC-DC Converter** sensing circuit is used to detect changes in input current to the power semiconductors. An increasing current indicates that the converter is supplying current to one (or more) of the nickel-cadmium cells in the battery pack.

The converter is depicted in the figure. The secondary of the power transformer consists of separate low-voltage output windings connected via diodes to each cell of the battery. During discharge the voltage across each cell is allowed to drop to a few tenths of a volt. This is sufficiently low for reconditioning. As the cell voltage drops, the diodes conduct, thus clamping the cell voltage at the converter output voltage level. This prevents cell voltage reversal. By sensing the converter input current, the device can also be used to monitor overall cell condition during normal operation, since the converter will supply current only when a cell voltage drops below the output threshold level.

This work was done by Robert E. Kapustka of **Marshall Space Flight Center.** *For further information, Circle 3 on the TSP Request Card.*

Inquiries concerning rights for the commercial use of this invention should be addressed to the Patent Counsel, Marshall Space Flight Center [see page A8]. Refer to MFS-23270.

Solid-State Particle Detectors

A new fabrication technique improves position sensitivity in nuclear-particle detectors.

Goddard Space Flight Center, Greenbelt, Maryland

A technique for fabricating position-sensitive solid-state nuclear-particle detectors consists of altering the resistance of the alkali metal diffused layer in a silicon wafer. Carefully-controlled mechanical abrasion during lapping and precisely-timed chemical etching are used to achieve the desired results. Changing the ratio of resistance to the thickness of the depletion layer enhances the sensitivity of silicon-based detectors. This procedure may also be useful in improving the sensitivity of germanium-based detectors.

The first attempts to fabricate the detector followed conventional procedures, and particular attention was given to ensuring ohmic contact with the lithium resistive layer. The ends of the lapped lithium side were gold plated by electroless deposition and masked with black wax. The entire crystal was etched for 3 minutes, removing 60 μm from the lithium side. After mounting the crystal in an epoxy glass holder, the black wax was removed; then contact with the gold-plated pad was made using silver epoxy and gold wire. The etching produced a groove around the pad as shown in Figure 1, causing a resistance between the contacts that was too nonlinear for a detector to have good position resolution.

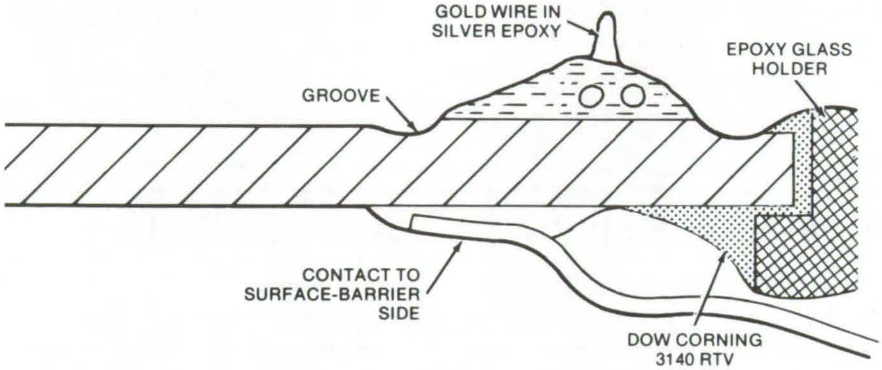

Figure 1. The **Solid-State Nuclear-Particle Detector** with 60 μm of the crystal removed from the lithium side after etching.

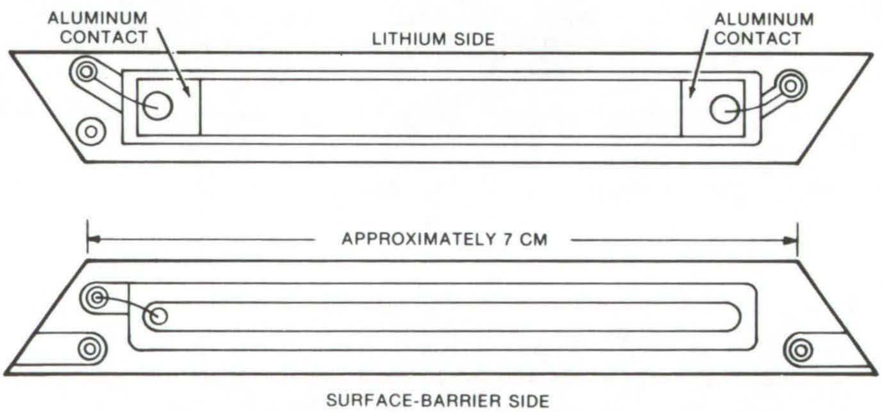

Figure 2. The **Modified Particle Detector** is made by removing more lithium and then vapor depositing aluminum contacts on the ends of the lithium side of the mounted detector.

The position detector was then reworked to achieve the desired characteristics. The lithium side was further lapped down and etched for 2 minutes; the overall material thickness was about 1.1 mm. The detector was mounted, and aluminum contacts were vapor deposited on the ends of the lithium side. (This detector is shown in Figure 2.) The nonlithium side consisted of a surface-barrier contact made by vapor depositing 160 Å (16 nm) of gold on the surface of the device.

This work was done by Joseph R. Gigante and Robert A. Lundgren of the University of Maryland for **Goddard Space Flight Center.** *For further information, Circle 4 on the TSP Request Card.*
GSC-11785

Removal of Encapsulating Materials

A technique to remove potting materials without damaging electronic parts

Goddard Space Flight Center, Greenbelt, Maryland

Often an entire encapsulated (potted) circuit or module fails due to the failure of a single component. In such a case the entire package is generally discarded, because there has been no reliable and efficient way to retrieve the other components. If the package consists of more than a few components or if the components are expensive and hard to replace, this represents an economic loss.

A new technique dissolves or softens many potting materials leaving the electronics unaffected. The encapsulated modules are placed in a sealed reactor capable of withstanding pressures of 15,000 psi (105×10^6 N/m^2) or higher. The reactor has a metal membrane sealed in one end cap, which will release at 5,000 psi (34.5×10^6 N/m^2) to provide pressure relief. Methylene chloride is added, and the reactor is sealed. The reactor is heated in an oven to elevated temperatures [100° C (212° F)] to obtain a pressure of approximately 500 psi (3.45×10^6 N/m^2). If plastics are exposed to specific solvents under these conditions for a period of time, the solvent is forced into the plastic, causing a rapid breakdown of its solid structure. The parts can then be removed, and the soft, loose, or actually dissolved plastic discarded.

The procedure may be used with almost any solvent or plastic and is limited only by the possibility that the temperature and pressure could cause damage to the parts. The parts should be checked for pressure and temperature sensitivity before using this method. It should be noted that the reactions of many chemicals under such conditions are not known and may cause explosive forces. Consequently maximum safety precautions should be taken before attempting such recovery.

This work was done by G. L. Jacobs of Sperry Rand Corp. for **Goddard Space Flight Center.** *No further documentation is available.*
GSC-11696

High-Temperature Flat-Conductor Cable

The working temperature is raised from 200° to 350° C.

Marshall Space Flight Center, Alabama

A development program aimed at increasing the working temperature of insulated multiconductor flat-conductor cable (FCC) has resulted in improved high-temperature performance of two types of common FCC: a 25-conductor signal cable and a 3-conductor power cable. The signal and the power cables were both fabricated by using woven and roll laminated techniques, respectively. New adhesives and their application to the cable have raised the safe uppermost temperature limit of woven and roll laminated FCC from 200° C up to 350° C.

Both the woven and roll laminated cables employ insulation materials made from polyimide/fluorinated ethylene propylene or polytetrafluoroethylene films. Since the polyimide and polytetrafluoroethylene films are not thermoplastic, an adhesive medium [fluorinated ethylene propylene (FEP)] is used to bond the polyimide film. However, the FEP is temperature limited to 200° C; above this temperature the material becomes thermoplastic and tends to soften and lose mechanical strength.

An alternate polyimide material (one of eight substitutes for FEP tested) was found to have a thermal resistance equal to or better than FEP. A layer of the new polyimide 0.003 in. (0.07 cm) thick was used to make a length of prototype cable. Several useful observations were made during the fabrication and testing of the cable:

Solvents released at the edge of certain test conductors cause bubbles to form.

Grooved rollers are necessary to fabricate cables enclosing conductors of 0.01 in. (0.02 cm) and larger in diameter.

Electrical characteristics are adversely affected by even low residual levels of solvents in the finished cable.

An inert gas atmosphere (or a vacuum) is required during post cure in order to prevent excessive darkening and embrittlement of the insulation film.

This work was done by Walter S. Rigling of Martin Marietta Corp. for **Marshall Space Flight Center.** *For further information, including data on the high-temperature performance of FCC, Circle 5 on the TSP Request Card.*
MFS-23451

Improved Soldering Iron Tip

Multipin electronic modules are removed faster and with less damage to adjacent components.

Lyndon B. Johnson Space Center, Houston, Texas

Repairs to electronic systems containing multipin electronic modules with the use of commercially-available flat soldering iron tips are time consuming and frequently unsatisfactory. Heating is uneven because initially contact can be applied only to the tops of the module pins. Localized uneven heating can damage adjacent components and board circuitry.

The problem can be resolved by the fabrication of special nickel-plated soldering iron tips, each having a machined recess matching the multipin pattern of a particular circuit module. The recess retains sufficient molten solder (see figure) to wet all of the pins of the module so that they are rapidly and uniformly heated. The tips are fabricated for use in standard electric soldering irons from oxygen-free, high-conductivity (OFHC) copper or from high alloy copper and are nickel plated to reduce oxidation and scaling.

This work was done by M. A. Vanasse of Rockwell International Corp. for **Johnson Space Center.** *For further information, Circle 6 on the TSP Request Card.*
MSC-19349

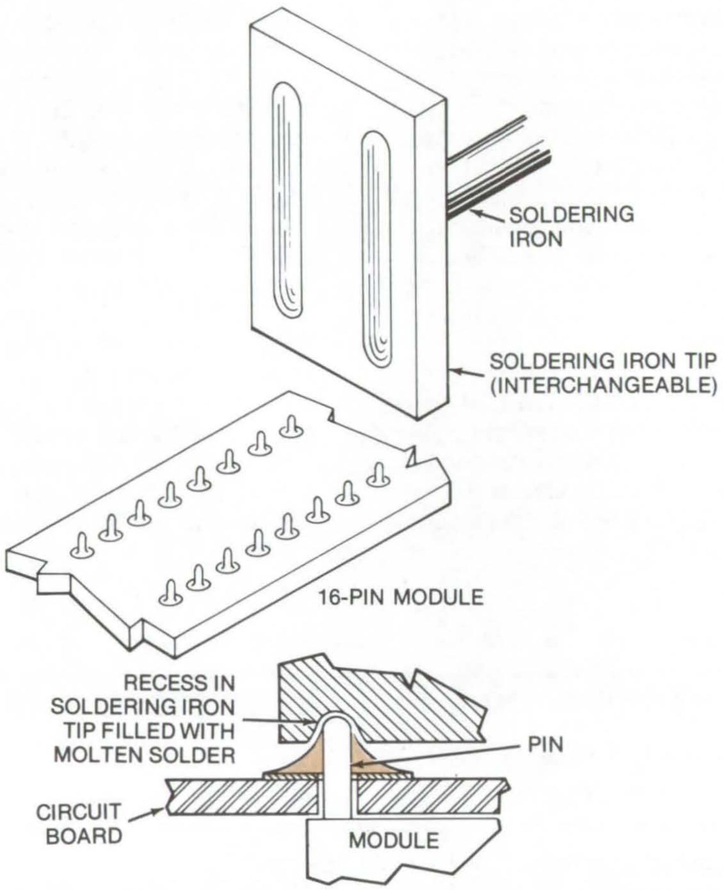

The **Improved Soldering Tip** used for desoldering is nickel plated to reduce oxidation and scaling. A recess machined into the tip retains molten solder which is used to wet all the pins for simultaneous heating and extraction.

Epitaxial Growth of $Ga_{1-x}Al_xAs$ on GaP

A new technique permits the growth of GaAlAs LED structures on transparent GaP substrates by the liquid-phase epitaxial method, thus obviating both the need for growing thick layers and for removing the substrates. High-efficiency infrared LED's can be developed as pumping sources for Nd:YAG lasers. Efficiency has been improved by thick layers of $Ga_{1-x}Al_xAs$ on GaAs, removing light-absorbing substrates and forming LED structures into a hemispherical geometry.
(See page 274.)

Solar-Cell Electrical Connections

Investigations of solderless methods of electrically connecting solar cells indicate that three bonding methods for mass production result in reliable, long-lasting electrical interconnects. Thermocompression bonding results in less cell breakage and surface oxidation. Parallel-gap constant-voltage welding yields good bonds over a wide range of weld time, pressure, and voltage. Ultrasonic welding is also suitable for many applications.
(See page 272.)

IGFET/SO1 Fabrication Method

A new method of fabricating insulated-gate field-effect silicon-on-insulator (IGFET/SO1) transistors increases switching speeds. These transistors have shorter channel length and reduced parasitic capacitance. There is also reduced gate overlap and minimum gate-to-channel capacitance. The p and n sections may be reversed, allowing the fabrication of complementary devices.
(See page 270.)

Connector Contact-Ring Bus

A means of terminating unconnected wires in a cable assembly eliminates crimp connectors and ferrules and results in a compact assembly.

Lyndon B. Johnson Space Center, Houston, Texas

One present method of terminating unconnected wires in a cable assembly requires the use of ferrules and closed-end solderless crimp connectors. If several wires are handled this way, the connector back shell becomes crowded, a situation that poses inspection and termination difficulties. The use of a contact-ring bus circumvents some of these problems by eliminating the crimp connectors and the ferrules. The result is a compact termination assembly and a more efficient use of back-shell space. This method may be used with both neutral and power-carrying wires, depending on the number of contact buses built into the terminating assembly (see Figure 1).

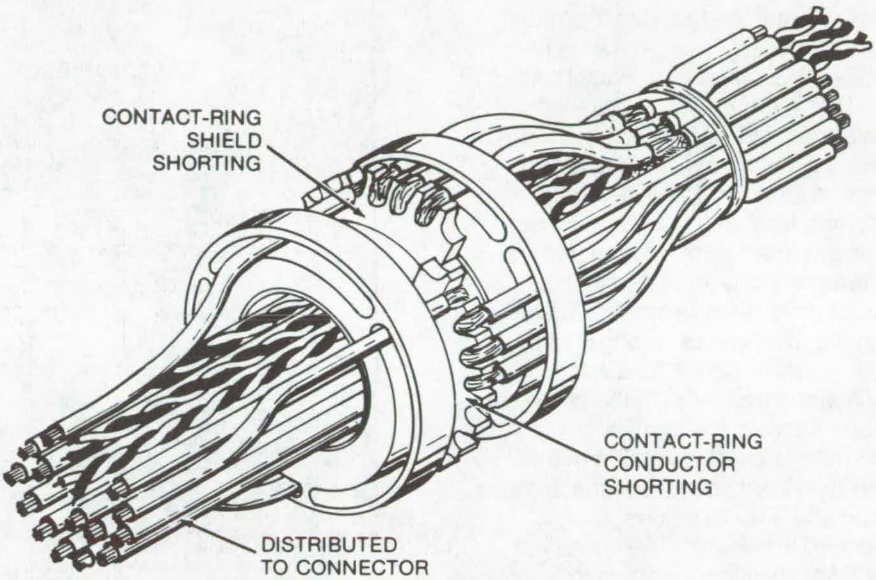

Figure 1. The **Connector** has neutral and power-carrying wires terminated depending on the number of contact buses built into the terminating assembly.

The assembly includes a pair of nylon disk caps, each mounted at either end of a nylon sleeve. Stainless-steel contact rings (one per desired termination) are located between the caps and are separated by nylon insulator rings. A pair of insulator rings, one at each end of the assembly, also provides spacing between the disk caps and the contact rings.

The adapter is fitted to the cable assembly after the harness is built but before the connector pins are attached to the wires. Wires to be terminated are soldered to their respective contant rings, and the entire adapter is insulated from the rest of the cable assembly with a tubular heat-shrink covering. The connector/back shell assembly is then screwed to the cable clamp (see Figure 2).

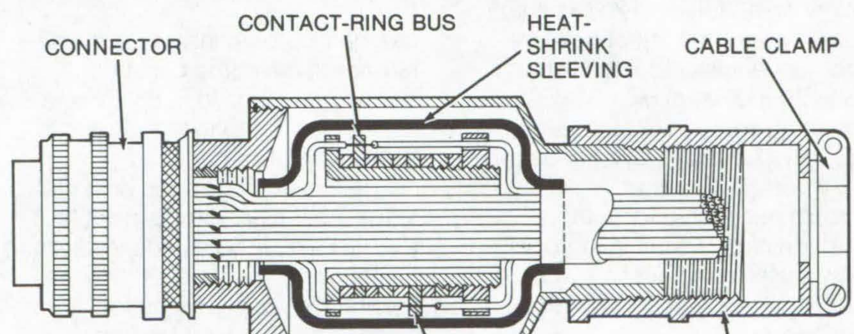

Figure 2. In the **Complete Cable Assembly** wires to be terminated are soldered to their respective contact rings, and the entire adapter is insulated from the rest of the assembly with a tubular heat-shrink covering.

This work was done by Jim Ligon of Rockwell International Corp. for **Johnson Space Center.** *For further information, Circle 7 on the TSP Request Card.*
MSC-19480

Waveguide-to-Coax Transition/Low-Pass Filter

A low-insertion-loss combination waveguide-to-coax transition and filter operates at 4.5 K and has a reflection coefficient of better than -21 dB.

Caltech/JPL, Pasadena, California

A low-pass filter is used to remove pump-frequency radiation from the input of a deep-space-network receiver. This pump frequency radiation that is emitted by a traveling-wave maser (TWM) must be attenuated to prevent possible calibration errors caused by TWM gain changes resulting from pump-frequency radiation into the signal waveguides. Differences in gain of as much as 0.5 dB have been recorded due to signal path changes during system calibration and are a function of impedance changes (at the pump frequencies) at the input of the TWM. An upgraded version of this filter type combines the signal transition and filter functions. It is matched at the signal frequency of the TWM, has low insertion loss, and operates at 4.5 K.

The filter, a coaxial type with 11 semilumped elements, had originally been incorporated into an X-band TWM system. It had a 12-GHz cutoff frequency, a signal rejection at the pump frequencies (18.4 to 19.6 and 22.6 to 24.8 GHz) of over 30 dB and a reflection coefficient at the signal frequency (7.7 to 8.8 GHz) of better than -21 dB. Because of these favorable rejection and match characteristics, a scaling factor of 2/3 was used to obtain an 18-GHz cutoff with the K_u-band TWM filter described.

A Teflon dielectric centering sleeve establishes adequate concentricity of the filter elements to the outer conductor. The element diameters in the scaled-down filter are reduced to compensate for the difference in dielectric constant. A sleeve was made to fit tightly over five of the six capacitive elements. (See the figure.)

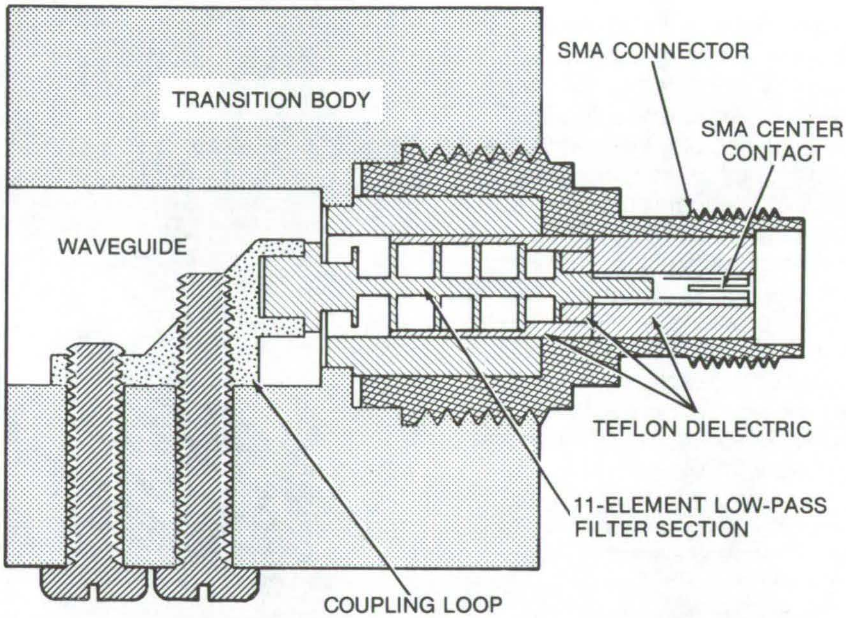

Combination Waveguide-to-Coax Transition/Low-Pass Filter is used to remove pump-frequency radiation from the input of a K_u-band receiver. The 11-element filter section is fitted via a Teflon dielectric centering sleeve.

The final tuning for the best match at the TWM signal frequency (14.3 to 16.3 GHz) is obtained by adjusting the length of the two 2-56 screws holding the coupling loop to the transition body. The filter section is located in the transition body between the coupling loop and the center contact of the SMA connector, a space previously occupied by a straight section of coaxial-cable center conductor. The transition body, the coupling loop, and the SMA connector-fitting assembly have the same outside appearance and dimensions of previous filters and are directly interchangeable with the present transition. The implementation of these filters will require no modification of the traveling-wave maser or its closed-cycle refrigerator system.

This work was done by Rex B. Quinn of **Caltech/JPL.** *For further information, Circle 8 on the TSP Request Card.*
NPO-13642.

Power-Control Switch

A constant-current source improves efficiency and rise-time consistency.

Marshall Space Flight Center, Alabama

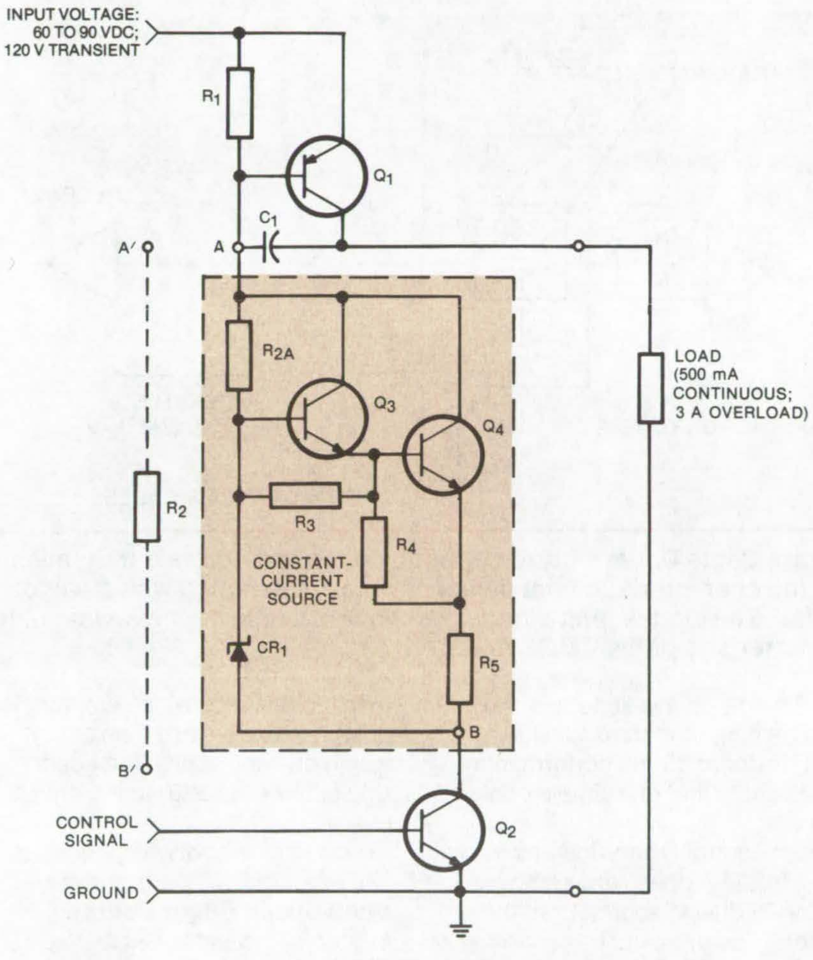

In the **Modified Power-Control Switch** the original resistive divider, R_1 and R_2 (circuit including A′B′ shown above) is replaced with a constant-current source (circuit including AB above).

Improvements have been made to a power-control switch (see figure) designed to operate with inputs from 60 to 90 V and with transients as high as 120 V. A series transistor (Q_1) that controlled the power applied to the load was driven by a second transistor (Q_2). A resistive divider, R_1 and R_2, between the positive input and the collector of Q_2 supplied the base current. The large variation in input voltage meant that R_2 dissipated excessive power at high input voltages because the resistance value was selected to provide adequate base current at the minimum input voltage.

In a new circuit R_2 is replaced with a constant-current source. This circuit provides the required drive current for Q_1 independent of the varying input voltage and thus reduces the power loss in the base drive circuitry by a factor of two at high input voltages. In addition to reducing power dissipation, the constant-current source maintains an essentially-constant charge rate for C_1, thus improving the rise-time consistency over the input voltage range.

This work was done by Leland L. Kessler of Westinghouse Electric Corp. for **Marshall Space Flight Center.** *For further information, Circle 9 on the TSP Request Card.* *MFS-23395*

CMOS-Compatible Tristate Cable Driver

A combination bipolar/CMOS cable driver draws no standby power.

Marshall Space Flight Center, Alabama

The CMOS advantages of low power consumption and high noise immunity are compromised when CMOS systems are interconnected using TTL cable drivers. CMOS-to-TTL interfaces require standby power and have worse noise immunity than the CMOS circuits being driven. To overcome these pitfalls, a CMOS-compatible tristate cable driver has been developed. It complements the CMOS low-power consumption as it, too, draws zero standby power. The driver is implemented via a bipolar complementary emitter follower controlled in each of the three states (output logic high, logic low, and high-impedance off) by CMOS switches, two per driver. The cable being driven is terminated (at the receiving end) by a pair of diodes. Although this termination scheme is not as effective as a line characteristic impedance matching resistor, it dissipates little power. The diode clamp limits cable reflections to about 1.5 to 2 volts, a level within the noise-immunity characteristics of the CMOS circuits.

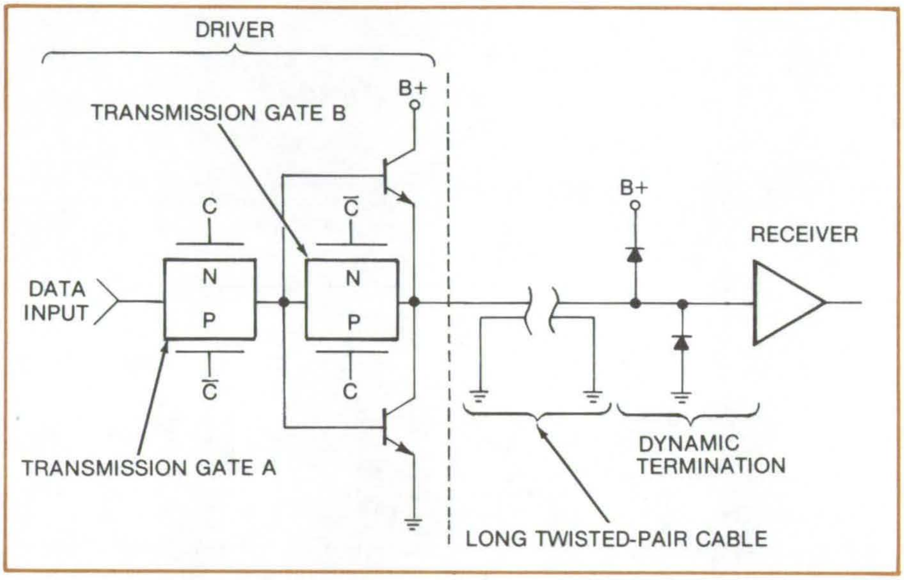

Tristate Cable Driver with zero standby power energizes a transmission line the characteristic impedance of which is matched with a pair of diodes. The diodes limit signal overshoot to within the noise immunity characteristic of the CMOS receiver.

The three cable driver states are varied via the CMOS transmission gates in combination with the bipolar complementary emitter follower as shown in the figure. The current that the emitter follower supplies to the line does not pass through the lower-power CMOS gates. Transmission gate A, for instance, in series with the input to the complementary emitter follower, transmits only the current supplied by the preceding CMOS stage. In this state, control gate C is high, and transmission gate B is open; circuit performance is identical to that of a simple cable driver.

When control C goes low, transmission gate A opens and removes the CMOS driving source from the emitter follower input. Transmission gate B is closed, presenting its "on" resistance between the input and output of the follower. The gate thus appears as a shunt resistance between the base and emitter of the emitter follower and keeps the transistor base potentials within less than a diode drop of the emitter. The driver transistors are then cut off which presents a high impedance (the output-off state) to the driven bus.

This work was done by Richard Lee Pryor of RCA Corp. for **Marshall Space Flight Center.** *For further information, Circle 10 on the TSP Request Card.*

Inquiries concerning rights for the commercial use of this invention should be addressed to the Patent Counsel, Marshall Space Flight Center [see page A8]. Refer to MFS-23410.

Electrical-Conduit Sizing Gage

An easily made template can be used to estimate the trade size number of conduit.

Lyndon B. Johnson Space Center, Houston, Texas

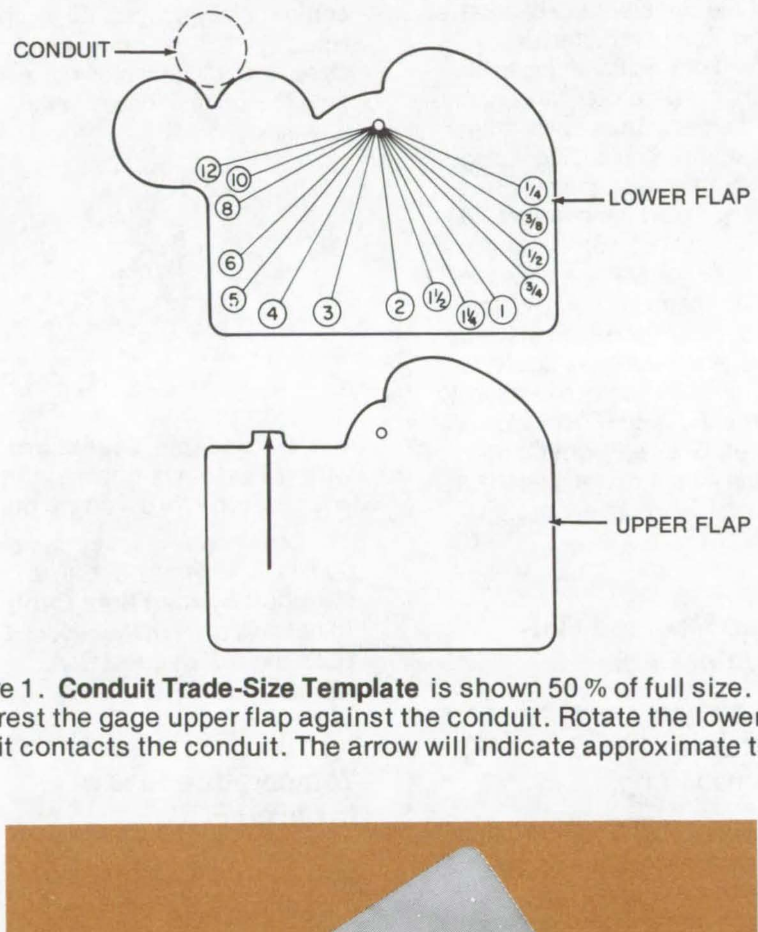

Figure 1. **Conduit Trade-Size Template** is shown 50 % of full size. To use, rest the gage upper flap against the conduit. Rotate the lower flap until it contacts the conduit. The arrow will indicate approximate trade size.

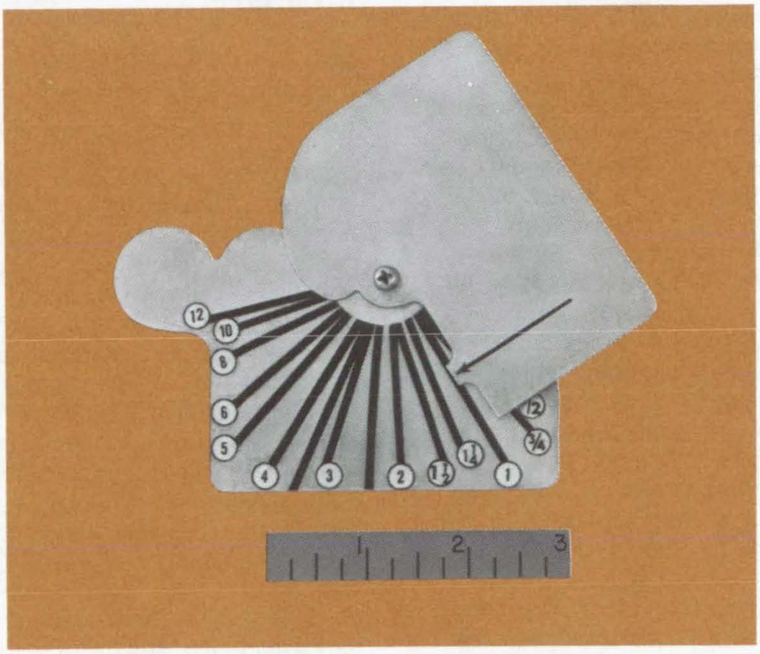

Figure 2. **Prototype Conduit Template** as fabricated. The lettering consists of rub-on dry-transfer lettering.

An electrical conduit is identified by a trade size number which has little relation to the exact diameter of the conduit. The number indicates the wire size and fill for which the conduit is designed. Experienced technicians can "eyeball" a conduit and judge its trade size. Inexperienced technicians have to measure the outside diameter with a caliper and use a conduit diameter-to-trade cross-reference table to determine the proper size. In many cases this leads to mistaken trade sizing or calling out incorrect sizes on drawings.

A simple gage has been developed to measure approximately the outer diameter of an electrical conduit and to relate it to the standard trade size. Trade sizes are standardized on the basis of the inside diameter of a conduit rather than its outer diameter. Thus, measurement of the outside diameter does not necessarily determine the trade size. Product literature indicates that conduit outer diameters vary from one manufacturer to another.

Since the outer diameters, though different, are not far apart, the gage can be made to show trade size range rather than exact diameter measurement. This enables the user to measure conduit trade size irrespective of manufacturer.

The gage, consisting of two flaps as seen in the figures, is made from thin aluminum sheet stock. Indicator lines can be scribed on the surface, or adhesive-backed decals can be used instead. To use the gage one of the gage flaps is rested against the conduit; the other flap is rotated until it contacts the conduit. An indicator arrow will point to the trade size being measured.

This work was done by Clarence E. Caveness of Rockwell International Corp. for **Johnson Space Center.** *No further documentation is available.*
MSC-19491

Books and Reports

These reports, studies, and handbooks are available from NASA as Technical Support Packages (TSP's) when a Request Card number is cited; otherwise they are available from one of NASA's Industrial Application Centers or the National Technical Information Service.

Testing Flat-Conductor Cable

Three-conductor FCC, is safety-tested to UL standards.

A report on the flat-conductor cable (FCC) which is designed for use in a surface nonmetallic protective covering is available; it is entitled "Testing of Flat Conductor Cable To Underwriters Laboratory Standards UL719 and UL83." The report describes the characteristics of a type of FCC which consists of three AWG No. 12 flat copper conductors laminated between two films of polyethylene terephthalate (Mylar) insulation with a self-extinguishing polyester adhesive. The insulation is rated at 100° C (212° F) and 600 volts. The self-extinguishing polyester adhesive has an oxide of antimony as the flame-retardant agent.

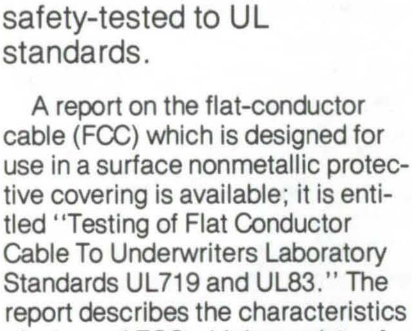

Flat-Conductor Cable Flow Test Apparatus is used to measure some of the ten parameters associated with the cable. The cable is tested to conform to UL719 and UL83 of the Underwriters Laboratories, Inc. safety code.

The tests were performed on samples according to the methods outlined in "Nonmetallic Sheathed Cables," subject UL719, and "Standard for Safety Thermoplastic-Insulated Wires," subject UL83, both of the Underwriters Laboratories, Inc. Ten parameters were tested. These included: (1) cable separability, (2) electrical continuity, (3) flame-retardant properties, (4) dielectric withstanding voltage, (5) tension and elongation, (6) unwinding at low temperature, (7) conductor pullout, (8) abrasion resistance, (9) crushing resistance, and (10) insulation flow. (A simplified representation of the insulation flow test is shown in the figure.)

This work was done by Robert W. Loggins and Ralph H. Herndon of **Marshall Space Flight Center.** *To obtain a copy of the report, Circle 11 on the TSP Request Card.* *MFS-23174*

Surface Mounted Flat-Conductor Cable

The drawbacks and advantages of FCC for home wiring

In the near future considerable improvements and changes will be made in home wiring to cope with increasing material and labor costs, electrical demands, new building materials and concepts, and the rehabilitation of old buildings. At present a 17-page technical memorandum entitled "Surface-Mounted Flat Conductor Cable For Home Wiring" is available. It presents the drawbacks and advantages of flat-conductor cable (FCC) technology in terms of its use in a home wiring system. According to the report FCC can be used throughout the home from the service-line entrance at the power panel to auxiliary wiring including telephone, intercom, and alarm systems.

Two types of surface-wiring schemes are considered: snap-on baseboard and extendable baseboard. The snap-on system can be installed in any type of existing or new structure, but requires more labor to install than extendable wiring. The extendable system illustrated with a three-prong-plug adapter is factory-made and is intended for new-home installation, but requires more development to be commercially successful. Both types of FCC, the report emphasizes, lower installation costs and time in this traditionally labor-intensive market.

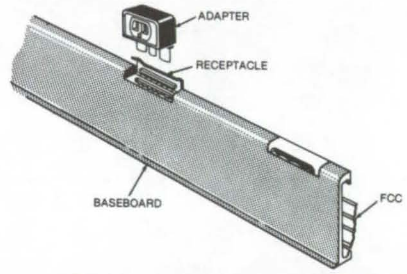

The **Extendable Baseboard** FCC wiring system is shown with an adapter for a three-prong plug.

This work was done by James D. Hankins and James R. Carden of **Marshall Space Flight Center.** *To obtain a copy of the report, Circle 12 on the TSP Request Card.* *MFS-23135*

Temperature Rise of Installed FCC

Temperature profiles of installed FCC for wood and tile surfaces

One of the advantages of flat-conductor cable (FCC) is its thinness as compared to round-wire cables carrying similar currents. As a result FCC can be installed in areas not previously possible by using methods not available to electrical contractors in the past. One such installation is the laying of FCC over a bare floor and under a short-pile carpet (and its sponge-rubber pad), and this is described in a 9-page technical memorandum. A three-conductor No. 12 AWG FCC was tested at twice the nominal current-carrying capacity, and the temperature rise of the carpet was noted.

The test results indicate that temperature rise is not a linear function of current with the FCC at this level.

Although the temperature of the carpet surface was not measured at the highest current, it felt barely warm to the touch, and the carpet material was not degraded. The report further notes that the floor surface acted as a thermal sink, as shown in the figure, further aiding FCC current-overload characteristics.

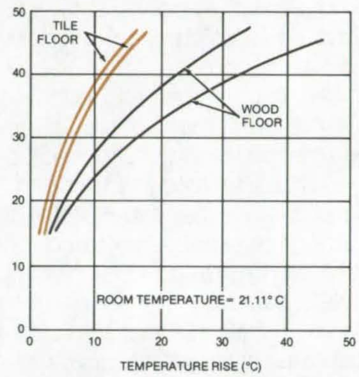

Temperature Rise is shown versus load for AWG No. 12 (copper) FCC installed under carpet.

This work was done by James D. Hankins of **Marshall Space Flight Center.** *To obtain a copy of the report, Circle 13 on the TSP Request Card.*
MFS-23127

Flat-Conductor Cable Baseboard

Test procedures for commercial and residential applications

A test of a flat-conductor cable (FCC) baseboard system has been performed, and the procedures and results are offered in a 26-page technical memorandum. The baseboard system is a prototype version built for use in residential and commercial applications, and it therefore was tested to appropriate Underwriters Laboratory standards.

The baseboard material used in the manufacture of the protective coverings and fittings is polyvinyl chloride (PVC), the receptacle cover is vacuum-formed PVC sheet material, and the receptacle box is metal. The system, with or without receptacles, will house nine No. 12 AWG flat conductors; three additional conductors of the same size can be accommodated for future system expansion. The cover and fittings are designed to snap onto the back channel, but if desired, PVC cement can be applied to make disassembly a deliberate operation.

The test procedure consisted of 20 stages. Mechanical, electrical, chemical, environmental, thermal, and analytical studies subjected the FCC and its baseboard system to considerably more severe conditions than would be encountered in normal service. The system withstood the tests favorably.

This work was done by James D. Hankins of the **Marshall Space Flight Center.** *For further information, Circle 14 on the TSP Request Card.*
MFS-23141

Manufacture of Flat-Conductor Cable

Discussion of manufacturing and design, includes a bibliography.

In less than 20 years the manufacture of flat-conductor cable (FCC) has grown from an experimental project at a space center to a multimillion-dollar industry. Military specifications have been published to standardize FCC for government applications, and the Institute of Printed Circuits has published a specification to cover industrial FCC.

A 77-page technical memorandum has been published outlining the manufacturing basics of FCC. The five chapters of "The Manufacture Of Flat Conductor Cable" describe basic cable design and the fabrication of both unshielded and shielded FCC and list additional references and bibliography. The memorandum describes the manufacture of unshielded and shielded cables, using a wide variety of materials and techniques.

Numerous cable configurations and production techniques have been developed. Fabricating processes include laminating (the most widely used), etching, extruding, and weaving. Rectangular conductors (usually bare or plated copper) are arranged parallel to each other and are held together in one plane by an insulating material. The conductors may be: (a) flattened round wires (the most-widely-used conductor type), (b) slit from foil or etched from a metal/plastic laminate, or (c) formed by electrolytic deposition. Insulation can be applied by several techniques, including lamination, extrusion, spray coating, and weaving. FCC can be fabricated for signal and power applications and, when necessary, can be shielded for the attenuation of both electrostatic and electromagnetic fields.

This work was done by W. Angele of the **Marshall Space Flight Center.** *For further information, Circle 15 on the TSP Request Card.*
MFS-23121

Electronic Circuits

Selected developments in instrumentation and communications technology

A recent NASA Compilation, SP-5972(07), entitled "Electronic Circuits," describes 29 circuits and circuit techniques developed for communications and instrumentation technology. This Compilation is one of a series of NASA Technology Utilization Publications which, like NASA Tech Briefs, make available aerospace technology that may have application in commerce and industry.

"Electronic Circuits" contains articles on communications techniques, including pulse-code modulation, phase-locked loops, data coding, and data recording. Articles on circuits for specialized instrumentation include descriptions of detection circuits, amplifiers, logic circuits, oscillators, and control circuits.

This work was done for **NASA Headquarters.** *To obtain a copy of SP-5972[07], Circle 16 on the TSP Request Card.*
HQN-10894

Electrical-Cable Design Guide

Data for filler materials, jacket wall thicknesses and cable diameters

The "Electrical-Cable Design Guide" is a 10-page compendium of formulas and tables to aid designers in determining electrical-cable jacket sizes, the number of wires per lay pattern, filler-material requirements, jacket wall thickness, and overall cable diameters. The guide provides a standard approach which assures consistency of end-product cable design parameters.

The formulas are intended to simplify the method of obtaining cable-bundle outside diameters. Four tables summarize the data. Table I has been compiled by using the nominal diameters of conductors of the same gage and diameter. Table II shows how to treat a cable as a single wire to determine final outside diameter by means of multiplying factors (1X, 2X, ... , nX). The reason for treating a cable as one wire is that a filler cable may be required to provide a circular cross section before jacketing of the cable assembly. (Fillers are used in place of spare wires to decrease weight and cost.)

Table III is used to obtain the correct inside diameter of the cable jacket, while Table IV gives applicable wall thickness of neoprene tubing. These calculations are applicable to all cables that are under 7.5 cm (3.0 in.) in diameter prior to jacketing.

This work was done by George A. Phelps of Rockwell International Corp. for **Marshall Space Flight Center.** *For further information, Circle 17 on the TSP Request Card. MFS-24280*

Installation of Surface-Mounted Flat-Conductor Cable

Tools, Hardware, and Procedures for residential and commercial buildings

A guide describing the installation of interior surface-mounted flat-conductor cable (FCC) used in residential and commercial buildings is offered. Although it is preliminary (since only two prototypical installations are described), the guide nevertheless shows in step-by-step fashion the tools, hardware, and procedures used at the sites of an apartment complex and an office.

Some topics covered in the 24-page booklet are: (a) vertical-wall cable routing and transition, (b) receptacle box assembly, (c) back-channel installation, (d) flat-conductor cable routing, (e) flat-cable-to-round-wire transitions, and (f) the installation of baseboard molding and front-cover hardware. Self-explanatory photographs show how cable-riser and baseboard covers are installed as well as receptacle assembly and receptacle-cover replacement.

This work was done by James R. Carden of **Marshall Space Flight Center.** *To obtain a copy of the report, Circle 18 on the TSP Request Card.*

Inquiries concerning rights for the commercial use of this invention should be addressed to the Patent Counsel, Marshall Space Flight Center[see page A8]. Refer to MFS-23266.

Guidelines for Multiple LSI Packaging

A design handbook for vertically layered thick-film microcircuits.

A handbook provides the integrated-circuit (IC) designer with specific guidelines related to ceramic multilayer circuit fabrication in terms of packaging density and interconnection methods. Current state-of-the-art IC technology provides logic circuits which will change state in only 1 nanosecond. The operating speed of a computer, for instance, is limited mainly by the length of interconnections between IC's. One method of reducing lead lengths is to use custom large-scale integration (LSI) chips. However, when special-application monolithic LSI circuits are not available, significant lead length reduction can be realized by a hybrid approach.

Ceramic multilayer interconnect systems permit many of the advantages gained through IC technology to be reliably utilized in a miniaturized custom-made form without incurring the expense and lead time involved in custom LSI chip design. However, as the physical size of the ceramic carrier interconnect circuitry decreases and active-device density increases, the probability of electrical, thermal, or mechanical problems increases proportionally.

Ceramic multilayer circuits consist of two or more layers of predetermined conductive interconnections, separated by dielectric layers and fired at an elevated temperature to form a solidly fused structure. The resultant ceramic interconnect matrix is used as a base to mount active and passive devices and to interconnect the desired electrical circuit.

The handbook, although tutorial, guides the designer from the initial stages of ceramic multilayer interconnection and artwork generation through test pattern utilization, assembly operations, and final inspection and test procedures. A step-by-step evaluation of a thick-film LSI microcircuit is offered, with actual test methods and results described to highlight final performance. The text concludes with a comprehensive evaluation of materials. A glossary of terms and a list of 98 additional references are included.

This work was done by C. J. Peckinpaugh of Electronic Communications, Inc., for **Marshall Space Flight Center.** *To obtain a copy of the handbook, Circle 19 on the TSP Request Card. MFS-23367*

Electronic Systems

Hardware, Techniques, and Processes

Automatic Fire/Weather Data Station

An integrated system collects and processes fire-index data.

Ames Research Center, Moffett Field, California

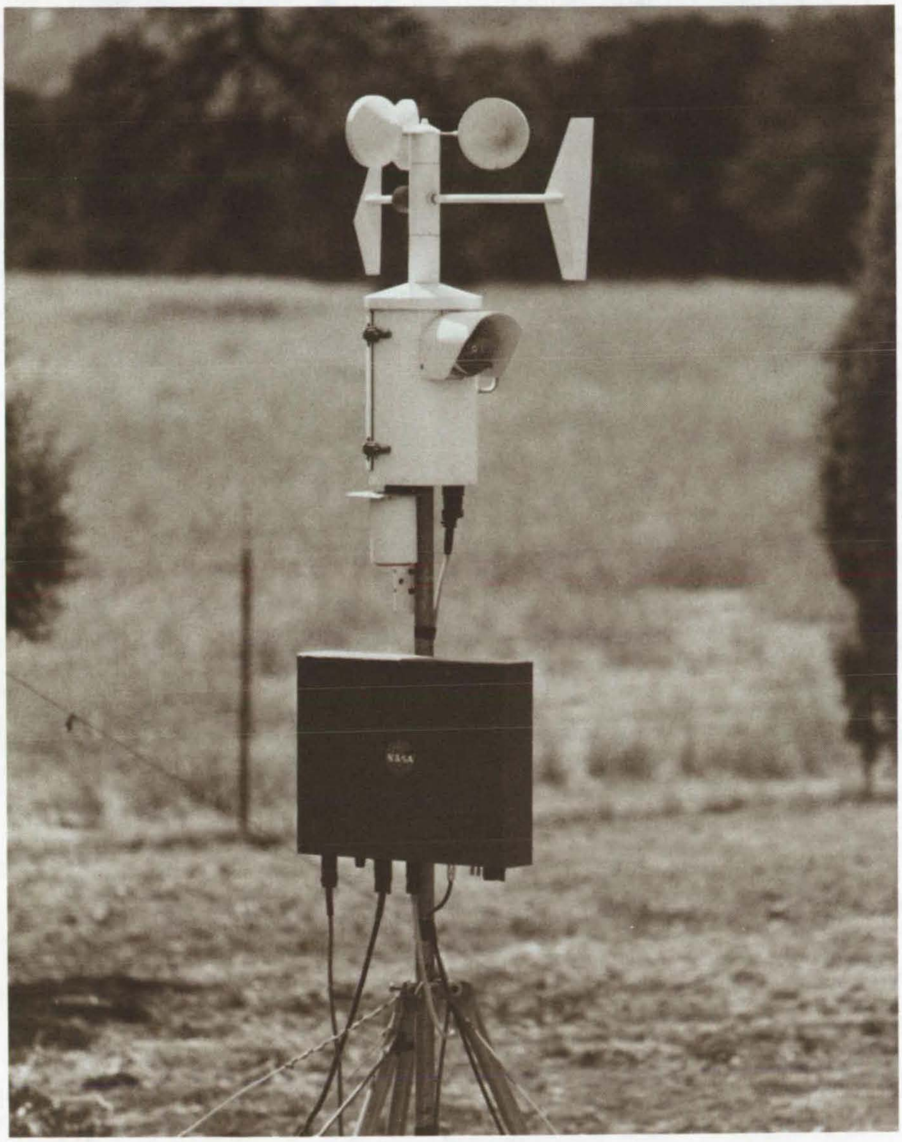

The **Automatic Fire/Weather Data Station** is a prototype unmanned integrated system which collects and processes fire-index data.

The prediction of fire/weather status is based on a "fire index" that is tabulated from measurements of five parameters: air temperature, relative humidity, wind direction, wind velocity, fuel moisture, and fuel temperature. Established methods for obtaining the fire index require personnel to make field measurements and to transmit data to an offsite center for tabulation, but data are not collected during firefighting or rainy seasons. Obviously, the accuracy of measurements are strongly dependent on personal judgments.

In order to improve the accuracy and frequency of fire/weather forecasting, an integrated system has been developed to collect and process fire-index data automatically. The system is based on state-of-the-art technology, and even though it uses low-cost hardware, it is highly reliable and needs little maintenance. The unmanned system (see the figure) operates on a year-round basis, so that models can be derived for long-range firefighting logistics.

Primary components of the automatic fire/weather data station are sensors for the six fire-index parameters listed above, a data-controlling and synchronizing (DCS) element, a microprocessor, and a power supply. The DCS element is used to generate all synchronizing and sequencing frequencies. The microprocessor contains conversion and calculation algorithms stored in programable read-only memories.

In operation, a sequencer interrogates each of the sensors at prescribed time intervals, converts the analog data to digital, and then transfers all digital data to an output data register. The signal from the output register is transmitted to the microprocessor where the digital data are converted to analog equivalents and the fire index is calculated from the converted data. The microprocessor output can be stored on disks for later reference, punched on paper tape for input to a computer for detailed analyses, or printed for hard-copy display.

This work was done by Henry Lum, Jr., of **Ames Research Center.** *For further information, Circle 20 on the TSP Request Card.*

Inquiries concerning rights for the commercial use of this invention should be addressed to the Patent Counsel, Ames Research Center [see page A8]. Refer to ARC-10993.

Unbalanced Quadriphase Demodulator

A new demodulator for supressed carrier pulse-code-modulated signals represents incoming signals as vectors.

Lyndon B. Johnson Space Center, Houston, Texas

A new demodulator is proposed to process an unbalanced quadriphase-shift-keyed (QPSK), suppressed-carrier, pulse-code-modulated (PCM) signal. An unbalanced QPSK signal is defined as one in which the four phase positions of the signal are not spaced by 90°. For example, the incoming QPSK signal may be represented as four possible voltage vectors spaced at 26°, -26°, 206°, and -206°, as shown in Figure 1(a). This unbalanced QPSK signal could be generated by adding a 20-percent relative-power PSK signal to a quadrature 80-percent relative-power PSK signal. The QPSK demodulator tracks the incoming signal with the use of two selectable phase-reference signals, I_{gen} and Q_{gen}, making up four phase positions for the reference signals, as shown in Figure 1(b).

The basic demodulator is shown in Figure 2. The two phase positions of I_{gen} and Q_{gen} are necessary to match the four possible incoming vectors. The incoming vector can be determined by a data demodulator which outputs an estimate of the data. When the product of data 1 and data 2 is positive, the incoming vector is V_1 or $-V_1$; so the switch selects position A, shifting the VCO reference +26°. Likewise, when the product is negative, the incoming vector is V_2 or $-V_2$, and position B is selected, giving a -26° phase shift of the VCO reference.

Therefore I_{gen} and Q_{gen} become the in-phase and quadrature reference tracking signals, respectively, whether the input vector is V_1 or V_2. The I and Q signals are then generated by the multiplication of each respective reference signal with the incoming signal. Next the I signal corrects the polarity of the Q signal in the I×Q multiplier, resulting in an error signal for tracking which is proportional only to the phase difference between the incoming signal and the tracking reference-signal phase.

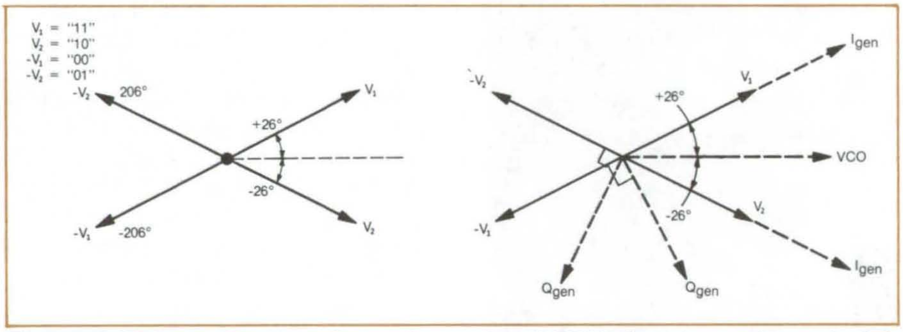

Figure 1. **Voltage Vectors** for an incoming QPSK signal are shown in (a) above. The Vi represent binary data pairs (data 1 and data 2). In (b) the vectors for reference signals at a phase-locked condition are shown.

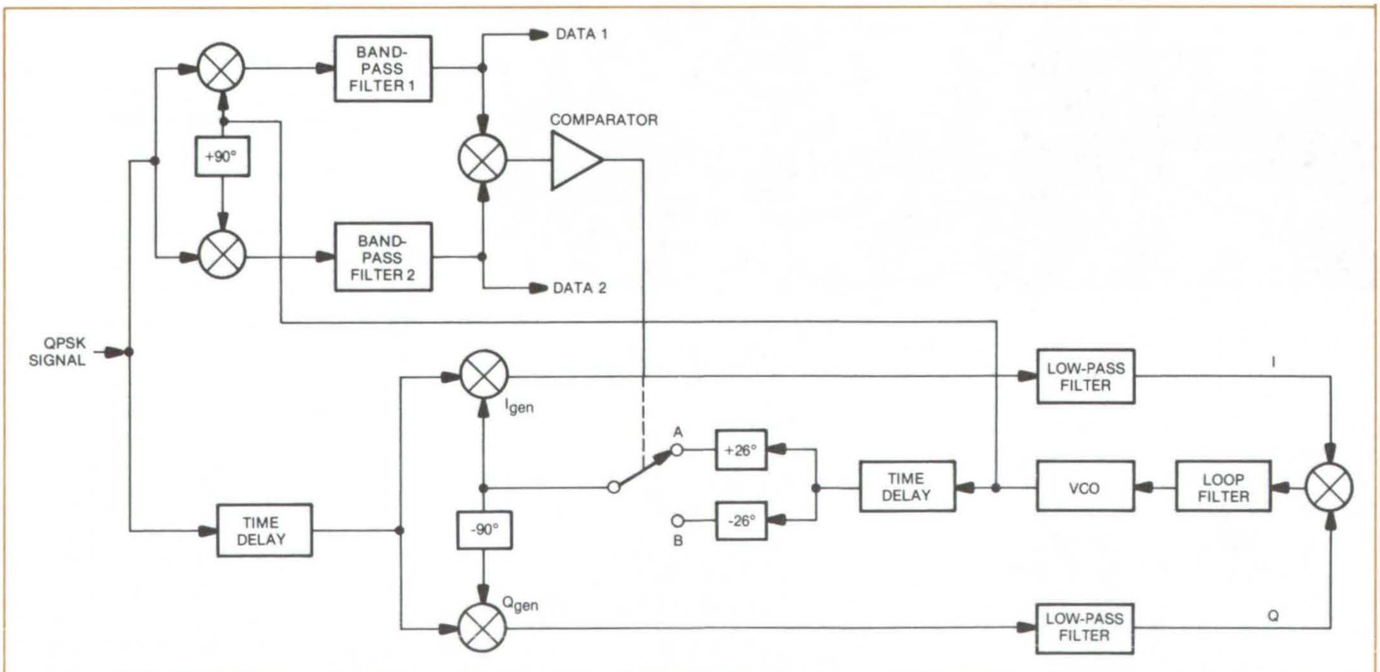

Figure 2. The **Unbalanced Quadriphase** Demodulator will process QPSK pulse-code-modulated signals with a suppressed carrier. Two phase-reference signals I_{gen} and Q_{gen} are used to track incoming signals.

Some important points about this demodulator are as follows:

- If the unbalance ratio of the QPSK signal is changed, then the selectable phase-shift networks should be set to a corresponding amount of phase shift. For example, the demodulator could receive a balanced QPSK signal if the selectable phase shifts are 45° and -45°.
- The tracking performance of the demodulator is not sensitive to voltage-level changes caused by gain and bias variations but only to the accuracy of the phase shifts.
- The difference between the absolute value (square) of the I and Q signals may serve as a lock detection signal for automatic acquisition and as a signal for automatic gain control.
- There are two ambiguities in the data output with an unbalanced QPSK signal: Each data input remains in its respective output form from the demodulator, but each may be of correct polarity or inverted. With a balanced QPSK signal, the data may also change outputs (four ambiguities).

This work was done by Herbert S. Kobayashi and Sydney P. Bradfield, III of **Johnson Space Center.** *For further information, Circle 21 on the TSP Request Card.*

Inquiries concerning rights for the commercial use of this invention should be addressed to the Patent Counsel, Johnson Space Center [see page A8] Refer to MSC-14840.

Free-Space Microwave-Power Transmission

Laboratory-scale wireless transmission of microwave power approaches 54 percent efficiency.

Marshall Space Flight Center, Alabama

In a new wireless energy transmission method, dc is converted to a 2.45-GHz signal and is transmitted through a horn antenna array. The microwave signal is received at a rectenna (rectifying antenna) where it is simultaneously collected and rectified back to dc at the receiving site. The dc is then processed for wired distribution, much as electrical energy is processed by a conventional generating station.

The increased efficiency is obtained through several developments:

- More-efficient and more-powerful GaAs Schottky-barrier diodes,
- A low-pass microwave filter input to the rectenna element,
- The development of a simplified but efficient half-wave rectifier circuit,
- The start of the development of a computer program which takes the fine structure of the rectenna element and the rectifier into consideration,
- The design of a rectenna to use in a high overall efficiency system and to maximize the amount of useful experimental data,
- An improved dual-mode horn antenna that delivers 95% of the microwave signal to the receiving site,
- The development of a design procedure for a microwave-beam transmission system of arbitrary transmission efficiency and transmission distance in which a point source of microwave power is used to excite the system, and
- A new design procedure for a low-cost ellipsoidal reflector.

This work was done by W. C. Brown of Raytheon Co. for **Marshall Space Flight Center.** *For further information, including a discussion of microwave energy transmission, design particulars of the improved system, and test data, Circle 22 on the TSP Request Card.*
MFS-23443

Long Binary Frame Sync Words

Prefixes of pseudonoise sequences for frame synchronization of binary PSK telemetry require only a small portion of the sync words to be stored in memory.

Caltech/JPL, Pasadena, California

Correlation criteria have been established previously for identifying whether a given binary sequence would be a good frame sync word for phase-shift keyed (PSK) telemetry. In the past, the search for a suitable k-bit sync word has involved the application of these criteria to the entire set of 2^k binary k-tuples. It is shown that restricting this search to a much smaller subset consisting of k-bit prefixes of pseudonoise (PN) sequences results in sync words of comparable quality, but requiring greatly reduced computer search times for larger values of K.

This procedure has been successfully used to find good sync words of lengths 16 to 63. The storage advantage is that these sync words can be generated by a 5-bit or 6-bit linear feedback shift register (FSR), so that only a small fraction of the sync word need be stored in memory.

This work was done by Barry K. Levitt of **Caltech/JPL.** *For further information, including a tabulation of sync words, Circle 23 on the Reader Service Card.*
NPO-13727

Demodulator Aids Synchronization

A decision-feedback loop synchronizes multiple-amplitude and phase-shift keyed signals.

Caltech/JPL, Pasadena, California

A method for highly efficient carrier synchronization has been demonstrated in connection with the study and development of multiple-amplitude phase-shift keyed (MAPSK) and quadrature-amplitude shift keyed (QASK) systems, the latter being a special case of MAPSK. As a result of the study, a demodulator has been designed which incorporates a decision-feedback structure for near optimum carrier synchronization. Single-threshold data detectors are replaced with multiple-threshold devices to accommodate the multiple amplitudes involved in MAPSK and QASK. Each decision-feedback loop employs an integrate-and-dump circuit and a decision-threshold level quantizer for QASK or a maximum-likelihood detector for MAPSK. The circuit can be used to generate a carrier reference for any MAPSK signal set.

The analysis of the system model includes the derivation of an expression for the effects of carrier synchronization on the error probability for MAPSK and an expression for the average probability of symbol error, given a fixed carrier-phase error. These are combined to give results for the degradation in average symbol-error probabilities in the presence of a noisy carrier reference signal.

This work was done by Marvin K. Simon and Joel G. Smith of **Caltech/JPL.** *For further information, Circle 24 on the TSP Request Card.*
NPO-13605

Analog-to-Binary Conversion of Video Data

A high-speed comparator circuit which ignores out-of-focus features and is insensitive to overall brightness changes in the picture.

Goddard Space Flight Center, Greenbelt, Maryland

A new technique for converting television information to binary form is both accurate and controllable. It was developed for systems requiring video signals to be used with automatic data-processing equipment. Modifications of the circuit parameters allow optimization of the binary conversion for given applications, including the detection of particle tracks in a nuclear emulsion and contrast enhancement in TV pictures.

A key element in the technique is an assembly of circuitry termed a "discriminator" which converts TV signals into binary data. The operation of the system is shown in the block diagram. For each horizontal line, the binary output from the discriminator is subsequently accumulated in a counter and is read by an IBM-1800 computer (or equivalent) in a parallel transfer.

This discriminator has several properties which make it stable and accurate and, hence, useful for many applications. For example, the circuitry will generally ignore out-of-focus features. This is controllable by selection of decay rates in the reference signal. Second, both the signal and the comparison signals are clamped prior to comparison at the blanking level. This makes the output independent of ordinary changes in overall scene illumination levels. Finally, the usage of a high speed comparator allows the resolution of fine detail in the image.

This work was done by Mario H. Acuna and Charles J. Pellerin of **Goddard Space Flight Center.** *For further information, Circle 25 on the TSP Request Card.*
GSC-11918

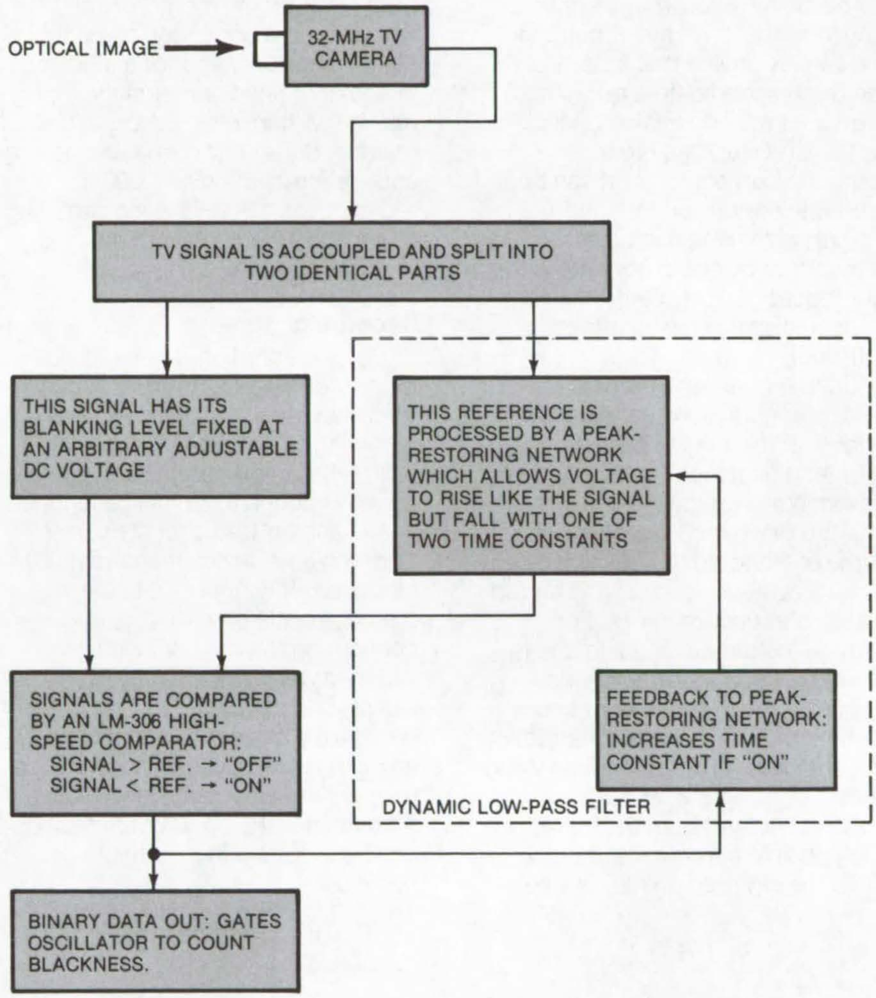

Analog-to-Binary Conversion of Video Data uses a high-speed comparator (LM-306) to compare the original signal with a reference derived from it. The binary output is derived from the comparator. Both the signal and comparison signals are clamped prior to comparison to make the output independent of ordinary changes in overall scene illumination levels.

Digital Video Image System

A computer-compatible data-storage interface permits video image manipulation.

Marshall Space Flight Center, Alabama

The digital video image system (DVIS) is an interactive recording and display device that acts as a very-high-speed data-input/output interface between analog (video) signals and standard digital-computer compontents. It can be used with various picture and memory sizes and can be controlled manually or by computer. There are four modes of operation:

- Video display (refresh static frame)
- Video record (one frame)
- Make digital tape (transfer contents of memory to bulk storage)
- Enter digital tape (load memory from bulk storage)

In the video record mode, one frame of standard (NTSC) video data is digitized at video rates and stored in a regular core memory. For display, the stored digital image is used to refresh a standard video monitor through repeated readout from memory and the reconstruction of a standard NTSC composite video signal.

Access to and from the memory is also possible at nonvideo rates. Thus, the digitized image may be read out from the memory and written onto a computer-compatible digital magnetic tape, or a digitized image contained on magnetic tape may be written into memory. This memory buffer technique results in a data-rate reduction of 1,000:1, reducing the 10-MHz video sampling rate to the 10-KHz rate of the recorder.

Recording

During recording, the bandwidth of the video signal (5 MHz) necessitates sampling and digitizing the incoming signal every 100 ns (10-MHz sample rate). Each sample (pixel) is coded to 8 bits in a high-speed analog-to-digital converter. The high data-acquisition rate (100 ns per pixel) is matched to the memory-cycle time (650 ns) by configuring the memory with a widened word size (32K by 65-bit words) and packing the data. Eight pixels (of 8 bits each) are packed in an input buffer register, allowing the memory to be cycled every 800 ns. A complete 512-by-512 video image can be recorded in 1/30th of a second.

Digital images stored on magnetic tape can be written into memory through the same input buffer register. In this case the basic clock cycle is determined by the digital tape recorder and the memory is cycled every 800 μs, so that a 512-by-512 pixel frame can be entered in approximately 90 seconds (including record gaps).

Image Memory

The maximum size of image which can be stored is determined by the amount of core memory provided. In the current system the memory capacity is 32K by 64-bit words or 256K by 8-bit bytes. This allows storage of a total of 262,444 pixels. All of these pixels can come from a single full-sized video frame or from several smaller pictures. Control features allow compression of recorded data and simultaneous display of several images for comparison.

Display

The memory output is the digitized image data obtained by a reversal of the memory input technique. Every

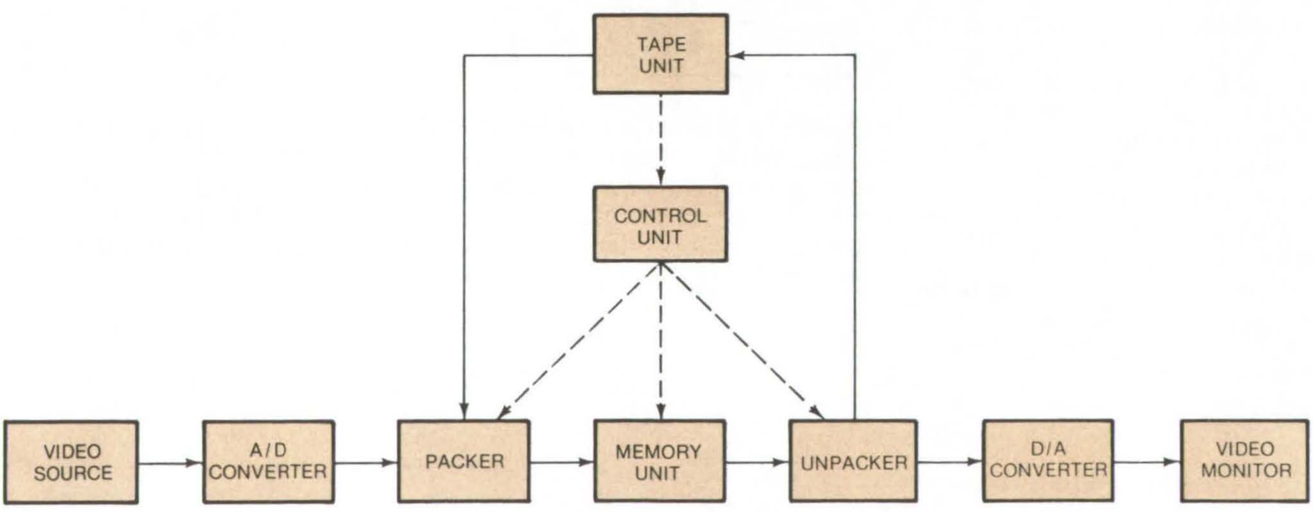

The **DVIS** is a modular system that makes use of standard computer hardware to generate computer-compatible tapes from analog video signals. Under direction of the control unit, the packer compresses data sampled by the A/D converter (or from tape) for insertion into memory; the unpacker expands data for display or tape storage.

memory cycle, a full 64-bit word is read out of memory and clocked into an output buffer register. For bulk storage the digital data are written onto magnetic tape through the same unpacking process. As before, the basic clock cycle is determined by the digital tape recorder.

The video output is a reconstruction of a composite video signal from the 100-ns pixel stream achieved through data conversion in a high-speed D/A converter, followed by reinsertion of the video synchronization signal and attenuation in a video amplifier. The stored image is continuously displayed at standard video rates until a new image is recorded or the tape mode of operation is used, either "enter tape" or "make tape." Upon completion of any of these modes, the system reverts automatically to the display mode and continues to display whatever image is currently in memory.

Automatic Operation

Images are recorded when a logic signal (STORE) is received from an external device. If required, data are written onto magnetic tape automatically after the STORE signal. The image is displayed for 10 seconds to allow the operator to decide whether to store it on tape. If no action is taken, the timer triggers the "make tape" mode; otherwise the operator may manually inhibit the "make tape" mode.

This work was done by Patrick L. Neely and Robert M. Brown of Computer Sciences Corp. for **Marshall Space Flight Center.** *For further information about the DVIS, including a description down to the subsystem level, Circle 26 on the TSP Request Card.*
MFS-23322

Interactive Imaging and Data Processing

High-speed memory system allows real-time image processing.

Caltech/JPL, Pasadena, California

Planetary missions of the future will use roving vehicles preprogrammed via computer control. In order to optimize programing time during the present design stage, the system is being assigned only specific limited goals. Other onboard interplanetary tasks, best performed via a man/machinery interface, are simplified by the use of a high-speed digitized video scheme implemented by digital imaging and data processing. This image processing method is capable of contrast enhancement, noise filtering, and photometric distortion removal in near real time. Personnel who are not trained in computerized signal analysis can view the resulting image transmitted from the craft on a conventional TV monitor.

The system uses digital image integration, and a digital video recorder is employed as an image buffer. Each frame of data is entered into a memory which consists of nonvolatile dynamic shift registers. The registers provide a readout of the stored TV frame.

As the linear video signal is applied to the input of the recorder, the system operates as a multiple additive frame grabber or integrator. The number of frames accumulated (or frame integration time) is controlled by an acquisition timer. This operates from the level of the received camera signal and improves signal-to-noise ratios from the camera system by a factor equal to the square root of the number of frames integrated. After increasing the signal-to-noise ratio, routine image processing in near real time is controlled by a minicomputer.

This work was done by Harold Alsberg, Robert Nathan, and John H. Morecroft of **Caltech/JPL.** *For further information, Circle 27 on the TSP Request Card.*
NPO-13655

Multiplane Binocular Visual Display System

An improved binocular display system for flight training may have applications with other display and remote-control systems.

Ames Research Center, Moffett Field, California

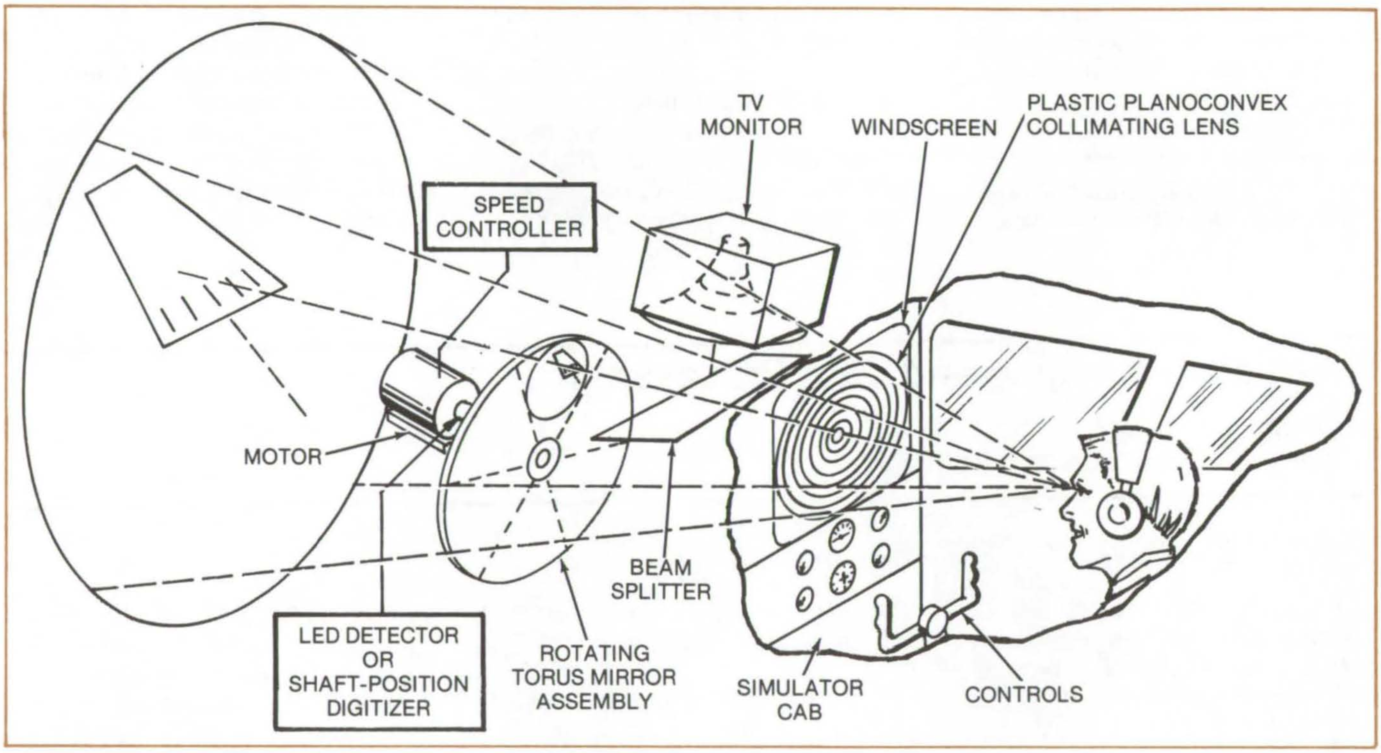

The **Multilayer Visual Display System** includes a television or digital-calligraphic monitor that is positioned above a 50-percent-reflectance, reverse-position beam splitter. A plastic planoconvex lens (60 cm in diameter) is placed ahead of the beam splitter in the windscreen of the simulator cab.

An electro-optic system has been interfaced with a digital computer in a flight simulator to generate simultaneous multiple-image planes in real time for out-the-window displays of a landing-approach scene over the entire range from the height of the pilot's eyes above the runway to infinity. The scenes have very compelling binocular stereo effects representing the major depth-perception cues that are not obtainable with the usual visual attachments.

The display system is shown in the figure. A large wheel behind the beam splitter supports either six offset mirrored sections or a torus mirror. The motor that spins the mirror system at 20 to 60 Hz is synchronized with the computer-controlled drawing of calligraphic-line or dot elements by means of a light-emitting-diode (LED) detector mounted behind the mirror wheel on the motor side; alternatively, a shaft-position digitizer and associated counters may be used for synchronization. The mirror wheel in the assembly must be matched to the size of the aircraft windscreen, collimating lens, and display monitor in order to create the illusion of depth.

The pilot is positioned with his eyes focused at the center of the collimating lens at a distance of about 60 cm (or one-half the focal length of the lens) so that he views a multiple virtual image. As the pilot moves the controls of the aircraft, the display will move as a consequence of changes in the aircraft six-degree-of-freedom dynamics processed by the digital computer. In order to produce the picture on the monitor and to draw it in its correct perspective and image plane, the display is turned on when the rotating wheel is in the correct viewing position. As many as six image planes can be drawn at any one time for the digitally generated displays, and for the TV display all image planes from infinity to the height above the runway can be drawn simultaneously (or from one to six image planes sequentially). In-and-out movement of the mirror-wheel assembly allows further freedom to position the far, near, and intermediate image planes to a satisfactory position for simulation purposes.

This work was done by Wendell D. Chase of **Ames Research Center.** *For further information, Circle 28 on the TSP Request Card.*

This invention is owned by NASA, and a patent application has been filed. Inquiries concerning nonexclusive or exclusive license for its commercial development should be addressed to the Patent Counsel, Ames Research Center [see page A8]. Refer to ARC-10808.

Physical Sciences

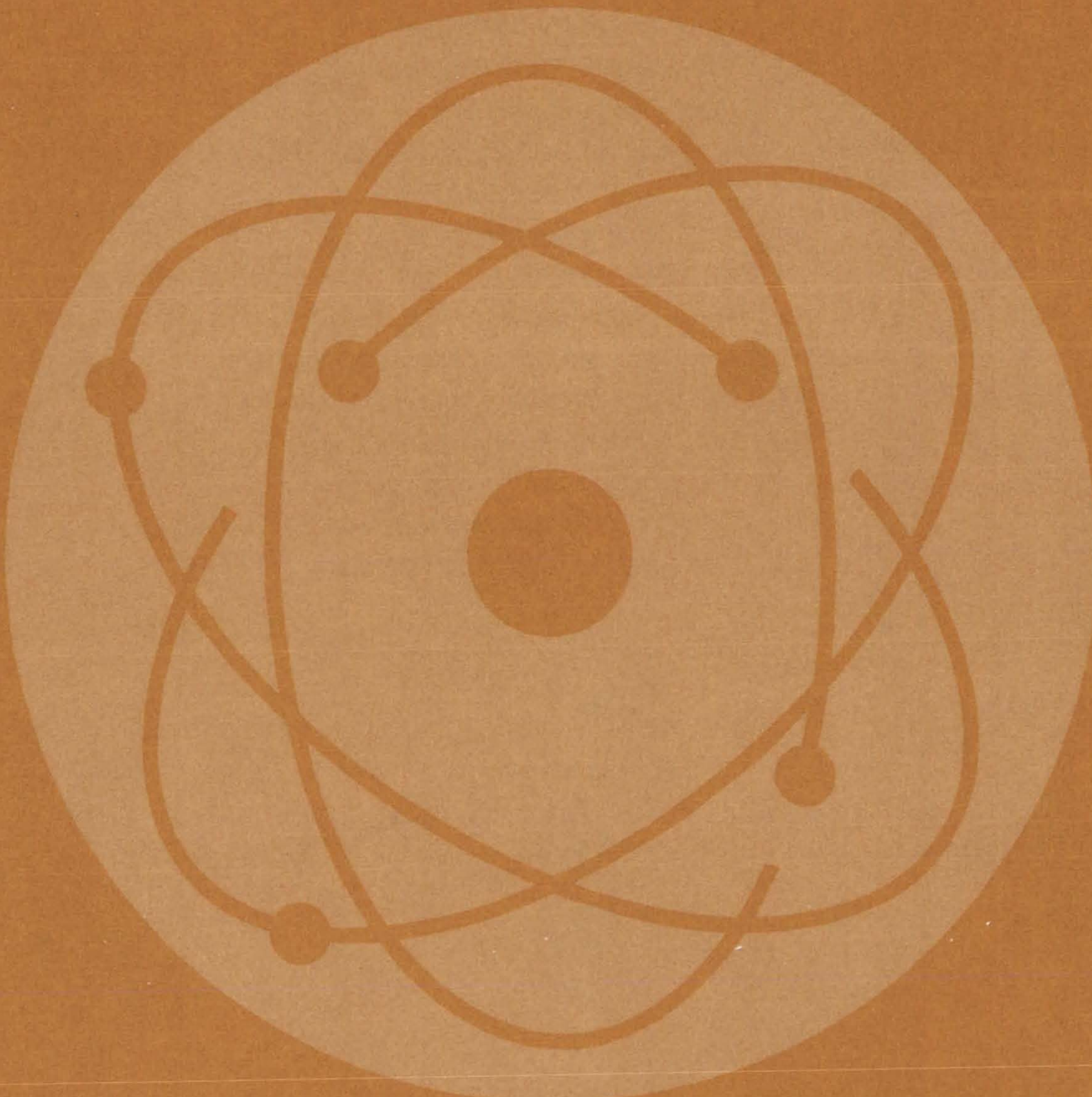

Double-Exposure Holographic Interferometer

An inexpensive
instrument for shock studies.

Caltech/JPL, Pasadena, California

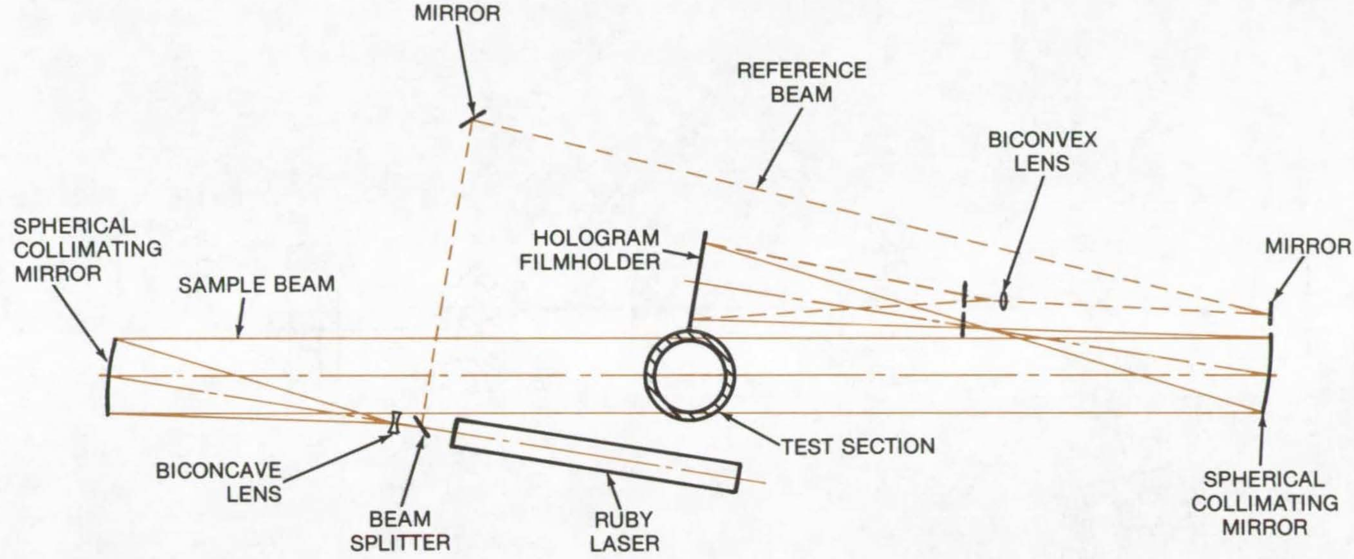

The **Holographic Interferometer** consists of a pulsed ruby laser system, a beam splitter, a sample beam expander, two spherical collimating mirrors, a reference beam expander, and a hologram filmholder. The laser is a pulsed ruby with a 20-ns pulse width and a coherent length from 1 to 5 m.

Expensive optical-grade components in a holographic interferometer are replaced with a plastic test section and a large-aperture spherical mirror to reduce distortions introduced by imperfections and cylindrical shape of the plastic. The modified interferometer is used for shock-tube gas density studies and is adaptable to wind-tunnel studies of vehicle windshields and other testing requiring instantaneous measurement of refractive index.

The laser beam (see figure) is split into sample and reference beams by a 0.5-cm-thick piece of plain glass. The reference beam is directed to the hologram plane by a prism and a series of plane mirrors and then is expanded by a biconvex lens. The sample beam is expanded with a biconcave lens, is collimated with a spherical mirror, is transmitted through acrylic-tubing test section, and is then focused upon the hologram plane by a second spherical mirror (where it intersects with the reference beam).

The pulsed holographic interferometer measures the fringe shift from the first film exposure (there is a neutral hydrogen/helium gas mixture in the test section) to the second exposure (there is shock-heated plasma in the test section) across the acrylic tube. The system can reconstruct quality image holograms of an object (such as a candle) within the test region without the acrylic tube. The finite fringes, spaced at about one per millimeter, are quite sharp and are well alined with a wire grid placed on each side of the test section.

With the acrylic tube in place (for shock-tube operation), the sample beam is expanded (the acrylic tube acts as a cylindrical lens of negative focal length), is scattered, and is refracted due to the plastic material. This is compensated for by use of the second spherical mirror. Knowing the displacement of grid wires enables one to interpret geometrically the recorded fringe shift accurately.

This work was done by Floyd R. Livingston of **Caltech/JPL.** *For further information, Circle 29 on the TSP Request Card.*
NPO-13796

Two-Wavelength Dye Laser

A double-pulse laser generates two independently-tunable closely-spaced pulses.

Langley Research Center, Hampton, Virginia

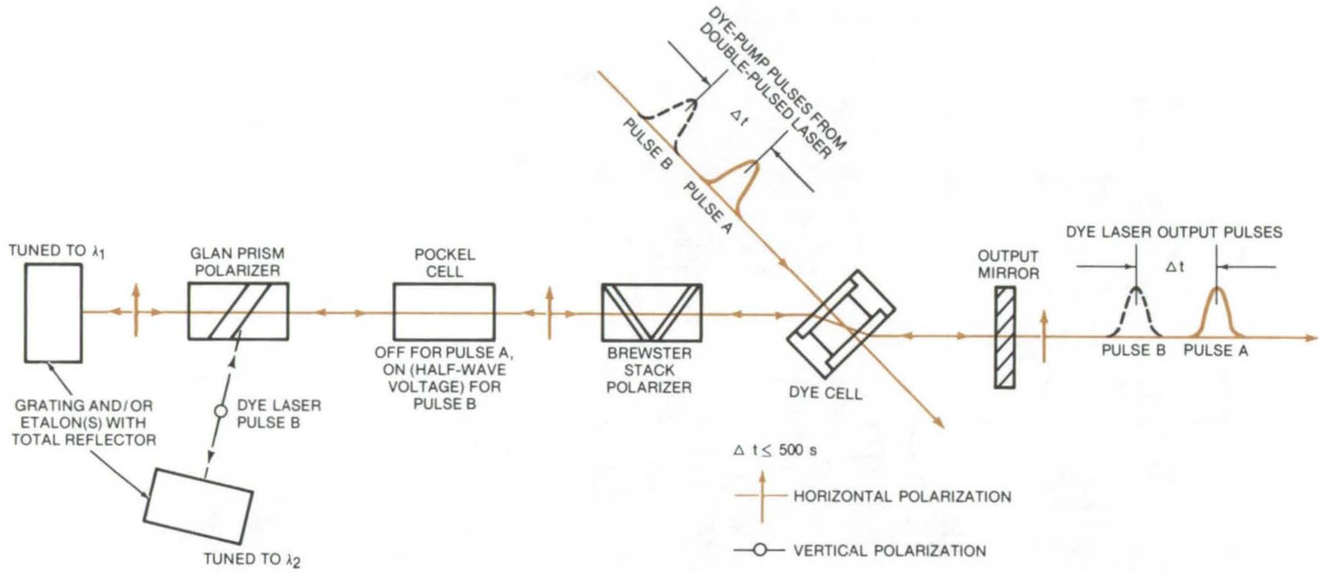

The **Two-Wavelength Dye Laser** receives horizontally polarized pulses from a double-pulsed dye-pump laser. Pulse A (color) is processed while the Pockel cell is off, remains horizontally polarized, and is reflected from a tuning element optimized for λ_1. Pulse B (black) is transmitted while the Pockel cell is on, is vertically polarized, and is reflected from a tuning element optimized for λ_2.

A double-pulse laser concept utilizes existing optical components in a unique design and is used in DIAL [differential absorption LIDAR (light detection and ranging)] experiments to remotely detect pollutant and trace gases in the atmosphere. It can be used with any double-pulsed pump laser or two single-pulse lasers that can be sequentially pulsed within a very short period of time. This laser provides two independently tunable wavelengths of light, which are required for the DIAL technique, in closely spaced pulses. These pulses are separated by less than 500 μs and minimize errors due to atmospheric scintillation. Also, requirements on the detection system are reduced as it is not necessary to simultaneously discriminate between two wavelengths of light which may be nearly identical. This system also provides such advantages as colinear propagation of both laser pulses and a nondispersive electro-optical switching element in the dye laser cavity, as well as reduced cost and increased reliability because only one double-pulse laser pump source is used.

The components of the two-wavelength double-pulse tunable dye laser are shown in the illustration. A double-pulsed laser, providing two closely-spaced laser pulses with a nominal time separation of less than 500 μs, is used to pump an appropriate dye in the flowing dye cell. The desired wavelength output of the dye laser restricts the choice of dye to be used, and the pump laser wavelength and the selected dye must be compatible. In the dye laser cavity, the flowing dye cell is orientated at near Brewster's angle to reduce reflection losses for horizontally polarized light, and the Brewster stack polarizer passes only the horizontally polarized light.

During laser pump pulse A, the Pockel cell has no voltage applied to it, and the light passes through it unchanged in its polarization direction. The horizontally polarized light is then transmitted by the Glan prism polarizer onto a grating and/or etalon(s) with a total reflector. The first dye laser output pulse is at λ_1 and is horizontally polarized. Between laser pump pulse A and pulse B, the half-wave voltage for light having a wavelength near λ_2 (including λ_1) is applied to the Pockel cell and is maintained for the duration of pulse B.

Light passing through the Pockel cell while the voltage is applied has its plane of polarization changed by 90° (horizontally polarized light from the Brewster stack polarizer is changed to vertically polarized light). This light is then reflected by the Glan prism polarizer onto a grating and/or etalon(s) with a total reflector. The tuning element is orientated to enhance the cavity gain for vertically polarized light at λ_2.

Upon being reflected back through the Pockel cell, the vertically polarized light is rotated back to horizontal polarization. The resulting second dye laser output

pulse is tuned to λ_2 and is also horizontally polarized. The time between the dye laser pulses is the same as between the laser pump pulses.

There are other optical components which can serve the same purposes as those illustrated in the dye laser cavity. There is also an alternative two-wavelength double-pulse tunable dye laser design which produces two nearly simultaneous pulses of light that are independently tunable.

This work was done by Edward V. Browell of **Langley Research Center.** *For further information, Circle 30 on the TSP Request Card.*

Inquiries concerning rights for the commercial use of this invention should be addressed to the Patent Counsel, Langley Research Center [see page A8]. Refer to LAR-12012.

Photorefractive Page Composer

A proposed optical memory would use a photorefractive hologram storage medium.

Marshall Space Flight Center, Alabama

An optical information-storage device based on a photorefractive page-composer concept is small, is easy to operate, and has low optical losses. This page composer uses an optical system in which the storage medium, a plate of photosensitive material, changes its refractive index upon exposure to light. A major design feature is that the page-composer plate does not require complete erasure between scans.

As conceived, the page-composer (see figure) includes a pulsed laser (laser 1) gated optically and followed by a raster-scanned two-axis deflector. A pulsed, modulated laser beam is scanned across the photorefractive page-composer plane. The plane is a 128-by-128 array of resolvable locations, each of which either receives a pulse which induces an index-of-refraction change, Δn, representing a digital one or receives no pulse, representing a digital zero. This pattern of index variations is stored in the memory plane until it is used with the reference beam to reconstruct the original signal.

The reconstructed beam would be phase-shifted in those areas corresponding to digital ones in the original beam. To convert the phase-shift information to intensity information compatible with the photodetector, a phase reference is used. This is done by recording the hologram of the empty page composer and filling the page composer with the desired series of 0° and 180° phase shifts. The hologram of this data is then superimposed on that of the reference page. The resulting interference patterns of the two holograms represents the stored pattern in an intensity format.

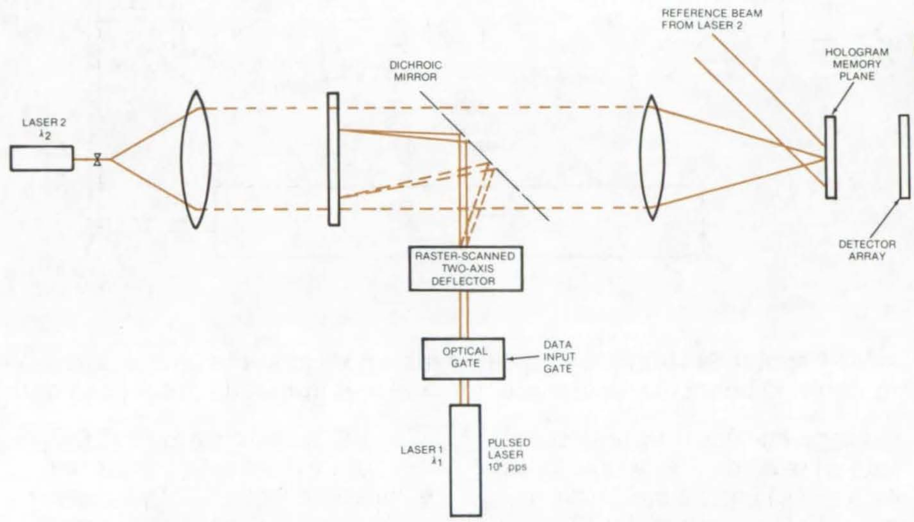

Photorefractive Page-Composer System with photorefractive plane consisting of a 128-by-128 array of resolvable locations: The array of serially entered bits is stored, and it is used as the object of which a hologram is made.

The page of data is recorded as a phase difference between a reference page and the data page. Values of the index of refraction in the reference page which are left unchanged in the data page will automatically cancel out. This means that the photorefractive plane does not have to be completely erased between pages. Material imperfections and beam inhomogeneities constant in time will have no effects on the information readout of the memory.

This work was done by Carl M. Verber of Battelle Memorial Institute for **Marshall Space Flight Center.** *For further information, Circle 31 on the TSP Request Card.*
MFS-23419

Wind Velocity Measurement

A single laser-Doppler system measures three-component wind velocity in "clear-air" conditions.

Marshall Space Flight Center, Alabama

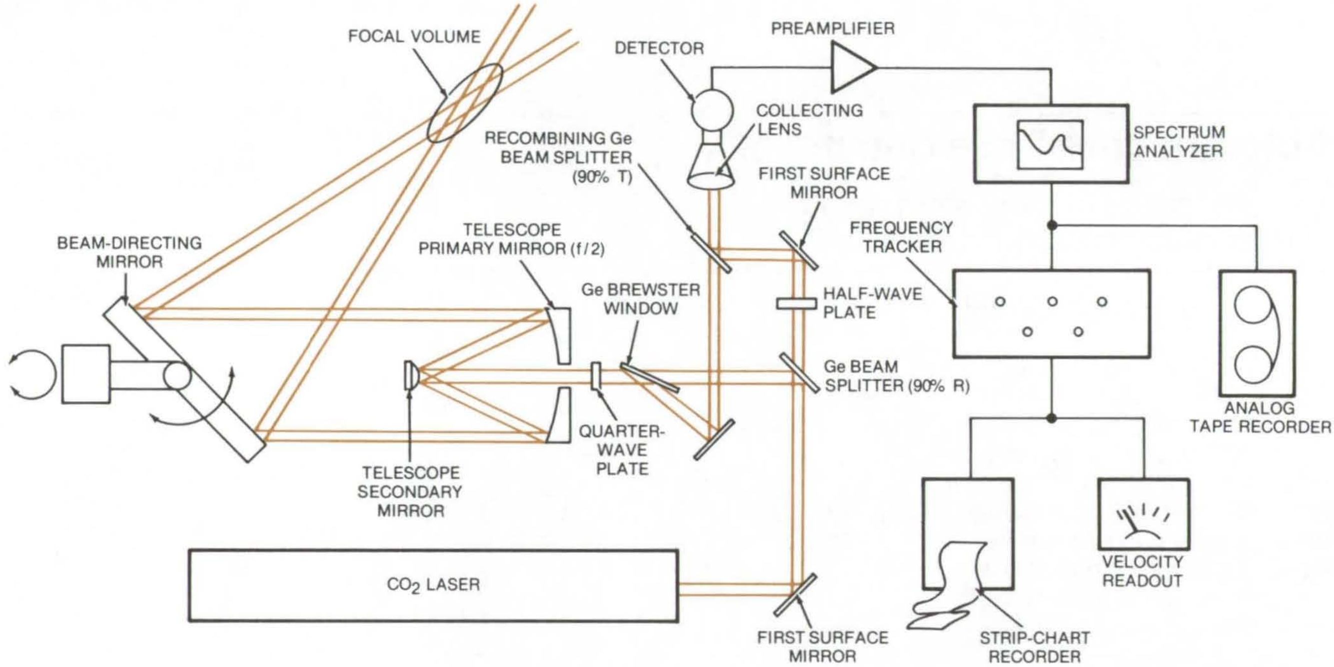

Laser-Doppler System projects laser radiation, collects backscatter, photomixes it and a portion of the transmitted beam in a photodetector, and electronically processes detector output.

Using a homodyne laser-Doppler system the wind velocity at altitudes of several kilometers can be determined in clear-air conditions. A Doppler spectrum of backscattered radiation from the ambient atmospheric aerosol gives the velocity component along the optical system line of sight. The continuous-wave laser homodyne system illuminates the scattering media, and the relative positions of two mirrors are varied to focus the beam at the desired altitude. The beam is scanned through a circular path (velocity azimuth display technique) to determine the three components of velocity. Only one system is needed to determine the three components of velocity. There is no need for seeding the airflow, the deployment of towers, radiosondes, or the like.

The laser source, a 20-watt CO_2 laser beam, horizontally polarized, is initially deflected 90° by a beam splitter (see the figure). The beam then passes through a Brewster window and a CdS quarter-wave plate that circularly polarizes it. The beam is expanded and reflected by a secondary mirror and then is focused into the atmosphere. A portion is vertically polarized by a half-wave plate after transmission through a beam splitter; it serves as the local oscillator. The backscattered radiation is collected by a primary mirror, collimated by the secondary mirror, and transmitted through the quarter-wave plate which vertically polarizes it.

About 78 percent of this backscatter is reflected off the Brewster window, transmitted through the beam splitter, and combined with the local-oscillator radiation. After the two beams are photomixed in a detector, the output is amplified with a 5-MHz bandwidth, 20-dB gain, low-noise preamplifier and is fed into a spectrum analyzer. The spectrum analyzer displays Doppler frequency (abscissa) against returned-signal strength (ordinate), and an analog signal tracker converts the output into a direct velocity readout. Data are presented on a strip-chart recorder and an FM tape recorder.

The scanning method is a velocity azimuth display technique. The telescope is focused at the desired altitude with the beam directed at zenith angle β. Scanning in azimuth traces out a circle. The instantaneous mean radial velocity, V_r, is given by

$$V_r = V_h \cos \Theta \cos (\beta - \beta_0) + \omega \sin \Theta$$

V_h and β_o, respectively, being the speed and the direction of horizontal wind motion, and ω the vertical motion at the height being sampled. Since the azimuthal dependence of V_r is sinusoidal, its amplitude, phase, and dc component are sufficient to yield horizontal speed and direction and vertical velocity, respectively.

This work was done by William C. Cliff, Robert M. Huffaker, and Werner K. Dahm of **Marshall Space Flight Center;** *T. R. Lawrence and M. C. Krause of Lockheed Missiles & Space Co., Inc.; and J. S. L. Thomson of Physical Dynamics Corp. For further information, Circle 32 on the TSP Request Card.*

This invention is owned by NASA and a patent application has been filed. Inquiries concerning nonexclusive or exclusive license for its commercial development should be addressed to the Patent Counsel, Marshall Space Flight Center [see page A8]. Refer to MFS-23362.

Combined GaAs Laser Outputs

The power of the combined output of diode lasers is increased using the free running mode.

Marshall Space Flight Center, Alabama

A new technique combines the output of a monolithic array of GaAs (junction diode) lasers to form a spatially coherent beam. A previous method of combining such laser outputs was to phase-coherently couple the lasers. In that method, however, not all of the energy was concentrated in the zero-order lobe, since several higher order lobes were caused by beam interference unless the spacing between lasers was very small. By using a free-running mode the spacing between lasers is less critical, and the optical power can be raised from less than 2 watts to 5 watts.

In the free-running mode the GaAs laser has an external-cavity anode of spherical lenses and plane mirrors. The laser array and plane mirrors are at the focal planes of the internal lenses of the optical cavity. A spatial filter replaces the conventional totally reflecting mirror, and a spatially coherent beam is formed based on the Fourier transform properties of the internal lenses.

The use of the spatial filter is responsible for the improvement in output power, as it selects the lowest-order transverse mode for each laser. The longitudinal modes vary randomly.

When the waves from the lasers are spatially superimposed, the random variations prevent the formation of a stationary interference pattern, and the intensities rather than the amplitudes of the waves are added. Thus, the field distribution at the output mirror has a single maximum and no additional lobes.

This work was done by Elisabeth M. Rutz of IBM Corp. for **Marshall Space Flight Center.** *For further information, Circle 33 on the TSP Request Card.*

Inquiries concerning rights for the commercial use of this invention should be addressed to the Patent Counsel, Marshall Space Flight Center [see page A8]. Refer to MFS-23397.

Airport Laser-Doppler

A laser system remotely senses aircraft-wake turbulence.

Marshall Space Flight Center, Alabama

A laser-Doppler radar, evaluated at Kennedy International Airport, New York, is capable of remotely sensing and tracking wake turbulence. The radar uses a continuous-wave 10.6-micron laser that monitors the motion of the ambient aerosol and thus the velocity, location, and flow of aircraft wake vortexes. It is the first instrument of its type available for wake turbulence evaluation and is described in a report, "Development of a Laser Doppler System for the Detection, Tracking, and Measurement of Aircraft Wake Vortices." Applications other than those of wake turbulence are suggested. These include: long-range (remote) detection of airflow, monitoring smokestack exit flow velocities, and observing winds at altitude.

This work was done by E. W. Coffey, C. E. Craven, B. B. Edwards, C. C. Huang, M. C. Krause, T. R. Lawrence, L. K. Morrison, K. R. Shrider, and D. J. Wilson of Lockheed Missiles & Space Co. for **Marshall Space Flight Center.** *For further information, Circle 34 on the TSP Request Card.*
MFS-23423

Analog Data Recording on MnBi Film

High coercive-force films have reduced sensitivity to wall-domain motion and can record at higher spatial frequencies.

Caltech/JPL, Pasadena, California

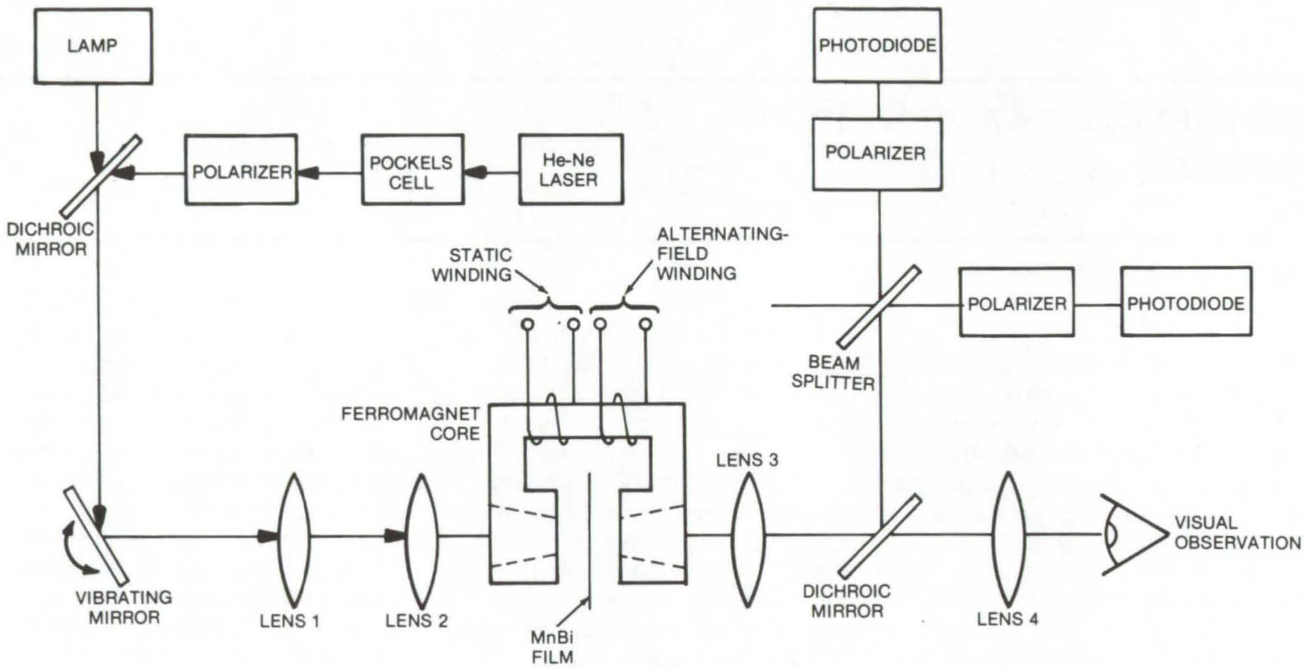

MnBi Film Recording Experiment: In a one-dimensional periodic motion, a focused 75-mW helium/neon laser was drawn across a stationary MnBi film. Tracks, typically 1 micrometer wide, were recorded at 500,000 micrometers/second.

A high-density analog recording process involves the use of a laser beam and a magnetic field to effect Curie-point switching of magnetic domains of a manganese bismuth (MnBi) film. The domain-wall motion, the range of maximum spatial frequency, and the degree of magnetization (gray scale) can all be varied for continuous analog recording. In the past, digital data have been recorded on MnBi film by switching discrete zones, or spots, from the magnetized to the unmagnetized state, or vice versa. Even greater data densities (analog data) could be achieved by Curie-point switching of successive portions of a track with no spacing between spots.

However, this technique is not without drawbacks; one is control of the degree of domain-wall motion observed in the switching of discrete spots. Another problem is the maximum spatial frequency that can be recorded. A portion of the film track, when cooled from the Curie temperature, goes through a temperature range in which its magnetization is set by the magnetic field present. When cooled to lower temperatures, the state of magnetization becomes immune to further magnetic field writing. The magnitude of these temperature ranges was initially unknown, and thus the degree of abruptness with which successive portions would become insensitive to applied magnetic fields.

MnBi films have now been prepared with a reduced sensitivity to domain-wall motion. The films range in thicknesses from 200 to 500 Å. Films are made by sequentially evaporating the compound constituents and heating the double layer into a glass substrate to allow them to react. The evaporation process is carried out in a bakable diffusion-pump vacuum system with an LN_2 trap with a titanium getter. Pressures prior to evaporations are typically between 10^{-8} to 10^{-9} torr. Bismuth and then manganese are evaporated at a rate of 10 Å/s; the pressure during evaporation is typically 3×10^{-8} torr. Protective coatings of sapphire are finally evaporated over the MnBi layer.

After treatment for a few hours at approximately 180° C, the double layers react to form a nonmagnetic film with a textured appearance. Depending on the amounts of Mn and Bi in the initial double layer, treatment at 250° to 300° C forms ferromagnetic MnBi.

Recording experiments were

carried out in an apparatus as shown in the figure. The laser beam was shuttered by a Pockels cell/polarizer combination and was focused on the MnBi film by a series of mirrors and lenses. A collimated beam from a mercury-arc lamp illuminated the film for visual observation. As the vibrating mirror rotated the laser beam at different angles off its optical axis, the beam was swept back and forth along the film track. The tracks were inspected visually and read out electro-optically.

The recording experiments consisted of switching tracks in various static and alternating magnetic fields surrounding the ferromagnet. When switched in a static field, the film showed two characteristics which depended mainly on its coercivity. Low coercive-force film, typically hundreds of amperes/meter, varied track width with the field applied during switching. Tracks became narrower in negative fields and broader in positive ones. Tracks switched in films with high coercive forces (typically 1,000 A/m) had track widths independent of the applied magnetic field. Also, the upper spatial frequency limit recorded by Curie-point switching in an alternating field was greater with high coercive-force film.

This work was done by John E. Guisinger and George W. Lewicki of **Caltech/JPL.** *For further information, Circle 35 on the TSP Request Card.*
NPO-13302

Low-Threshold Light-Emitting-Diode Laser

A light-emitting diode with reduced bandgap change reduces strain in the active region of the laser.

Langley Research Center, Hampton, Virginia

A new technique has been developed to produce low-threshold laser diodes which are made from (AlGa)As and emit in the visible spectrum. The technique consists of reducing the bandgap change at the heterojunction to 0.1 eV and avoiding deep-level impurities such as Si and Ge.

The lowest-energy bandgap for the alloy used for the diodes ($Al_xGa_{1-x}As$) is about 1.92 eV at room temperature and 2.0 eV at 77 K for x equal to 0.34. Thus red-emitting laser diodes can be made to operate at 77 K. However, in order to obtain the high efficiency and low threshold required for continuous-wave (CW) operation, the dopant and the alloy composition in the active region of the device must be controlled closely.

CW laser diodes ($\lambda \approx 6{,}500$ to 6,600 Å) with threshold current densities as low as 400 A/cm² can be made with an improved version of the multiple-layer epitaxial techniques previously used for GaAs-(AlGa)As infrared-emitting heterojunction diodes. Diodes that emit visible laser light have been made with two basic structures: (1) the simple double heterojunction and (2) the large-optical-cavity configuration where a p-n junction is introduced between the heterojunctions.

A key feature in the fabrication is the exclusive use of Zn as the acceptor. Normally Si and Ge have been used as acceptors to produce the best infrared heterojunction diodes, but both of these introduce impurities that impair efficiency. The other important consideration in fabrication of the visible diode is maintenance of a very small (about 0.1 eV) bandgap discontinuity at the heterojunction. This reduces the strain in the active region of the laser.

This work was done by Frank Z. Hawrylo and H. Kressel of RCA Corp. for **Langley Research Center.** *For further information, Circle 36 on the TSP Request Card.*

Title to this invention has been waived under the provisions of the National Aeronautics and Space Act [42 U.S.C. 2457(f)] to the RCA Corp., Princeton, N. J. 08540.
LAR-11477

Beam Splitter/Combiner

Secondary reflection is almost eliminated, using a wedge-shaped laser beam splitter.

Goddard Space Flight Center, Greenbelt, Maryland

An optical beam splitter uses total internal reflection in a wedge configuration to avoid interference caused by unwanted, stray reflected beams. It is particularly suitable for laser heterodyne systems used in communications, radar, radiometry, and spectroscopy. The beam splitter produces only two predictable beams which can be recombined in the same manner as they were split. The beam splitter is not wavelength dependent, and the angle of incidence is not dependent on the intensity of the split (or combined) beams. The splitter uses total internal reflection of the incoming light beam to remove the unwanted beams. The reflective properties are the result of three factors: (1) the shape (angle of sides) of the wedge, (2) the wedge index of refraction, and (3) the angle of incidence formed by the light beam at the surface of the wedge.

The splitter is installed at a transmitter and/or receiver, depending upon its application. The wedge surfaces are coated with an antireflective substance to help minimize the effects of secondary light beams formed with the desired twin beams.

Figure 1 illustrates the beam-splitter principle. Incident beam i enters the splitter at point A on surface a. This surface may have a partially reflective (50 percent) coating. Beam i is split into reflected beam r and beam $\bar{t}$ inside the splitter element. At point B most of $\bar{t}$ leaves the element to form transmitted beam t.

Surface b is coated with the antireflective substance. Only a small fraction of $\bar{t}$ (typically 0.5 percent or less) is reflected to form beam m. The angle of incidence δ_i, the wedge angle ε, and the index of refraction n are chosen so that the angle of incidence ω for beam m at point C exceeds the minimum angle necessary for total internal reflection. Beam m therefore is totally reflected at points C, D, E, etc. Beam m leaves the element only when reaching the ground rim c where it is diffusely scattered.

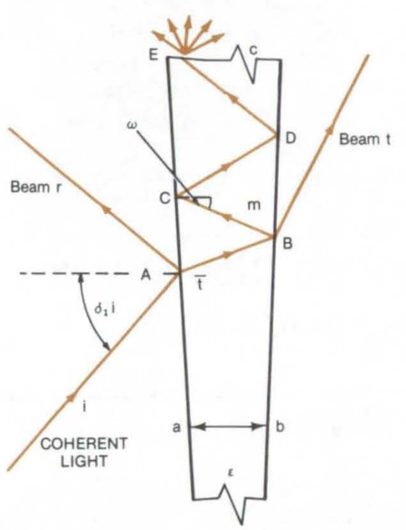

Figure 1. **Coherent-Light Beam Splitter:** Coherent light energy entering the splitter at point A is separated into lesser intensity beams, r and t. The splitter can be made insensitive to beam wavelength and temperature variation by diverging secondary beam m away from r and t.

Figure 2 shows the element configured as a beam combiner. Two beams, i_1 and i_2, are incident on surfaces a and b, respectively. Beam i_2 propagates as in the splitter. A small part of i_2 is reflected at R even though an antireflective coating is applied to surface b. The reflection is shown as beam $\bar{r}_2$. Remaining beam $\bar{i}_2$ is split into $\bar{t}_2$ and r_2 at point A. Beam $\bar{t}_2$ propagates similarly as $\bar{t}$ in the beam splitter. The result is two combined and collinear beams: r_1, r_2 and t_1, t_2. The only unwanted beam is $\bar{r}_2$, but the beam amplitude is low and considerably divergent from beams t_1 and t_2. Beam $\bar{r}_2$ can be eliminated by using an absorbing stop.

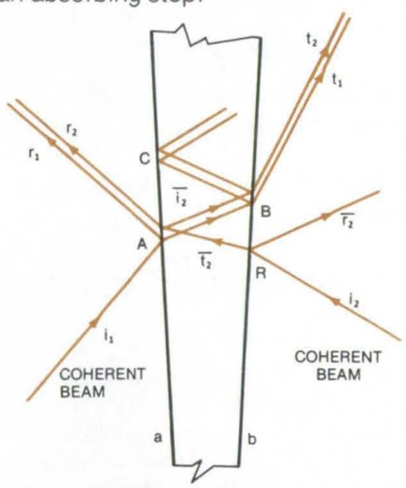

Figure 2. **Coherent-Light Beam Combiner:** Two coherent beams, i_1 and i_2, combine at point A to form two pairs of lesser intensity beams, r_1, r_2 and t_1, t_2. Secondary beam $\bar{r}_2$ does not adversely affect either primary beam pair. Secondary interference problems are thus eliminated.

This work was done by Walter Leeb of the National Research Council for **Goddard Space Flight Center.** *For further information, which consists of additional data describing the beam splitter, Circle 37 on the TSP Request Card.*

This invention is owned by NASA and a patent application has been filed. Inquiries concerning nonexclusive or exclusive license for its commercial development should be addressed to the Patent Counsel, Goddard Space Flight Center [see [see page A8]. Refer to GSC-12083.

Optical Alinement System

A rapid alinement technique can be used in daylight.

Ames Research Center, Moffett Field, California

Using a new technique, the geometric center of a light source, such as the Sun, a laser, or a solar simulator, can be alined with a mirror quickly and in daylight. The source is alined by precisely superimposing the colored images of the source, as viewed along two different paths.

Light originating from a source initially off axis is divided by a beam splitter (see figure). After passing through a spectral filter F_2, the transmitted beam is reflected by a mirror back to the beam splitter and thence to the image plane of the theodolite. Light reflected from the beam splitter is returned by a trihedral prism after passing through spectral filter F_3, and it passes through the beam splitter to the image plane of the theodolite. Filters F_2 and F_3 spectrally complement one another, except for a small overlap in the yellow region. For example, if F_2 is red and F_3 is green, and if they overlap in the yellow region, the source images at the theodolite will appear red or green except where they overlap.

The colored images can be differentiated easily, and their region of overlap is distinct. It is possible to aline the images to within 5 arc seconds with high-quality theodolites. An adjustable iris, S, is used to balance the relative intensity of the red and green images, and the source intensity is further attenuated as required by neutral density filter F_1.

Because the prism retroreflects the incident light for large angles of incidence, the resulting angular displacement between the two optical images is independent of small angular misalinements of the prism with respect to the source or the observing telescope. In addition, the angular displacement of the two images is independent of small relative misalinements of the various components that make up the assembly. It depends only upon twice the angle between the normal to the mirror and the axis defined by the mirror and the source.

To aline a telescope to a light source, it is merely necessary to install a properly illuminated reticle or slit in an image plane that is centered on the optical axis of the telescope. The degree of alinement is indicated by superposing the image of the slit or reticle upon the image of the source. Two mirrors facing each other or two light sources can also be alined in this way.

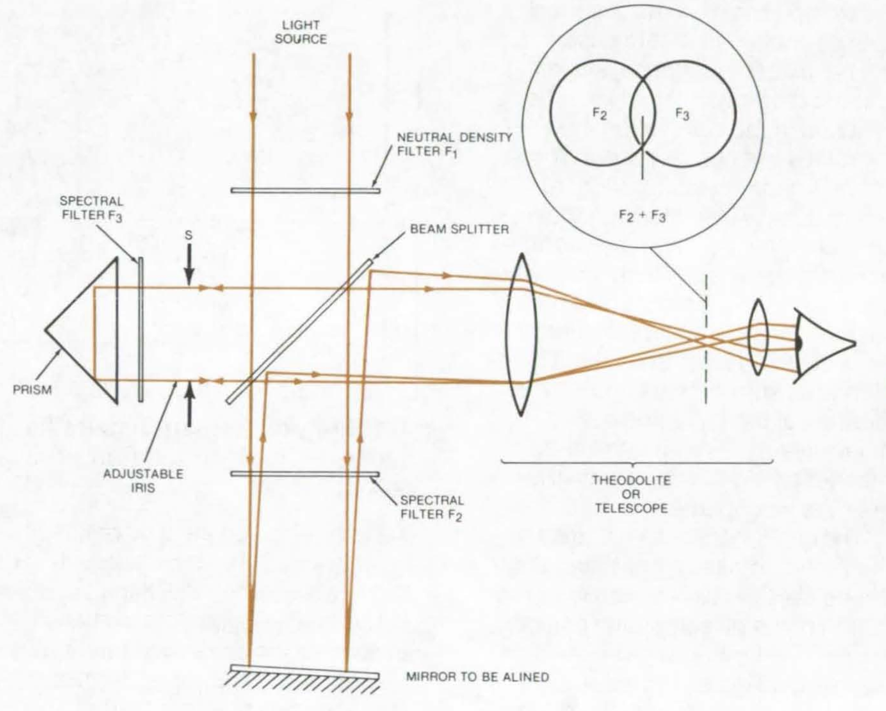

The **Optical Alinement System** is used to adjust the plane of a mirror to make it perpendicular to the axis of light from a source. As shown above, the mirror is out of alinement. When alined, F_2 and F_3 will overlap completely.

This work was done by Norman L. Thomas of Lockheed Missiles & Space Co., Inc., for **Ames Research Center.** *No further documentation is available.*

Inquiries concerning rights for the commercial use of this invention should be addressed to the Patent Counsel, Ames Research Center *[see page A8]*. *Refer to ARC-10932.*

Field Distribution in a Thin Lens

A quasi-optical formulation gives an optical field distribution by computing only two terms.

Langley Research Center, Hampton, Virginia

Very often in optical engineering, ray tracing based on geometrical optics is not sufficient to describe the behavior of an optical system, and the diffraction effect must be included in the calculation. Typical examples are optical pattern recognition, image reconstruction, and holography. When studying these optical systems, a complex combination of many optical elements may be reduced to a simple equivalent system consisting of a thin lens of a finite size and input and output planes as shown in the figure. The location of the input and output planes is arbitrary, and the electromagnetic field distribution is given over the input plane.

The quasi-optical formulation of the system makes it possible to calculate the field distribution over the output plane by computing only two terms. The first term represents the geometrical optics effect, and the second term represents the diffraction effect. Thus, the mathematical expression is greatly simplified; and considerable computer time is saved.

The optical system shown in the figure consists of an input plane, a thin lens, and a detector plane (or output plane). An arbitrary distribution of the optical field is specified over the input plane (x_1,y_1), and the field distribution over the output plane (x,y) is sought. The radius of the thin lens is b, its focal length is f, and it is located in the plane (x_2,y_2).

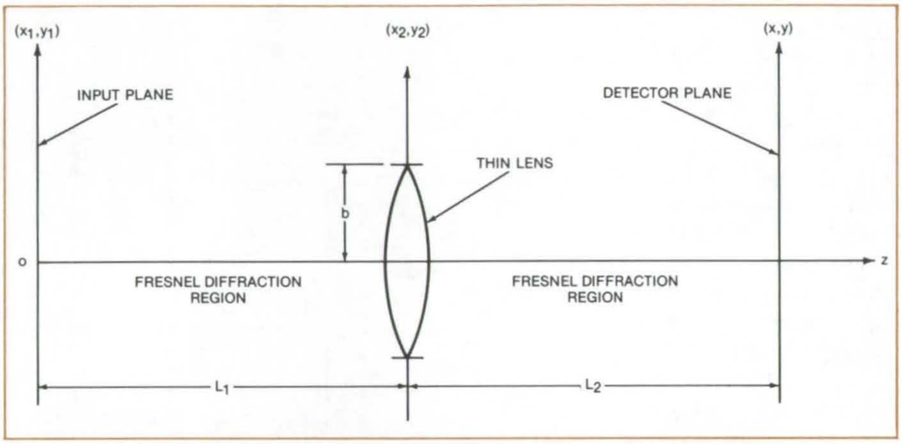

A **Thin-Lens System** has its field distribution represented by a mathematical formulation valid over the entire region of input and output planes.

The quasi-optical formulation is an asymptotic expansion (stationary phase) for a small wavelength in which the two dominant terms are retained. It includes the geometric ray tracing, the diffraction effect of the spatial filter due to the finite size of the lens, and the diffraction effect in the shadow region. The calculation begins with a sequence of three checks to determine whether: (1) a stationary point exists, (2) the regions of interest satisfy the Lagrangean condition, and (3) the shadow region is in the region

$$p \leqslant \frac{3\lambda}{4\pi b} \quad \text{or} \quad p > \frac{3\lambda}{4\pi b}$$

where:

λ = wavelength,
b = radius of the lens, and

$$p = \sqrt{\left(\frac{x_1}{L_1}+\frac{x}{L_2}\right)^2 + \left(\frac{y_1}{L_1}+\frac{y}{L_2}\right)^2}$$

The formulation is then valid for the entire region of the input and output planes.

This work was done by Chang H. Chi of Perkin-Elmer Corp. for **Langley Research Center.** *For further information, Circle 38 on the TSP Request Card.*
LAR-11392

Simplified Deflection-Coil Linearity Testing

Ordinary white light striking a tube-mounted precision pinhole mask provides a convenient reference video signal when adjusting coil linearity.

Marshall Space Flight Center, Alabama

A mask placed over the face of an image-dissecting photomultiplier tube can be used to simplify linearity testing of the tube and its associated focus/deflection coil. The mask has a precision array of pinholes that permit light to impinge on the tube at known points. The deflection signals fed to the coil which locks onto each point are recorded, permitting the linearity of the tube and coil assembly to be determined. The test method eliminates the need for the precision test configuration and the complex operator procedure previously used.

The key to task simplification is the precision pinhole mask. An array of 25-micron-square apertures is symmetrically spaced on 0.050-in. (0.127-cm) centers. The mask fabrication technique is the same as that developed for microelectronic circuits. Pinhole spacing provides 80 to 100 points (depending on the tube area covered) while holding test time for a complete linearity run to less than 45 minutes.

A readily-available white-light source was used to determine that a 25-micron-square pinhole aperture would provide 3.1×10^{-10} watts over the pinhole area, or roughly 50 times the energy that would be focused on the tube cathode by a 50-mm lens in a zero magnitude star flux. The 25-micron dimension is chosen to be from 30 to 60 times the wavelength of concern over the tube photocathode spectral response. Diffraction problems in tube setup are thus minimized.

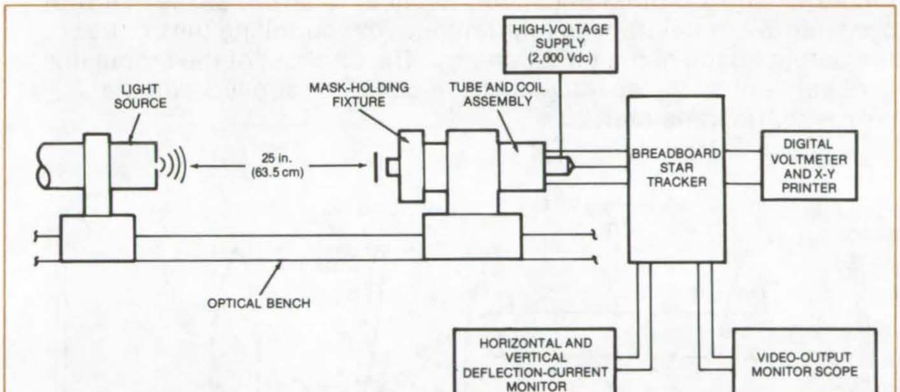

In the **Deflection-Coil Linearity Tester,** light strikes the pinhole mask and impinges on the face of the pickup tube as a precise pattern of dots. The resultant video signal is used as a reference to set x-axis and y-axis deflection-coil potentiometers. As scanning voltages are fed to the deflection coil, the X-Y plotter prints the dot pattern, thus indicating coil linearity. Further data processing yields deflection gradients, axis skew, and linearity function.

The tube/coil test fixture is set up as shown. Two preliminary adjustments are required prior to starting the data run. The centermost horizontal row of pinholes is alined to the horizontal coil axis. The oscilloscope used to monitor horizontal and vertical currents is adjusted so that the scope graticule provides a convenient reference for each of the pinholes. A simple tool holds the pincushion mask against the tube face, yet it enables the mask and the tube to be rotated as an assembly. This enables alinement of the mask axes with the deflection-coil axes.

The test procedure consists of varying the deflection-coil current so that the tube outputs at each of the pinholes is read in a predetermined sequence. A square matrix of (x,y) coordinates is obtained. An automatic X-Y plotter system is triggered, and following a 10-second integration period for both values of x-axis and y-axis deflection currents, the coordinates are printed out. The data points are computer processed later to acquire deflection gradients, axis skew, and linearity-error function data.

This work was done by George P. Kramer of Sperry Rand Corp. for **Marshall Space Flight Center.** *For further information, including pinhole dimensional data and a sample computer readout of plotter data, Circle 39 on the TSP Request Card.*
MFS-23400

Contrast Enhancement of Transparencies

The contrast of a photographic transparency is enhanced or reduced for printing or projection by using constructive and destructive interference of a collimated laser beam.

Goddard Space Flight Center, Greenbelt, Maryland

Several methods presently exist to change the contrast of a poorly-exposed (or developed) photographic transparency. These methods range from simple trial-and-error hand dodging to a correction process which is based on costly CRT printing with electronic feedback and control of image contrast. In all of these systems, real-time evaluation of the corrected image contrast is not possible, or empirical analysis of the transparency is required before contrast enhancement or reduction can begin.

A new relatively-inexpensive optical apparatus enhances or reduces contrast of photographic transparencies (positive or negative) in real time. The device, shown in Figure 1, consists mainly of two parallel, closely spaced, and partially reflecting mirrors. The volume

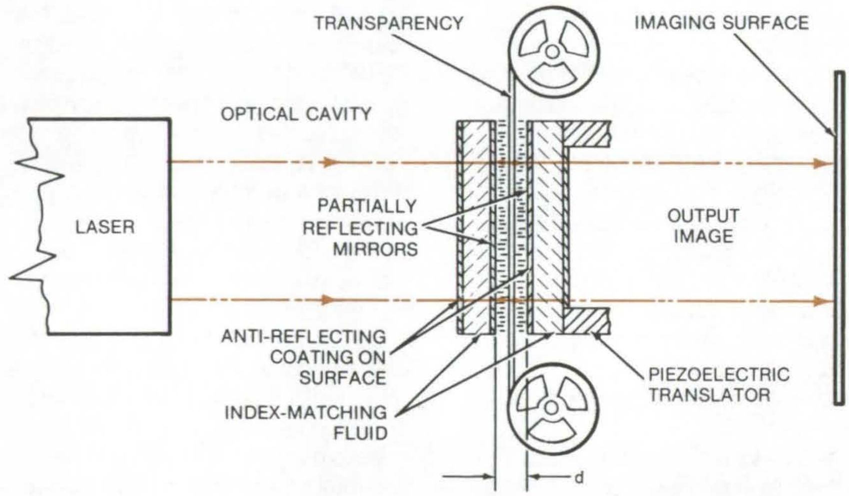

Figure 1. The **Contrast Enhancer/Reducer** is an optical device with constructive or destructive interference for controlling the contrast of the output image of the transparency: The contrast of the output image is dependent on the spacing d, which can be controlled with the piezoelectric translator.

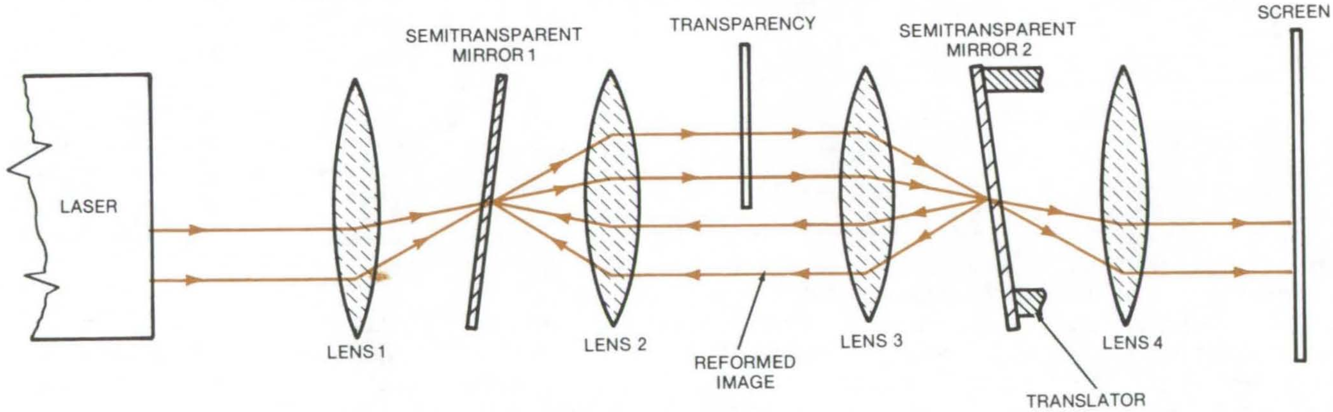

Figure 2. For **Spatial Filtering,** two double convex lenses, 1 and 4 are positioned outside the optical cavity. As explained in the text, collimated light passing through the transparency is reformed as a spectrum on mirror 2. This light passes back through the optics, bypassing the transparency, to form another image spectrum on mirror 1. This spectrum is reformed as an image coincident with the original transparency image. Distance between the mirrors can be varied to cause destructive or constructive interference that changes the contrast of the image formed on the screen.

between mirrors is filled with a fluid matching the index of refraction of the transparency to avoid phase changes in the light as it passes through the transparency.

A collimated laser beam is reflected back and forth in the optical cavity by the partially reflecting mirrors. If the distance between the mirrors (d) is an integer (η) multiple of one-half the wavelength (λ) of the coherent laser light (e.g., $d = n\lambda/2$), constructive interference occurs, and the contrast is increased. If the distance between the mirrors is an odd-integer $(2n + 1)$ multiple of one-quarter the wavelength [e.g., $d = (2n + 1)\,\lambda/4$], destructive interference occurs, and the contrast is reduced. Light from the cavity is projected onto a screen (for viewing or printing).

In addition to contrast processing, an alternate version of the apparatus permits spatial filtering (see Figure 2). The laser beam is focused via lens 1 to a point on a semitransparent mirror. The light then passes through the semitransparent mirror and is collimated by lens 2, on the transparency. A third lens reforms the light from the transparency to a spectrum on a second semitransparent mirror. The light from the second semitransparent mirror is partially reflected back through lenses 3 and 2, bypassing the transparency and forming another image spectrum on the initial mirror. Reflected light from this spectrum at the first mirror is reimaged by lens 2 on the transparency.

Spacing between the mirrors is adjusted by a pair of translators which can vary the interference pattern on the transparency, formed by light transmitted directly through the first mirror and light reflected from the first mirror. The fourth lens takes the spectrum formed on the translated mirror to form the processed image on a screen. Spatial filtering is performed either on the first or second mirror, and path length can be varied to control the location of the spatial filtering. Filtering can not only change the output image from a low to a high contrast (or vice versa) but can also change it from a positive to a negative, or vice versa. Projected images may also be processed with this device by replacing the input transparency with a photochromic material.

This work was done by Arnold R. Shulman of **Goddard Space Flight Center** *and Sing H. Lee of the University of California. For further information, Circle 40 on the TSP Request Card.*

This invention is owned by NASA, and a patent application has been filed. Inquiries concerning nonexclusive or exclusive license for its commercial development should be addressed to the Patent Counsel, Goddard Space Flight Center [see page A8]. Refer to GSC-11989.

Faceted Solar Energy Collectors

Faceted collector surfaces and a dyed working fluid improve the performance of thermal radiation collectors.

Lyndon B. Johnson Space Center, Houston, Texas

Two new concepts can be used to enhance the efficiency and flexibility of solar energy collectors: faceting the collector surface and adding a coloring agent to the working fluid. Solar energy collectors concentrate heat from the Sun and transfer it to a heat exchanger using a working fluid such as water. From the heat exchanger, the energy is stored or converted to a useful form.

Normally the collector is placed on a structure built especially to give the collector maximum exposure to the Sun or on a structure that can be continuously oriented. If the collector is placed on an existing structure not designed for solar energy collectors (e.g., the roof of a house), the efficiency is far from optimum. This problem can be overcome to a significant extent by faceting the collector.

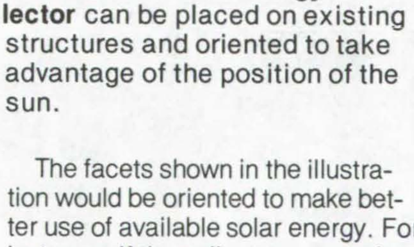

The **Faceted Solar Energy Collector** can be placed on existing structures and oriented to take advantage of the position of the sun.

The facets shown in the illustration would be oriented to make better use of available solar energy. For instance, if the collector were to be installed on the roof of a house, the facets might be oriented to take advantage of the general direction of the Sun during the coldest months. The efficiency of the collector could be further enhanced by placing a magnifying surface over the facets.

In most conventional solar collectors water is used as the working fluid. The water runs on a specially-coated (usually black) absorbent surface and picks up heat by conduction. The only way to change the absorbance of the system is to recoat or replace it. By adding a coloring agent to the working fluid, the total absorbance can be increased, and the absorbance can be altered if required.

This work was done by Donald R. Segna of **Johnson Space Center.**

No further documentation is available.
MSC-12687

Double-Focusing Mass Spectrometer

A simplified magnet assembly is lighter, more compact, and easier to aline.

Caltech/JPL, Pasadena, California

A typical miniature double-focusing magnetic-sector mass spectrometer operates with two magnetic fields. One is used to turn the ion beam, and the other is used to operate the ion pump (see Figure 1). The elements required to generate these fields represent the major portion of the assembly. The bulk of the system is further increased because of a nonmagnetic steel duct used in guiding the ion beam. A large heavy magnet is used to accommodate the duct. Because of its mass the magnet is difficult to aline in relation to the duct. Shock and vibration easily misaline the magnet.

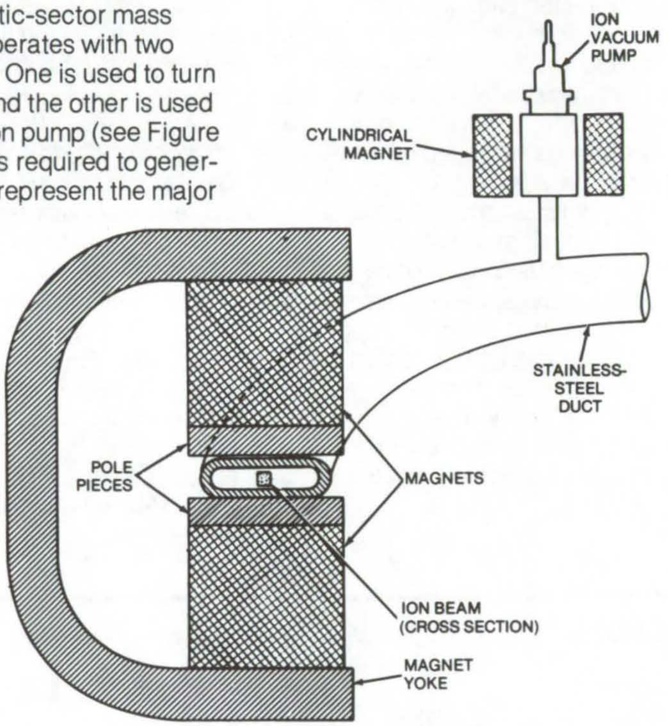

Figure 1. A **Conventional Magnet Assembly** used for a double-focusing mass spectrometer includes a duct to the vacuum pump.

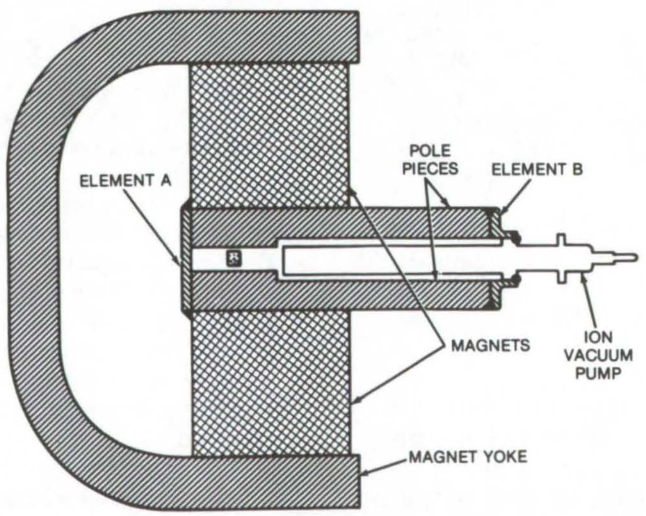

Figure 2. The **Compact Magnet Assembly** for a double-focusing mass spectrometer uses the pole pieces (elements A and B above) as a duct.

The simpler magnet assembly shown in Figure 2 is lighter and easier to aline. It provides the conventional magnetic field required to interact with the ion beam, as well as the different-strength magnetic field required by the ion vacuum pump.

The new assembly has no duct. A new evacuated duct is formed by the pole pieces, elements A and B, that support the vacuum pump. In this configuration the magnetic gap for the ion beam is reduced from 0.183 in. (4.64 mm), as required in Figure 1, to 0.100 in. (2.54 mm), and the weight of the magnet assembly is reduced 36 percent, from 5.2 to 3.2 lb, (2.4 to 1.5 kg).

Key features of the new assembly pole pieces include:

- A conventional homogeneous magnetic field as required by the magnetic analyzer,
- A second homogeneous magnetic field for the ion vacuum pump, and
- Walls for the new duct through which the ion beam travels.

This work was done by Charles E. Giffin, Alfred O. Nier, and Leonard M. Sieradski of **Caltech/JPL.** *For further information, Circle 42 on the TSP Request Card.*

This invention is owned by NASA, and a patent application has been filed. Inquiries concerning nonexclusive or exclusive license for its commercial development should be addressed to the Patent Counsel, NASA Resident Legal Office-JPL [see page A8]. Refer to NPO-13663.

Low-Reflectivity Spectrally Selective Coating

A new coating is used as a neutral-density reflection filter for an optical tracking system.

Goddard Space Flight Center, Greenbelt, Maryland

A mirror, with an area of low reflectivity, has replaced the neutral-density transmission filter in a star-tracking system, and it may have applications in other optical systems. Reliability is increased because the mechanism needed to insert and remove the transmission filter is no longer needed. In the star tracker, a fine-error sensor to track brighter stars is achieved by reducing the energy transmitted to the sensor to as little as 1 percent of the amount entering the sensor system over the wavelength range of 400 to 700 nm. A small area of low reflectivity on a normally highly reflective mirror permits both bright and dim objects to be processed within the operating region of the optical detector by simply moving the mirror slightly.

The low-reflectivity area is a multilayered coating having low reflectivity in the spectral region of interest. It comprises a vacuum-deposited film sequence of aluminum, dielectric spacer, semitransparent metal, and dielectric spacer. Numerous combinations of materials and thicknesses for the dielectric and metal films were tried. Data for the best combination are shown on the graph.

The proper thicknesses of the various layers are achieved by optically monitoring the reflectivity of the substrate. The first three layers are monitored at a wavelength of 433 nm, and the aluminum is deposited until reflectivity reaches a maximum. The first dielectric layer (magnesium fluoride) is then deposited until a minimum is reached. As the semi-transparent metal film (inconel) begins to form, the reflectivity continues to drop until another minimum is reached, and this deposition is allowed to continue until reflectivity increases to about 20 percent of what it was when the inconel epavoration started. The fourth and final layer, magnesium fluoride, is deposited until the reflectivity at a wavelength of 546 nm reaches another minimum.

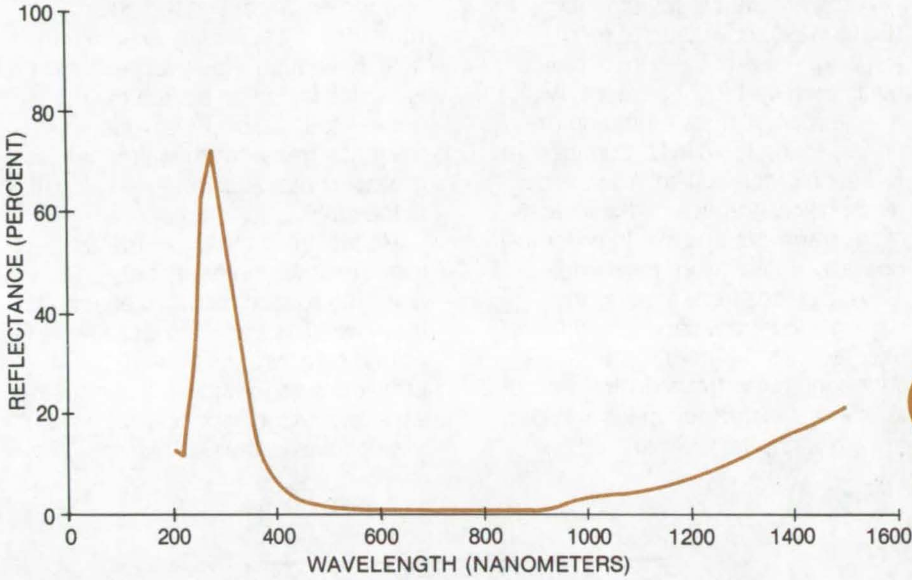

Reflectance Data for the Best Coating System: The average reflectance of the coated mirror is 1.4 percent in the 400-nm to 700-nm spectral range, which is lower than had previously been attainable.

A technique has also been developed to use the low-reflectivity coating only on a small area, such as a square 0.5 to 1 mm per side, of the acquisition mirror, which has a high-reflectivity coating on the balance of its surface. The process used to achieve this is as follows:

a. The entire surface of the acquisition mirror is coated with a high-reflectivity material.
b. The coated surface is then overcoated with photoresist, and the area to have low reflectivity is exposed to a light source through a mask having an appropriately sized aperture.
c. The exposed photoresist is removed via the usual developing process, leaving a layer of resist only in the unexposed area.
d. The low-reflectivity coating previously described is deposited over the entire mirror surface.
e. The resist and the coating directly over it are removed by immersion in a solvent, leaving the low-reflectivity coating in the area from which the resist has previously been removed.

This work was done by John J. Zaniewski and Howard Herzig of **Goddard Space Flight Center.** *No further documentation is available.*
GSC-12114

Pulse Transformer for GaAs Laser

Transformer and laser are separated, but impedances remain matched.

Marshall Space Flight Center, Alabama

A high-radiance gallium arsenide (GaAs) laser operating at room temperature is utilized in an optical navigation system. The laser, with an injection-current repetition frequency of up to 10 kHz, confines the radiation of the 300-microns-wide diode homostructure to the lowest-order transverse mode. In order to operate efficiently in this mode, 10-kHz pulses from a generator having a low-impedance output are injected into the laser via a wideband pulse transformer. For an efficient transformer-to-laser impedance match, the laser should be connected directly to the pulse transformer secondary winding. In this application, however, the laser is placed inside an optical cavity, necessitating a physical redesign of the pulse transformer which has too great an outside diameter to also fit in the cavity.

Redesigning the pulse transformer allows the necessary physical separation between it and the laser. The transformer primary is wound on a toroidal core. The one-turn secondary winding is connected via a low-impedance coaxial transmission line to the GaAs diode. The secondary-winding impedance (approximately 0.5 ohm) matches the impedance of the forward-biased diode (about 20×10^{-3} ohm) and is capable of passing the injection current (150 A peak at 50 ns maximum duration).

The conduction current induced by the magnetic field in the toroid is radial in the upper and lower part of the secondary winding. The secondary winding is coupled to the transmission line by the continuity of the radial conduction current in the upper part of the secondary winding and the radial displacement current in the coaxial transmission line.

The low-impedance coaxial transmission line is dielectrically loaded. The characteristic impedance of the cable is 0.28 ohm, and the line extends into the optical cavity 0.48 inch (1.21 cm). The low characteristic impedance of the transmission line and its short length contribute to a primarily resistive impedance of $20 \times 10^{-3} + j2.8 \times 10^{-3}$ ohm at 25 MHz, the upper frequency limit of the pulse transformer.

This work was done by Elisabeth M. Rutz of IBM Corp. for **Marshall Space Flight Center.** *For further information, Circle 43 on the TSP Request Card.*

Inquiries concerning rights for the commercial use of this invention should be addressed to the Patent Counsel, Marshall Space Flight Center [see page A8]. Refer to MFS-23399.

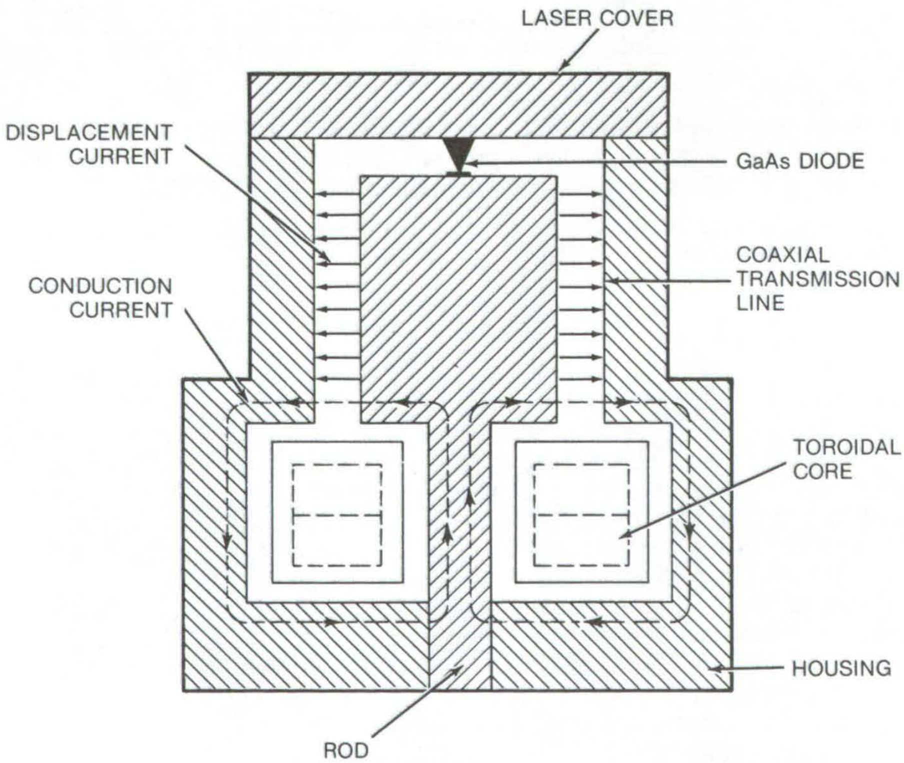

The **Pulse Transformer** has a primary winding, (not shown) of four turns. It is made of an isolated 4-mm copper strip wound tightly on the toroidal core, covering most of the core material. The secondary winding of one turn has circular symmetry about the core center and is formed by the housing, the rod, and the laser cover. The secondary winding tightly encloses the primary winding, thus minimizing the leakage induction of the transformer.

Books and Reports

These reports, studies, and handbooks are available from NASA as Technical Support Packages (TSP's) when a Request Card number is cited; otherwise they are available from one of NASA's Industrial Application Centers or the National Technical Information Service.

Solar Thermal Energy Utilization

A bibliography with abstracts

In the support of the national effort to develop alternate sources of energy, an ongoing bibliography of reports and papers related to the practical thermal utilization of solar energy entitled "Solar Thermal Energy Utilization: A Bibliography with Abstracts" is being compiled and published by the NASA-sponsored Technology Application Center at the University of New Mexico. The bibliographic series, which is periodically updated, cites documents published since 1957 and is indexed by author, corporate source, title, and keywords. Topics include: "Overview Documents," "Insulation Data," "Radiative Properties," "Components" (e.g., flat-plate collectors, concentrating collectors, and thermal storage units), "Thermal Characteristics of Buildings," "Process Heat Applications," and "Solar Thermal Power Generation." The bibliography organizes much of the significant worldwide literature devoted to solar energy.

Thermal use of solar energy takes such diverse forms as building heating and/or cooling, water desalinization, crop processing, metallurgical research, and power generation. All solar thermal systems are similar in that they use a collection device to transform the solar electromagnetic radiation into thermal energy. Collectors either gather solar energy in its dilute Earth surface form or concentrate it with an optical system to achieve high temperatures. This thermal energy is then used to produce the desired output immediately or is stored to satisfy a future demand. Either input heat or output product can be stored to overcome the intermittent nature of solar energy at the Earth's surface. A backup system using some other energy source is frequently used to insure reliability and economy.

The utilization of solar energy for the heating and/or cooling of buildings and the production of potable water supplies is presently most economic and feasible. In many areas of the United States, solar heat is economically competitive with electric resistance heating. While the economics of solar heating/cooling are considered to be better for larger structures, such as public buildings, schools, office buildings, and apartment complexes, the most numerous applications have been in single-family residences and small laboratories. So-called "active" solar space conditioning uses collector and storage devices that are added to a building and uses fans or pumps to collect and distribute the heat. So-called "passive" techniques use building orientation, the structure as collector and storage, and construction details such as roof overhangs and movable insulation to collect and distribute the heat. Both approaches have their respective strengths, weaknesses, and places in solar space conditioning.

This work was done by the Technology Application Center at the University of New Mexico for **NASA Headquarters.** *Copies of "Solar Thermal Energy Utilization: A Bibliography with Abstracts" and subscriptions to the update service [TAC ST 74-600] ,ay be obtained at cost from the Technology Application Center, University of New Mexico [see page A7].*
HQN-10900

Optics and Lasers

Selected development in lasers, spectroscopy, and photography

A recent NASA Compilation, SP-5973(03), entitled "Optics and Lasers," describes 27 optical concepts developed for holographic viewing, spectral transmission, and film camera technology. This Compilation is one of a series of NASA Technology Utilization Publications which, like NASA Tech Briefs, make available aerospace technology that may have application in commerce and industry.

"Optics and Lasers" contains articles on laser technology, including holographic interferometry laser-Doppler systems, laser beam-deflection controls, an alinement microscope for rotating laser scanner, and a coplanarity measurement tool. Articles on spectroscopy and general optics include descriptions of a solid-state TV camera, spectral matching of alkali-metal vapor lamps, X-ray photography, and a membrane light-valve computer memory. Other articles describe camera components, such as shutters, focus control, and film calibration.

This work was done for **NASA Headquarters.** *To obtain a copy of SP-5973[03], Circle 45 on the TSP Request Card.*
HQN-10893

Optical Devices

Selected developments in optical instrumentation, light generation, and lasers

A recent NASA Compilation, SP-5965(01), entitled "Optical Devices," describes 30 concepts and techniques developed for optical instrumentation and light transmission and generation. This Compilation is one of a series of NASA Technology Utilization Publications which, like NASA Tech Briefs, make available aerospace technology that may have application in commerce and industry.

"Optical Devices" contains articles on spectrometer components, such as choppers, monochromators, light sources, and beam splitters. Other articles on telescopes and microscopes include design techniques, mounts, mirror

(continued next page)

drives, and applications. Finally, a section on laser techniques describes holographic cameras and devices and several improvements in laser design.

This work was done for **NASA Headquarters.** *To obtain a copy of SP-5965[01], Circle on the TSP Request Card.*
HQN-10891

Hydrogen Energy

A bibliography with abstracts

Recognizing the need for complete and up-to-date information on the use of hydrogen as an energy carrier, the NASA-sponsored Technology Application Center (TAC) at the University of New Mexico is now publishing a bibliographic series entitled "Hydrogen Energy: A Bibliography with abstracts." Computerized literature search techniques as well as manual research methods are used in compiling each issue in the series. In addition to the cumulative volume, an annual supplement is available for 1974, and a quarterly update program serves 1975 and the current calendar year.

Hydrogen, per se, is not a primary energy source but a synthetic fuel or "energy carrier." A source of energy such as nuclear, solar, or wind energy must be utilized in order to produce hydrogen. Method commercially available today to produce hydrogen are the electrolysis of water, the gasification of fossil fuels, and the the thermochemical decomposition of water. In addition, the use of hydrogen, either in gaseous or liquid form, will necessitate the development of a large-scale transmission and distribution system. The growing literature reports a variety of opportunities for utilizing hydrogen, notably in space vehicles, aircraft, and other vehicles and in fuel cells. The residential and commercial use of hydrogen also appears both feasible and practical, especially in new buildings. Also, the use of hydrogen in electrical power generation may provide higher efficiencies than are presently possible in conventional generating plants.

Recent high interest in the area of the hydrogen economy has been shown by the increasing number of conferences, study groups, and meetings held on the topic. Among the latest and most outstanding of these were the "Cornell International Symposium and Workshop on the Hydrogen Economy," the "Working Symposium on Liquid-Hydrogen-Fueled Aircraft" held at NASA's Langley Research Center, and the NASA/ASEE 1973 Systems Design Institute held on the topic of "Hydrogen as a Future Energy Carrier" at Johnson Space Center, all held in 1973, and the Hydrogen Economy Energy Conferences held in Miami in 1974 and 1976.

Hydrogen Energy represents an attempt to list and organize the literature devoted to hydrogen as an energy carrier. Each issue in the series is divided into the following sections: "General"; "Production"; "Utilization: Transmission, Distribution, and Storage"; and "Safety." Author, corporate source, title, and keyword indexes are included.

This work was done by the Technology Application Center at the University of New Mexico for **NASA Headquarters.** *Copies of "Hydrogen Energy: A Bibliography with Abstracts," the 1974 annual, and subscriptions to the update service [TAC H-74-500] may be obtained at cost from the Technology Application Center, University of New Mexico [see page A7].*
HQN-10898

Computer Programs

These programs may be obtained at very reasonable cost from COSMIC, a facility sponsored by NASA to make new programs available to the public. For information on program price, size, and availability, circle the reference letter on the COSMIC Request Card in this issue.

SANDTRACKS

World Map and Stations Predictions Computer Programs

SANDTRACKS computes a time history of the subsatellite point and the visibility from a station to a given satellite by integrating a given epoch state.

Given a geocentric satellite epoch state, several user-defined options, starting and ending times, and station coordinates, the SANDTRACKS program generates a "world map" and/or "look angles." A "world map" is a time history of the subsatellite point (groundtrace) and the satellite height. This groundtrace is given in terms of geodetic latitude and longitude, while the satellite height is a measure of the normal between the satellite and the computational ellipsoid. "Look angles" consist of the azimuth, elevation, and range from a given station to the satellite.

The satellite ephemeris is generated by an iterative process according to the theory developed by Brouwer. The theory is not valid for orbits near the critical inclination of 63.4°, but is otherwise valid for eccentricities between 0.001 and 1 together with all inclinations. Atmospheric drag and solar radiation pressure are unmodeled. These forces are known to perturb a satellite orbit. Consequently, any comparison of results from SANDTRACKS with those from other programs must take into account the compatibility of the dynamic modeling between the two programs.

FORTRAN, Interactive Mode
IBM 360/95

This program was written by Richard J. Sandifer of **Goddard Space Flight Center.** *For further information, Circle 47 on the COSMIC Request Card.*
GSC-12099

Materials

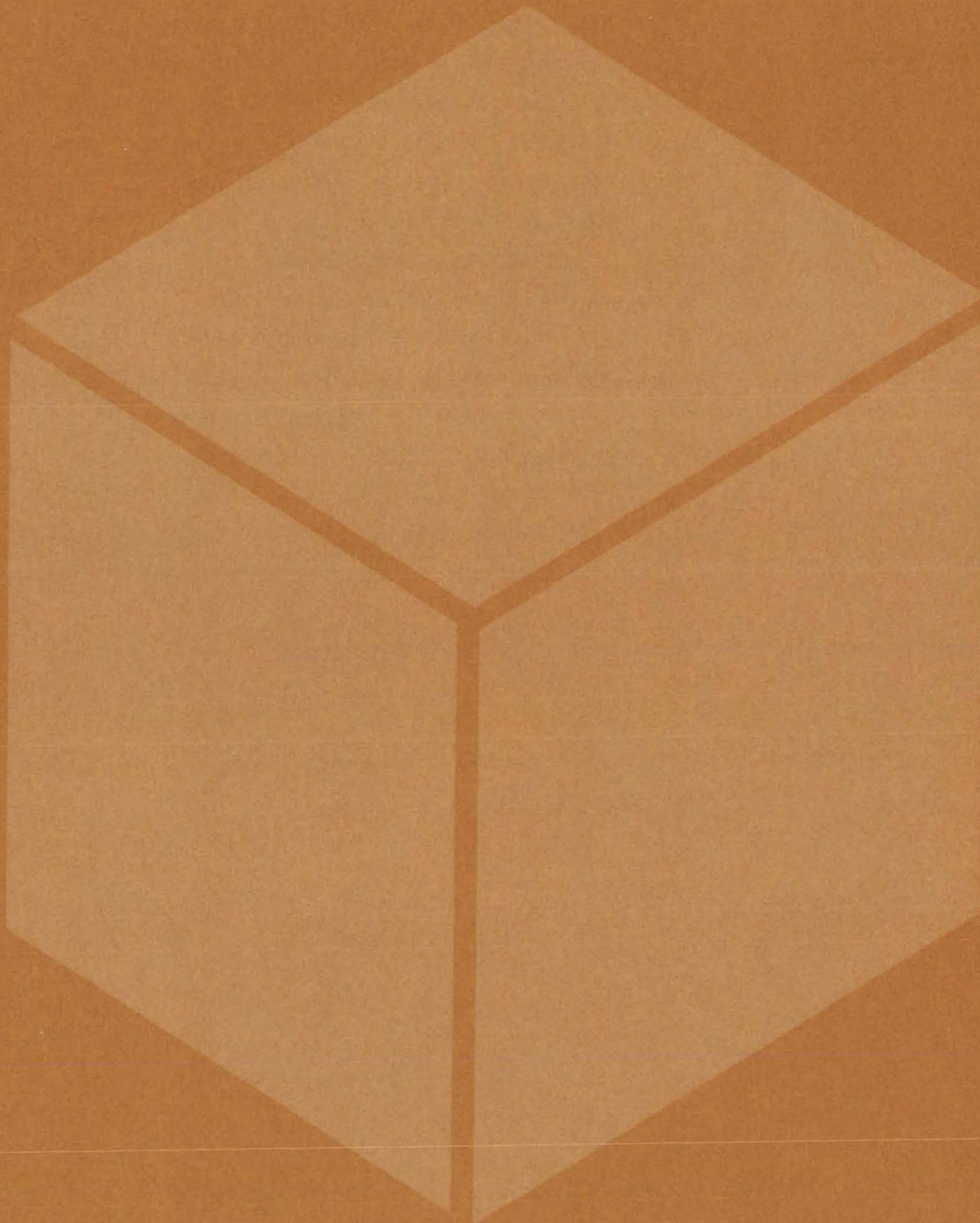

Hardware, Techniques, and Processes

Books and Reports

Chemiluminescent Prediction of Service Life

A new technique predicts degradation of polymers, such as potting compounds, without imposing artificial conditions.

Lyndon B. Johnson Space Center, Houston, Texas

A chemiluminescence technique can be used to predict the oxidation degradation of polymers and other organic materials under the actual expected-use conditions. Degradation is usually so slow or small that conventional aging tests require artificial intensification of critical parameters such as temperature. When extrapolated to actual conditions, this type of data does not necessarily give accurate predictions of service life.

A true degradation rate, under actual environmental conditions, can be determined by measuring the weak chemiluminescent emission that accompanies the oxidation of many organic materials. The emission mechanism is believed to proceed by way of free-radical chain oxidation with the formation of excited ketones in the chain determination step. A small fraction of the ketone emits light or transfers excitation energy to another compound that decays with light emission.

An apparatus designed to measure this weak emission is shown in the figure. It has been used to measure emission from samples of *cis*-polybutadiene, Viton, Teflon, silicone, and a boron-epoxy composite at temperatures from 25° to 150° C. Excellent correlations between temperature and chemiluminescence have validated independent accelerated-aging tests (at elevated temperatures) used to predict service life of these compounds.

In addition, smooth or linear correlations are obtained between chemiluminescence and physical properties (tensile strength, viscosity, and loss tangent) of purified polymer gums. The data are obtained much more easily than with conventional methods. Another application, studying the effects of mechanical deformations on polymers, is suggested by the chemiluminescent emission observed on milled samples of polymer gums.

This work was done by John A. Hassell, G. David Mendenhall, and Richard A. Nathan of Battelle Memorial Institute for **Johnson Space Center.** *Further information may be found in NASA CR-147463 [N76-18276/LK], "Space Shuttle Nonmetallic Materials Age Life Prediction," a copy of which may be obtained at cost from the National Technical Information Service, Springfield, Virginia 22151. MSC-16010*

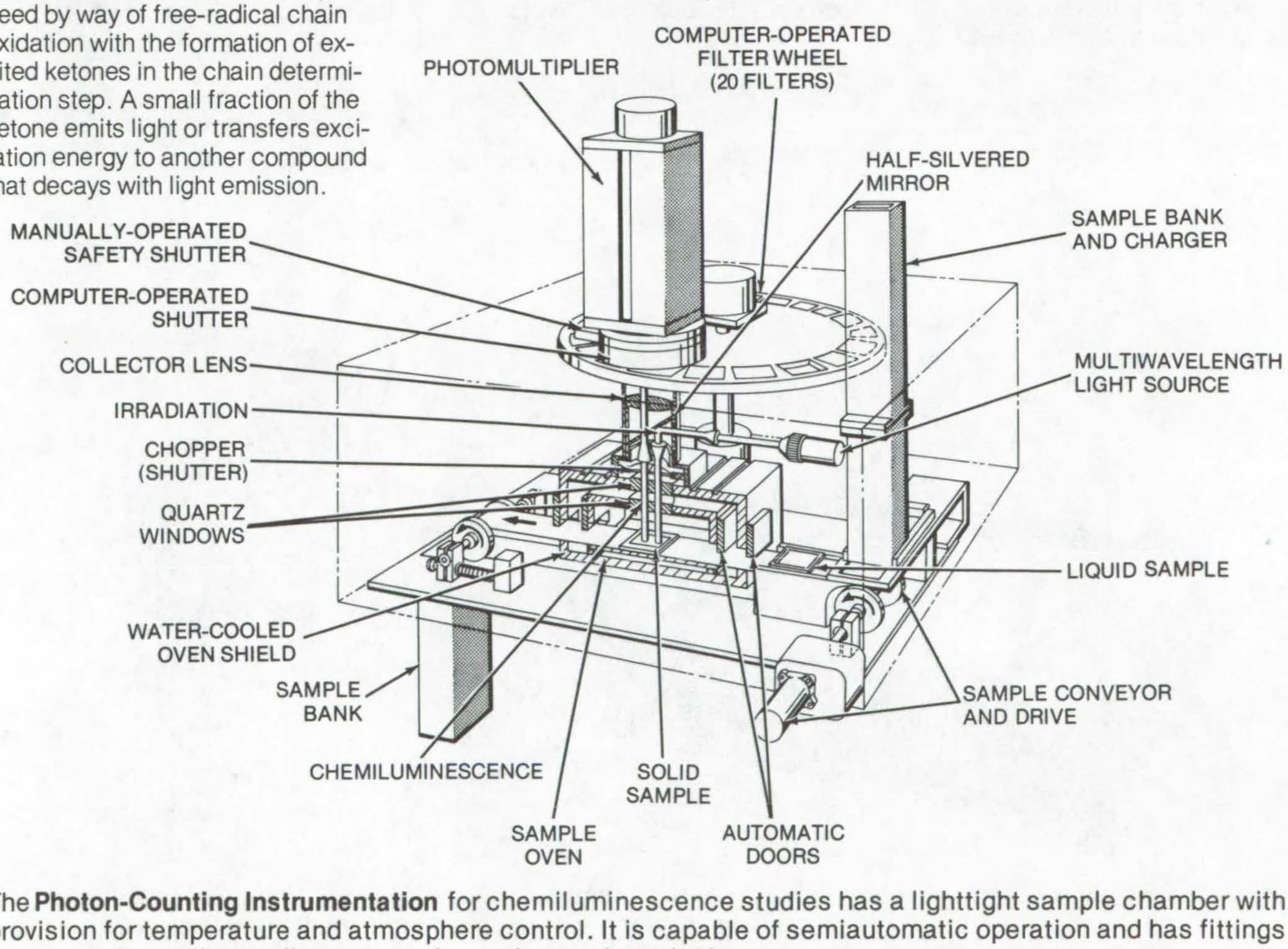

The **Photon-Counting Instrumentation** for chemiluminescence studies has a lighttight sample chamber with provision for temperature and atmosphere control. It is capable of semiautomatic operation and has fittings for measuring and recording extremely-weak sample emissions.

Thermoluminescence for Forensic Analysis

Thermoluminescence apparatus is designed for determining whether two samples are from the same source.

Caltech/JPL, Pasadena, California

The need to assess the commonality of origin of physical evidence frequently presents problems in the criminalistics laboratory. In such a case, it is only necessary to establish whether two or more items issued from the same or different sources; their compositions need not necessarily be analyzed. The present experimental methods used for such determinations include optical microscopy, infrared and emission spectroscopy, density gradient techniques, and the measurements of the refractive index. All of these methods are time consuming and involve a long delay for processing the samples.

A new technique for evaluating evidence materials has been developed which utilizes the phenomenon of thermoluminescence. Thermoluminescence is defined as the emission of light produced by the heating of a solid nonelectrical conductor to a temperature below that of incandescence. The solid is first exposed to ionizing radiation (such as natural radioactivity, cosmic rays, X-rays, or beta particles) which produces a cloud of displaced electrons within the lattice structure of the solid. Some of these electrons are caught in lattice traps: imperfections and vacancies in the crystal lattice. When the temperature of the lattice structure is raised, thereby supplying the kinetic energy necessary to cause a recombination of the traps, these electrons escape and in doing so emit light. This phenomenon is measured as a function of increasing temperature [73 K to 293 K (-328° to 68° F) for low temperatures and 293 K to 623 K (68° to 662° F) for high temperatures] versus light emitted to give a characteristic glow curve. Small variations in crystalline structure and/or in the levels of impurities cause large changes in the nature of the glow curves produced by different samples of the same type of material.

The thermoluminescence system is illustrated in Figure 1. Two principal types of light-measuring systems were considered: a photon or pulse counting system and an analog or current measuring system. While the photon counting system allows the measurement of very low light levels, it is expensive and complex. The analog system, in which the

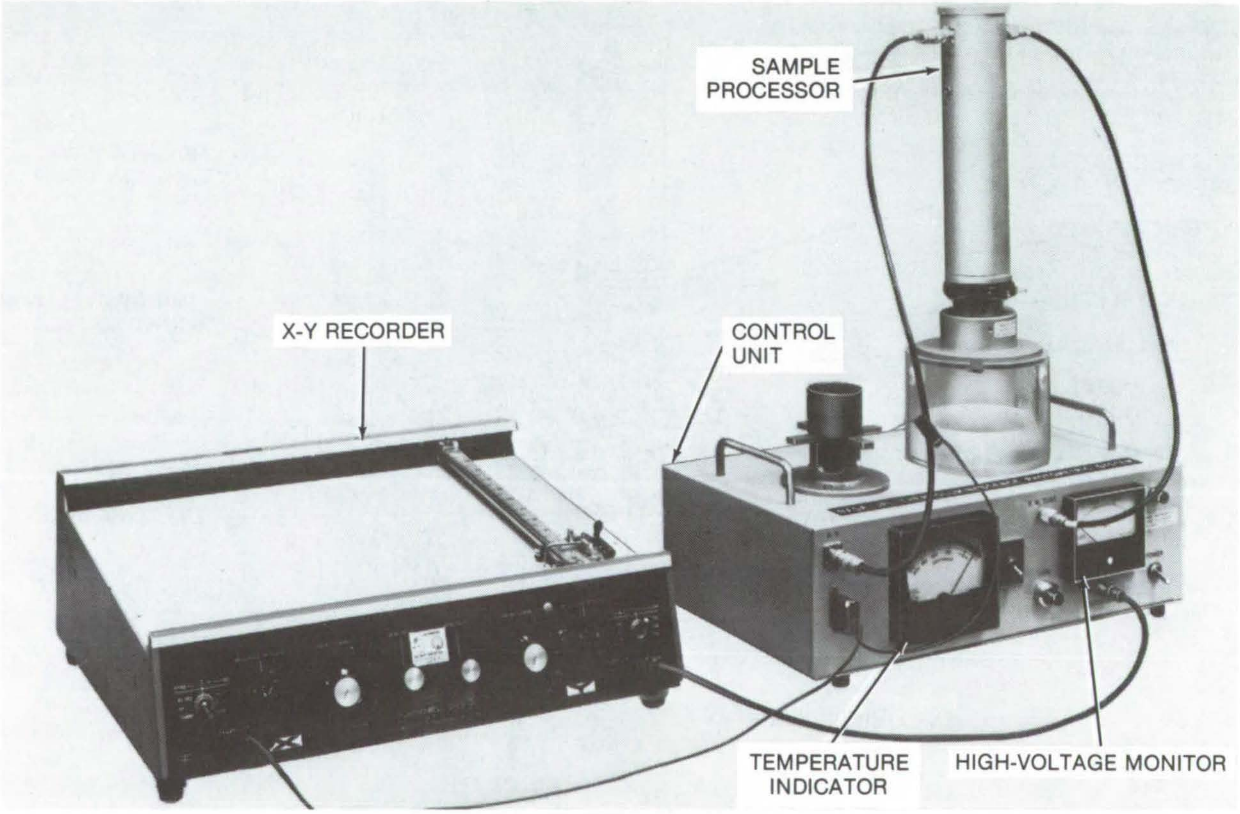

Figure 1. **Thermoluminescence System,** an analog (current measuring) device, employs a photomultiplier tube, the output of which is measured by an electrometer. The control unit contains the photomultiplier high-voltage supply and low-voltage sample heater source.

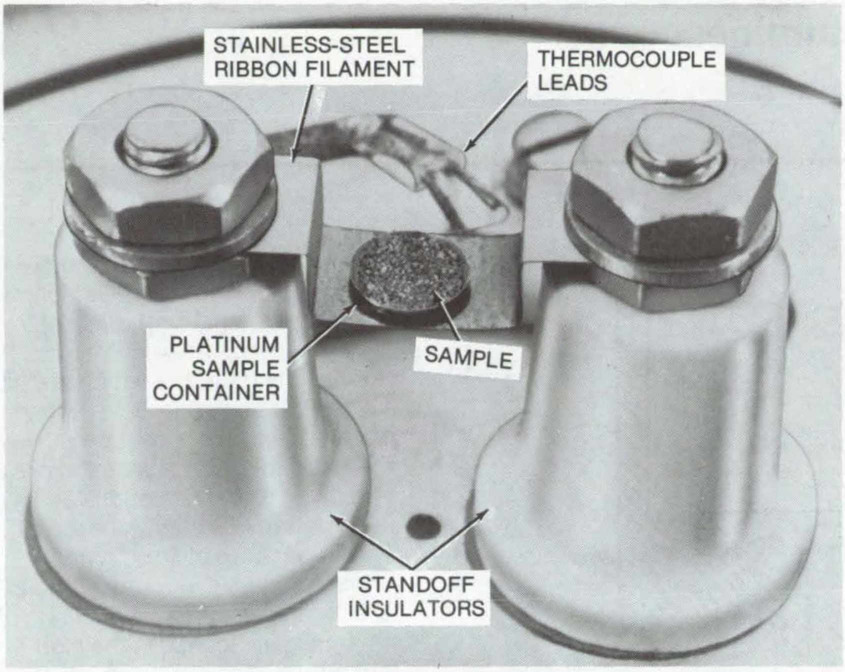

Figure 2. **Sample Container and Sample Heater** are suspended by ceramic standoffs. A 10-mg sample of material is placed in the sample dish after being granulated and sieved. The sample is then exposed to ionizing radiation. Radiation levels are determined by trial and error.

photomultiplier tube output is measured by an electrometer, is economical and straightforward and for general usage is the most versatile and requires the least operator skill.

A 10-stage photomultiplier tube was selected for use in both systems because of its high sensitivity to blue light and negligible sensitivity to red radiation. This helps to reduce black body radiation as an upper temperature limitation. Also, the light collection or sensitive area of the tube is large, about 14.2 cm^2 (2.2 $in.^2$), which makes it possible to detect less than a 0.1 microlumen of light. With the exception of this tube, the remainder of the system is constructed using only solid-state components.

The sample is first granulated and sieved to give a uniform particle size. Then the sample is exposed to 50 kilorads of ionizing radiation. In some materials, more or less than 50 kilorads of radiation may be required to get a useful glow curve. The exact radiation levels can be determined only by a trial and error procedure for each sample pair.

Figure 2 shows the sample container and the arrangement for heating the sample.

A uniformly increasing temperature is generated in a platinum sample cup by electrically heating the stainless steel ribbon with a high current/low voltage input to the ribbon. The temperature ramp is generated by increasing the voltage to the ribbon. The temperature of the system is measured by an iron/constantan thermocouple. The thermocouple supplies output to the meter on the thermoluminescence unit and to the X axis of an X-Y recorder.

The sample container arrangement is unique in that, contrary to the usual practice in the study of this phenomenon, the sample cup handles extremely small samples, on the order of 10 milligrams (3.2×10^{-4} oz). The usual container for other instruments handles samples on the order of one-half gram or more. Sample preparation involves crushing the specimen to obtain a fine consistency powder and sieving through a 100-mesh screen. The control unit contains the high-voltage supply, which is applied to the photomultiplier tube, as well as the low-voltage sample heater supply. In addition, it contains a sweep motor to provide a ramp voltage which is used to effect a gradually-increasing sample temperature.

This work was done by Daniel D. Lawson of **Caltech/JPL.** *For further information, Circle 48 on the TSP Request Card.*
NPO-11607

Graphite-Reinforced Bone Cement

Chopped graphite fibers, when added to surgical bone cement, form a bonding agent with mechanical properties more nearly matched to those of bone. To prepare, chopped fibers are added to a polymethylmethacrylate composition. Bone stiffness is increased without affecting flexural strength, but compressive strength is reduced. The inhibiting effect of the fibers results in a maximum cure temperature of 55° C.
(See page 221.)

Double-Focusing Mass Spectrometer

A double-focusing magnetic-sector mass spectrometer uses a lighter, more-easily-alined, magnet assembly to provide the field required to interact with the ion beam. It has no separate duct; instead, an evacuated duct is formed by the pole pieces which support the vacuum pump. The magnetic gap and magnet assembly are reduced from 4.64 to 2.54 mm and from 2.4 to 1.5 kg, respectively.
(See page 192.)

Low-Reflectivity Spectrally Selective Coating

A new multilayer coating for mirrors imparts a 1-percent reflection in the region 400 to 700 nanometers. It is a vacuum-deposited film sequence of aluminum, dielectric spacer, semitransparent metal, and dielectric spacer. The proper thicknesses of the layers are achieved by optically monitoring the reflectivity of the substrate.
(See page 193.)

Low-Temperature Thermoluminescence

Improved thermoluminescence technique is applicable to water pollution technology.

Caltech/JPL, Pasadena, California

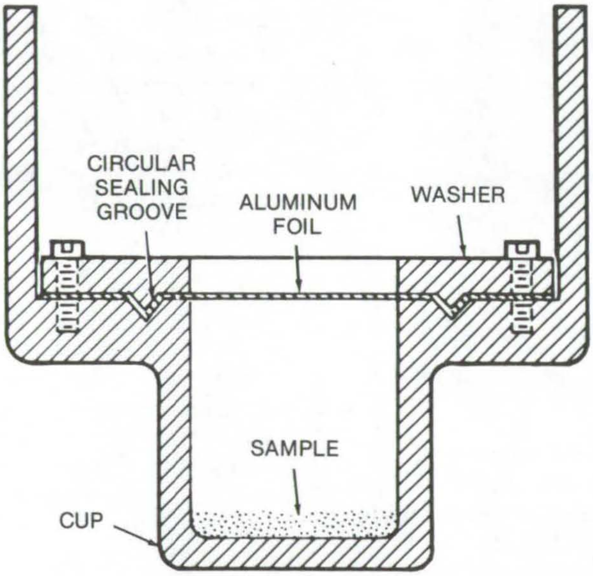

Figure 1. A **Low Temperature Sample Cup** with a sealed aluminum membrane that is pierced by a knife once the cup is inserted into heating and sensing equipment.

The usefulness of thermoluminescence techniques for establishing the commonality of origin of forensic evidence materials can be extended to materials which are not solids at room temperature and to materials which are heat sensitive, such as paper, drugs, and the like, by making test observations at low temperatures. Testing is begun at the temperature of liquid nitrogen and is concluded at room temperature. The use of the phenomenon of thermoluminescence in the high-temperature regime, from 293 K to 723 K (68° to 842° F) has been described in the preceding article, Thermoluminescence for Forensic Analysis (NPO-11607).

A serious problem encountered in low-temperature thermoluminescence measurements, which is not

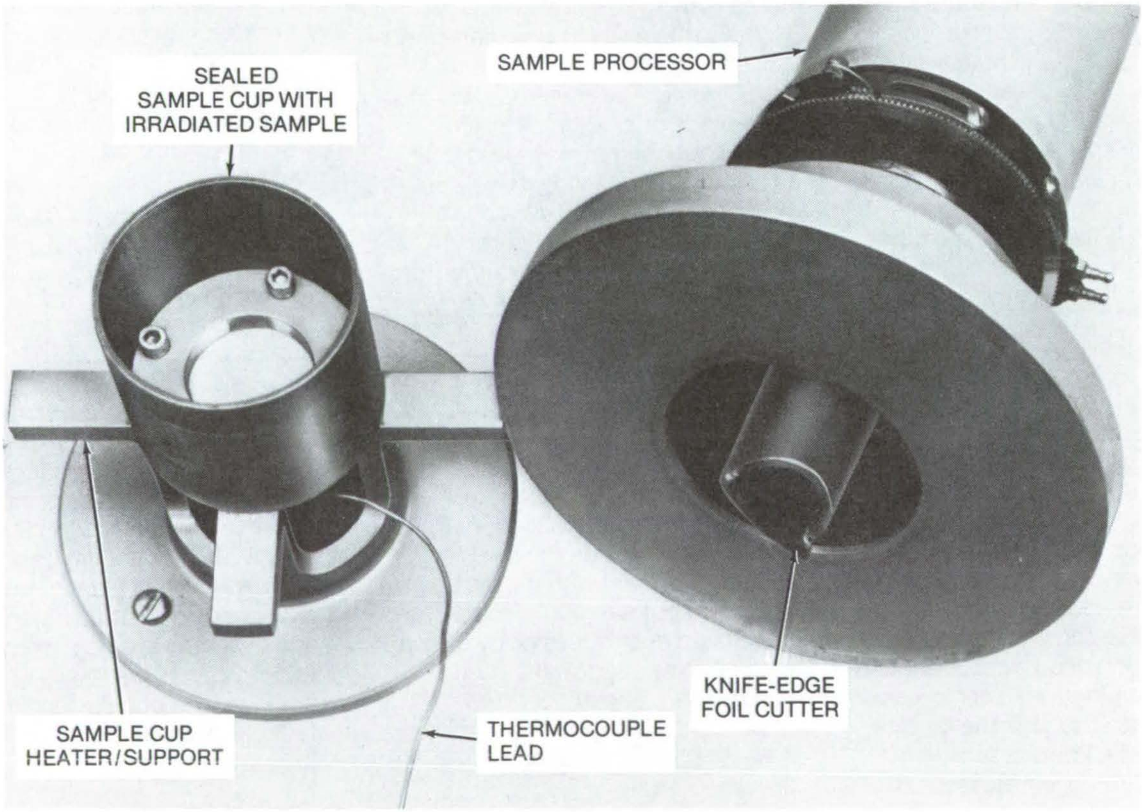

Figure 2. The **Sample Cup in Heater/Support, and Sample Processor** which contains a tube with the knife-edge foil cutter at the end of it.

encountered in high-temperature measurements, is the contamination of the sample by the condensation of water vapor from the atmosphere during the liquid nitrogen cooling. This problem is solved by using a sealed sample cup. An aluminum foil membrane is clamped over the sample cup to provide sealing and remains intact during the cooling and irradiation steps. When the sample cup is inserted into the heating and sensing equipment, a knife pierces the membrane and is rotated to move the foil out of the light path to the photomultiplier tube.

The sample is heated by passing hot air around the cup. Airflow must be at a constant rate in order to effect the relatively linear recording of light levels versus time (for good correlation with rising temperature). The nonlinearity of thermocouples at low temperatures and the consequent nonlinearity exhibited on the temperature axis of the glow curve are also problems with this technique. The sample cup is shown in Figure 1.

The cutter which opens the aluminum foil so that the emitted light may be sensed by the photomultiplier tube can be seen in Figure 2. The cutter is a vertical knife edge which is retained at the end of a tube. The tube is mounted in the sample processor below the shutter so that the latter may control the amount of light emission which is seen by the photomultiplier tube, as in the high-temperature system.

One area of potential usefulness lies in assessing the commonality of the origin of oil pollutants, such as are produced by ships at sea dumping oil. It is also believed that the technique may be useful for mapping certain features of lakes and/or oceans and for the identification of the source of materials, such as plastics, rubber, solvents, water solutions, and the like.

This work was done by Daniel D. Lawson and John D. Ingham of **Caltech/JPL.** *For further information, Circle 49 on the TSP Request Card.*
NPO-11935

Solventless Intumescent Coatings

A new intumescent coating requires no hydrocarbon solvent and can be applied in smooth layers.

Ames Research Center, Moffett Field, California

An intumescent coating that requires no solvent can be made by reducing the concentrations of intumescent compound and fibrous materials that are used in sprayable compositions. The formulation is then cast or molded into shapes that subsequently can be cut and bonded onto contoured surfaces. Although a variety of intumescent coating compositions are currently in use, among the most versatile in the formulation NASA-313, which consists of a three-part mixture of polysulfide resin, the ammonium salt of *p*-nitroaniline-*m*-sulfonic acid, siliceous fibers, and polymerizable epoxy-resin substrate in a solvent base.

The following modification of the NASA formulation consists of only two parts and does not require a solvent to make a smoothly manageable composition:

Part A—**Ingredient**	**Weight** %
Polysulfide liquid polymer	21.4%
Liquid epoxy resin	17.1%
Ammonium salt of *p*-nitroaniline-*m*-sulfonic acid	56.5%
Quartz microfibrils	5%
Part B—	
Tri(alkylamino)phenol	2.5%

The amount of part B to be used is about 15 percent by weight of the amount of epoxy in part A. The composition will provide a char yield of about 45 percent at over 540° C (1,000° F), and the temperature of intumescence is about 260° C (500° F).

Compositions of the type represented by the above formulation can be cast between plastic sheets to provide smooth-surface forms. Alternatively, the compositions can be pressed or molded into a variety of shapes. The smooth-surfaced sheets or preforms can then be fastened to the surfaces of structures with thin films of adhesives. By these expedients, smooth intumescent layers can be applied to aerodynamic surfaces (sprayed coats are too rough). Moreover, preforms can be cemented to surfaces that cannot be overcoated by the usual spray-coating techniques.

This work was done by Seymour Schwartz of Hughes Aircraft Co. for **Ames Research Center.** *Further information may be found in NASA CR-137706 [N75-28228], "Development of an Optimized Intumescent Coating," a copy of which may be obtained at cost from the Aerospace Research Applications Center, Indiana University* *[see page A7]*.
ARC-10996

Thermal/Acoustical Insulation Foam

Lightweight controlled-density foam used in aircraft has excellent fire resistance

Lyndon B. Johnson Space Center, Houston, Texas

A low-density foam, based on a composition of alumina/silica/ceramic fibers, is an improved material particularly suitable for use in aircraft insulation. The foam has several properties which makes it an attractive insulant: Material density can be controlled over the range of from 0.6 to 1.2 lb/ft³ (9.6 to 19.2 kg/m³), and the foam has good thermal and acoustic properties. The controlled-density foam can replace the resin-bonded fiberglass batting used to insulate aircraft; and it offers a safety improvement over the lightweight foam material which supersedes the batting, since the new low-density foam contains no asbestos as does the foam insulation it replaces.

The foam is fabricated by dispersing the foam fibers and other fibrous ingredients with a surface-active agent. A soluble organic resinous binder and a medium such as water are added to disperse the fiber mixture. Subsequent drying and heat treatment produce a porous, nonfluid foam. Two different resin systems used to produce laboratory samples of the foam are equally effective organic binders.

The figure illustrates the results of tests, as comparing these to other foams and insulative materials. The flame-impingement tests consisted of heating one side of each foam sample with a 2,250° F (1,232° C) oil burner; as indicated the backface temperature of the controlled-density foam is no greater than 650° F (343° C) during the test period. Little or no fumes were generated during the test.

Noise-reduction properties have not yet reached a satisfactory level, but may be improved by incorporating fine-diameter glass fibers in various percentages of foam composition. Further acoustical optimization procedures and tests are required.

This work was done by Ruey Y. Lin and Edward A. Struzik of The Carborundum Co. for **Johnson Space Center.** *Further information may be found in NASA CR-141498 [N75-15803], "Development of a Thermal Acoustical Aircraft Insulation Material," a copy of which may be obtained at cost from the National Technical Information Service, Springfield, Virginia 22151.*

This invention is owned by NASA and a patent application has been filed. Inquiries concerning nonexclusive or exclusive license for its commercial development should be addressed to the Patent Counsel, Johnson Space Center [see page A8]. Refer to MSC-14795.

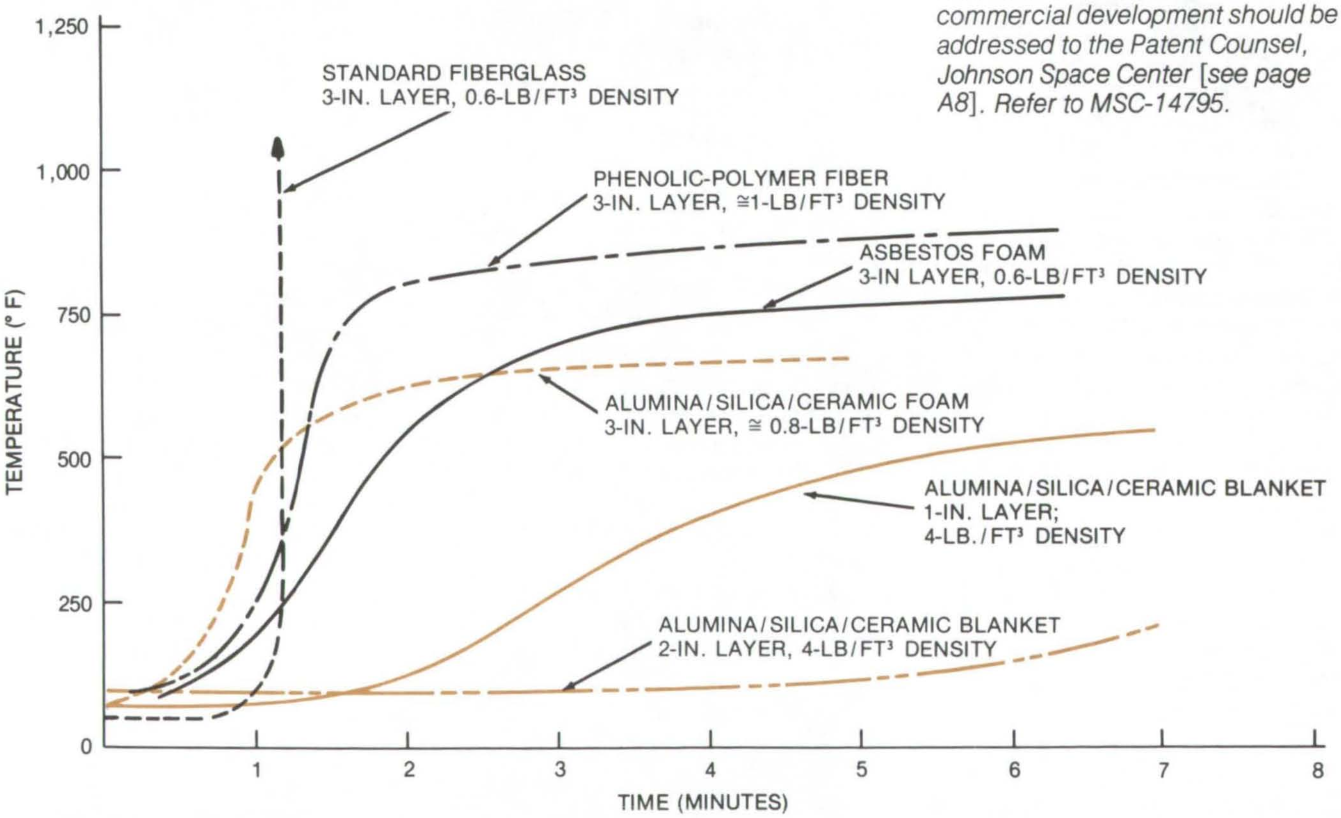

Flame-Impingement Tests of the low-density foam reveal the ability of the material to withstand direct flame, as compared to standard fiberglass, phenolic-polymer, and asbestos foam insulants. The backface temperature of the controlled-density foam was no greater than 650 ° F during the test period.

Coating for Solar Panels

An inexpensive coating requires no primers and has high absorptivity and low emissivity.

Marshall Space Flight Center, Alabama

A pigment to vehicle-solids weight ratio of 0.075 is obtained by ball-milling carbon black with polyvinyl butyral (both as commercially available preparations) dissolved in 95 percent ethyl alcohol. The pigment grind is reduced with an ethanol solution of the polyvinyl butyral, and the finished coating is thinned with a 65:35 mixture of xylene/diacetone alcohol. Panels are wiped with toluene, sprayed with a coating 0.25-mil to 1.0-mil thick, and baked at 177° C for 45 minutes. No primer is needed for good adhesion to aluminum, copper, or stainless steel. The coating is a simple means of increasing the efficiency of solar collectors because of its high absorptivity and low emissivity.

The properties and composition are shown in Tables 1, 2, and 3.

Table 1. Paint Composition

Component	Weight %
Mill Base	
Carbon Black	0.53
Polyvinyl Butyral	1.77
Ethyl Alcohol	16.81
Water	0.88
Reducer	
Polyvinyl Butyral	5.31
Ethyl Alcohol	74.70

Table 2. Finished Paint Data

Component	Weight %
Solids	
Carbon Black	0.53
Vehicle Solids	7.08
Total Solids	7.61
Thinner	
Diacetone Alcohol	35
Xylene	65

Table 3. Properties of Coating

Absorptivity	0.95
Emissivity	0.74
Resistance Salt Spray	Good
Adhesion	Good
UV Stability	Good
Humidity Resistance	Good
Thermal Cycling	Good
Pigment to Vehicle-Solids Ratio	0.075

This work was done by Ronald W. Gumbs of R. Gumbs Associates for **Marshall Space Flight Center.** *For further information, Circle 50 on the TSP Request Card.*

Inquiries concerning rights for the commercial use of this invention should be addressed to the Patent Counsel, Marshall Space Flight Center [see page A8]. Refer to MFS-23420.

Improved Insulation Material

A multilayer insulation material is useful for thermal-protection systems and cryogenic containers.

Lyndon B. Johnson Space Center, Houston, Texas

Conventional multilayer insulating materials usually have plain surfaces which wrinkle unavoidably during installation. This wrinkling may cause random diffusions of radiant energy, degrading the effectiveness of the insulation because of the fractions of energy diffused laterally along the layers and eventually reradiated into the insulated volumes.

A new insulating material consists of embossed, silver-coated Mylar, nylon net, and silk net. The embossing on the coated Mylar is in a square pattern which creates small (¼-inch) boxlike forms in the surface. The embossing serves two purposes: (1) to help separate the radiation barriers and (2) to control the diffusion of radiant energy. As the radiant heat waves impinge on each barrier, the small square embossed pattern tends to trap the energy and reradiate it in the opposite direction. Theoretically, this action should reduce the amount of random radiation that actually arrives at the pressure vessel.

The nylon and silk nets used are commercially available materials with approximately 300 holes per square inch. These materials are used to separate the Mylar radiation barriers. Originally, the netting spacers were used as received. However, they were found to contain sizing matter that could potentially cause trouble when used in a vacuum (e.g., in the wall of a Dewar container) due to outgassing.

Each layer of Mylar is separated by one or two layers of net. Nylon net is more effective at temperatures above 400° F (222 K), and silk is more effective below that temperature. This insulating material requires no maintenance after installation. The new embossed, silverized Mylar may well prove to be more sensitive than plain surface materials and may be useful in designing thermal-protection systems on cryogenic containers.

This work was done by the Beech Aircraft Corp. for **Johnson Space Center.** *For further information, Circle 51 on the TSP Request Card.*
MSC-14642

Automated Solvent Concentrator

Designed for automated drug-identification system (AUDRI), the solvent concentrator increases concentration by 100.

Caltech/JPL, Pasadena, California

An automated solvent concentrator has been developed for use with an automated drug identification system (AUDRI). The concentrator provides the input material to the analysis subsystem. Samples to be analyzed range from relatively small to relatively large volumes of fluid. Each sample is first filtered by passage through a suitable filter medium contained within a long-tailed extraction tube. The filter removes particulate contaminants and simultaneously reduces the water content of the sample.

The sample is then extracted from the filtered residue by a specific solvent (for example, chloroform). Most of this solvent must then be removed from the active sample before analysis. The solvent concentrator removes the bulk of this solvent as the first step of a two-stage procedure. The remainder is then removed by the precolumn processor discussed in the next article, "Precolumn for Extract Concentration" (NPO-13083). While many types of manually operated concentrators are presently in use, none are suitable for an automated system such as the AUDRI without extensive further development.

The solvent concentrator required by the AUDRI must reduce the ratio of solvent to specimen by about 100 to 1. The maximum concentration time is 10 minutes, in which a sample content of 100 ml must be reduced to 1.5±1.0 ml of product. The output is required to flow against a back pressure of about 10 in. of water (2,490 N/m²) produced in a following precolumn processor.

A suitable solvent concentrator has been fabricated from a helix of 12-mm (0.47-in.) Pyrex glass tubing consisting of about four turns, 6 in. (15 cm) in diameter, on a slope of about 3° (see figure). The helix terminates in a glass collector cone or sump. A series of electrical resistance heaters wound on the outside

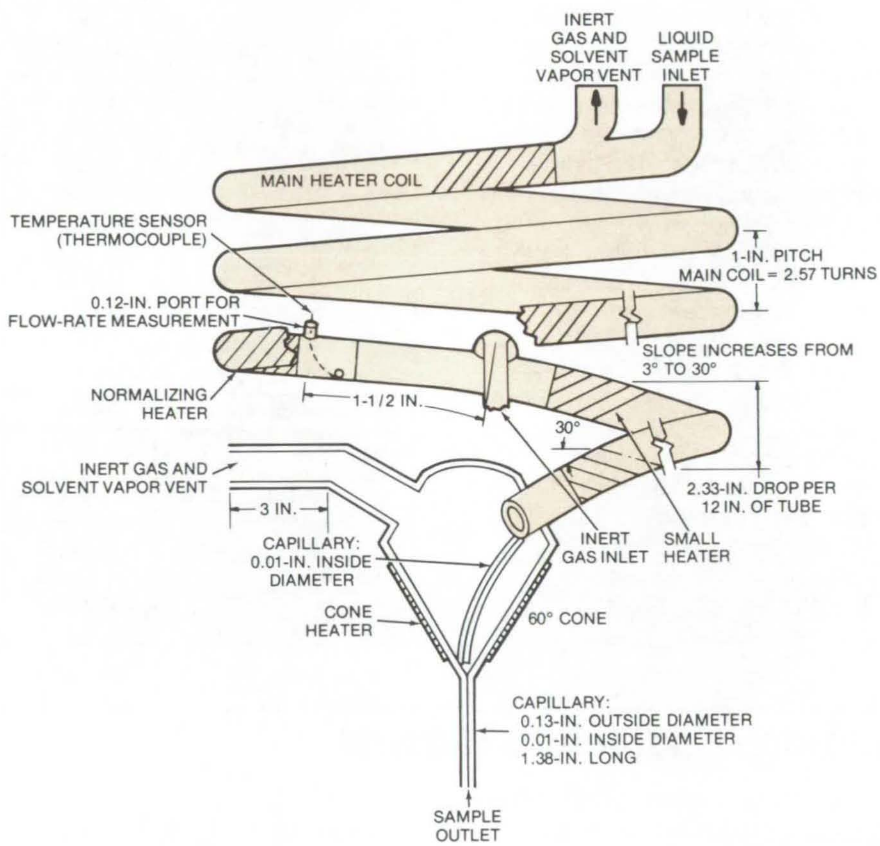

The **Automated Solvent Concentrator** is fabricated from a helix of 12-mm Pyrex glass tubing consisting of about four turns on a slope of about 3°. The helix terminates in a glass cone or sump.

of the tubing evaporate the solvent as the solution flows by gravity down the helix. The sump has a separate heater to aid in the final evaporation. The construction of the helix, using long thin glass tubing of low thermal conductivity, facilitates the independent heating and control of various sections of the tubing.

An inert gas such as nitrogen is introduced about 3/4 the distance down the helix. The gas sweeps the vapor upward and downward and out through vents, and it also serves to maintain a nearly-uniform low temperature in the tubing. This reduces the loss of solute by undesired evaporation. This is possible because the solvent has a low boiling point and the analysis sample has a much higher boiling point.

A thermocouple temperature sensor is located in an unheated section of the helix, just above the flush gas inlet. The sensor is located inside the tubing, in the flowing liquid. At that position, 70 to 95 percent of the solvent has already been evaporated. At a relatively constant flush gas flow and gas-liquid interface area the temperature drop due to evaporative cooling will be inversely proportional to the solvent flow rate at this point. The thermocouple measures the temperature of the cooled flowing liquid which is an indication of the flow rate.

The signal from the sensor provides a flow-rate control signal to the

single electronic controller which adjusts the heat input in certain sections of the helix tubing in accordance with the liquid flow rate. The liquid maintains a relatively constant, repeatable, stream or track resulting in a minimum dryout and deposition of solutes in the helix. Solute hangup is readily removed by increasing the flow rate slightly to redissolve the solute between samples.

Two outlets and an input port are provided for the flush gas, with an option to use them in any combination. Outlet flow restrictors insure the proper division of gas flow. These arrangements provide nearly-pure flush gas for cooling the liquid in the vicinity of the flow-rate temperature-sensing thermocouple.

Two glass capillary tubes are used. One conducts the concentrated product from the end of the helix to a point near the apex of the cone providing essentially continuous flow instead of droplet flow, and the second drains the product from the cone. The cone is an accumulator or storage device for high flow conditions during malfunctions or system startup. The cone heater is capable of evaporating moderate amounts of excess fluid obviating the need for a special drainage system. The lower capillary acts as a restrictor for large liquid flows.

This work was done by John S. Griffith and Jerry L. Stuart of **Caltech/JPL.** *For further information, Circle 52 on the TSP Request Card.*
NPO-13068

Precolumn for Extract Concentration

A precolumn extract concentration increases sensitivity in an automated drug identification system (AUDRI).

Lewis Research Center, Cleveland, Ohio

The automated drug identification system (AUDRI) requires that test samples be separated into families of organic compounds for subsequent insertion into several parallel gas chromatographs. A sample is first extracted by selective organic solvents. Solvent is then removed from the extract to increase the ratio of extract to solvent. This step significantly increases system sensitivity.

With each gas chromatograph in the AUDRI system there is a preprocessing unit (the PGC) which includes a solvent concentrator, [described in the previous article, *"Automated Solvent Concentrator"*

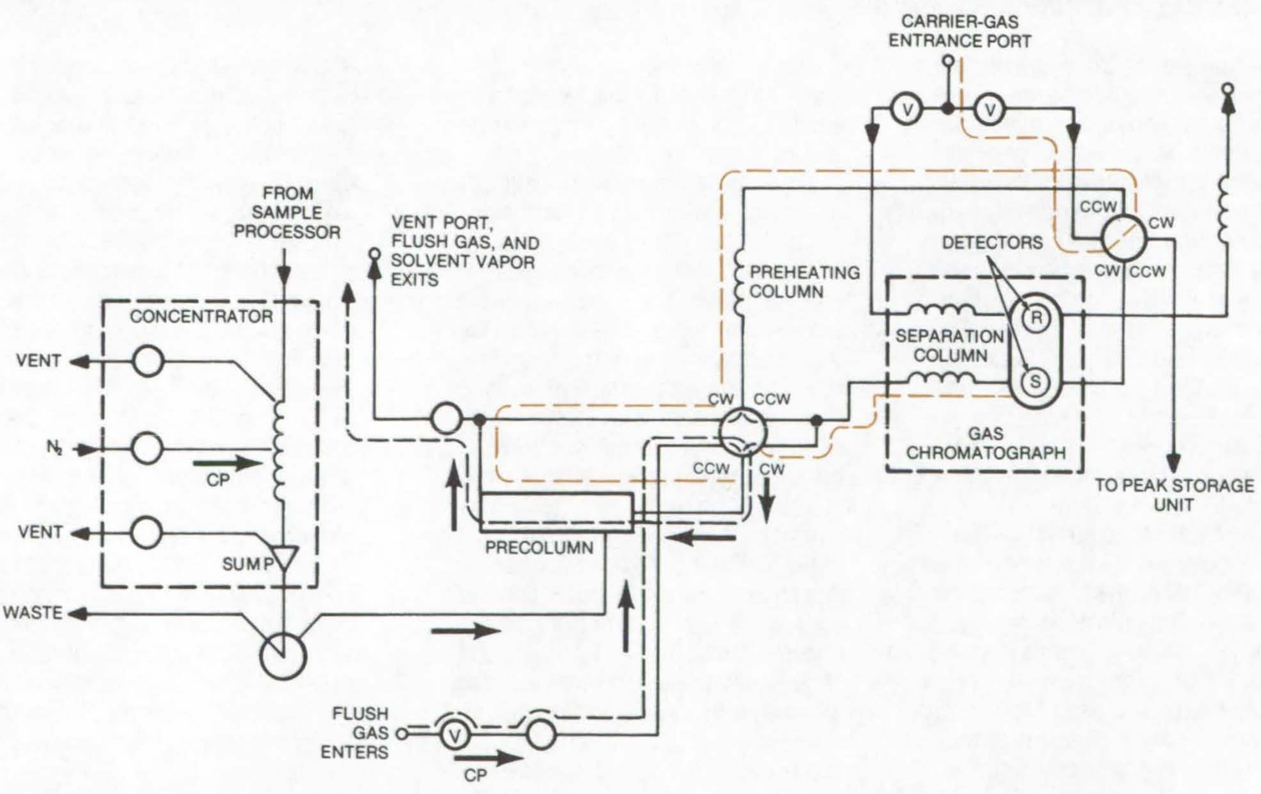

The **AUDRI Flow Schematic** shows the concentrator, precolumn, and a gas chromatograph. In the precolumn the concentrated sample is further reduced to an enriched extract for input to the gas chromatograph.

(NPO-13068)], and a precolumn to further reduce the solvent concentration. The precolumn assembly contains a column similar to a conventional gas chromatograph column. It further concentrates the sample by evaporating solvent; then it injects the extract into the analytical gas chromatograph.

Figure 1 is a schematic drawing showing the concentrator, the precolumn, and a gas chromatograph. After passage through the concentrator, the reduced product is transferred from the sump to the precolumn where it is further reduced to an enriched extract which can be accommodated by the gas chromatograph. In Figure 1 it is assumed that the reduced volume of extract and solvent enters the precolumn from the right and moves towards the left end.

While the sample from the concentrator is introduced, flush gas is passed through the precolumn along the dotted line. The temperature of the precolumn is selected to enhance the vaporization of the solvent and to permit the extract to be retained. The solvent vapor is then vented out of the system through the vent port. The precolumn reduces the solvent-and-extract volume to a few microliters, a volume which can be inserted into a gas chromatograph.

The flush-gas flow is stopped, and the carrier gas is introduced into the system along the dashed line. The carrier gas goes through a preheating column to raise the temperature of the precolumn sufficiently to volatilize the sample residue. The carrier gas then flushes the extract out of the precolumn in a direction opposite to that in which it entered. The now vaporized extract is forced into the separation column of the gas chromatograph.

The gas flow during solvent vaporization and deposition is opposite the flow during injection into the gas chromatograph. This backflushes the precolumn to more efficiently cleanse it before processing subsequent extracts, thus significantly reducing the build up of contaminants in the precolumn. Further, it is easy to replace the precolumn with a new column when desired.

This work was done by Vilhelm J. Jahnsen and William G. Bloom of **Caltech/JPL.** *For further information, Circle 53 on the TSP Request Card.*

Title to this invention, covered by U. S. Patent No. 3,859,209 has been waived under the provisions of the National Aeronautics and Space Act [42 U.S.C. 2457(f)], to Caltech/JPL, Pasadena, California 91109
NPO-13083

Fraction-Storage Unit for Drug-Identification System

Gas chromatograph samples are stored for input to an IR spectrometer.

Caltech/JPL, Pasadena, California

The automated drug identification (AUDRI) system utilizes gas-chromatographic separation of sample constituents followed by spectral analysis with an infrared (IR) spectrometer to provide information for computer identification of drugs. The test sample is processed in the sample processor as described in the preceding articles (NPO-13068 and NPO-13083). The different extracts are then simultaneously analyzed in separate, parallel, gas chromatographs (GC's). GC analysis is followed by spectral analysis in a single IR spectrometer.

As a result of the simultaneous parallel operation, several samples may be ready for IR analysis at the same time. Furthermore, a singel GC may occasionally elute constituents at a faster rate than the IR can analyze them. The use of four separate rapid-scanning infrared spectrometers or mass spectrometers would largely resolve these problems. However, four spectrometers would increase the system cost beyond acceptable limits.

This problem has been avoided by a fraction-storage unit which connects the outputs of all the GC's to a single, relatively-inexpensive, IR spectrometer. The storage unit provides buffer storage of the samples until the infrared spectrometer is ready to accept them. The fraction-storage unit consists of several sets of gas-chromatograph columns equipped with appropriate valving, plumbing, heaters, detectors, and electronics. It independently controls the input and output of the storage columns and back-flushes each storage column after use in order to clean it.

Typically there are three columns for each chromatograph. Constituents from each GC may be stored and transferred one at a time to the IR. Even simultaneous peaks, if produced by different GC's, can be stored in separate holding columns. The storage unit can also be used to separate overlapping peaks.

A diagram of the peak storage unit is shown in the figure. For clarity only one set of holding columns is depicted. It comprises three holding columns, two pressure-balancing columns, and the necessary valves. In addition to a similar set for each GC, the fraction-storage unit includes a balancing column, a selector valve, and a pair of detectors.

When a constituent passes through a GC detector toward the fraction-storage unit, its elution time is computed by either the chromatograph or the computer. If, based on the computation, the constituent is not of interest, it is directed out the vent port (dashed lines). If however, the constituent is of interest and

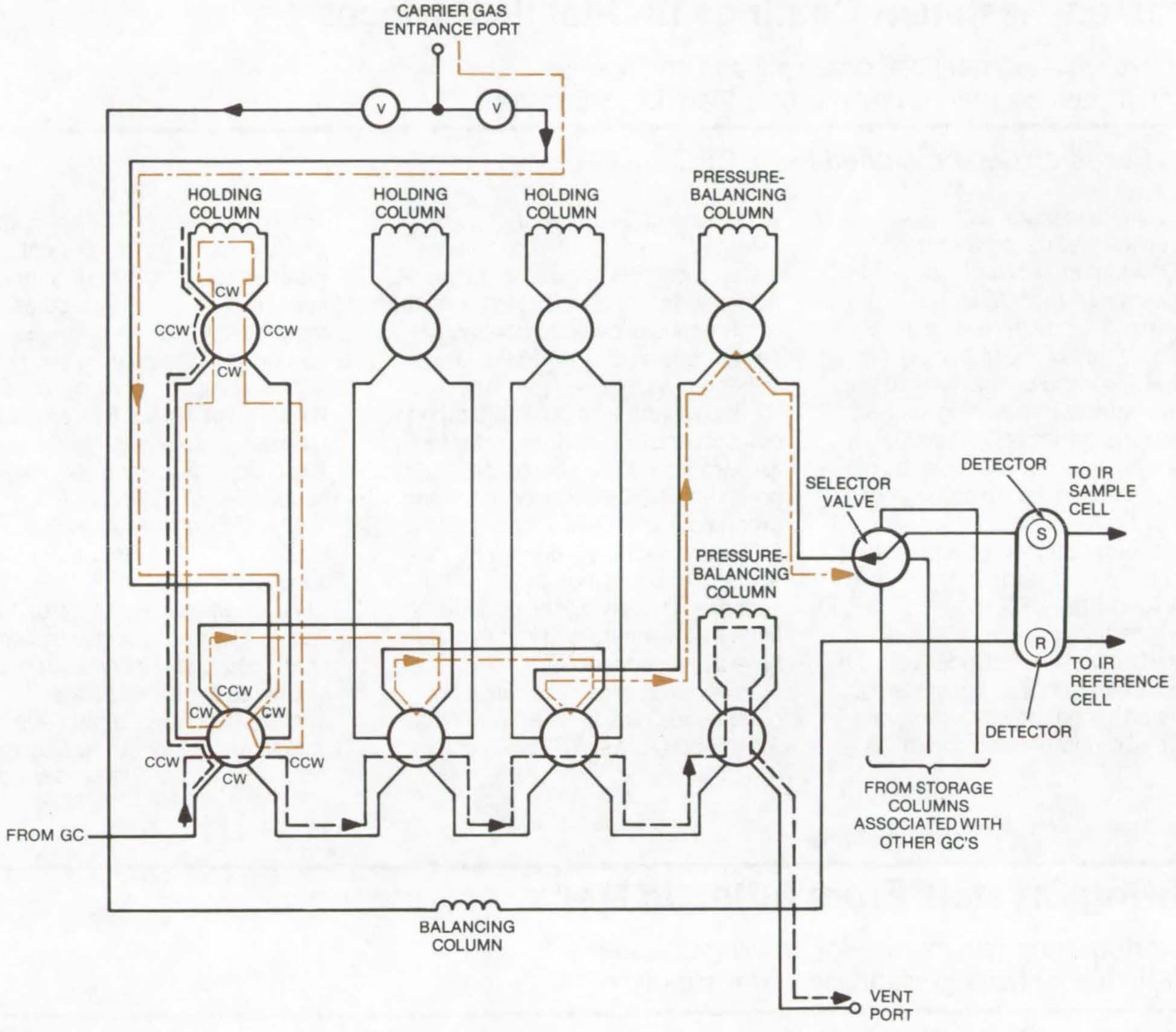

The **Fraction-Storage System for One Gas Chromatograph** consists of three holding columns, two pressure-balancing columns, detectors, and the appropriate valving.

should be analyzed in the spectrometer, it is directed to a holding column (dotted lines). When the spectrometer is ready to receive the constituent for spectral analysis, a carrier gas forces the constituent out of the column and through the selector valve to a detector and thence to the IR sample cell (dashed-dot lines). The carrier gas is also directed to the IR reference cell through the balancing column and a detector. Any number of holding columns may be included for each GC, depending upon the expected rate of elution of constituents of interest and the length of time it takes the IR spectrometer to complete a scan cycle.

This work was done by Charles F. Campen and Jerry L. Stuart of **Caltech/JPL.** *For further information, Circle 54 on the TSP Request Card.*
NPO-13111

Abrasion-Resistant Coatings for Plastic Surfaces

An optically clear coating of organosilicon compounds insulates plastic surfaces and protects them from abrasion.

Ames Research Center, Moffett Field, California

Scratch tests made with a diamond stylus clearly show that the scratch resistance of a plastic surface coated with a plasma-polymerized silane derivative is superior to that of the uncoated surface. Also, the uniformity and optical clarity of the coating applied by plasma polymerization is superior to those applied, for example, by dip coating, electron-beam coating, or ultraviolet polymerization.

The plasma polymerization technique has been described in detail in NASA Tech Brief B73-10507. Briefly, the substrate to be coated is mounted between electrodes in a vacuum chamber, and the system is evacuated. Then the monomer, or a mixture of monomer and diluent, is let into the chamber so that a preselected pressure can be maintained, power is applied to the electrodes to establish a plasma, and the discharge is allowed to continue until a coating of desired thickness is obtained. As an example, vinyltrimethoxysilane was polymerized on a polycarbonate substrate under the following conditions: chamber pressure, 0.260 torr; monomer and argon flow, 5 and 14.5 cm^3/min (STP), respectively; power, 30 watts; and deposition time, 3,000 seconds. By varying the conditions, films of 400-nm to 800-nm thickness have been deposited.

In general, organosilicon compounds may be used which have the general formula $Si(OR)_2$ or $Si(OR)_3R'$, where R is any appropriate organic group. Diluent gases (such as oxygen, nitrogen, and sulfur dioxide) may also be used in the process and may increase the hardness of the coating even more.

This work was done by Theodore Wydeven of **Ames Research Center** *and John R. Hollahan of Tegal Corp. Further information may be found in U. S. Patent No. 3,847,652 and NASA Tech Brief B73-10507. No further documentation is available.*

This invention is owned by NASA, and a patent application has been filed. Inquiries concerning nonexclusive or exclusive license for its commercial development should be addressed to the Patent Counsel, Ames Research Center [see page A8]. Refer to ARC-10915.

Growing Crystals From Eutectic Melts

An inverted Bridgman method for growing crystals results in higher homogeneity and better structure.

Marshall Space Flight Center, Alabama

A new process called the Inverted Bridgman Method is an improvement over the ordinary Bridgman Method for growing crystals of alloys which contain two or more components. The new process yields crystals of higher homogeneity and better structure than those grown by the ordinary Bridgman Method.

The ordinary Bridgman Method involves melting the alloy in a crucible and then directionally solidifying it, starting from the bottom. This is accomplished by lowering the mold containing the alloy into and through the furnace, or by moving the furnace itself in the opposite direction, or by moving a cooling jacket around the mold. The crystal may be grown with or without a seed. The problem is created by the temperature gradient which is always present at the solid-liquid interface. This results in the migration of components either toward the interface or away from it (a phenomenon known as thermotransport, or the Soret effect).

Thermotransport introduces non-homogeneity into the crystal which may seriously impair its properties. This is a general effect and is applicable to most alloy systems. The degree of nonhomogeneity depends on several variables: (a) the type of alloy system, (b) the duration of crystal growth, and (c) the temperature gradient in the liquid melt. Eutectics and other polyphase alloys seem to be affected by thermotransport to a greater degree than single-phase alloys.

The Inverted Bridgman Method (see Figure 1) eliminates this nonhomogeneity and yields better

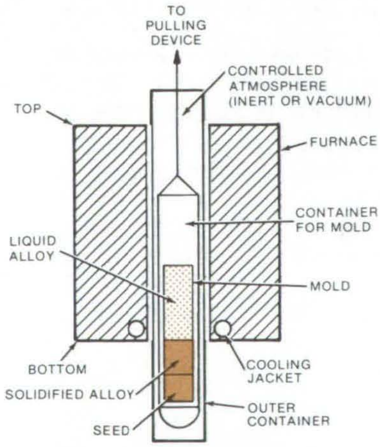

Figure 1. The **Bridgman Apparatus** for the inverted Bridgman method reduces nonhomogeneity (due to thermotransport) to yield a better crystal.

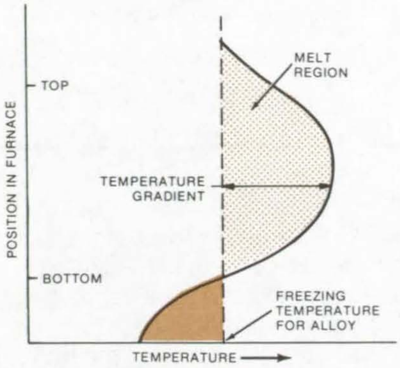

Figure 2. The **Temperature Distribution in Bridgman Apparatus:** For a temperature gradient of 50 ° C per cm the rate of growth is about 1 mm per day.

crystals. It does so by taking advantage of the fact that thermotransport can be controlled. Desired amounts of segregation can be introduced into a molten alloy simply by holding it in a known temperature gradient for a known period of time. The alloy then is cooled rapidly to quench in the state of segregation. The sample next is inverted so that the hold end becomes the cold end. The crystal is then grown in the usual manner.

The new method may also be used for growing single crystals, although at present it is only applicable to eutectic melts. Again using the aluminum-copper system for an example, there is a eutectic of α and Θ phases forming at 17.4 atoms/percent copper. When directionally solidified, this alloy has a lamellar structure. If the freezing is interrupted in the Bridgman apparatus, thermotransport will occur, and the copper will migrate to the colder regions. Hence the liquid at the solid-liquid interface will become supersaturated and unstable. The excess copper will precipitate as Θ phase on the existing lamellae of Θ phase in the solid. A single crystal of $CuAl_2$ is obtained in this fashion.

The rate of growth will be determined by the thermal diffusion coefficient and the temperature gradient. Using the new technique, the crystal is seeded at the bottom. The crucible containing the alloy and the seed is slowly raised in the furnace until part of the seed is melted. The crucible is held at that position for a time sufficiently long for precipitation to occur. The rate of growth depends on the temperature gradient and the thermal diffusion coefficient.

For a temperature gradient of 50° C per cm, the rate of growth is approximately 1 mm per day. The sample is then pulled down by that amount, and further growth of Θ phase occurs. These steps are repeated. Copper in the melt may be replenished by adding solid Θ from the top (this arrangement is not shown). Copper migrates in the temperature gradient and deposits on the growing Θ phase.

Single crystals of Θ phase, several millimeters long, have been grown in the laboratory. This method is readily applied to any other eutectiferous system where thermotransport is appreciable. Pb-Se and Pb-Te appear to be good candidate systems, the criterion being that the component migrating to the cold end should be able to precipitate and grow either as a primary phase or as an intermediate phase.

This work was done by Biliyar N. Bhat of the National Research Council for **Marshall Space Flight Center.** *For further information, Circle 55 on the TSP Request Card.*

Inquiries concerning rights for the commercial use of this invention should be addressed to the Patent Counsel, Marshall Space Flight Center [see page A8]. Refer to MFS-22926.

Compressed Air Cylinder Pallet

An inexpensive handling and storage device for up to 20 compressed air cylinders.

Lyndon B. Johnson Space Center, Houston, Texas

A pallet support can be used to handle up to 20 cylinders of compressed gas of any standard size, simultaneously and with improved safety.

The inexpensive storage and handling arrangement for gas cylinders is shown in the figure. A pallet of wood or plywood has a support structure that holds from 1 to 20 cylinders in the vertical position. The wooden picture-frame support is secured vertically to the center of the pallet with plywood gussets. A saddle is attached to the top of the picture frame. The cylinders are placed in the saddle and strapped to the picture-frame support.

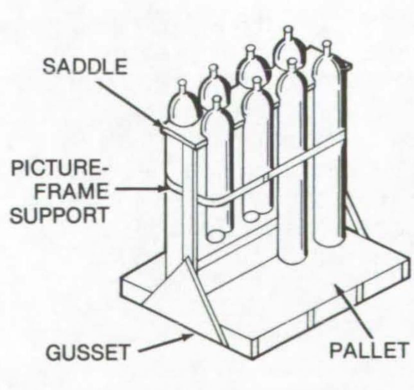

The **Compressed Air Cylinder Pallet** may be made as shown or larger to hold up to 20 cylinders.

This work was done by Kenneth G. Highley of Rockwell International Corp. for **Johnson Space Center.** *No further documentation is available.*
MSC-19217

Pyroionic Infrared Detector

A new infrared detector operates near room temperature and is not sensitive to vibrations.

Langley Research Center, Hampton, Virginia

A pyroionic detector that is infrared sensitive and functions near room temperature was developed as a replacement for the semiconductors and pyroelectric materials normally used in infrared detectors. Semiconductors are limited in their usefulness because of the necessity of being maintained at cryogenic temperatures, while pyroelectric detectors are sensitive to vibrations and have detectivities which are below the radiation noise limit and, thus, are often smaller than would be useful. Ionic materials, LaF_3 in particular, may have a higher detectivity than others that operate near room temperature, and they are not vibration sensitive as their piezoelectric coefficient is so low that it has not been measured.

Many ionic solids, particularly the rare-earth trifluorides, exhibit a strongly-temperature-sensitive ionic conductivity and surface polarization capacitance. The combination of these effects is referred to as the pyroionic effect to distinguish it from the pyroelectric effect, a phenomenon associated with ferroelectric materials. This temperature variability can provide the basis for a bolometer-like device (see Figure 1) that is sensitive to radiation ranging from ultraviolet to microwave frequencies. However, the principal use for such detectors is in the infrared-to-microwave part of the spectrum.

Radiation strikes a thin black layer, chosen to absorb radiation in the frequency interval to be detected. (This layer can be eliminated if the frequency interval lies in the range where the pyroionic material has a strong absorption band.) Next is a thin (~0.1 μ to 0.5 μ) conducting layer which serves as an electrical contact. A thin metal contact is also deposited on the back surface of the pyroionic material. The detector circuit is the combination of a battery, the device, and a load impedance. The signal voltage is developed across the load.

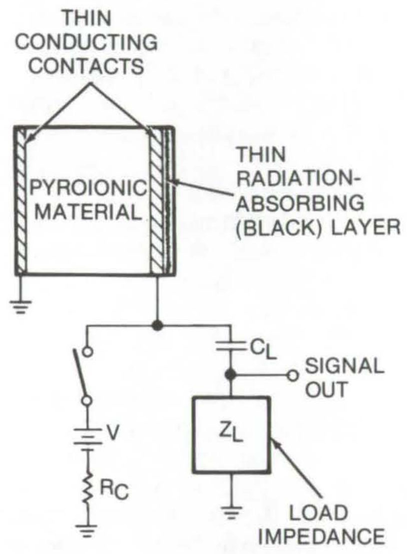

Figure 1. The **Detector Circuit** is a combination of a battery, the device, and a load impedance.

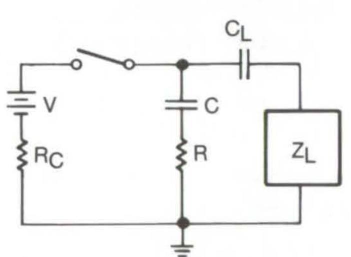

Figure 2. The **Equivalent Circuit** of the infrared detector is a series resistance (R) and capacitance (C).

The equivalent circuit of the device can be represented by a series combination of a capacitance (C) and a resistance (R). Thus, with a load (Z_L), the circuit of the system is as shown in Figure 2. When charged to voltage (V) and the device is functioning, the switch is opened to avoid noise generated by the battery. Capacitor (C_L) is chosen to be large compared to capacitor (C) as its purpose is to prevent the device from discharging through the load.

Since the capacitance in pyroionic materials is dominated by a surface phenomenon, the effective volume that must be heated to modulate capacitor (C) may be far smaller than the sample volume. This would enhance the sensitivity of the device. Also, if the ambient temperature of the device is increased, then capacitance increases and resistance decreases, but the device time constant stays almost steady. However, since noise-limiting resistance is reduced at higher temperatures, noise is reduced. A detector operating at 400 K would have a detectivity of about 5×10^9 ($Hz^{1/2}cm/W$).

This work was done by Arden Sher of the College of William and Mary for **Langley Research Center.** *For further information, Circle 56 on the TSP Request Card.*

Inquiries concerning rights for the commercial use of this invention should be addressed to the Patent Counsel, Langley Research Center [see page A8]. Refer to LAR-11921.

Separation of Water From Air Samples

A gas chromatograph is modified to separate water from preconcentrated air samples.

Ames Research Center, Moffett Field, California

The analysis of air samples for volatile organic constituents by the combination of gas chromatography and mass spectrometry requires a preconcentration step so that substances which are present in quantities of less than a few parts per billion can be brought up to detectable limits. The preconcentration may be accomplished by passing measured quantities of the air sample through a cryogenic trap to condense the organic substances until a sufficient quantity is obtained for analysis. However, the trapped organics are so greatly diluted by the water content of air that analytical procedures are often compromised by the large amounts of water.

A preparative gas chromatograph with a sorbitol column has been used successfully in a three-part system for separating collected water from organic materials. The first part, a preconcentration subsystem, comprises a collecting trap and a sorption pump that are cooled to 77 K. The air sample is drawn by the pump at a uniform regulated rate through the trap, which is a stainless-steel tube packed with glass beads. After the desired volume of air sample has passed through the collection trap, the trap is warmed, and the condensed water and organics are transferred by a stream of helium carrier gas to a second trap (an open stainless-steel tube cooled to 198 K) connected by valves to a preparative gas chromatograph.

When the second trap is warmed, the vapors are carried by helium onto the sorbitol column in the gas chromatograph. Effluents from the column are collected in the third part of the system (a stainless-steel tube packed with glass beads and cooled to 77 K) until just prior to the emergence of water, as monitored by a thermal conductivity detector. At that time the water is vented, the third trap is warmed, and the organic sample is carried by helium into the analytical system.

The chromatograph column is made of stainless steel, packed with 15 percent sorbitol and 5 percent Igepal on 60/80 mesh HMDS-treated Chromosorb P (or equivalent). The sorbitol column is useful for many compounds which elute prior to water, e.g., aldehydes, pyrans, furans, oxides, and certain classes of terpenes. Other columns may be used, as long as there is a significant difference in retention characteristics for water and the compounds of interest.

This work was done by Bennett J. Tyson and Glenn C. Carle of **Ames Research Center.** *Further information may be found in: "Gas Chromatographic Separation of Water from Cryogenically Collected Air Samples — Enhanced Concentration of Trace Organic Volatiles Prior to GC-MS Analyses," B. M. Tyson and G. C. Carle, Analytical Chemistry, vol. 46, No. 4, p. 610, 1974. No further documentation is available.*
ARC-10890

Books and Reports

These reports, studies, and handbooks are available from NASA as Technical Support Packages (TSP's) when a Request Card number is cited; otherwise they are available from one of NASA's Industrial Application Centers or the National Technical Information Service.

Vapor Corrosion Inhibitors

Effectiveness and materials compatibility of amine nitrites

A report on vapor corrosion inhibitors (VCI's) which is of potential value to those interested in long-term corrosion protection is now available. It is known that any salt which liberates nitrite ions in neutral or alkaline solutions will act to inhibit corrosion. There are many nitrogen-containing organic compounds that react in aqueous solution, whose nitrous acid salts have been shown to be excellent corrosion inhibitors for ferrous metals. The VCI products are a family of such compounds which combine this inhibiting action with controlled volatility. Thus they are available in various volatility ranges.

These solid amine nitrites are slightly volatile at atmospheric temperatures, making possible the prevention of the atmospheric corrosion of the ferrous metals in containers or packages. In application, VCI vapors are transported by convection and diffusion to all surfaces of the metal where they condense, giving a thin layer of crystals. In the presence of even minute quantities of moisture, these crystals dissolve, giving their nitrite ions to the condensed or absorbed moisture, thereby protecting the metal. The volatility of the inhibitors is merely a means of transport.

Where long-term protection is required, dicyclohexyl ammonium nitrite is recommended. This material has a vapor pressure of approximately 0.00012 mm Hg (0.0160 N/m^2), which is one-tenth that of mercury, and since it is not readily dissipated from an enclosed area, it provides long-lasting protection. When rapid initial protection is desired, diisopropyl ammonium nitrite is recommended. The vapor pressure of this material is approximately

(continued next page)

4 times that of mercury and 40 times that of dicyclohexyl ammonium nitrite. A combination of these two incorporates the desirable features of both nitrites, namely, rapid early protection with long service life.

Tests have demonstrated that VCI vapors will effectively protect complex parts or assemblies which are normally difficult or impossible to treat with other types of protectives. The vapors also diffuse into remote corners and small recesses, giving uniform protection within the interior of a wrap. The presence of an oil or other preservative film on the part to be protected does not impair the protection afforded by the vapors. The vapors will not penetrate the oil film but will protect where the film has been ruptured or removed. Further, the ability of VCI's to prevent further rusting of rusted steel has been demonstrated in the laboratory.

Since the vapor pressure of the VCI is low, the material is not lost rapidly through vaporization, if it is not subjected to a free circulation of air. Even when exposed directly to outdoor air at normal temperatures, its retention is remarkable. However, since the VCI is slightly water soluble, it is necessary to provide waterproof barriers to packages subject to rain or any leeching action by liquid water. Subject to these conditions, short-term protection is very easily achieved. Using reasonable care, protection periods of several years are possible.

Tests on nonferrous metals indicate that varying degrees of protection are obtained, while the effects of VCI on nonmetallic materials (such as plastics, protective coatings, rubbers, adhesives, fabrics, woods, inks, leathers, papers, and cork) have also been studied. Toxicity studies with small animals have shown that VCI's are similar in such properties to sodium nitrite (a commonly-used food preservative) and would have about the same degree of hazard.

This work was done by Lawrence A. Bielman of Rockwell International Corp. for the **Marshall Space Flight Center.** *For further information, Circle 57 on the TSP Request Card.*
MFS-19232

Life Sciences

Hardware, Techniques, and Processes

Computer Programs

Occlusive-Cuff Controller

Pressure and time are set automatically for plethysmographic studies.

Lyndon B. Johnson Space Center, Houston, Texas

Occlusive cuffs are a system component used in venous occlusion plethysmography, which is a technique for measuring the change in the volume of a limb segment by interrupting venous blood return without seriously impeding arterial inflow. The cuffs are placed on the limbs proximal to the plethysmograph and are inflated to a specific occlusion pressure for a preselected time period. The change in limb volume during occlusion can be used to determine the capacitance and resistance of blood vessels within the limb. With this technique it is possible to measure blood flow, detect arterial blockages, evaluate venous capacity and competency, and assess the responses of blood vessels to various therapeutic drugs (e.g., vasoactive drugs).

A new occlusive-cuff controller can be set to supply the desired amount of pressure for a given time automatically and may be triggered manually or from the patient's electrocardiograph. Pressurized gas (maximum 2.07×10^6 N/m^2 or 300 psi) is fed to the flow control/regulator and is regulated to within 0.7×10^6 N/m^2 (100 psi) at a nominal flow value of 0.14 m^3/min (5 ft^3/min). The fill/hold and dump solenoid valves are normally closed. Prior to an inflation cycle the fill/hold valve is deenergized (closed) and the dump valve is energized (open) to assure zero pressure in the cuff. The initiation of an inflation cycle opens the fill/hold valve and closes the dump valve. When the desired pressurization of the cuff is achieved the fill/hold valve closes. At the end of the timing cycle the dump valve opens and the cuff deflates.

The cuff inflation is controlled automatically by the electronics control unit. The unit has two time settings of 20 s and 2 min and two pressure settings of 30 and 50 mm of Hg (4×10^3 and 6.7×10^3 N/m^2). Any combination of settings may be repetitively and automatically cycled at selectable frequencies from 30 s to 10 min.

This work was done by J. T. Baker and G. W. Hoffler of Technology, Inc. and W. Hursta of **Johnson Space Center.** *For further information, Circle 58 on the TSP Request Card.*

Inquiries concerning rights for the commercial use of this invention should be addressed to the Patent Counsel, Johnson Space Center [see page A8]. Refer to MSC-14836.

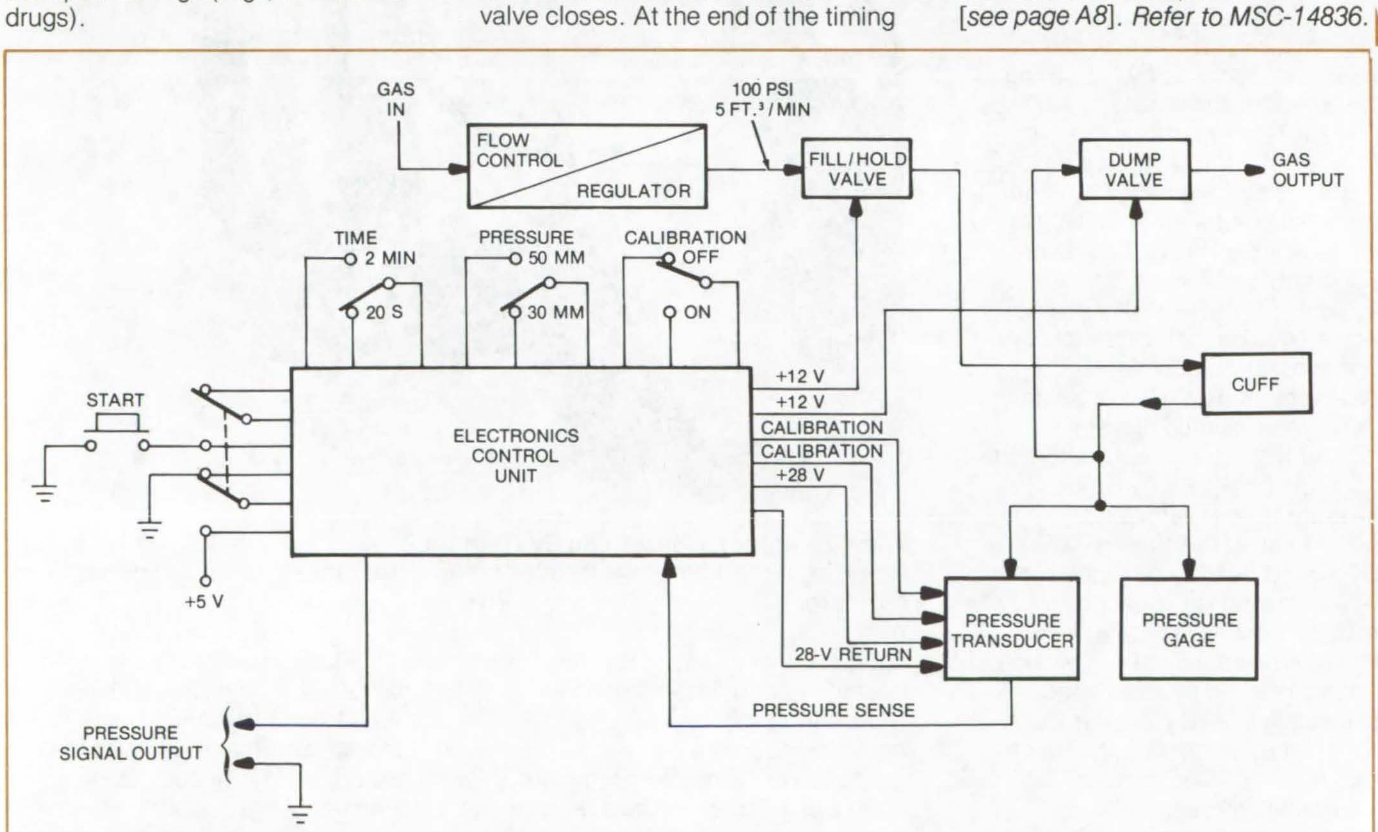

The **Occlusive-Cuff Controller** includes a flow control/regulator, fill/hold and dump valves, a pressure transducer, and a pressure gage, all connected to an electronics control unit.

Firefighter's Breathing System

A new breathing system is lighter and less bulky than conventional apparatus.

Lyndon B. Johnson Space Center, Houston, Texas

There has long been a demand for an improved firefighter's breathing apparatus. Among other problems, conventional systems are heavy and bulky and often interfere with the wearer's mobility. An improved firefighter's breathing system overcomes many of the disadvantages associated with prior devices. It is lighter and less bulky, yet still provides 30 minutes of air supply. Human factors, such as comfort, visibility, donning time, and breathing resistance, have also been improved. The apparatus is simple to recharge and maintain, and its cost is comparable to previously available systems.

The system is based on an open-loop demand-type compressed air concept, which was found to best satisfy the requirements for a moderate duration system at a reasonable cost. The bulk of the vessel was reduced by increasing the air-storage pressure to 4,500 psi (31×10^6 N/m^2), and weight was reduced by using a storage tank (see figure) made from a high-strength composite material: glass fibers in resin, wrapped over a one-piece aluminum liner.

The 4,500-psi air pressure is regulated to breathing demand by a high-pressure reducer and a mask-mounted demand regulator. The frame-mounted pressure reducer regulates pressure from the 4,500-psi (maximum) supply pressure to an intermediate pressure of 80 to 140 psig (0.55×10^6 to 0.97×10^6 N/m^2). The pressure reducer contains two reducing valves in parallel. These are controlled automatically to provide redundancy and to actuate the warning device. The mask-mounted demand regulator is easily detached from the facepiece, and the user can breathe through the large opening in the facepiece while in a nonhazardous environment. The demand regulator incorporates a spray bar that channels the inlet flow over the visor during inhalation to reduce visor fogging. A depletion-operated warning is contained in the demand regulator.

The **Firefighter's Breathing System** includes a light-weight air tank, a frame-mounted pressure reducer, and a facemask-mounted demand regulator.

A flexible facepiece bubble, held in place by a nylon net and a single adjustable strap, provides excellent visibility and sealing, and it reduces helmet/facepiece interference. The small, thin, flexible shell and the restraint simplicity make this facepiece considerably lighter than those currently available. The placement of the components allows a clear frontal area, and the support harness places the apparatus weight on the hips and lower back so as to

reduce shoulder fatigue. The firefighter's breathing system has been evaluated by several cities in actual firefighting and an improvement in firefighting efficiency was demonstrated.

This work was done by Pat B. McLaughlan of **Johnson Space Center;** *Eugene A. Giorgini, John L. Sullivan, and Milo R. Simmonds of Scott Aviation; and Emory J. Beck of Martin Marietta Corp. For further information, Circle 59 on the TSP Request Card.*

This system was developed under NASA contracts and a U. S. Patent No. 3,957,044 has been granted on the automatic redundant fluid pressure controls with fluid actuated alarm. Title to one version of the pressure tank design has been waived to the Martin Marietta Corp. under the provisions of the National Aeronautics and Space Act [42 U.S.C. 2457 (f)]. Inquiries concerning nonexclusive or exclusive license for its commercial development should be addressed to the Patent Counsel, Johnson Space Center [see page A8] Refer to MSC-14733.

Manual Dexterity Evaluator

A hand-controlled tracker is used to measure eye-to-hand coordination.

Langley Research Center, Hampton, Virginia

The manual dexterity evaluator pictured was developed at Langley Research Center to be used, in collaboration with physical therapists, in the study and evaluation of eye-to-hand coordination. Many areas of physical therapy are in need of better, more-quantitative data to define and measure the severity of physical afflictions and to determine the progress of treated patients. This device was designed for use in the area of neuromuscular dysfunction, which includes afflictions such as ataxia, bradykinesia, and tremor.

The manual dexterity evaluator, basically, incorporates a hand-controlled tracker that moves over a horizontal two-dimensional surface. The tracker is relatively inexpensive to construct and very simple to operate. It uses either linear or sine/cosine potentiometers and a transformation logic to locate the position of the bull's-eye of the tracker head. The subject's task is to move the bull's-eye ring over a 900-cm² surface so as to follow a moving image (light spot). The light spot is driven in two dimensions along the path that is chosen to best define the physical disability being tested. Only a few minutes of practice in performing the task are necessary to obtain a leveling off of the learning curve. The data obtained consist of time histories of single-axis error, magnitude of two-dimensional vector error, and other forms of analysis desired of these errors, such as rms, power spectral density, and model matching.

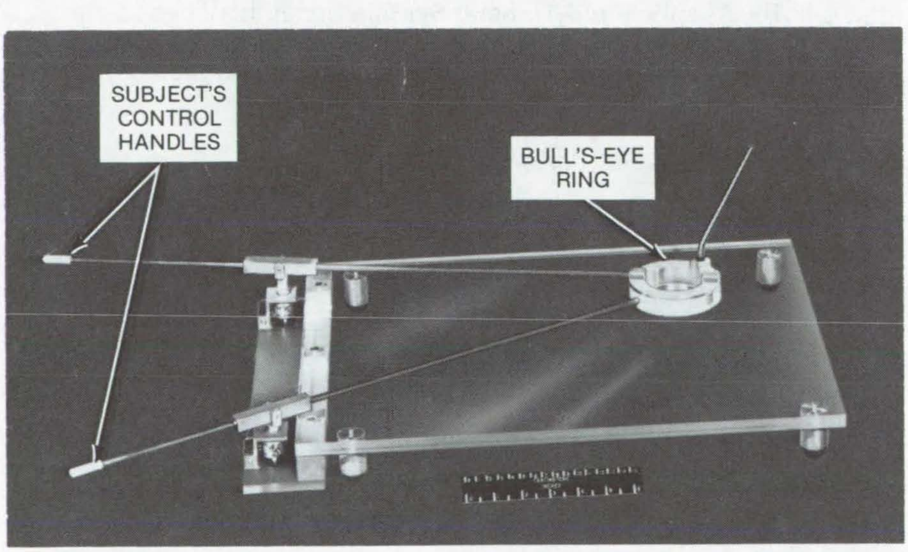

The **Manual Dexterity Evaluator** is operated by using the control handles to make the bull's-eye ring follow a moving light spot.

While the tracker was designed for a specific problem, the basic concept can be applied to several other uses. As a two-dimensional or a three-dimensional tracker or plotter, it can perform as:

An X/Y curve plotter.

- A device to calculate the area under a randomly shaded curve or of an arbitrarily-shaped two-dimensional surface.
- A displacement tracker in either two-dimensional or three-dimensional space.
- Other general measurements in either two-dimensional or three-dimensional space.

This work was done by Hugh P. Bergeron, James D. Holt, and Patrick A. Gainer of **Langley Research Center.** *For further information, including design details and operating characteristics, Circle 60 on the TSP Request Card.*
LAR-12022

Aseptic Fluid-Transfer System

An inexpensive storage and transfer system allows blood and other fluids to be added or removed without contamination.

Caltech/JPL, Pasadena, California

Blood and many other biological fluids are normally stored and handled in a sterile environment to prevent microbial contamination. Special care must be taken when the fluids are transfered from one container to another. For example, blood is commonly stored in a two-bag arrangement. The bags are connected by a tube during fabrication. Blood is first collected in one bag while the other remains empty. When the plasma and red blood cells are separated during blood fractionation, the plasma is expressed into the empty satellite bag. The tube connecting the two bags is then sealed and detached. Although this arrangement is safe it is cumbersome and costly. In addition, nothing can be added to or removed from these bags without the risk of contamination.

A new aseptic fluid-transfer system shown in Figure 1 is simpler, safer, and less costly. On the left side is a conventional sterile container of biological fluid which is fitted with a flexible plastic tube ending with a newly developed terminal. On the right side is an empty sterile container. Shown in the center is a device which clamps the two terminals together. The device heat-sterilizes all external surfaces of the terminals that may become contaminated during handling, and it forms a sterile passageway between the terminals.

Cross sections of the two terminals are shown in Figure 2. Each terminal is a flexible tube fabricated from Teflon, or equivalent, that can be heat sealed at sterilizing temperatures. Bonded around the inside surface, as shown, is a plastic liner that cannot be heat sealed.

Before the fluid is transferred the two terminals are placed together and clamped by the clamping device. The upper jaw of the device is a flat plate; the lower has several raised ridges to direct the flow of melted plastic. The jaws are electrically heated and then cooled through a programed temperature/time cycle. The heating process melts the Teflon which flows away from the raised areas and forms sealed flaps and an opening between the two terminals. The plastic liners stay intact. After the terminals are fused the jaws are cooled and released, leaving the terminals as shown in Figure 3.

The entire process takes less than a minute. It is safe in a contaminated environment because the heat created during fusion destroys the microbes on the Teflon surface.

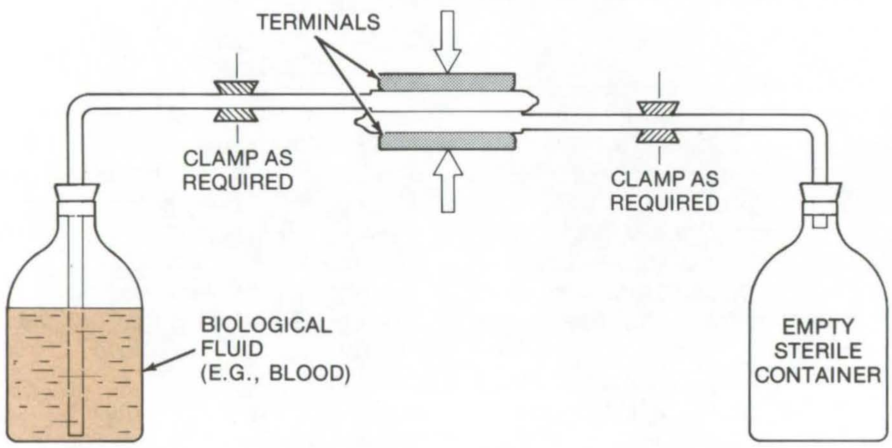

Figure 1. The **Aseptic Fluid-Transfer System** consists of two sterile containers connected by flexible plastic tubing. The key feature is the heating clamp for the terminals, which sterilizes the surface of the plastic tubing.

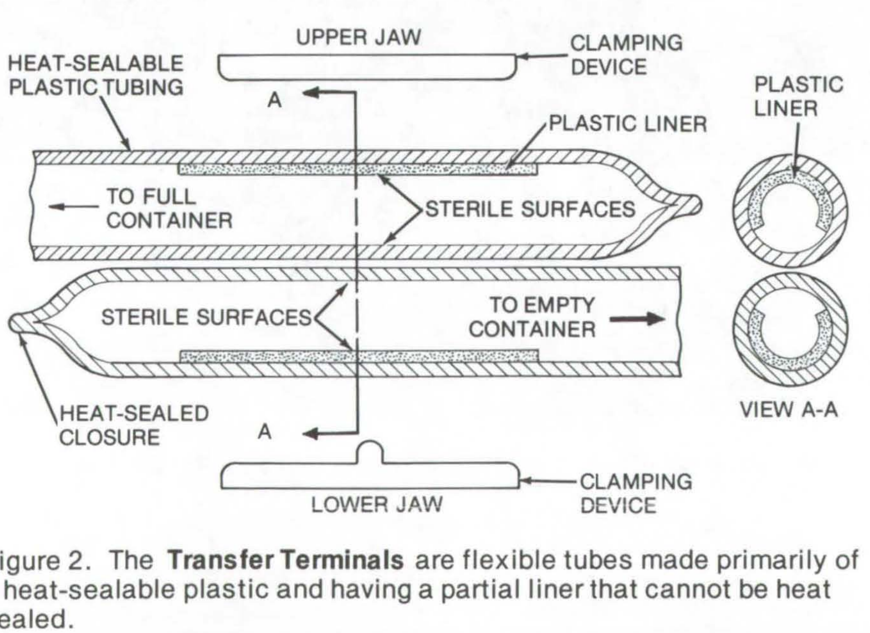

Figure 2. The **Transfer Terminals** are flexible tubes made primarily of a heat-sealable plastic and having a partial liner that cannot be heat sealed.

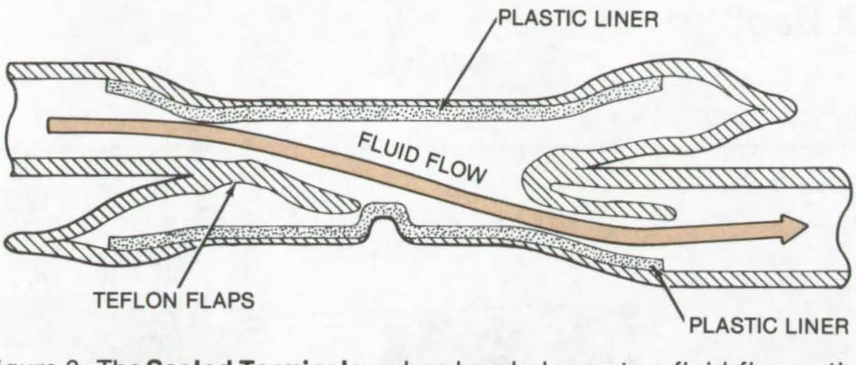

Figure 3. The **Sealed Terminals**, when bonded, create a fluid-flow path because of the opposed unsealable plastic liners.

This work was done by James C. Arnett, Richard M. Berkman, and Edward L. Cleland of **Caltech/JPL.** *For further information, Circle 61 on the TSP Request Card.*

Title to this invention has been waived under the provisions of the National Aeronautics and Space Act [42 U.S.C. 2457(f)] to the California Institute of Technology, Pasadena, California 91109.
NPO-13743

Graphite-Reinforced Bone Cement

Adding chopped graphite fibers improves stiffness and lowers curing temperature.

Caltech/JPL, Pasadena, California

Chopped graphite fibers, when added to surgical bone cement, form a bonding agent with mechanical properties more nearly matched to those of bone. In addition, the curing reaction produces less heat, resulting in reduced traumatization of body tissues.

Preparations of the improved cement are made by adding chopped graphite fiber to a polymethylmethacrylate composition. Weight ratios of 30 percent monomer, 60 percent polymer, and 10 percent fiber work well, but it may be possible to improve this composition.

The addition of graphite fibers has several effects. The stiffness (elastic modulus) is increased significantly without affecting the flexural strength. Compressive strength is reduced, although this problem might be overcome with process improvements. The inhibiting effect of the fibers results in a maximum cure temperature of 55° C, compared to over 100° C for similar test specimens without fibers. In addition, the coefficient of thermal expansion of the graphite-reinforced cement more nearly matches that of bone.

This work was done by Albert C. Knoell of **Caltech/JPL.** *For further information, Circle 62 on the TSP Request Card.*

This invention is owned by NASA, and a patent application has been filed. Inquiries concerning nonexclusive or exclusive license for its commercial development should be addressed to the Patent Counsel, NASA Resident Legal Office — JPL [*see page A8*]. *Refer to NPO-13764.*

Physician's Modern "Black Bag"

A compact medical kit contains most of the instrumentation of a well equipped physician's office.

Lyndon B. Johnson Space Center, Houston, Texas

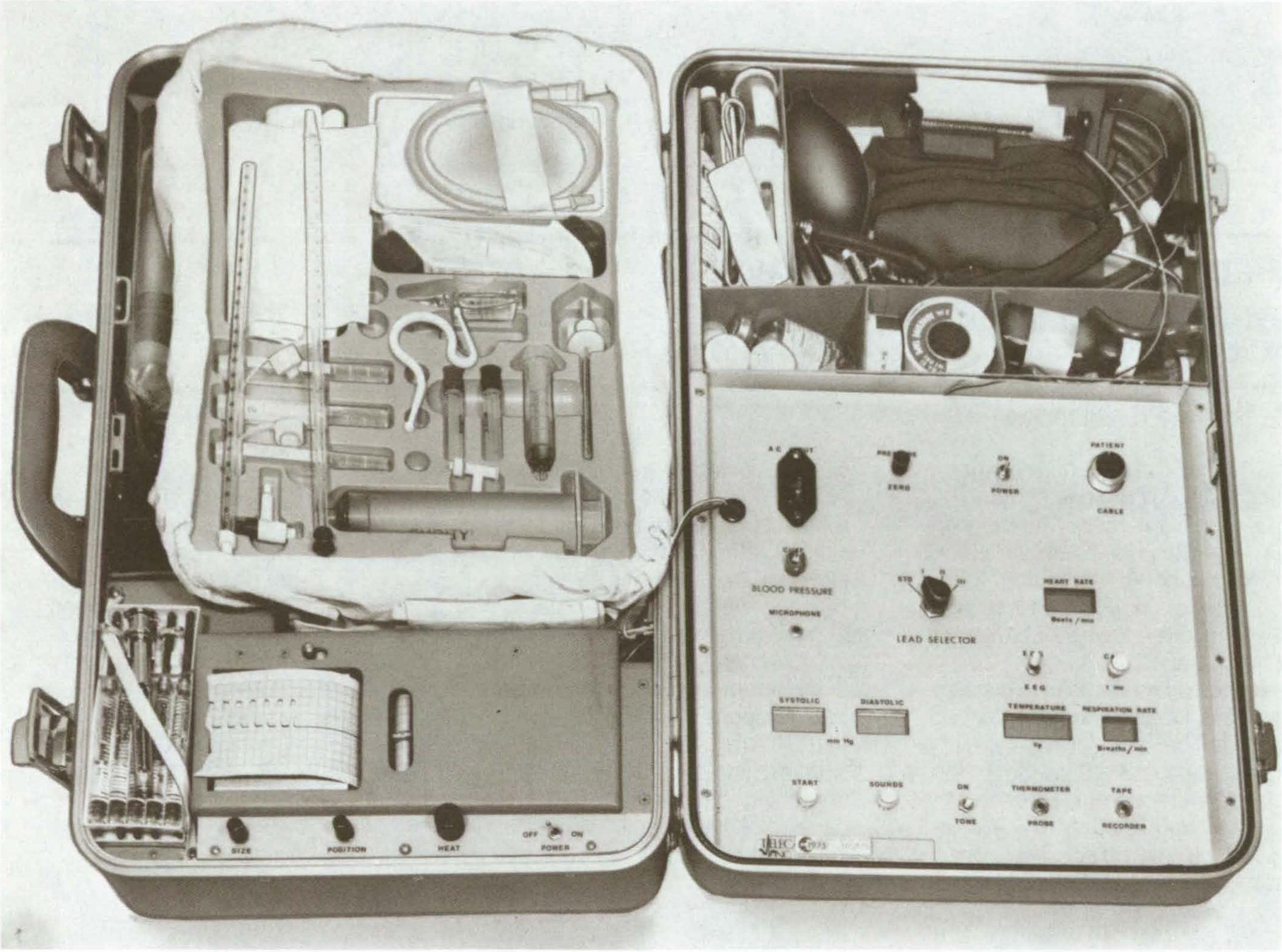

The **Physician's Modern "Black Bag"** is a lightweight, compact package that contains practically all the instrumentation of a well-equipped medical office.

Physicians on house and emergency calls usually carry a familiar "black bag." The bag contains instruments and drugs necessary for on-site diagnosis and treatment. Heavier, more sophisticated equipment is kept in hospitals and doctors' offices to examine the patients more thoroughly. A physicians capabilities for on-site treatment are greatly extended by a new "black bag" that contains practically all the instrumentation of a well-equipped medical office. The entire unit which is packed in a suitcase weighs less than 14 kg (30 lb).

The unit includes the electronic equipment, drugs, bandages, and instrumentation necessary for relatively thorough diagnosis and treatment. It is packed into an 18-cm by 56-cm by 36-cm (7-in. by 22-in. by 14-in.) suitcase for hand carrying.

The electronic components include an electrocardiograph (ECG) and electroencelphalograph (EEG). Data are recorded either on a built-in strip-chart recorder or on a cassette tape recorder, and a built-in telephone coupler can be used for data transmission over a standard telephone line. A single printed-circuit card is used to

control the measurement and display of vital data, such as heart rate, respiration rate, temperature, and blood pressure. The card is also used to precondition ECG and EEG signals for the strip-chart recorder or the telephone.

A small self-contained rechargeable battery pack supplies power for all the electronics. The battery can be used for 12 hours and may be recharged from a standard ac outlet. Battery life is enhanced in this system because the instrument data are displayed with power-saving liquid crystals.

In addition to the electronic equipment, the kit contains nearly 50 other diagnostic instruments and supplies. These include a combination laryngoscope-otoscope-ophthalmoscope, a stethoscope, an emergency supply of drugs, hypodermic syringes, thoracentesis, and spinal-puncture trays. All of this equipment is compactly packaged within the "black bag."

The advantages of the new "black bag" are many: It extends the quality of treatment a physician can administer on emergency and house calls and helps obtain more complete diagnosis prior to hospital admission. Furthermore the electronic instrumentation is sophisticated enough to be used as part of the standard equipment in the physicians office.

This work was done by C. K. LaPinta and J. L. Day of **Johnson Space Center** *and A. E. Schulze and G. A. Zivley of Telecare, Inc. For further information, Circle 63 on the TSP Request Card.*
MSC-14936

Fraction-Storage Unit for Drug-Identification System

In a drug-identification system which simultaneously identifies several drugs via separate, parallel gas chromatographs followed by IR analysis, one of the chromatographs may elute at a faster rate than others. A fraction-storage unit which connects to each chromatograph output and buffer stores the samples until the infrared spectrometer is ready to accept them. It controls storage column input and output and backflushes each after use to clean the column.
(See page 208.)

Precolumn for Extract Concentration

An automated drug-identification system requires that test samples be separated into families of organic compounds for subsequent insertion into several parallel gas chromatographs. A sample is first extracted by selective organic solvents. Solvent is then removed from the extract to increase the extract-to-solvent ratio. This step, which increases system sensitivity, is used with each chromatograph.
(See page 207.)

Automated Solvent Concentrator

When used in an automated drug-identification system, the concentrator reduces the solvent-to-specimen ratio by 100:1. It feeds input material to the analysis subsystem where each sample undergoes filtration in an extraction tube. The filter simultaneously removes particulate contaminants and reduces the sample water content. The sample is extracted from the filtered residue by a specific solvent.
(See page 206.)

Computer Programs

These programs may be obtained at very reasonable cost from COSMIC, a facility sponsored by NASA to make new programs available to the public. For information on program price, size, and availability, circle the reference letter on the COSMIC Request Card in this issue.

Birth/Death Process Model

A first-order Markov model implemented on a digital computer

A computer model has been developed for a population having the following characteristics:

- The population must be composed of entities that have at most three attributes.
- Entities are born into the system and leave the system with definite attribute values.
- Within the system an entity may change its attribute values a number of times.

The system consists of over 22 programs designed to model various attributes of the population and includes the supervisory program POPMOD, which interactively allows the user to select the desired options. POPMOD uses subroutines for its five basic tasks: (1) input; (2) P-matrix generation; (3) iteration; (4) checking, changing input values, and branching at the end of an iteration; and (5) output. The system is user interactive, self-documenting, and does not require the user to have a complete understanding of the underlying model details. It contains thorough error-checking algorithms on input and powerful default capabilities.

In order to make the system convenient to use, restrictions have been placed on the number of attributes allowed within the population and the types of changes in attribute value that are permissible. The system allows the entities to be distinguished through the use of up to three attributes. For a given entity, the value of the first attribute is fixed. The values of the second and third attributes are allowed to increase or decrease one unit at a time or stay as they are. That is, if an entity has the attribute values denoted by the set (X,Y,Z) at a time period t, then the entity could have attribute value sets (X,Y,Z-1); (X,Y,Z); (X,Y,Z+ 1); (X,Y,+ 1,Z-1); (X,Y+1,Z); or (X,Y+-1,Z+1) at time period t+1. These are the only transitions allowed.

FORTRAN
UNIVAC 1108, EXEC VIII

This program was written by Carleton B. Solloway of Caltech/JPL and Wayne Wakeland of Harvey Mudd College for **NASA Pasadena Office.** *For further information, Circle B on the COSMIC Request Card.*
NPO-13616

Mechanics

Constant-Rate Fluid-Delivery System

Mechanical-feedback-regulated modulating valve maintains a constant pressure within a flexible bag, causing fluid to be expelled at a constant rate.

Lyndon B. Johnson Space Center, Houston, Texas

A constant-rate fluid-delivery system was originally developed for a medical intravenous-feeding system. In an early version of that system, a pair of plates squeezed a flexible bag to force out the fluid. As fluid was expelled, the bag changed size; and this caused the contact area between the plate and the bag to change. Thus, although a constant pressure was applied across the plates, both the pressure within the bag and the fluid-delivery rate varied.

This problem has been overcome, and a constant rate of fluid delivery achieved, using a feedback-regulated modulating valve. This relatively simple system maintains a constant internal pressure in the flexible bag. It could be used in a variety of pneumatic control systems or to maintain a constant pressure in viscoelastic materials, as would be desirable in compression molding plastics requiring a uniform density.

The delivery system, as shown in the figure, is operated by pressurized gas that expands a bellows that squeezes the bag. The important new feature is the valve that keeps the pressure within the bag equal to that within the bellows.

As gas first enters the system, it passes by the valve poppet and into the bellows. The bellows expands, and the bag is squeezed between the stationary plate and the movable plate/disk. As it is squeezed, the bag exerts a pressure (equal to its internal pressure) back against the movable plate and disk. When the bag pressure equals the gas pressure at the inlet port, the poppet closes the valve. As fluid is expelled, the bag pressure drops, the disk and poppet move against the bag, and the valve opens.

The fluid-delivery system as described is able to keep flow constant to within $\pm$ 8 percent at low flow rates and to within $\pm$ 5 percent at high flow rates. The valve and the feedback principle could also be used with systems where the bellows are replaced by cylinders, bladders, or diaphragms.

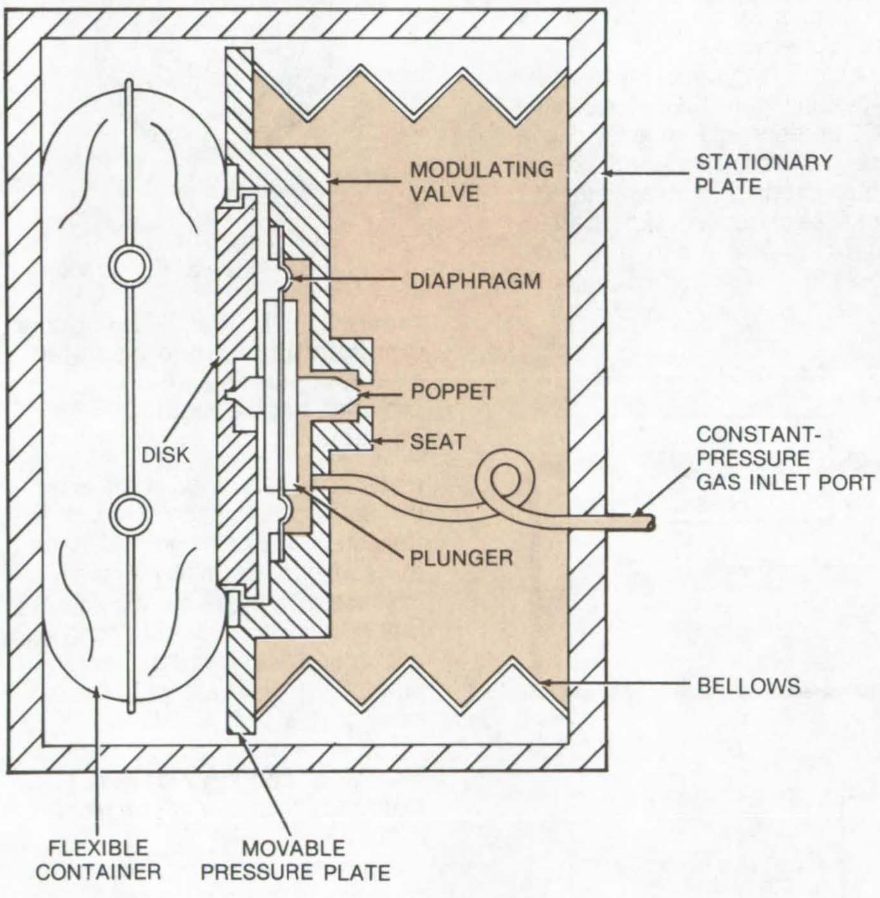

The **Modulating Valve** is shown here as part of a constant-rate fluid-delivery system. The disk and valve are rigidly connected. When the inlet pressure is greater than the internal bag pressure the valve will be open. When the bag pressure reaches the inlet-gas pressure, force on the disk and poppet closes the valve to shut off the gas supply. The valve will open and close as necessary to keep the bag pressure equal to the inlet pressure.

This work was done by D. S. Jacob of Beckman Instruments Inc. for **Johnson Space Center.** *For further information, including performance data, Circle 65 on the TSP Request Card.*

Inquiries concerning rights for the commercial use of this invention should be addressed to the Patent Counsel, Johnson Space Center [see page A8]. Refer to MSC-14905.

ROUS System

Reflection-Oscillator
Ultrasonic Spectrometer System

Langley Research Center, Hampton, Virginia

The ROUS system is a novel ultrasonic generator/monitor that can be used to measure ultrasonic parameters and therefore determine certain physical properties of the region under test. Some applications of the device are to measure noninvasively lubricants and hydraulics for contaminants, changes in stress in metals, bolt tension (an honest stress wrench rather than a torque wrench), and blood and other liquids for particulates, bubbles, or clots. The fundamental parameters measured are the change in mechanical resonance frequency and the change in "Q" of the system, both of which may be related to the monitored physical property.

The ROUS is a closed-loop feedback oscillator and therefore is related to the transmission-oscillator ultrasonic spectrometer (TOUS). Like the TOUS, the ROUS is sensitive, inexpensive, and, for resonance measurements, takes advantage of sensitivity enhancement. Unlike most other continuous-wave (CW) techniques, the ROUS requires contact to only one side of the sample, similar to pulse-echo measurements. However, being CW, the ROUS has high-frequency stability, has no duty-cycle effects, and is relatively simple in both construction and use.

A block diagram of the system is shown in Figure 1. Changes in the "Q" or resonant frequency due to changes in the sample are read out with appropriate instruments. Changes in frequency of 1 part in 10^7 or in "Q" of 1 part in 10^5 are possible. The one-sided contact CW

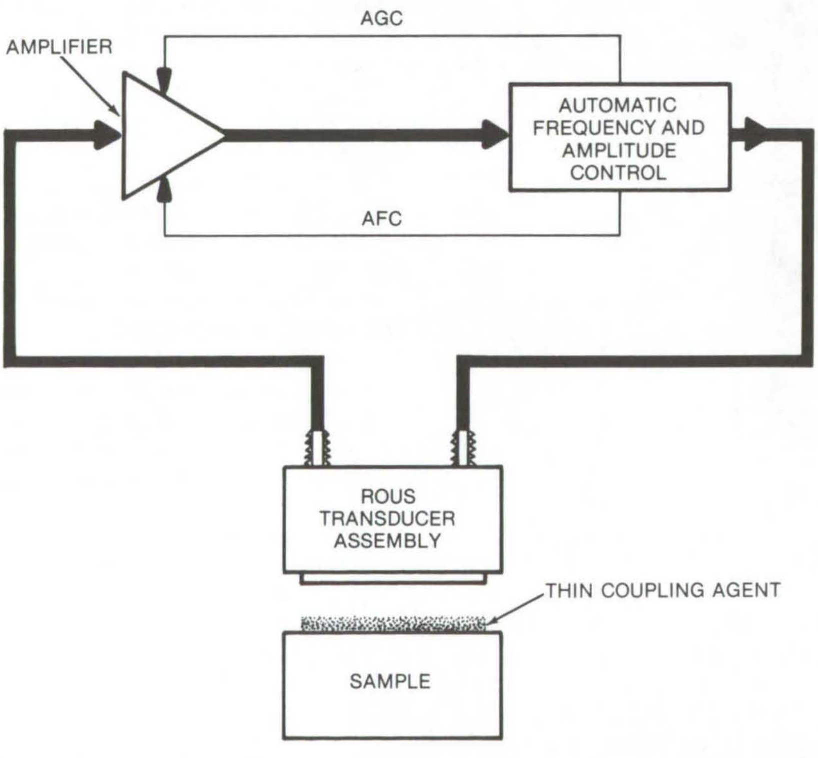

Figure 1. The **ROUS System** includes a transducer in contact with the sample under test: the automatic frequency and amplitude controls are set to operate as a closed loop oscillator at the peak of a mechanical resonance.

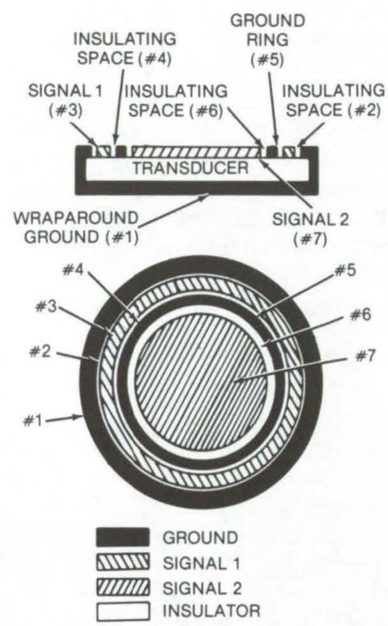

Figure 2. The **ROUS Transducer Configuration** features isolated contact geometry which provides good acoustic coupling.

measurement is made possible by the isolated contact geometry on the transducer shown in Figure 2. With this configuration, high electrical isolation with good acoustic coupling is achieved; and with the closed loop oscillator, the system has many attributes appropriate for both laboratory as well as field use.

This work was done by Joseph S. Heyman of **Langley Research Center.** *For further information, Circle 66 on the TSP Request Card.*

Inquiries concerning rights for the commercial use of this invention should be addressed to the Patent Counsel, Langley Research Center [see page A8]. Refer to LAR-12015.

ROUS Bolt-Tensioning Monitor

The reflection-oscillator ultrasonic spectrometer is used to accurately measure bolt tension.

Langley Research Center, Hampton, Virginia

By measuring changes in the high harmonic resonant frequency of bolts, a bolt-tensioning monitor (see figure) provides accurate information on the stress exerted in the bolts. The monitor features the use of a ROUS (reflection-oscillator ultrasonic spectrometer), which is a closed-loop feedback circuit similar to the TOUS (transmission-oscillator ultrasonic spectrometer). The operating frequency of the system is a linear function of stress in the bolt to which an ultrasonic transducer is attached. The design of the transducer provides high electronic isolation between input and output as well as good acoustic coupling between the reflected acoustic wave and the output of the transducer. The resulting electronics have many applications as they are simple, inexpensive, and flexible.

The torque wrench is the most common device used for tensioning bolts but is inherently inaccurate due to friction. Pulse-echo ultrasonic measurements of bolt elongation are more accurate than torque wrenches but have the disadvantage of not only requiring complicated electronics but also expensive generation and monitoring equipment. The advantages of the ROUS bolt-tensioning monitor are its simplicity, higher accuracy, and potential low cost. Other applications of the device are related to stress measurements for critical loading, physical property monitoring, and use as a strain gage or as a load cell. The electronics and the transducer can be modified for specific applications.

The ROUS bolt-strain monitor makes use of a special transducer incorporating the bolt under test as part of a high "Q" close-loop feedback amplifier/oscillator. The ROUS, with automatic gain (AGC) and frequency (AFC) locking, therefore tracks resonant-frequency shifts related to strain (due to bolt elongation) with either a frequency counter readout (error less than 0.01 percent) or an analog readout of the AFC voltage (95 percent accurate).

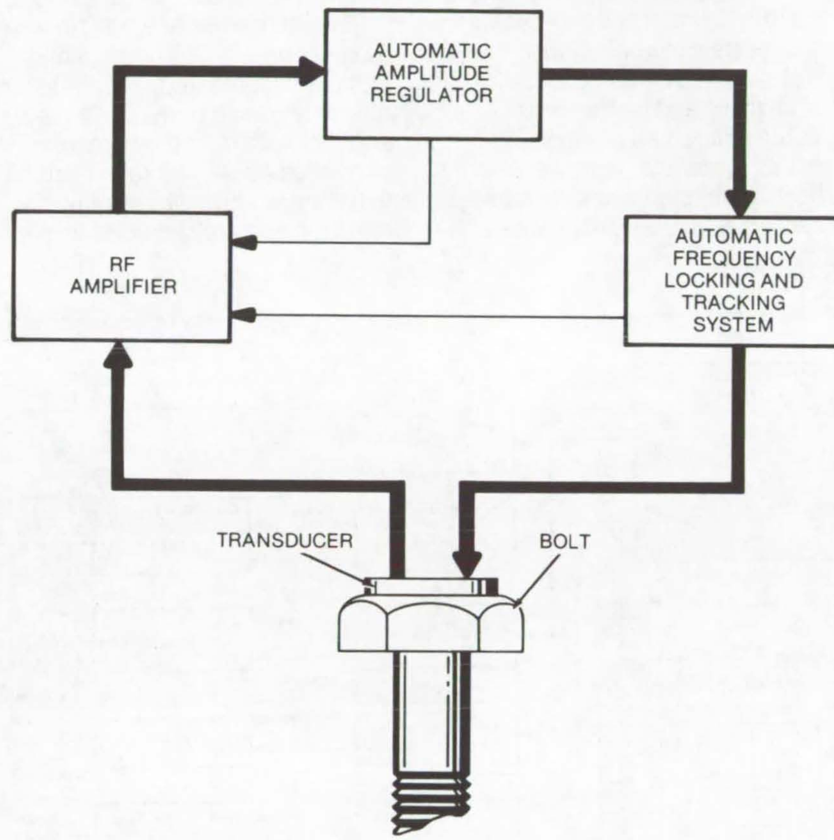

The **ROUS Transducer Assembly** is attached to the bolt, using a thin coating of coupling grease. After circuit adjustments (locking on a mechanical resonance), the bolt is tightened to the desired change in frequency (calibrated while bolt is under stress).

This work was done by Joseph S. Heyman and F. Dale Stone of **Langley Research Center.** *For further information, Circle 67 on the TSP Request Card.*

Inquiries concerning rights for the commercial use of this invention should be addressed to the Patent Counsel, Langley Research Center [see page A8]. Refer to LAR-12016.

Computer-Automated Ultrasonic Inspection System

A computer system automatically analyzes and records ultrasonic weld inspection data.

Marshall Space Flight Center, Alabama

Ultrasonic testing is an excellent nondestructive method for detecting flaws in welds. However, the method is limited by complicated signal analysis and test records. A computer-automated ultrasonic inspection system for weldments has been developed that automatically analyzes and records the test data and the results of the analysis.

The unit can be operated in three modes: manual, automatic, and computer-controlled. The first two modes are used primarily for setup and calibration. In the computer-controlled mode, the results of the test-data analysis are displayed in real time and are recorded on paper copies and in the computer disk files.

As shown in the figure, the system includes an ultrasonic unit, a mechanical scanner, a control console, an ultrasonic head assembly, a computer and the associated electromechanical interface, and a display and paper-copier

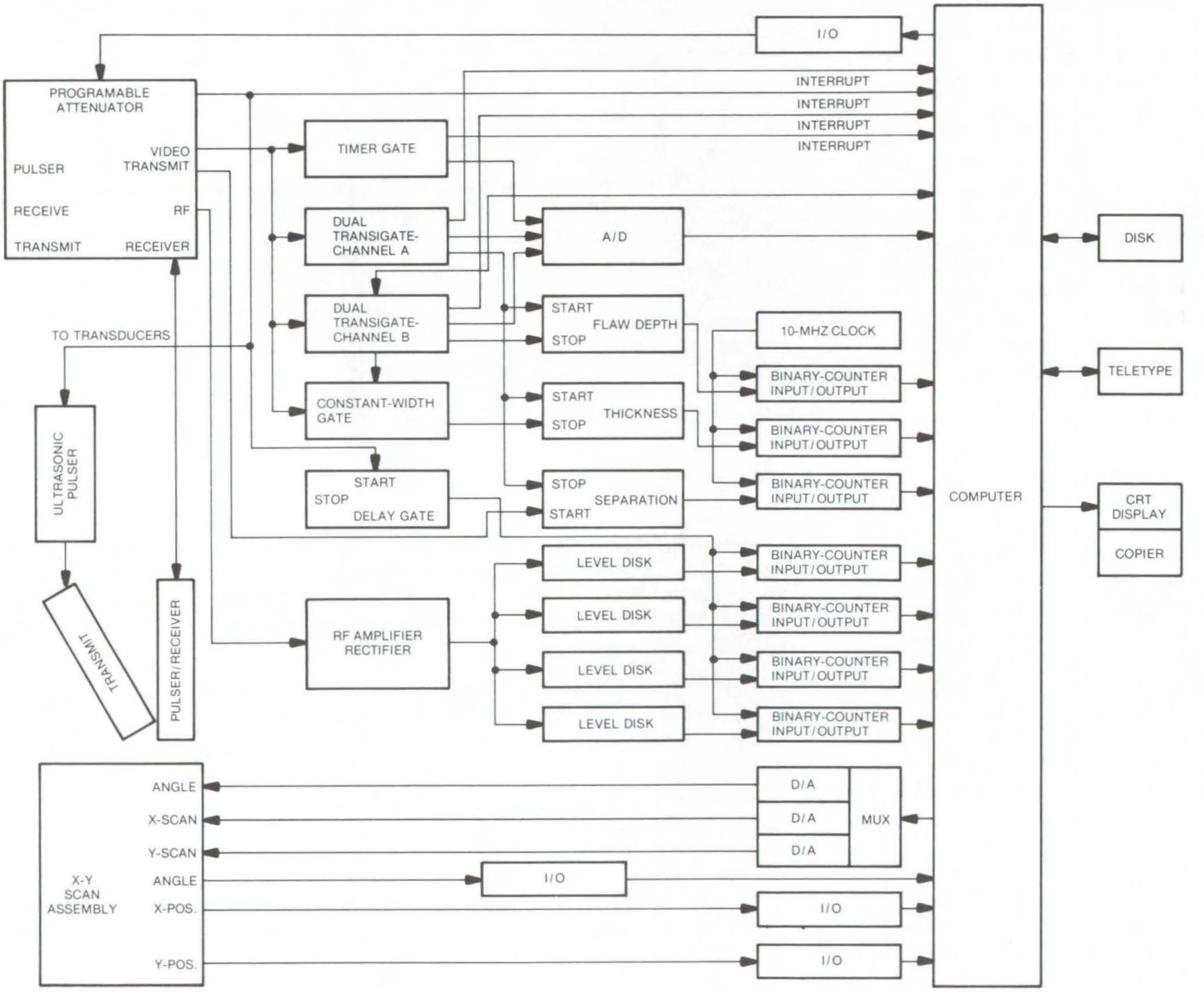

The **Automated Ultrasonic Testing System** consists of four subsystems: (1) the ultrasonic unit; (2) the mechanical scan assembly, control unit, and ultrasonic head assembly; (3) a minicomputer; and (4) the displays. The X-Y scan assembly directs the ultrasonic test beam and indicates its location to the computer. The computer controls the scanner by means of analog signals generated by the D/A converter. The analog output of the ultrasonic unit is converted to digital form by the A/D converter for computer compatability.

unit. The X-Y scan assembly directs the ultrasonic test beam and indicates its location to the computer. The computer controls the scanner by means of analog signals generated by the D/A converter. The analog output of the ultrasonic unit is converted to digital form by the A/D converter for acceptance by the computer.

The computer system includes:

- A 20K memory
- Two disk-cartridge data-storage units with a total capacity of 2.4 million words
- An 8-channel D/A converter
- A 4-channel A/D converter
- A 5-channel D/D converter
- A high-speed paper-tape reader and punch
- Special-purpose counters

The scanner has a speed of from 0.1 to 10 in./s (0.25 to 25 cm/s) in either axis and an index in the alternate axis of from 0.010 to 0.200 in. (0.025 to 0.51 cm) in increments of 0.010 in.

The computer analyzes incoming ultrasonic signals for anomalies. Any anomaly with an amplitude above a predetermined threshold is recorded as a flaw, and it is indicated along with other pertinent parameters. The computer compensates for transducer variations, equipment variations, and far-field effects. In addition, it monitors the liquid coupling between the transducers and the component under inspection and allows inspection to begin only when the ultrasonic energy is adequately coupled into the component under test.

The system may be used with ultrasonic-reflection (compressional-wave), shear-wave, or delta-scan methods for weld inspection. Results are displayed in real time at a selected threshold level. During the post-inspection analysis they can be displayed at any desired level to facilitate the discrimination of critical flaws.

This work was done by D. Dunmyer, A. H. Gardner, E. E. Kerlin, J. S. Kunselman, A. R. Robinson, T. C. Walker, T. G. Wells, and B. G. W. Yee of General Dynamics, for **Marshall Space Flight Center.** *For further information, including descriptions of major subcomponents and ultrasonic equipment, Circle 68 on the TSP Request Card.*

Inquiries concerning rights for the commercial use of this invention should be addressed to the Patent Counsel, Marshall Space Flight Center [see page A8]. Refer to MFS-23338.

Fail-Safe Hydraulic Shaker Protection

Fail-safe system controls the acceleration and force on a structure undergoing vibration stress testing.

Caltech/JPL, Pasadena, California

Seven critical parameters and three optimal parameters associated with the safe operation of an electrohydraulic servosystem are monitored by a fail-safe protection system. The failure of any parameter closes a relay which operates solenoid valves that clamp the hydraulic ram position and shut down power, thereby preventing damage to the test object.

The system has nine channels. Each channel processes a voltage corresponding to one electrohydraulic servosystem parameter. Each channel converts its input into a unipolar voltage which is then applied to a comparator. The comparator determines whether the signal is within specified limits and outputs an appropriate go/no-go command. The go/no-go commands are routed to logic gates which ultimately select the abort commands cutting off the hydraulic power.

A peak acceleration limiter develops an abort command whenever the instantaneous acceleration level exceeds a prescribed value. Two separate channels are used for the peak force/strain limiter to accommodate the two force gages normally used to interconnect the shaker head to a fixture when force measurements are made. If the force or strain exceeds a critical value an abort command is developed.

The other parameters monitored are as follows:

- The excitation signal (5-kHz carrier) for sensors which monitor the position and direction of the hydraulic ram
- The dither signal (815 Hz) applied to the hydraulic ram to minimize static friction (which produces erratic ram motion)
- The excessive dither signal (which could cause servo valve wear or servoamplifier overload)
- Three critical voltages associated with the servo power amplifier: +300 volts, -300 volts, and -600 volts
- Displacement of the hydraulic ram beyond safe operating limits.

The system also has a manual abort which is independent of the electronics.

This work was done by Raymond C. Woodbury of **Caltech/JPL.** *For further information, Circle 69 on the TSP Request Card.*
NPO-13726

Pump Failure Monitor

High-frequency vibration analysis predicts failure in pumps.

Marshall Space Flight Center, Alabama

A high-frequency vibration analysis technique, originally developed for the detection of ball-bearing defects in a control-moment gyro, is utilized to diagnose potential failures in pumps. The concept is based on the fact that when a mechanical component is impacted, it will ring (vibrate) at one of its natural (resonant) frequencies, normally at the lowest mode. When the lower modes are restrained by mounting clearances, the component will resonate at higher unrestrained modes. The high modes are usually not entirely restrained; extremely small deflections associated with high force (g) levels are smaller than the dimensions of the surface finish imperfections of the mating surfaces.

The diagnostic technique compares the spectra of a pump mechanism in service against a plot of an identical pump which has compiled only a few hours of service life. The spectra, viewed on a real-time analyzer, are first electronically processed to strip away the low-frequency components, leaving only the high frequencies for viewing. This signal transformation process is called envelope detection and is identical to the method used in a broadcast radio receiver to recover audio signals from the IF carrier.

A set of accelerometers connected to the pump are used to feed signals from the pump to a frequency-modulated tape recorder. The tape recorder is operated at 30 ips (76.2 cm/s); however, the FM electronics for 7.5 ips (19 cm/s) are used. This is done to reduce FM center-frequency pick up on the direct channels. The frequency response of the direct channels is 0.2 to 100 kHz. The frequency response of the FM channels is 0 to 2.5 kHz.

After the signal has been transferred via envelope detection, it is passed through a filter network to determine the repetition rate of the highest amplitude frequency component. The source of impact or rub within the pump is thus located.

The following steps summarize the technique:

- High-frequency resonances are identified, and their amplitudes are measured.
- The resonance is band-pass filtered and demodulated.
- The frequency content of the demodulated signal is determined.
- From knowledge of the excitation and pump mechanism the excitation source is found.
- The amplitude of the signal at the given frequency is observed.
- Pump condition is determined based on the amplitude of resonance and envelope frequency content.

This work was done by John L. Frarey, Donald S. Wilson, and Richard F. Burchill of Shaker Research Corp. for **Marshall Space Flight Center.** *For further information, including test setup and procedures, Circle 70 on the TSP Request Card.*
MFS-23366

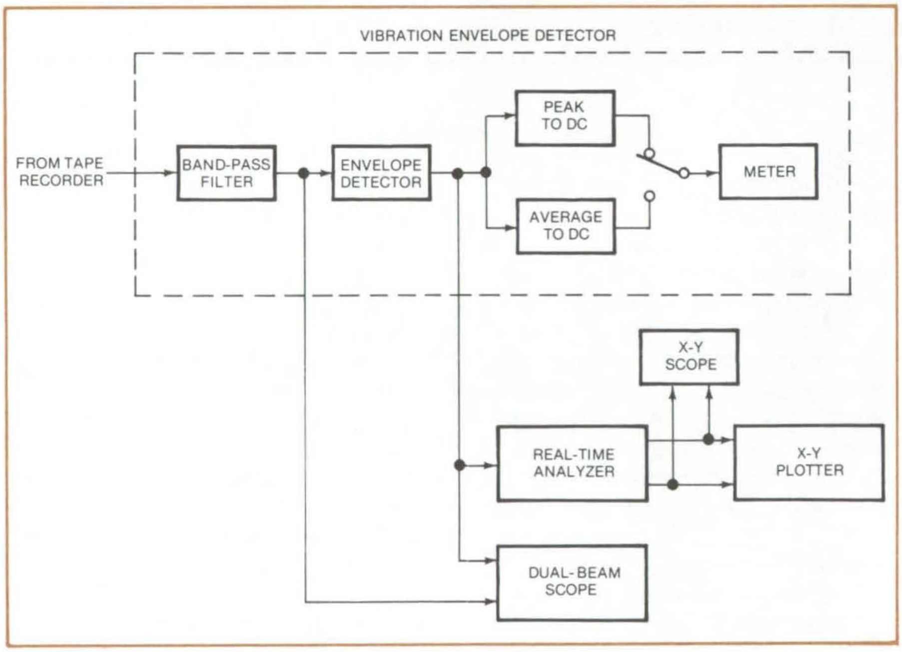

For **Data Reduction for Envelope Characteristic Identification,** signals from a frequency-modulated tape recorder are fed to a vibration envelope detector (VED) to produce real-time analyses of the filtered wave shapes.

Vapor/Liquid Interface Sensor

A fluidic circuit senses the level of liquid nitrogen in a pipe or container by responding to pressure changes.

Lyndon B. Johnson Space Center, Houston, Texas

A method of detecting a vapor/liquid interface has been developed to sense liquid nitrogen in a pipeline or to sense the liquid-nitrogen level in a container. Conventional methods employ electrical sensors and valve controllers. Because there is considerable condensed moisture associated with liquid nitrogen, the electrical sensors and valves are subject to corrosion.

In this technique, (see figure) air flowing through a small tube serves as the sensor. The oxygen in the air is liquefied when it is in contact with the cryogenic nitrogen. This liquefaction causes a pressure drop in the tube. The pressure drop then is sensed and amplified by a fluidic circuit. A signal at one of the outputs (O_1 or O_2) indicates whether the sensing tube is in or out of the liquid nitrogen.

This work was done by Jack E. Briegy of **Johnson Space Center.** *No further documentation is available.*
MSC-12474

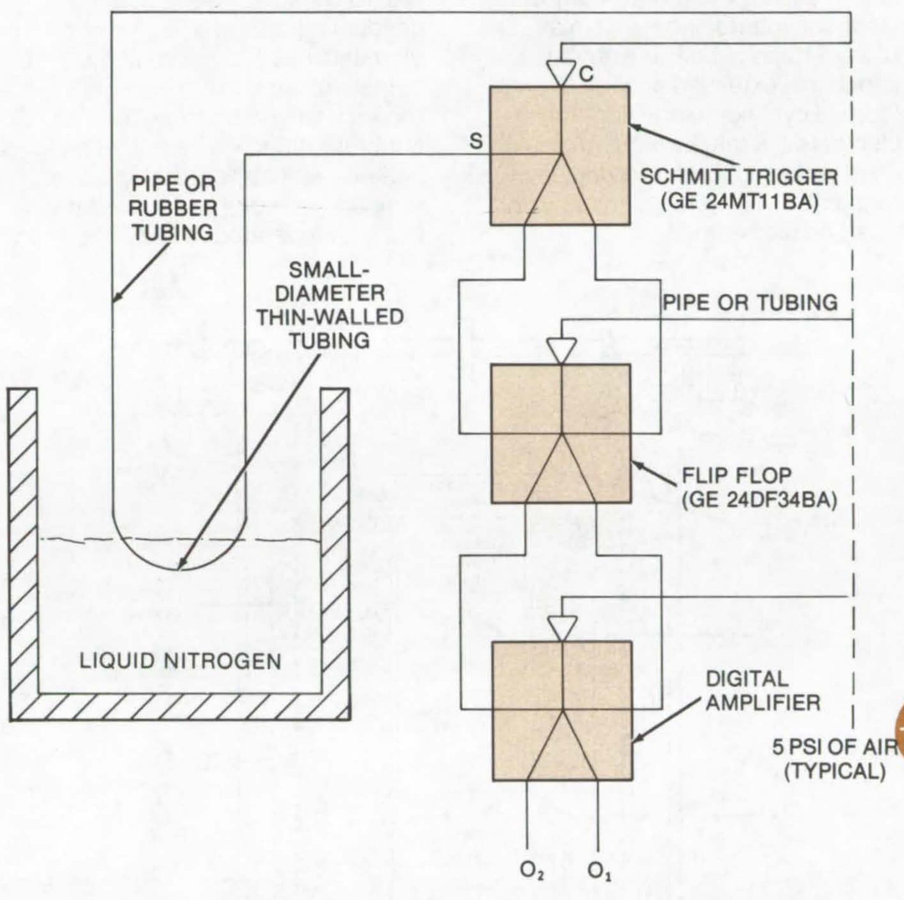

In the **Vapor/Liquid Interface Sensor** the oxygen in the air under pressure in the thin-walled tube is liquefied when it contacts the cryogenic nitrogen. The liquefaction causes a pressure drop in the tube, which is sensed and amplified.

Improved High-Temperature Heater With Stabilized-Zirconia Elements

Improved conducting-ceramic heating elements extend performance and life expectancy of 2,100° C furnace.

Marshall Space Flight Center, Alabama

Improvements in ceramic oxide quality and in platinum-to-ceramic electrode interfacing result in a reliable furnace heater element capable of extended and rapid thermal cycling. In addition, these elements operate in vacuum or in inert, reducing, and oxidizing environments, adding to their versatility as an ohmic heater.

A furnace (see Figure 1) fabricated from stabilized-zirconia conducting-ceramic heater elements has been used at 1,940° C to melt a platinum/20-percent rhodium alloy. The same furnace structure, fitted with a pair of main heater elements for axial gradient temperature control, (see Figure 2) has been operated at 2,050° to 2,100° C during the melting of high-purity alumina. A shorter, 7.6-cm-long, secondary heater element consisted of a platinum/10-percent rhodium alloy. The primary heater element (stabilized-zirconia ceramic) was placed on top of the secondary. The axial temperature gradient was 250° C/cm based on the heater-element wall temperature. These temperatures do not reflect the upper bounds for the furnace element; rather they are limits relative to the instrumentation used.

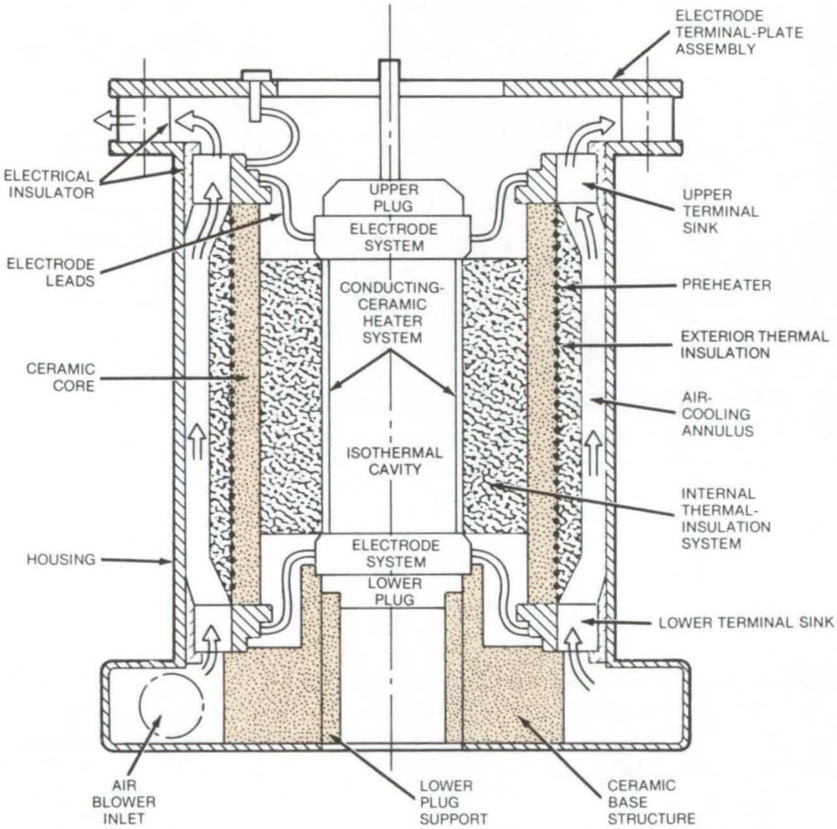

Figure 1. The **Isothermal Furnace** has three insulation systems: (1) the internal insulation system between the ceramic heater and the preheater, (2) the exterior system between the preheater and air-cooling annulus, and (3) the upper and lower plugs. The plugs control direct axial thermal losses, and the internal and external systems control radial losses. By proper sizing of the insulation system, preheating can raise the cavity temperature enough to ignite the main heater without overheating the preheaters.

These characteristics are in part due to the comparable and linear thermal-expansion properties of ZrO_2 and platinum. Therefore platinum metal can be used with the stabilized zirconia-ceramic heater element for forming an electrode interfacing the flow of electrons with oxygen ions. Zirconia was selected for both the isothermal and the axial gradient furnace systems because it contributes increased strength and reliability.

The geometry of the parallel tubes also improves the resistance to thermal stresses. For moderate rates of temperature change, thermal-stress resistance is inversely proportional to specimen dimensions. For very high rates of change, this size effect is only important for small dimensions. In general, sharp corners or edges and parts with adjacent thick and thin sections should be avoided.

Transient response (e.g., cooldown tests) was excellent. For example, a command for a 100° C lower setting had a 99-percent response in 25 seconds. With an industrial solid-state power controller, cavity-temperature error was less than ±1° C.

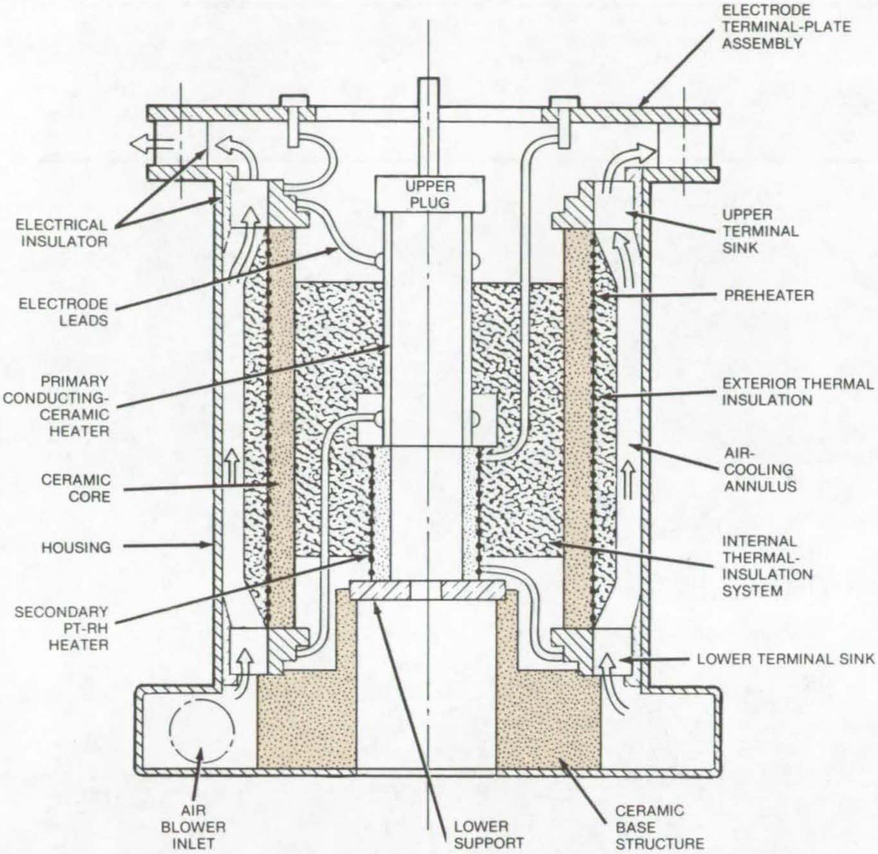

Figure 2. The **Axial Gradient Furnace** has a two-zone heater element. The housing, base, preheater, and external physical dimensions are identical to those of the isothermal furnace. Two heater-element zones are controlled separately. Nominal working cavity size is 2.5 cm in diameter and 10.0 cm long.

This work was done by Carl R. Halbach and Russell J. Page of Advanced Research and Technology for **Marshall Space Flight Center.** *For further information, including system operating parameters, Circle 71 on the TSP Request Card. MFS-23351*

Simplified Deflection-Coil Linearity Testing

A mask placed over the face of an image-dissecting photomultiplier tube has a precision array of pinholes that permit light to impinge on the tube at known points. Signals are fed to the deflection coil which sweeps the beam across each point to be recorded; tube/coil linearity is thus determined without complex operator procedures.
(See page 189.)

Chemiluminescent Prediction of Service Life

The oxidation degradation of polymers and other organic materials is predicted under actual expected-use conditions. Very-low-intensity light emission, which occurs during degradation, is monitored under actual-use temperatures, e.g., from 20° to 150° C. This data can be used to calculate an actual rate of degradation.
(See page 199.)

Transistor-to-Substrate Bond Quality

X-ray images of bonded power transistor chips are interpreted by using a light meter to examine the images to determine the percentage of voids in the bond. The light meter provides a quantitative measurement of void area. X-rays of identical assemblies are always taken at identical machine settings.
(See page 151.)

Hot-Wire Probe

A platinum probe measures turbulence at high temperatures and hypersonic velocities.

Ames Research Center, Moffett Field, California

A high-temperature hot-wire probe can be used to measure turbulence and Reynolds shear stresses in high-temperature compressible flows. It is especially suitable for measurements in hypersonic boundary layers since it does not vibrate at high velocities and does not react like a strain gage on warmup.

The probe is made from a platinum/platinum alloy mounted on a rigid high-temperature ceramic support of special design. The diagram illustrates typical arrangements for dual and triple hot-wire probes. The space between the supports is filled with a high-temperature alumina-based ceramic paste that has an alumina content high enough to ensure formation of a rigid high-temperature ceramic upon curing. After curing, the ceramic filler between the hot-wire supports is ground to sharp wedges in which the steel supports are just exposed at the faces of the wedges.

Filaments of platinum/10 percent rhodium, 5 to 10 μm in diameter, are spot welded onto the exposed leading edge of the steel supports. The precious-metal wires are cemented to the leading edge of the exposed ceramic insulator by a thin layer of liquid ceramic. After the cement has cured, a current is passed through the precious-metal filaments, and the current is increased in steps until the filaments appear red hot. Finally, the ceramic is carefully removed from the forward parts of the filaments.

Inasmuch as the precious-metal filaments are supported along their entire lengths by heat-resistant ceramic, they can be operated in the high temperatures of supersonic wind tunnels (e.g., 1,300° C) without risk of destruction, and they can be depended upon to give accurate measurements.

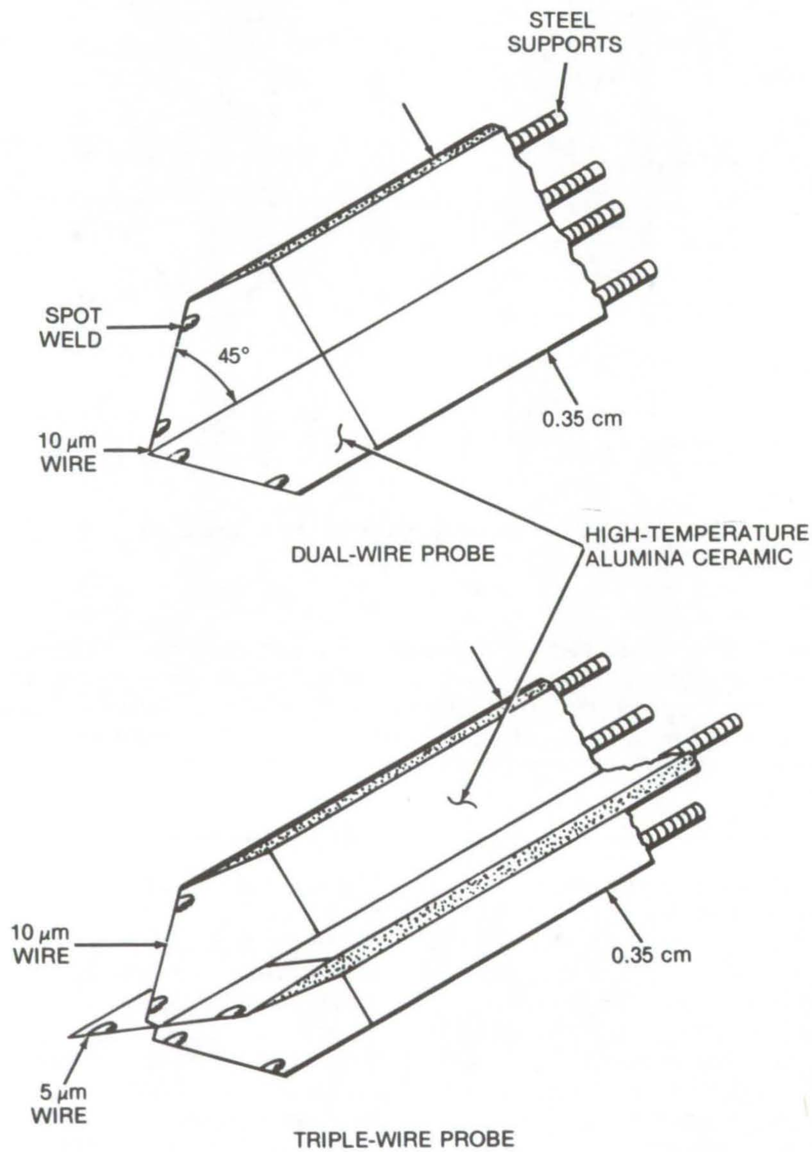

Dual and Triple Hot-Wire Probes are shown. The hot wire is made of a platinum/platinum alloy, and the supports are ordinary hot-wire stainless steel.

This work was done by Volker Mikulla of **Ames Research Center.** *For further information, Circle 72 on the TSP Request Card.*

This invention is owned by NASA, and a patent application has been filed. Inquiries concerning nonexclusive or exclusive license for its commercial development should be addressed to the Patent Counsel, Ames Research Center [see page A8]. Refer to ARC-10900.

"Thermal-Diode" Heat Pipe

A heat pipe transfers heat in one direction and blocks heat transfer in the other.

Ames Research Center, Moffett Field, California

In certain cases, such as a highly-variable thermal environment, it is desirable to vary the heat-transfer characteristics of a heat pipe so that flow in one direction is greatly inhibited. For example, when the space radiator of a satellite-borne heat pipe that is designed to cool electronic equipment is exposed directly to the Sun, the heat pipe must not transmit in the reverse direction and overheat the electronic equipment. Normal, reversible heat-pipe action can be inhibited by introducing a section between the condenser and the evaporator to act as a "thermal diode", that is, a section that transmits heat efficiently in one direction and very inefficiently in the other direction.

Normal heat-pipe operation can be modulated by mechanical means such as thermally controlled valves or by passive techniques, such as freezing the working fluid, noncondensable gas blockage of the vapor space, inclusion of excess working fluid to block the vapor space, or a liquid trap to dry out all or part of the wick.

In an application requiring the transmission of 20 watts in one direction at a minimum conductance of 2.25 watts per degree (K) and not more than 1.4 watts in the reverse direction with a maximum conductance of 0.01 watt per degree, blockage by excess liquid was found to be the most suitable method. A shutoff temperature of 27.7° C (82° F) made impractical a "diode" action based on freezing the working fluid. The relatively-large reservoir volume required for the noncondensable gas blockage technique was too bulky and too heavy.

When a heat pipe is charged with an excess of working fluid, there will be a strong tendency for the excess to accumulate as a slug in a colder portion of the pipe, except when it is displaced by surface tension or by gravity. Because of its low conductivity, the liquid effectively limits the rate of heat transfer between two sections of pipe. Thus the "diode" section consists of a cold zone between the evaporator and the condenser where excess liquid can accumulate and interfere with the transfer of vapor.

To overcome the effects of gravity, the vapor space in the blocked section of the shutoff "diode" must be thin enough to insure that capillary forces will support the pressure head of the liquid slug. (The vapor space must self-fill with liquid and remain filled in the reverse mode.) Naturally, this can impose thin vapor spaces and concomitant large vapor pressure drops during normal heat-pipe operation.

Satisfactory "diodes" have been produced with spiral arteries fabricated from stainless-steel screen and tubing that provide large film coefficients and adequate vapor cross sections. A 6-percent overcharge of ammonia at 30° C (86° F) was found satisfactory.

This work was done by John P. Kirkpatrick of **Ames Research Center** *and Burton Swerdling and Robert Kosson of Grumman Aircraft Corp. For further information, Circle 73 on the TSP Request Card.*
ARC-10997

Fatigue Life of Spur and Helical Gear Sets

A mathematical model for determining surface fatigue life of spur and helical gears.

Lewis Research Center, Cleveland, Ohio

Gears used in power transmissions may fail in several different ways — such as tooth breakage caused by high bending stresses in the gear teeth, scoring of the gear tooth surface due to an inadequate lubricant film, or surface pitting caused by high surface contact stress. Design techniques have been developed for the prevention of the tooth breakage and scoring problems. However, surface pitting will eventually end the useful life of even the best designed gear. The problem was how to accurately predict the time to failure.

The fatigue life model by Lundberg and Palmgren is the commonly accepted theory for determining the fatigue life of rolling-element bearings. A life theory similar to Lundberg and Palmgren's theory was derived for surface fatigue life of gears.

The factors affecting gear life are number of stress cycles, maximum critical stress beneath the gear surface, the depth below the surface at which the critical stress occurs, and the total amount of stressed volume of gear material. The theory can also be used to calculate the dynamic capacity, which is defined as the transmitted tangential load which gives a 90-percent probability of survival of the gear set for 1 million pinion revolutions.

It was assumed that the gears were geometrically ideal with no profile errors or tooth spacing errors. The effect of dynamic loads induced by tooth flexibility and gear inertia was neglected. Uniform line contact between mating gear teeth was assumed.

The equations, when simplified by setting the helix angle to zero, can then be used for spur gears. Fatigue tests were conducted using vacuum-arc-remelted AISI 9310 steel spur gears. The theory and experimental results were in close agreement.

This work was done by Dennis P. Townsend and Erwin V. Zaretsky of **Lewis Research Center** *and John J. Coy of the U. S. Army Air Mobility R&D Laboratory. Further information may be found in:*

NASA TN-D-8045 [N75-30564] "Life Analysis of Helical Gear Sets Using Lundberg-Palmgren Theory" and

NASA TN-D-8029 [N75-29434] "Analysis of Dynamic Capacity of Low-Contact-Ratio Spur Gears Using Lundberg-Palmgren Theory."

Copies of these reports may be obtained at cost from the New England Research Application Center *[see page A7]*.

LEW-12596

Faster X-Ray Analysis of Semiconductor Wafers

By bending the wafer, the useful X-ray flux is increased, and the exposure time reduced.

Marshall Space Flight Center, Alabama

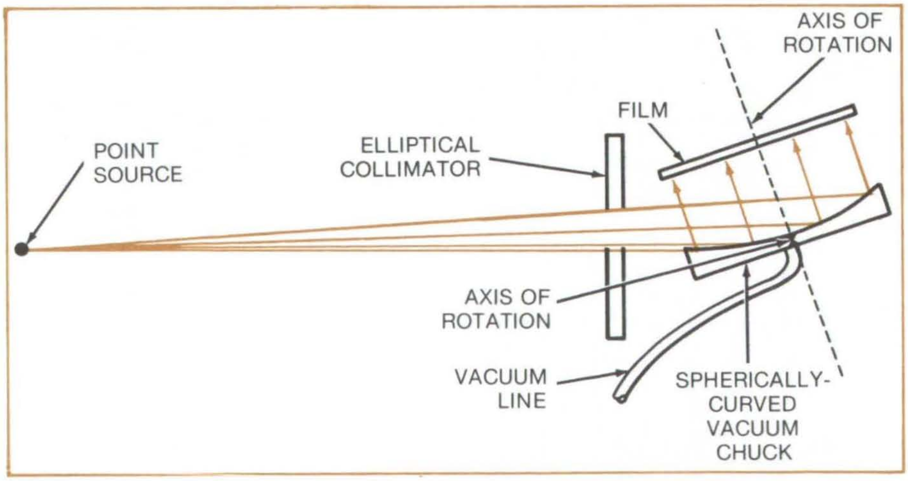

The **Bent-Crystal X-Ray Camera** is a modified Berg-Barret system. The wafer may be rotated about two axes through its center: one in the plane of the figure and one perpendicular to that plane.

X-ray topography is probably the best nondestructive test for damage to the crystal lattice of semiconductor wafers. For most manufacturers, however, the cost of equipment and the time required for an exposure make the process too expensive for production testing. By reducing the exposure time at least an order of magnitude, a new X-ray camera significantly reduces the cost per topograph.

The new camera, shown in the figure, features a vacuum chuck that bends the wafer such that the X-rays from a point source simultaneously satisfy the Bragg condition for a given set of lattice planes. Thus the instrument is able to incorporate

Rowland focusing. The ideal shape of the chuck (and thus of the elastically deformed wafer) is an exponential spiral.

No satisfactory method was found to accurately machine the exponential spiral within required tolerances, and a concave spherical shape was chosen instead. However, no single setting of the spherically deformed wafer will diffract X-rays simultaneously from the entire wafer surface. To compensate, the crystal and film are rotated on an axis through the center of the wafer and perpendicular to the central scattering plane.

Attached to the face of the chuck is a flat edge to match the wafer flat and allow a sequence of wafers from the same batch to be photographed with a minimum of individual adjustments. With this configuration one person can take from 20 to 30 topographs per hour. Proposed improvements could possibly double this throughput.

This work was done by D. L. Parker and W. A. Porter of Texas A. & M. University for **Marshall Space Flight Center.** *For further information, including camera specifications and experimental procedures, Circle 74 on the TSP Request Card.*
MFS-23315

Attenuation of Sound in Ducts with Acoustic Treatment

A generalized approximate equation for duct-lining sound attenuation can be used for design and analysis.

Lewis Research Center, Cleveland, Ohio

A generalized approximate equation for duct-lining sound attenuation has been written. The equation can be used for initial acoustic-liner design as well as to provide an understanding of the duct sound-propagation problem usually obscured in the exact calculation.

Previous approximate sound-attenuation equations by P. M. Morse [P. M. Morse, "Vibration and Sound," 2nd edition (McGraw-Hill, New York, 1948)] are valid for nearly hard walls and give good results over a limited range. However, as the liner resistance is reduced and the exact calculations using the wave equation predict higher sound attenuations, the Morse approximate equations become inaccurate.

The generalized approximate equation is based on the nearly circular shape of the constant attenuation contours in the wall acoustic impedance plane. This circular approximation is illustrated in the figure. The specifications of two parameters, the peak attenuation and the optimum impedance, completely determine the sound attenuation for any acoustic mode at any selected wall impedance. For impedances far from the optimum, the generalized equation reduces to Morse's approximate expression.

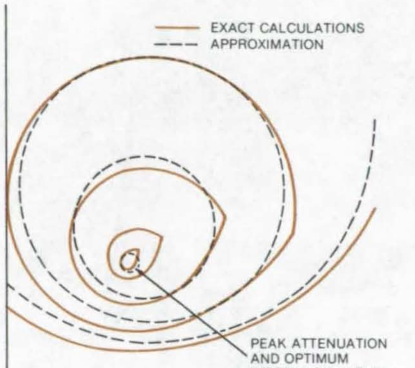

Equal Sound Attenuation Contours with inlet Mach number of 0.4 are shown.

Sample calculations using the generalized approximate attenuation equation show that the peak and the bandwidth of the sound attenuation spectrum can be represented by quite simple functions of the ratio of the actual wall acoustic resistance to optimum resistance.

This work was done by Edward J. Rice of **Lewis Research Center.** *Further information may be found in NASA TM-X-71830 [N76-12827], "Attenuation of Sound in Ducts with Acoustic Treatment — A Generalized Approximate Equation," a copy of which may be obtained at cost from the New England Research Application Center [see page A7].*
LEW-12686

Frozen-Fluid Line Repair

Improved line-freezing equipment permits
fluid line repairs in previously inaccessible areas.

Lyndon B. Johnson Space Center, Houston, Texas

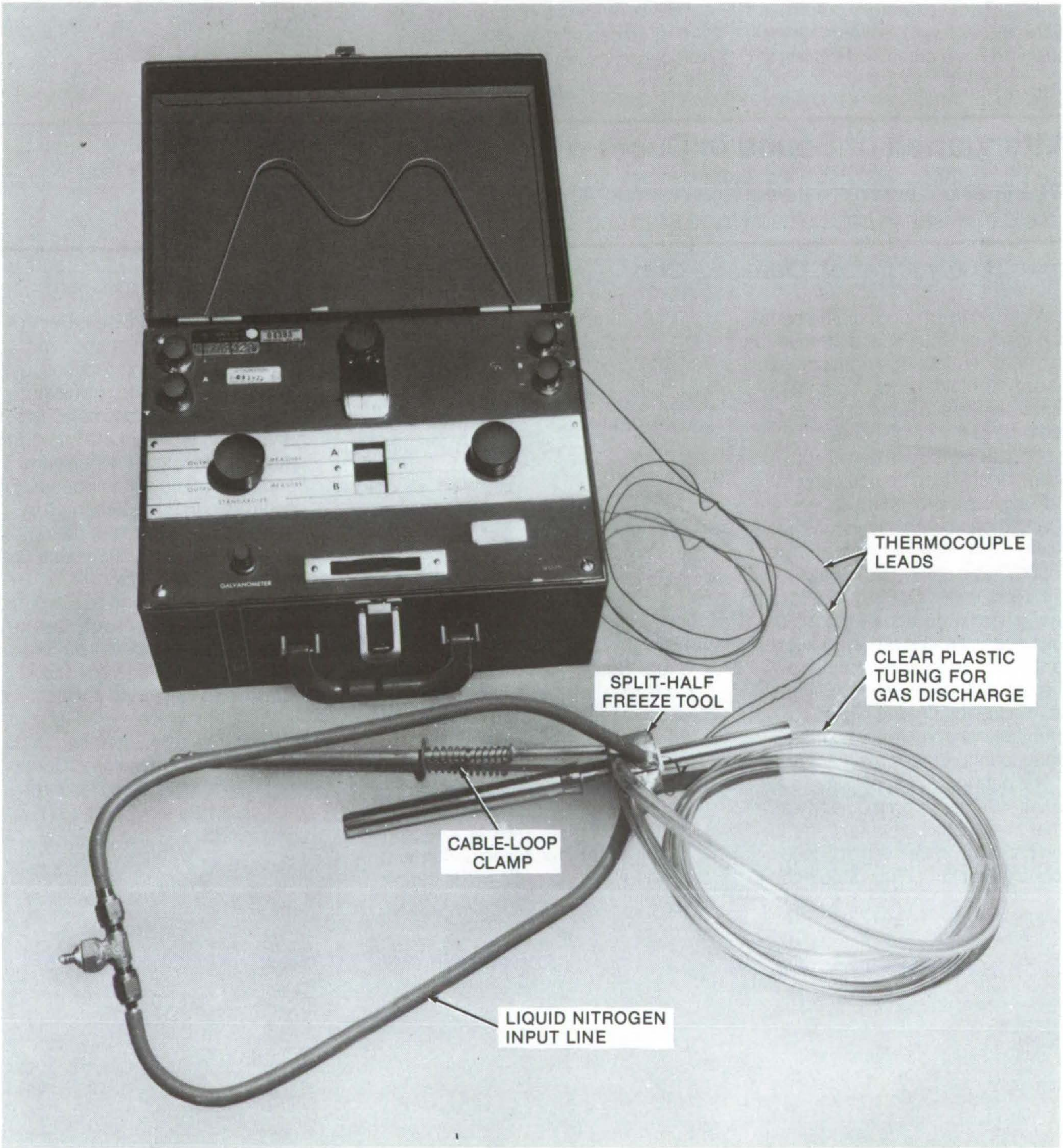

Figure 1. **Frozen-Fluid Line Repair Equipment** consists of a freeze tool attached to an extension-type cable loop clamp. Silicone tubing covers the liquid-nitrogen inlet lines. Thermo couples and readout equipment are used to remotely monitor the freeze site.

Fluid lines are often repaired by freezing a fluid in a section of the line so that it acts as a plug. The line can then be repaired without draining the system. The frozen plug can be formed by circulating liquid nitrogen through a freeze tool that consists of two halves that are bolted around the line. This standard technique can be improved on by using a spring-retracting cable-loop clamp that allows lines to be frozen in limited access areas and by using remote temperature monitoring equipment.

The improved line-freezing equipment is shown in Figure 1. The freeze tool is attached to the cable-loop clamp that permits the tool to be attached to a line in a confined or difficult-to-reach area. Silicone tubing is used to cover the liquid-nitrogen inlet lines, and the cooling-gas discharge lines are made of clear plastic. Also shown in Figure 1 are the thermocouples and readout equipment that allow the temperature at the freeze site to be monitored remotely.

The construction of the split-half freeze tool is shown in Figure 2. The tool is constructed from 0.040-in. (0.102-cm) aluminum. It has also been found that the heat transfer from the line can be improved by simply using a wet paper towel.

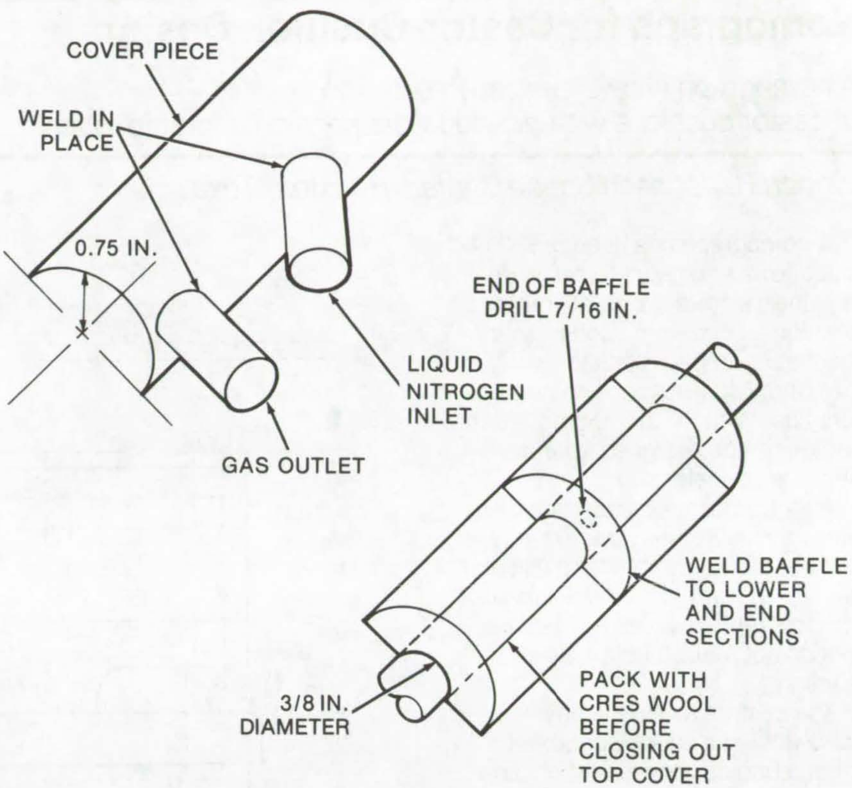

Figure 2. The **Split-Half Freeze Tool** has two chambers (formed by a baffle) in each half. Right-hand and left-hand halves are made; the actual size will depend on the diameter of the line to be frozen.

This work was done by John A. Stein of Rockwell International Corp. for **Johnson Space Center.** *No further documentation is available.*
MSC-19132

Simplified Explosive-Weld Evaluation

Wave patterns of explosive-charge weldments are visually analyzed after being coated with a thin layer of molybdenum disulfide.

Lyndon B. Johnson Space Center, Houston, Texas

Explosive welding is increasingly used to join both similar and dissimilar metals. When materials are bonded together explosively, wave patterns are generated at the mating surfaces which are a direct indication of the quality of the bond. To evaluate the quality of a bond made in this way, micrographic inspection coupled with physical testing is a normal procedure. As the parts are physically connected, it is necessary to make sections in several places and to prepare micrographic specimens for inspection.

A technique has been developed to allow visual inspection of the significant indications of bonding, thus saving time and cost in comparison with prior methods. The surfaces to be welded are first coated with a thin layer of molybdenum disulfide, which is commercially available in an aerosol spray can. The surfaces are then subjected to the welding process, as usual. Under these conditions, however, bonding will not occur, and the wave pattern generated may be visually inspected. This inspection normally reveals more information than does sectioning, and it is particularly useful in evaluating explosive initiation points, shock fronts, and the effects of changes in the geometry of the parts or the explosives. With the use of this technique, fewer trial welds are necessary, making explosive bonding more competitive in all applications.

This work was done by D. M. McLarty of Martin Marietta Corp. for **Johnson Space Center.** *No further documentation is available.*
MSC-14654

Nomograph for Castor-Cushion Design

A nomograph allows inexpensive design
of castor cushions with individual suspension characteristics.

Lyndon B. Johnson Space Center, Houston, Texas

A nomograph has been developed that allows engineers to easily design inexpensive shock-absorbing cushions for castors. Dollies that must carry impact-sensitive cargo have individual suspension characteristics. With this nomograph, each castor can be designed for individual-impact deceleration.

Although shock castors are currently available, they are expensive and are not adjustable for particular loads. Furthermore, unlike this system, currently-available shock castors do not make a dolly self-leveling.

The castors are modified by sandwiching a shock-absorbent material, such as neoprene, between the castor base plate and the mounting plate on the dolly (see figure). The neoprene acts as a natural shock absorber. When the castor is mounted eccentrically (e.g., as is a swivel castor), there is a mechanical advantage that improves the system, by reducing the compression on the neoprene.

The cushions could be manufactured inexpensively and marketed as accessories by castor manufacturers, or they could be designed and made onsite by the ultimate users.

This work was done by Gary L. Dillard of Rockwell International Corp. for **Johnson Space Center.** *For further information, Circle 75 on the TSP Request Card.*
MSC-17094

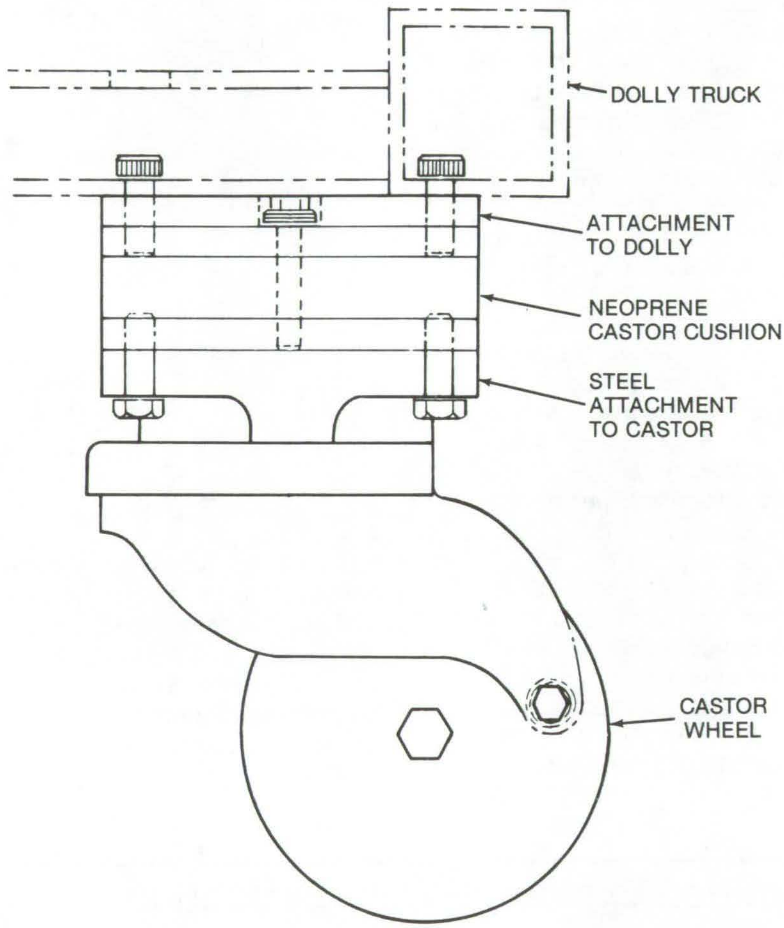

The **Dolly-Wheel Castor Cushion** is sandwiched between the castor base plate and a mounting plate on the dolly.

Cable-Load Equalization System

The winding speeds of a dual cable/winch drum system are synchronized, using a limited-slip differential.

Lyndon B. Johnson Space Center, Houston, Texas

A limited-slip differential can be used to drive dual-cable winches as shown in the illustration. This system synchronizes winding speeds and insures the equal loading of both cables. Redundant motors and clutch/brakes are mounted on a limited-slip differential in the synchronizing shaft connected to the dual-cable reels. The loads in the cables are equalized through the balancing effect of the limited-slip differential.

The application of this technique depends on the selection of an appropriately designed differential. However, the fundamental concept should be of interest to the manufacturers and designers of lifting equipment, such as cranes and elevators.

This work was done by Richard W. Benjamin of Rockwell International Corp. for **Johnson Space Center.** *No further documentation is available.*
MSC-17494

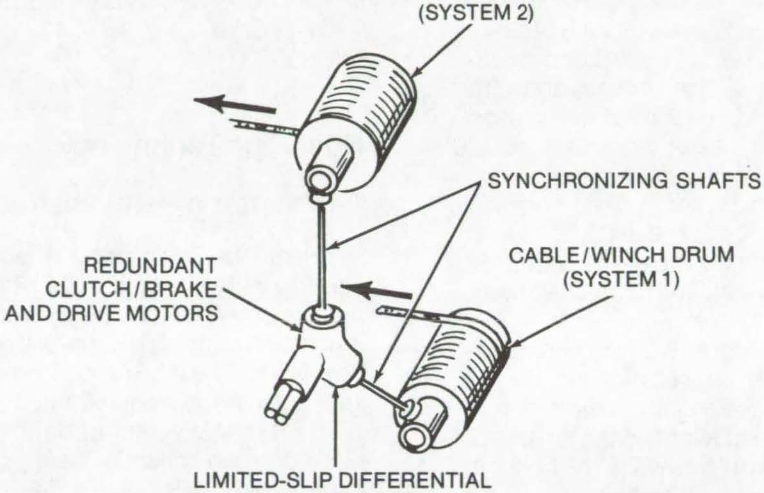

The **Cable-Load Equalization System** is a limited-slip differential connected to synchronizing shafts used to maintain common winding speeds of the winch sets. The system thus assures equal cable loading.

Books and Reports

These reports, studies, and handbooks are available from NASA as Technical Support Packages (TSP's) when a Request Card number is cited; otherwise they are available from one of NASA's Industrial Application Centers or the National Technical Information Service.

Analysis of Bonded Joints

Single-lap, double-lap, and flush joints are analyzed for peel and sheer stresses.

The use of bonded joints in primary structures is becoming increasingly common. In such joints the adhesive, which transfers the load from one member to another, is subjected to a shear stress and to a normal stress in the thickness direction (peel stress). The joint, when subjected to static or fatigue loads, can fail from excessive shear or peel stresses in the bond. Thus, for a proper design of bonded joints, reasonably accurate estimates of maximum peel and shear stresses are needed.

A refined elastic analysis of bonded joints, in which the transverse shear deformation and transverse normal stress were considered, was developed at Langley Research Center. Previous analyses neglected these stresses and strains. The refined elastic analysis was developed to obtain the stresses and displacements in the plates and in the bond. The displacements were expanded in terms of polynomials in the thickness coordinate; the coefficient of these polynomials was a function of the axial coordinate. The stress distribution was obtained in terms of these coefficients by using strain-displacement and stress-strain relations. The governing differential equations were obtained by integrating the equations of equilibrium.

In this study, single-lap, double-lap, and flush joints were analyzed. The effects of adhesive properties, plate thicknesses, material properties, and plate taper on maximum peel and shear stresses in the bond were investigated. For a single-lap joint the two main plates, which were constant, tapered, or stepped in thickness, were joined by direct bonding. For a double-lap joint the two main plates were joined by bonding two plates, one on each side. For a flush joint the two main plates were joined by bonding a lap plate on one side only.

(continued next page)

This analysis of bonded joints revealed that maximum peel and shear stresses in the bond can be reduced by the following methods:

- Making the bond flexible (in all types of joints) either by increasing the adhesive thickness or decreasing the adhesive elastic moduli.
- Using a combination of flexible and stiff bonds (in all types of joints) with flexible bonds in regions of high stresses and stiff bonds in regions of low stresses.
- Using thinner but higher-modulus lap plates in double-lap joints.
- Using thicker and higher-modulus lap plates in flush joints.
- Tapering the plate or plates in single-lap and double-lap (only peel stress) joints.

Of the three types of joints analyzed, for a given total adhesive thickness and joint volume, the double-lap joint had the smallest maximum stresses in the bond; the flush joint had the highest.

This work was done by Saroja R. Srinivasa of Argonne National Laboratory for **Langley Research Center.** *Further information may be found in NASA TN D-7855, "Analysis of Bonded Joints," a copy of which may be obtained at cost from the North Carolina Science & Technology Research Center [see page A7].*
LAR-11871

Fluid Handling Equipment

Selected developments in fluid lines, filters, and other fittings and equipment

A recent NASA Compilation, SP-5976 (03), entitled "Fluid Handling Equipment," describes 24 concepts and methods developed for fluid transport technology. This Compilation is one of a series of NASA Technology Utilization Publications which, like NASA Tech Briefs, make available aerospace technology that may have application in commerce and industry.

"Fluid Handling Equipment" contains articles on fluid lines, including a description of a flexible-line insulation technique, a break-resistant flexible hose, and a manual tubing cutter. Articles on filters, valves, and other fittings include descriptions of a chatter-free check valve, a metal-to-plastic tubing connector, a remote-controlled quick disconnect, a transpiration seal, and a poppet valve pretest device.

This work was done for **NASA Headquarters.** *To obtain a copy of SP-5976[03], Circle 76 on the TSP Request Card.*
HQN-10890

Heat Pipe Technology

A bibliography with abstracts

"Heat Pipe Technology: A Bibliography with Abstracts" is a bibliographic series which attempts to organize the growing literature on heat pipes. The NASA-sponsored Technology Application Center (TAC) at the University of New Mexico began collecting heat pipe information in 1970, and today it acquires on a continuous basis the technical reports, books, conference papers, foreign reports and translations, patents, and other documents devoted to heat pipes. At the present time, publications on heat pipes are increasing at a rate of about 200 per year. TAC's special collection of heat pipe literature ranks as one of the most comprehensive collections available on the topic. It also forms the basis of the bibliographic series.

The heat pipe is a simple and inexpensive device which can transport thermal energy with little drop in temperature. This unique heat-transfer device utilizes the evaporation, condensation, and surface tension characteristics of a working fluid to transfer up to 500 times more heat per unit weight than a solid thermal conductor of the same cross section. By using various working fluids, heat pipes can be designed to operate at temperatures from the cryogenic region up to 3,600° F (2,255 K) and are only limited at higher temperatures by materials technology. The heat pipe has no moving parts and will operate silently and reliably for long lifetimes. Heat may be transferred to or from the heat pipe by radiation, convection, or conduction, and the heat pipe may be used with a variety of heat sources, such as open flames, electric heaters, or nuclear heat sources.

There are several companies and laboratories currently active in research and development on the heat pipe. The heat pipe concept has been attributed to G. M. Grover and associates of the Los Alamos Scientific Laboratory, Los Alamos, New Mexico. Los Alamos pioneered the heat pipe technology and developed the heat pipe operational theory.

Heat Pipe Technology has kept up with the various applications of heat pipes utilized in solving various heat conduction problems. Each issue in the series is divided into the broad areas of: "General Information," "Heat Pipe Applications," "Heat Pipe Theory," "Design and Fabrication," "Testing and Operation," and "Patents." Author, subject, and patent indexes are included. The initial cumulative volume was published in 1971, and yearly supplements have followed. A quarterly update program serves 1975 and the current calendar year.

This work was done by the Technology Application Center at the University of New Mexico for **NASA Headquarters.** *Copies of "Heat Pipe Technology: A Bibliography with Abstracts," the annual updates, and subscriptions to the quarterly update service [TAC HP 72-100] may be obtained at cost from the Technology Application Center, University of New Mexico [see page A7].*
HQN-10901

Cryogenic Storage Tank Thermal Analysis

Nomographs and curves of the thermal insulation requirements for cryogenic liquid tanks

The results of an analytical study of the thermal insulation requirements for cryogenic liquid tanks are presented as a series of nomographs and curves. The multilayered superinsulators discussed in the study are primarily considered for space applications, but the basic analysis and equations used are

generally applicable to industry. This material might be useful to engineers storing or handling cryogenic liquids, including liquefied natural gas.

The analysis was prepared in parametric form to show the relationship between cryogenic boil-off and such parameters as tank size, insulation thickness and performance, structural-support heat leaks and the use of vapor-cooled shields. No attempt was made to arrive at an optimum system, since that selection of parameters is dependent on a number of cost factors that could not be assessed or evaluated in such a study.

This work was done by James P. Wright of Rockwell International Corp. for **Johnson Space Center.** *To obtain a copy of the study, Circle 77 on the TSP Request Card.*
MSC-19103

Solar Heating and Cooling Performance

Techniques are developed for evaluating solar energy systems.

A recent study defines several important considerations for the evaluation of solar heating and cooling systems. A technique has been developed for comparing solar heating and cooling devices with conventional devices to determine whether conventional energy resources may be saved. The technique is applicable to cooling and heating systems that are driven by solar energy directly and also to systems using solar energy to drive Rankine-cycle engines.

Solar and nonsolar energy devices are compared in terms of primary performance characteristics, including efficiencies, auxiliary energy requirements, and solar energy requirements. Analytical expressions for efficiency are derived, and graphical data for solar energy requirements to break even in a system are presented for various coefficients of performance.

This work was done by J. W. Littles and J. C. Cody of **Marshall Space Flight Center.** *To obtain a copy of the report, Circle 78 on the TSP Request Card.*
MFS-23432

Thermal Network Modeling Handbook

A reference for standard formulas, techniques, and terminology

The "Thermal Network Modeling Handbook" describes the basic techniques used in constructing thermal mathematical models. The purpose of the handbook is threefold:

1. To acquaint a new user with the terminology and concepts in thermal mathematical modeling,
2. To present a more experienced user with a quick reference, and
3. To initiate a catalog of standard formulas which may be applied to automated conversational language techniques.

The handbook includes two major sections, one discussing thermal mathematical modeling and the other, operational-parameter relationships. The section on mathematical modeling presents thermal networks as analogous to electrical networks. Techniques are used in which Ohm's and Kirchhoff's laws are applied to the thermal networks.

The basic approach in the thermal analysis of the bodies is to subdivide them into a number of finite subvolumes. The thermal properties of each subvolume are said to be concentrated at its central nodal point. (The subvolumes are referred to as nodes.) Three types of nodes are presented: (1) a diffusion node represented by a temperature and a thermal capacitance, (2) an arithmetic node (zero capacitance) represented by only a temperature, and (3) a boundary node represented by a fixed temperature. The processes of defining the nodes and the conductors (conduction, convection, and radiation) for the thermal network are explained for several configurations.

Further discussion includes computational methods for conduction conductors, convection conductors, and radiation conductors. A number of graphs and tables are used in support of the mathematical formulations for the convection and radiation conductors. Various finite differencing algorithms are discussed for the applicable heat-transfer equations.

Finally, the section on operational-parameter relationships presents the interrelations of the finite differencing parameters (node size, time step, number of iterations, convergence, and damping factor) and their influence on solution accuracy and computational time/costs. Two examples, a one-dimensional metal bar and a two-dimensional metal plate, are used to illustrate these relations.

This work was done by TRW Systems Group for **Johnson Space Center.** *A copy of the report, NASA CR-144418 [N75-30483] "Thermal Network Modeling Handbook" may be obtained at cost from National Technical Information Service, Springfield, Virginia 22151.*
MSC-14964

Impedance of Curved Ducts

An expression for acoustic impedance is developed for circular bends.

The concept of acoustical impedance is useful in the analysis of the behavior of acoustic systems. Interaction of different acoustical segments can be determined if impedances of those segments are known. In the absence of reflections, specific acoustic impedance of straight ducts is $z = \varrho c$, and is thus independent of frequency and duct geometry.

Until recently, the specific acoustic impedance of bent ducts was unknown because of the inability to formulate the equations expressing the impedance for these geometries. A newly derived mathematical solution has now permitted showing that, for circular bends in hardwalled ducts of rectangular cross sections, the specific acoustic impedance depends on both the frequency and the

(continued next page)

geometry of the bend. That is

$\varrho c \cdot (kR_1)/\nu \cdot (r/R_1)$

which, when integrated and averaged over cross section, is

$$z_{bend} = \varrho c \frac{kR_1}{2\nu}(a+1)$$

where ϱ is the fluid density, c is the velocity of sound waves in unlimited space, $k = w/c$ is the wave number, ν is the angular wave number, $w = 2\pi \cdot$ frequency, and $a = R_2/R_1$ is the radii ratio of the outer to the inner cylindrical walls of the bend.

The frequency parameter kR_1 has to be known or assumed for any given problem.

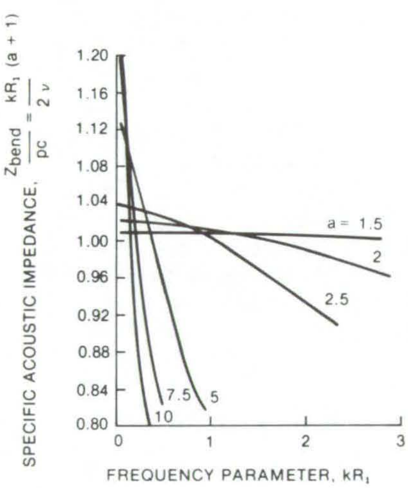

The **Graph of Impedance** for a circular bend in a hardwalled duct with a rectangular cross section gives z_{bend} for various values of $a = R_2/R_1$, the ratio of the radii of the outer (R_2) and inner (R_1) walls of the duct. The parameter k is defined in the text.

Since the corresponding angular wave number ν cannot be easily calculated, the expression for z_{bend} has been evaluated for a range of frequency parameters at several radii ratios and is given in a graphical form (see figure). It will be noticed that the specific acoustic impedance of bends z_{bend} may be greater or smaller than the specific acoustic impedance z of straight ducts, but there is always one frequency at which $z_{bend} = z$.

The expression for the specific acoustic impedance has application in acoustical engineering and in all problems of fluid flow where wave motion should be considered in circular bends of hardwalled ducts.

This work was done by W.A. Rostafinski of **Lewis Research Center.** *The theories which allowed the derivation of the expression for impedance has been verified by experiments conducted by A. Cummings of the Institute of Sound and Vibration Research, University of Southampton, Southampton, England. These were published in the Journal of Sound and Vibration (1974), vol. 35(4), pp 451-477.*

Further information may be found in:

NASA TM-X-2698 (N73-15705) "Propagation of Waves of Acoustic Frequencies in Curved Ducts" and

NASA TM-X-71827 (N76-13881) "Acoustic Systems Containing Curved Duct Sections."

Copies of these reports may be obtained at cost from the Aerospace Research Applications Center, Indiana University *[see page A7].*
LEW-12636

Remote Sensing of Natural Resources

A quarterly literature review

At present the growing literature devoted to remote-sensing research and applications is scattered and difficult to locate. The "Quarterly Literature Review of the Remote Sensing of Natural Resources" compiles citations and abstracts from eight major abstracting and indexing services such as STAR and IAA for quick, easy access. In addition, each issue has an author/keyword index to assist the researcher. The Review is compiled by the Natural Resources Program staff at the NASA-sponsored Technology Application Center (TAC) at the University of New Mexico.

The potential for remote-sensing applications increases daily. The broad subject divisions of each issue reflect this potential:

- Geology and Hydrology,
- Agriculture and Forestry,
- Marine Sciences,
- Urban and Land-Use,
- Instrumentation, and
- General.

In the attempt to review the literature of remote sensing which is so strongly an interdisciplinary science, a definition of boundaries is necessary. The editors include literature which reports data obtained or techniques used from space, aircraft, or ground-based stations with regard to remote sensing. All of the documentation is related to remote-sensing sensors or the remote sensing of the natural resources. Meteorites and extraterrestrial sensing is normally not selected.

This work was done by the Technology Application Center at the University of New Mexico for **NASA Headquarters.** *Copies of "Quarterly Literature Review of the Remote Sensing of Natural Resources" and subscriptions to the 1976 Review may be obtained at cost from the Technology Application Center, University of New Mexico* *[see page A7].*
HQN-10899

Computer Programs

These programs may be obtained at very reasonable cost from COSMIC, a facility sponsored by NASA to make new programs available to the public. For information on program price, size, and availability, circle the reference letter on the COSMIC Request Card in this issue.

NECAP

NASA Energy-Cost Analysis Program

A computer program was needed for evaluating the design and operation of facilities in regard to building energy consumption. The NASA Energy-Cost Analysis Program (NECAP) was developed to determine and minimize building energy consumption. The program is a highly-sophisticated and powerful computerized simulation system, embodying within it all of the state-of-the-art techniques of ASHRAE (American Society of Heating, Refrigerating, and Air-Conditioning Engineers) for performing thermal load calculations and energy usage predictions.

NECAP includes such features as: (a) taking into account building thermal storage and hourly weather data, (b) using new weighting factors for building lights and environmental equipment schedules, (c) allowing infiltration to vary with wind velocity, and (d) allowing internal temperature to vary with equipment capacity schedules. For user convenience the program has built-in input for certain standard analyses.

NECAP provides users with data for selection of the most economical system, system size, fuels, window area, thermal barriers, and the like, during the design phase. After installation, users can optimize operating schedules, determine the most economical temperature settings for components, and obtain other valuable information.

NECAP is actually a set of six individual programs. However, each building design or analysis problem does not necessarily require the use of all six of these programs:

1. **Response Factor Program** — For wall or roof structures different from the typical ones built into NECAP, the Response Factor Program, using a layer-by-layer description of the surface, will calculate and output the set of response factors required to perform transient-heat transfer analysis.
2. **Data Verification Program** — The Data Verification Program interrogates the building-description input data to check for proper order, range, and format of the card input data.
3. **Thermal Load Analysis Program** — The Thermal Load Analysis Program performs hourly transient-heat transfer calculations for each building space, utilizing actual hourly recorded weather, the geometry and construction of the building, scheduled internal loads, and the effects of solar radiation.
4. **Variable Temperature Program** — The Variable Temperature Program adjusts the thermal loads, calculated in the Thermal Load Analysis Program, to account for temperature swings occurring within each space due to thermostat action, equipment capacity, and equipment scheduling.
5. **System and Equipment Simulation Program** — For thirteen common types of distribution-systems and most types of energy-conversion equipment, the System and Equipment Simulation Program determines the total load on the energy-conversion equipment, and based upon part-load efficiencies determines the building monthly demand and consumption of all forms of fuels and energy.
6. **Owning and Operating Cost Program** — For the expected life of the building, the Owning and Operating Cost Program calculates the expected annual expenditure to own and operate the building utility systems.

CDC FORTRAN, Version 2.3
CDC 6000/CYBER 70 Series

This program was written by **Langley Research Center** *and GATX, Inc. For further information, Circle C on the COSMIC Request Card.*
LAR-11888

Shock Interference Patterns and Heating

Prediction of supersonic and hypersonic interference flow fields and surface heating

Small areas of high heat transfer and pressure can occur on the surface of a vehicle due to the influence of an impinging shock on the local flow. Methods were needed to determine peak pressure and heating in these areas.

In order to determine peak pressure and heating in these areas, a system of computer programs has been developed. The programs calculate two-dimensional shock interference patterns for six types of interference flows. Results in the package also include properties of the inviscid flow field and the inviscid/viscous interaction at the surface, along with peak pressure and peak heating at the impingement point.

The six types of interference flow patterns considered are as follows:

1. Type I interference pattern occurs if two weak shocks of opposite families (bow shock and impingement shock) intersect when the flow upstream of the impingement point is supersonic. Peak heating at the surface is the result of a shock/boundary layer interaction. In the case of a blunt body this type interference pattern takes place well below the sonic point.
2. Type II interference pattern occurs when two shocks of opposite families (bow shock and impinging shock) intersect. Both shocks are weak, as in type I, but are of such strength that in order to turn the flow a Mach reflection must exist in the center of the flow field, with an embedded

(continued next page)

subsonic region occurring between the intersection points and the accompanying shear layers. Peak heating is caused by the shock/boundary layer interaction at the surface. Type II interference pattern occurs on a blunt body when the impinging shock intersects the bow shock near the sonic point.

3. Type III interference pattern occurs when a weak impinging shock intersects a strong detached bow shock. High surface heating is the result of shear layer attachment. On a blunt body the shock intersection occurs near or above the lower sonic point.
4. Type IV interference pattern can occur when the impinging shock intersects a strong bow shock ahead of a subsonic flow region. On a blunt body this shock intersection is located between the lower sonic point and just above the body axis. The impinging shock causes a displacement of the bow shock and the formation of a supersonic jet that is embedded in the subsonic region. A jet bow shock is produced when the jet impinges on the surface, creating a small region with high stagnation heating.
5. Type V interference pattern involves the interaction of two weak shocks of the same family. The interaction produces a shear layer, a supersonic jet, and a transmitted impinging shock. Surface heating is caused by a shock/boundary layer interaction. On a blunt body the shock interaction occurs near the upper sonic point.
6. Type VI interference pattern involves the intersection of two weak shocks of the same family which leads to an entirely supersonic flow field. This type of interference pattern is important because it provides a means for predicting the onset of type V interference pattern.

Peak-heating correlations for laminar and turbulent shock/boundary-layer interactions are included in the programs for types I, II, V, and VI interference patterns. Heating correlations for laminar and turbulent reattaching shear layers, obtained from separation studies, are included in the program for type III interference pattern.

FORTRAN IV
CDC 6000 Series

This program was written by Dana J. Morris and J. Wayne Keyes of **Langley Research Center.** *For further information, Circle D on the COSMIC Request Card.*
LAR-11497

COMOC

A finite-element algorithm for the Navier-Stokes equations

The finite-element procedure has proved highly adaptable to the solution of linear elliptic boundary-value problems involving complex boundary conditions; however, its adaptation to quasi-linear and/or nonlinear problems such as the solution of the Navier-Stokes equations has been deemed both theoretically and computationally difficult.

A new finite-element algorithm has been devised to facilitate solution of the two-dimensional Navier-Stokes equations governing the kinematics and thermodynamics of a variable-viscosity, compressible, multiple-species fluid. This algorithm has been implemented into the COMOC (Computational Continuum Mechanics) computer-program system.

In the theoretical development, the primitive dependent variables are replaced by a vorticity/stream-function description, which provides a uniformly elliptic differential equation system description for all computational variables. The preferred differential equation systems are established in rectangular, cylindrical, and spherical coordinate systems. The finite-element algorithm is derived for the generalized, nonlinear elliptic boundary-value problem of mathematical physics and contains no requirements for either computational mesh or solution domain closure regularity. Boundary-condition constraints on the normal flux and tangential distribution of all computational dependent variables, as well as velocity, are routinely piecewise enforceable on domain closure segments arbitrarily oriented with respect to a global reference frame. The intrinsic finite-element shapes for one-, two-, and three-dimensional domains spanned by linear approximation functions are the line, the triangle, and the tetrahedron, respectively.

The area-coordinate concept of structural mechanics has been utilized to establish a natural coordinate function description for the finite-element approximation to the Navier-Stokes equations. Adaptation of these functions represents a significant advance that has for the first time allowed analytical formulation of the complexly nonlinear matrix representations for specific terms in the equation system — in particular, the vorticity transport equation.

The consequence of integration by parts of select nonlinear terms in the differential equation system is examined in detail, and the assumptive constraints are established according to which the generated surface integrals can be neglected or made to cancel. The establishment of the natural coordinate function description allows recognition of the many standard matrix forms that constitute the finite-element algorithm for the nonlinear terms in the equation system and provides broad insight into the mechanics of the algorithm.

The finite-element solution algorithm for the characteristic equation system has been embodied into the COMOC computer-program system, specific variants of which have produced solutions in three-dimensional subsonic and supersonic viscous flow fields and nonlinear transient-heat conduction, in addition to the Navier-Stokes solutions. The COMOC system consists of four basic macromodules, the first of which is Input wherein discretizations are formed and dependent variables are initiated. The Geometry module establishes the nonstandard element matrices for each finite element of the discretization and evaluates the matrix multipliers required for the standard matrices. All

(continued next page)

computations are performed in a local Cartesian-coordinate system with automatic accounting for the lack of coordinate transformation invariance for other-than-rectangular Cartesian systems.

The Integration module embodies solution algorithms for large-order ordinary differential and algebraic equation systems, either of which is produced by the application of the finite-element algorithm to the parent, partial differential equation system. For discretized-equivalent initial-value problems, the basic operation is the evaluation of the derivative vector on an element basis and the assembly of the global vector, using Boolean algebra. For the solution of an algebraic system, the diffusion (that is, "stiffness" in elasticity) matrix is formed on an element basis, and the equation system inhomogeneity is evaluated if present. Each is then assembled into the global representation through Boolean algebra. The matrix-equation system rank is established by evaluating boundary-condition constraints, and the effective inverse is found by equation-solver techniques. The final Output module serves its standard function.

CDC FORTRAN IV, Version 2.3
CDC 6600
SCOPE
Memory Requirements Less Than 77K Octal 60-Bit Words

This program was written by A. J. Baker, A. M. Bauer, P. D. Manhardt, and J. A. Orzechowski of Bell Aerospace Co. for **Langley Research Center.** *For further information, Circle E on the COSMIC Request Card.*
LAR-11480

Predicting Off-Design Performance of Radial-Inflow Turbines

A one-dimensional model accounts for stator, rotor, incidence, and exit losses.

A computer program has been developed for calculating off-design performance of a radial-inflow turbine. The program uses a one-dimensional solution of flow conditions through the turbine along the mean streamline. The loss model accounts for stator, rotor, incidence, and exit losses.

A previous program used turbine geometry and design point performance as input and computed the performance and velocity-diagram parameters over a range of speeds and pressure ratios. The loss model of the previous program was modified, and new features were added to account for stator and rotor trailing-edge blockage and to compute the conditions for pressure ratios at or beyond stator and/or rotor choke. These features are desirable since they give more flexibility to the program and offer a greater range for off-design turbine analysis. Overall turbine geometry and design point values of efficiency, pressure ratio, and mass flow are needed as input information. The output includes performance and velocity-diagram parameters for any number of given speeds over a range of turbine pressure ratios.

Experimental performance from two radial-inflow turbines was compared with the results from this new computer program and the previously used program. The overall computed results from the new program showed a marked improvement over those of the previously used program and good agreement with experimental data.

The new program can be used in two ways. For an existing turbine where the performance at the design operating point may be known, this program provides a convenient way to estimate off-design performance without making actual tests. The program is also useful as a design guide. This program supersedes the previously-issued computer program, LEW-10764 (Tech Brief 69-10267), by C. A. Todd and S. M. Futral, Jr.

FORTRAN IV
IBM 7094/7044 DCS

This program was written by Charles A. Wasserbauer and Arthur J. Glassman of **Lewis Research Center.** *For further information, Circle F on the COSMIC Request Card.*
LEW-12500

Crack-Growth Analysis

A computer program predicts crack growth for structural analyses.

In order to include the important consideration of structural failure due to the presence of flaws and cracklike defects in aerospace hardware, it is necessary to have a computer program capable of performing crack-growth analysis that is easy to use and generally applicable. The need for a computer program (as opposed to simple hand calculations) arises from the complexity of growth descriptions required for crack-growth analysis of real materials in complex structure under a variety of loading and environmental conditions. The Marshall Space Flight Center Crack-Growth Computer Program was designed to meet this need.

The MSFC Crack-Growth Computer Program calculates crack growth for part-through cracks, through-the-thickness cracks, and cracks which are transitioning from part-through cracks to through-the-thickness cracks. The computer program has been written to be flexible in its operation and to be easily adapted and changed as fracture mechanics technology changes and/or the design usage of the program changes.

This computer program is essentially an integration routine which calculates crack growth from an initial defect size and terminates calculation when the crack is sufficiently large for a critical condition (instability or rapid growth) to be reached. In addition, if a design life is not met for a particular structure, the program has the capability of varying the thickness of the structure so as to establish the thickness which will meet the design requirements.

During the period when a crack is a part-through crack, crack growth in the depth and surface directions may be different due to variations in stress-intensity factors and/or directional dependence of material properties. The MSFC computer program considers both of these effects and hence incorporates realistic crack-shape changes.

(continued next page)

During the period when a crack is transitioning from a part-through crack to a through-the-thickness crack, the crack lengths on the back side and the front side are different. The program tracks the growth of these two dimensions separately, evaluating the stress-intensity factors at each surface until these dimensions are the same and the crack has completed its transition to a through-the-thickness crack.

The program is flexible in the methods that can be used. It incorporates the recently-developed Collipriest-Ehret equation as well as the Paris and Forman crack-growth equations. Either may be used to describe a material in a run case.

Retardation effects are also considered. Three models are available: (1) Wheeler, (2) Willenborg, and (3) Grumman Closure.

As many runs (each with varying-input conditions) as desired may be stacked. As additional runs are made, only that section of data which is changed (i.e., loads, material properties, or geometry) need be reentered. Output for each run may be controlled by the user. Minimum output for each run consists of information on input data and failure (crack lengths, cycles, and the like), as well as stress-intensity factors and crack-growth rates for the first and last cycles of each stress level in the first load block applied as a part-through crack, a transitional crack, or a through crack. Additional information (crack lengths, stress-intensity factors, and crack-growth rates) for particular blocks and loading steps may be requested by the user.

Program execution requires approximately 10.6K 36-bit words of central memory.

UNIVAC FORTRAN V
UNIVAC 1108, EXEC VIII

This program was written by C. Bianca of **Marshall Space Flight Center** *and M. Creager of Del West Associates. For further information, Circle G on the COSMIC Request Card.*
MFS-23320

Machinery

Hardware, Techniques and Processes

Books and Reports

Tool Removes Brazed Fittings

A new tool and technique removes brazed-fitting stubs of all sizes and wall thicknesses.

Langley Research Center, Hampton, Virginia

The present technique for the removal of brazed fittings from thin wall tubing utilizes a collet-type removal tool. The fitting is first cut midway between the tubes at a point previously determined by a radiograph or other method. The standard stub removal tool is then inserted into the cut end of the fitting stub and is expanded by means of a collet to positively engage the fitting wall. The fitting stub and the collet are enclosed by the brazing tool, and the heat cycle is initiated to bring the braze alloy to a fluid condition. The fitting stub is then withdrawn from the tube end by the spring force of the removal tool. This method has several problems: (a) The removal tool may bond to the fitting stub, (b) the fitting stub wall may melt, and (c) the tube end may erode.

A simple, expendable, stainless steel split ring (see figure) is placed over the collet of the removal tool prior to its insertion into the fitting stub. The collet is expanded which in turn expands the ring which engages the wall of the stub. The braze tool is attached as previously, and the heat cycle is applied to melt the braze alloy. However, the increased heat capacity provided by the ring prevents the erosion of the tubing end and the melting of the stub wall. In addition, the ring acts as a capillary trap for the melted brazing alloy. This may result in the expendable ring becoming bonded to the stub wall but prevents the bonding of the removal tool to the wall. The new technique is applicable to brazed fitting stubs of all sizes and wall thicknesses.

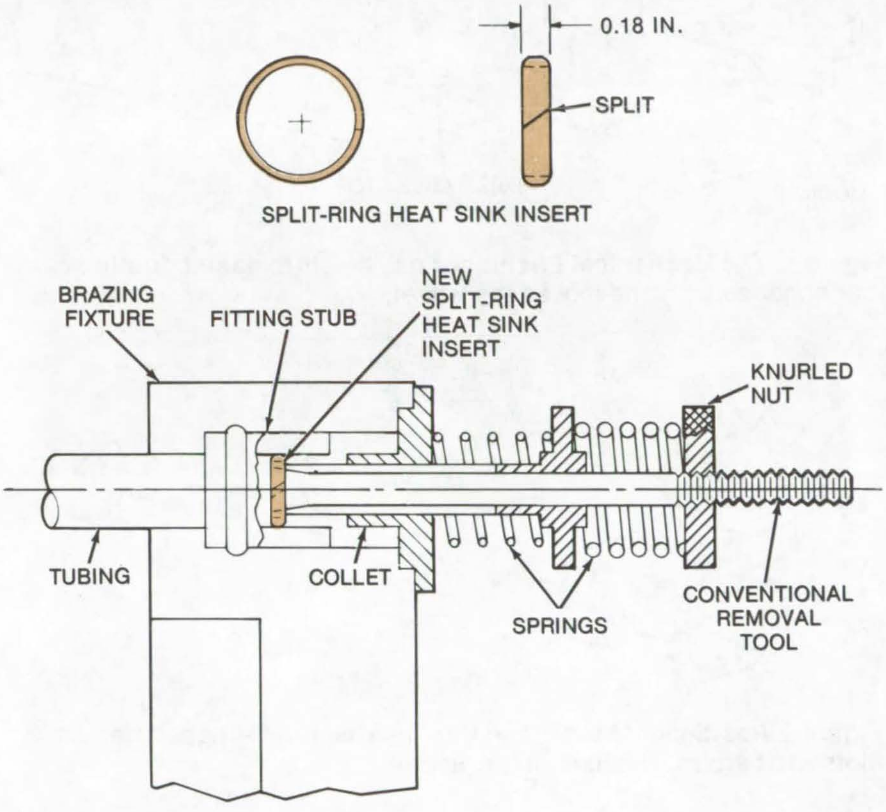

The **Brazed Fitting Removal Tool** with a stainless-steel split ring is placed over the collet that engages the wall of the stub.

This work was done by W.J. Hurley and S. E. Nelson of Martin Marietta Corp. for **Langley Research Center.** *For further information, Circle 64 on the TSP Request Card.*

Inquiries concerning rights for the commercial use of this invention should be addressed to the Patent Counsel, Langley Research Center [see page A8]. Refer to LAR-10944.

Mechanical Positioner

A mechanical positioner for castor wheels can be used to position heavy loads.

Lyndon B. Johnson Space Center, Houston, Texas

The mechanical positioner shown in Figure 1 has been designed for castor wheels on heavy equipment. It can be used to rachet the wheel forward and backward and to stop and steer the wheel. All of these operations are controlled manually.

The device employs a self-engaging self-releasing friction cam that engages with and moves the wheel. The wheel is mounted in a U-shaped frame, and the cam is connected to a lever arm approximately 4.5 ft (1.3 m) long. The frame has slots on each side, which allow it to be attached to the axle of a caster wheel (see Figure 2).

The wheel is moved by raising and lowering the lever arm, which causes the cam to engage with the wheel and ratchet it forward or backward. Adjustable stops control the degree of pressure exerted on the wheel, and a lock pin holds the device in a neutral steering configuration. A hand guard has been added for safety.

This work was done by George A. Tuthill and Garth O. Magnusson of Rockwell International Corp. for **Johnson Space Center.** *For further information, Circle 79 on the TSP Request Card.*
MSC-15817

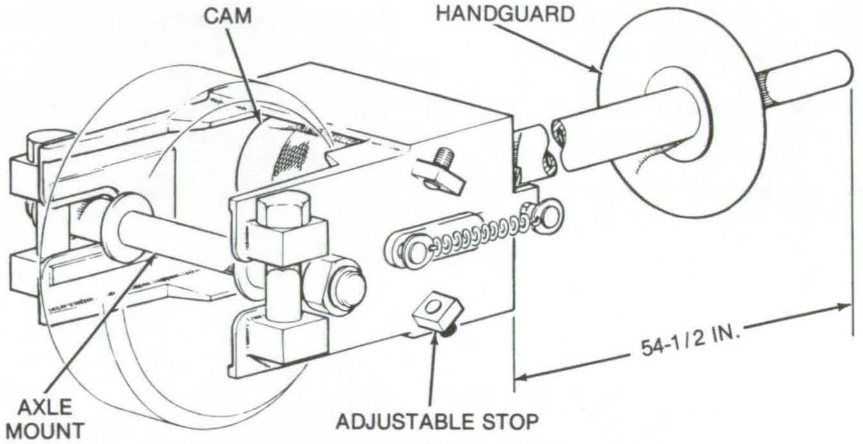

Figure 1. The **Mechanical Positioner** has a self-releasing friction cam that engages with and moves the wheel.

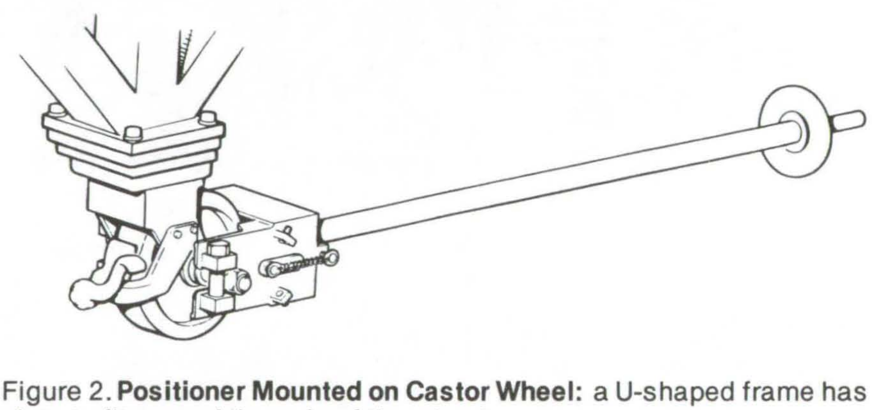

Figure 2. **Positioner Mounted on Castor Wheel:** a U-shaped frame has slots to fit around the axle of the wheel.

Improved Soldering-Iron Tip

Nickel-plated soldering-iron tips are used to remove multipin electronic hardware from printed-wiring boards. The pattern of the recess, machined into the tip, matches the circuit module. Pin heating and subsequent hardware removal is easier. The tip is fabricated from oxygen-free, high-conductivity copper and is nickel plated to reduce oxidation and scaling.
(See page 158.)

Method of Removing Drilling Chips

A special chuck, used to bore or drill long, large-diameter holes, receives a mixture of water and pressurized air during operation. The mixture is directed to a coolant passage within the drill bit. The water and air flush the hole being bored in the workpiece and thus remove chips.
(See page 275.)

Technique for Joining Metal Tubing

Uniform wall thickness and uninterrupted heat transfer in metal tubing joints can be achieved by using a shaped metal insert as wall material for the joint. The insert acts as a support during brazing, after which excess material is ground away to bring the joint to the original tubing size.
(See page 289.)

Radial Level

Accurate and simple measurement of the angle a surface makes with the ground plane.

Langley Research Center, Hampton, Virginia

The radial level is an instrument which is capable of determining any angle without requiring any component to be set, moved, or adjusted. It is very simple, not only in construction but principle of operation, and has distinct advantages over other angle-indicating instruments. The radial level requires no specialized training for its use, and an angle can be determined more rapidly as there are no bubbles to adjust, knobs to turn or lock, or other such operations to perform.

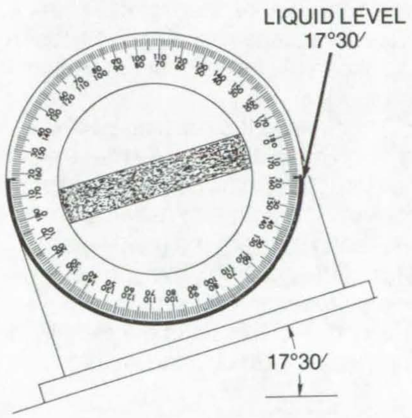

The **Radial Level** has a transparent tube around its periphery that is exactly 50 percent filled with a liquid. Either end of the liquid indicates the angle of the base with ground level.

This angular-indication instrument is capable of accurately determining the angle of a surface or a line of sight in relationship to gravitational level. It is functional and accurate within the full 360° spectrum and instantly determines the angle of any surface without having to make any adjustments as the radial level has no moving parts. A liquid, captured inside a cylindrical transparent tube that is radially mounted around or under a 360° scale, is the actual angle indicator. The liquid occupies 50 percent of the volume of the tube while the remaining 50 percent is evacuated. With this condition, either surface of the liquid indicates the angle of the instrument.

The basic instrument consists of a lightweight frame, a flat base, a 360° scale, and a tube mounted radially around the scale. The center of the frame serves as a handle. The tube is occupied 50 percent by mercury, and the remaining volume is evacuated to eliminate the possibility of bubbles becoming trapped. Mercury is used as the liquid due to its favorable thermal expansion rate; a change in volume due to temperature fluctuation is canceled by the linear expansion rate of the glass or plastic tube. The principle and the simplicity of the instrument are shown in the illustration. The angle being determined is 17° 30 minutes off the horizontal, and this angle is clearly indicated on the instrument.

A single radial level may incorporate multiple scales to enhance its function and versatility. Two angular indication scales are desirable: one to indicate the angle off the horizontal and one to indicate the angle off the vertical. A scale to indicate rise per foot could indicate the pitch of a roof. A scale to indicate percent of grade would be beneficial in the construction of roadways, grading, and the like.

This instrument is not limited to surface contact applications. Mounted on a tripod and equipped with a sighting mechanism alined with the zero-degree indices, the angle, the rise per foot, or the percent of grade can be instantly determined, further expanding its diversified capability. It could also be used to determine quickly the height of an object. If the angle and distance are known, the height can be easily determined.

This work was done by Donald L. Posey of **Langley Research Center.** *No further documentation is available.*

Inquiries concerning rights for the commercial use of this invention should be addressed to the Patent Counsel, Langley Research Center [see page A8]. Refer to LAR-11982.

Split-Ring Seal

A gland-type seal requires
little installation space and infrequent servicing.

Lyndon B. Johnson Space Center, Houston, Texas

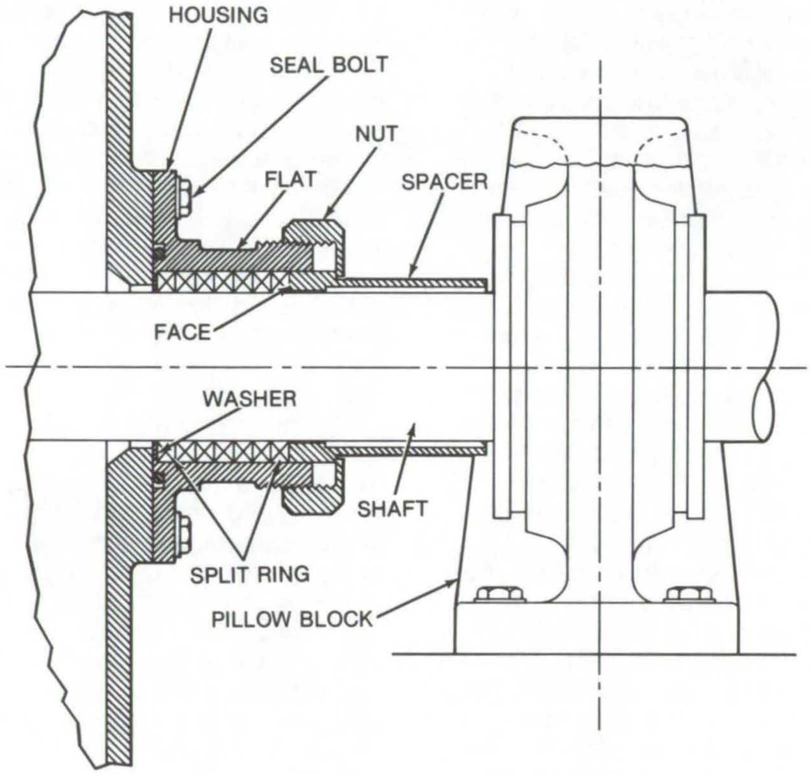

Figure 1. When the **Split-Ring Seal** nut is torqued down, the ring is compressed against the washer, the spacer face, the shaft outside diameter, and inside diameter of the housing.

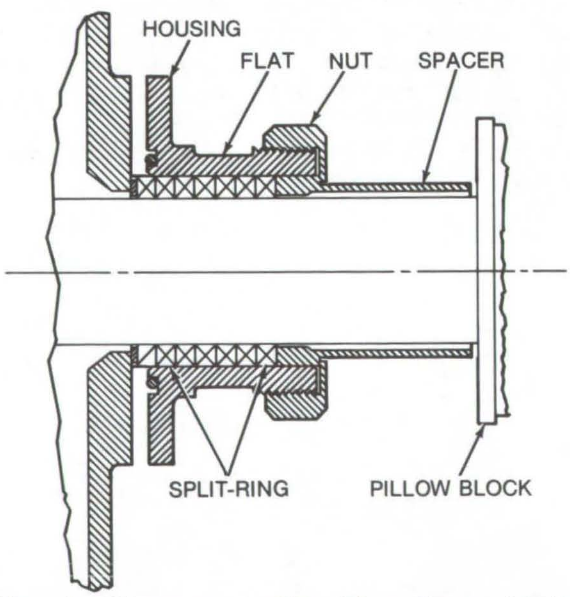

Figure 2. In the **Housing Disconnected Position,** the seal bolts are removed using a wrench which contacts flats on the housing. The housing is turned relative to the nut.

The split-ring seal shown in Figure 1 may be used with hydraulic and pneumatic actuators and similar equipment. It is designed for applications with partial vacuums and requires little space for installation and servicing.

The shaft is sealed (Figure 1) when the nut compresses the split ring against the washer, the face of the spacer, the outside diameter of the shaft, and the inside diameter of the housing. The seal is disconnected from the housing by removing the seal bolts as shown in Figure 2. The seal may then be inspected or serviced by manually sliding the housing assembly to the position shown in Figure 3.

The flats on the housing permit a wrench to be attached so that the housing may be turned relative to the nut. The split ring may thus be broken away from the inside diameter of the housing. The spacer prevents the rings from sliding with the housing, and the seals will remain in full view and readily accessible.

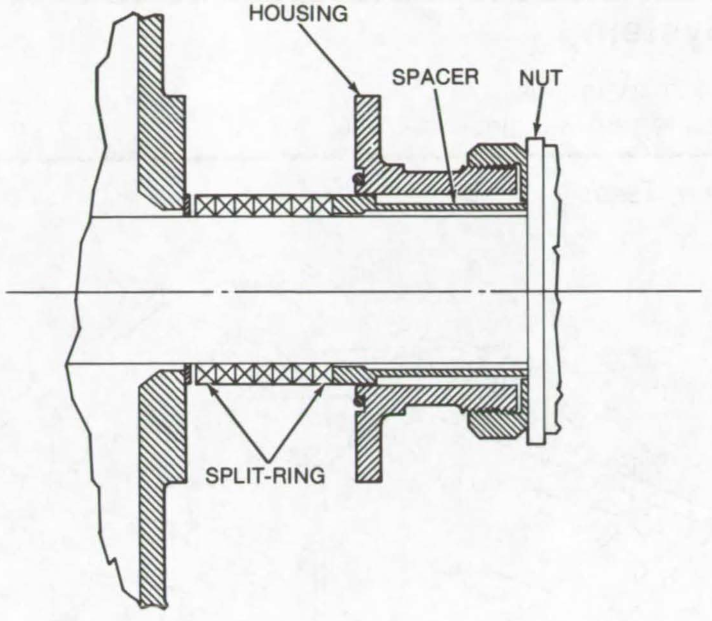

Figure 3. The **Seal is Exposed** for inspection or service by manually sliding the housing to the position shown above.

This work was done by Elia A. Gallo of Kentron Hawaii, Ltd. for **Johnson Space Center.** *No further documentation is available. MSC-14304*

Rotary Broaches

A roughing-out and finishing tool is designed for limited-access areas.

Marshall Space Flight Center, Alabama

A useful tool (see figure) has been designed for counterboring or back-spot facing recesses for boltheads or nuts in difficult-to-reach locations, such as near webs, bosses, or flanges. Two versions of the tool have been designed: one rotary broach for roughing out and another rotary broach for finishing.

Both broaches have a flat area to facilitate insertion into a pilot hole. This flat area is placed against the casting when using the tool. Around the periphery of the broach, each cutting tooth extends slightly further out than its predecessor. Thus each tooth removes slightly more material, and the hole is machined to its final diameter in a single rotation of the broach.

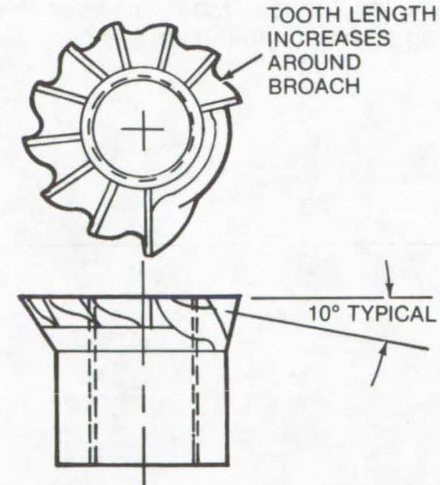

The Roughing-Out Tool with staggered cutting teeth will drill out the proper diameter in one revolution.

This work was done by Charles Libertone of Rockwell International Corp. for **Marshall Space Flight Center.** *For further information, Circle 80 on the TSP Request Card. MFS-23374*

Vehicle Load-Equalization System

A closed-loop cable-and-pulley arrangement maintains constant wheel-to-ground contact in an all-terrain vehicle.

Lyndon B. Johnson Space Center, Houston, Texas

Two wheel beams are connected by cables to form a closed-loop system which equalizes vehicle-wheel loading, regardless of terrain. The closed loop causes reactions at each of three wheels in response to loading action at the remaining wheel.

The wheels on each side of the vehicle (see figure) are attached to a wheel beam, which in turn is attached to the vehicle chassis by a central pivot. The respective ends of the opposite-side wheel beams are connected by a cable-and-pulley arrangement. The wheel beams provide for pitch-axis motion; the cable system completes the closed loop and provides for roll-axis motion of the beams.

The cable system can be replaced by a linkage arrangement or a hydraulic system, and it may be damped by the addition of shock absorbers. The simplicity of this design should be of interest to designers and manufacturers of construction equipment and off-road vehicles.

This work was done by W. K. Creasy of **Johnson Space Center.** *No further documentation is available.*
MSC-12466

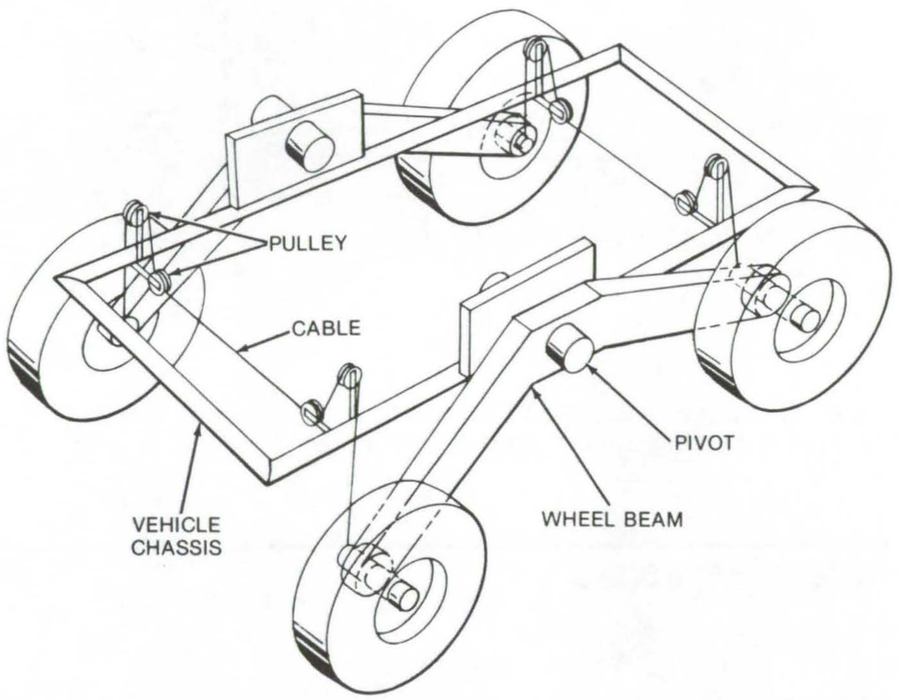

Vehicle Load-Equalization System uses cables and associated pulleys to form a closed-loop suspension system for terrain compensation. The loop causes reactions at each of three wheels in response to loading at the remaining wheel.

Large-Diameter Fasteners of CRES Alloy

Double-hex-head bolts can be made with diameters of up to 1-1/4 in. and with a tensile strength of 220,000 psi.

Lyndon B. Johnson Space Center, Houston, Texas

A specially designed bolthead permits bolts of MP 35N high-strength corrosion resistant steel (CRES) alloy to be made with diameters up to 1 ¼ in. (3.2 cm). High-strength fasteners of this material have been previously limited to a maximum diameter of ¾ in. (1.9 cm). This limitation exists, primarily, because the conventional 12-point tension heads (double hex heads) cannot be cold formed to retain the required minimum tensile strength of 200,000 psi (13.8×10^9 N/m^2).

The conventional double hex head is shown in Figure 1. Figure 2 depicts the modified head, which can be cold formed with a tensile strength of 220,000 psi (14.18×10^9 N/m^2) and high fracture toughness. The standard bolt design can be used for bolts up to ¾ in. (1.9 cm) in diameter; the modified design has been developed for bolts from 7/8 in. to 1 ¼ in. in diameter (2.3 to 3.2 cm). Aside from the difference in head design, both bolt types are fabricated in essentially the same manner.

This work was done by J. F. Charles and M. L. Marke of Rockwell International Corp. for **Johnson Space Center.** *For further information, Circle 81 on the TSP Request Card.*
MSC-19313

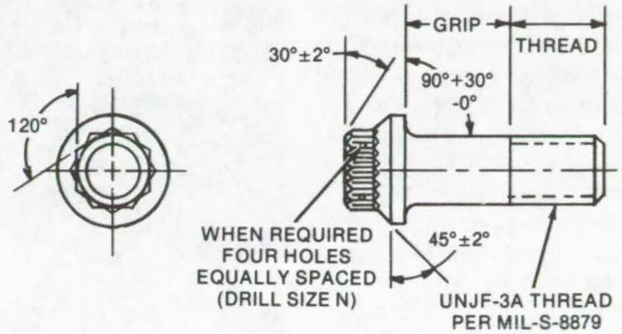

Figure 1. **Conventional Design** of large-diameter fastener of CRES alloy can be used to fabricate bolts up to 3/4-in. diameter.

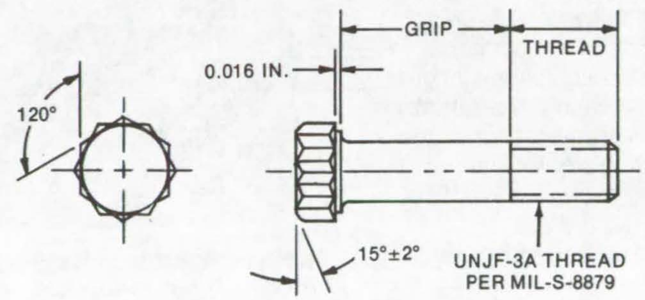

Figure 2. **Modified Bolt Design** depicts cold-formed head of up to 1-1/4 in. in diameter having a tensile strength of 220,000 psi.

High-Temperature Heating Array

A graphite element is less costly
and easier to replace than a quartz lamp.

Lyndon B. Johnson Space Center, Houston, Texas

A heating array (see figure) for thermally conditioning the reusable surface insulation panels of thermal-protection systems is capable of heating samples to 2500° F (1644 K), at pressures ranging from 0.5 to 760 torr (66.6 to 10.1×10^4 N/m^2). Low-cost, easily-replaceable, graphite heating elements instead of quartz lamps are used in the heating array. Advantages of the array include:

- The operating cost is lower because quartz lamps have a relatively short life and are expensive to replace.
- The graphite heating elements function well at lower pressures whereas quartz lamps do not.
- The graphite heating elements give more uniform heating than quartz lamps. However, protection of the graphite heating elements from air oxidation may cause some difficulty.

This heating array may be useful for high temperature processing or conditioning of materials. The heater elements heat a susceptor plate (in this case, a coated columbium-beaded plate) which in turn heats the test panel. The elements are surrounded by a nitrogen atmosphere to prevent oxidation of the graphite; air is forced between the susceptor plate and the test article to provide an oxidizing atmosphere around the test article. The unit is economical to operate and maintain. It is shown in the figure with the heating-array elements installed but before the heating-array enclosure is installed.

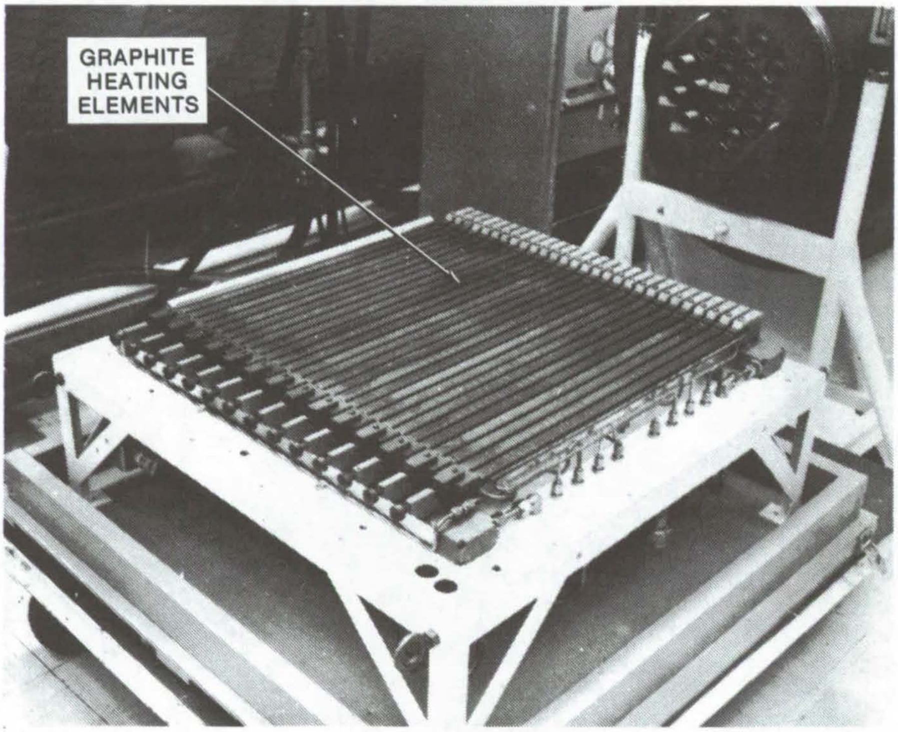

High-Temperature Heating Array is capable of heating samples to 2500° F at pressures ranging from 0.5 to 760 torr. The illustrated array is used to thermally condition reusable surface insulation panels of thermal-protection systems. It is shown with the individual graphite elements installed and with the array enclosure removed.

This work was done by Harold E. Christensen and B. G. Cox of McDonnell Douglas Corp. for **Johnson Space Center.** *For further information, Circle 82 on the TSP Request Card.*
MSC-14287

Load-Regulating Latch

Automatic regulation of latch-tension load, prevention of overload, and load sharing in a multiple-latch system

Lyndon B. Johnson Space Center, Houston, Texas

A load-regulating latch has been designed for remotely latched doors or for doors on which the latch cannot be reached for adjustment after the door is closed. The latch, as shown in the illustration, has a hook that engages a strike roller. The surface of the hook is shaped to cam the strike roller to the engaged position when a predetermined load is applied between the hook and the roller.

A compression spring is mounted in a housing and around the latch stem to allow the latch to move along the spring centerline and compress the spring. The desired preload tension, equal to the maximum load desired when the door is latched, is set by an adjusting bolt. The final hook-and-strike position is selected so that the minimum desired load is exceeded. This causes the hook to move toward the strike by an amount exceeding tolerances in the strike-and-load interface.

In addition to the spring travel, further motion is allowed for structural deflections occurring over the life of the latch. As an increased load tends to open the door, the spring exerts a greater force on the latch. To prevent overload, the housing has a shoulder that limits travel of the hook to the point where the washer meets the shoulder.

The shapes of the spring and the hook also cause the load of closing to be shared more evenly among latches when there are several on a single door. Normally, the latches farthest from the hinge do all the work until just before the door is completely closed. This is also the case for loads due to door or jamb warpage and seal compression. However, with this system, even though latches nearer the hinge are slightly closer to their strike, they share the load because the spring-supported hood contacts the strike earlier in its stroke. The illustrated latch has a 45° stroke and makes contact within the first 20° or less of closing motion, immediately picking up load and relieving the other latches.

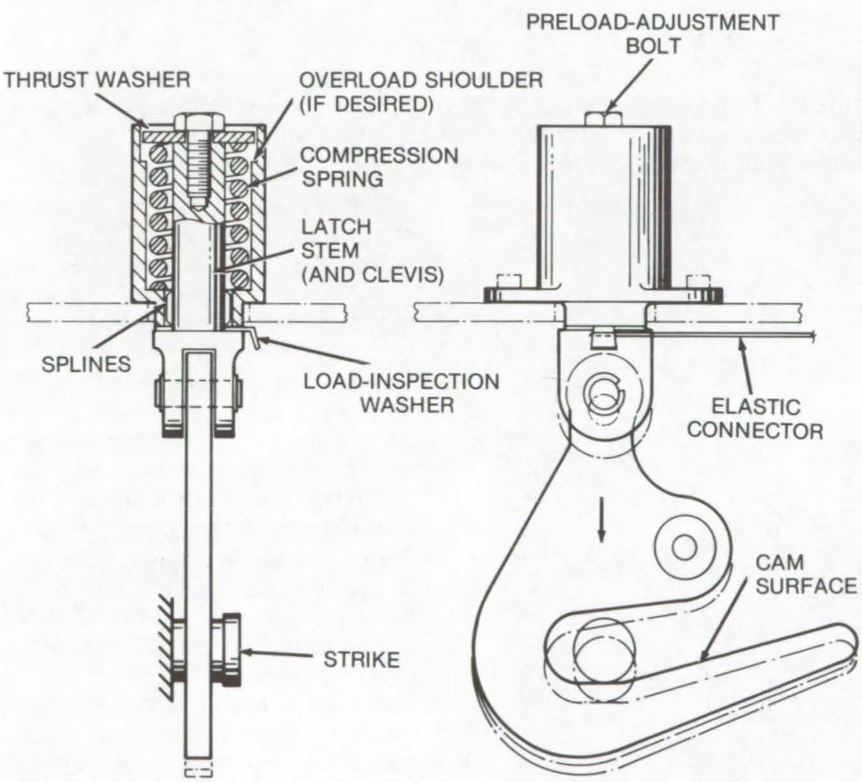

The **Load-Regulating Latch** is splined to the spring housing. The splines allow the hook to move along the centerline but prevent rotation. A typical spring is sized to travel 0.125 in. It is preloaded to 220 lb and produces a force of 280 lb when fully compressed.

This work was done by Walter T. Appleberry of Rockwell International Corp. for **Johnson Space Center.** *For further information, including alternate versions of the latch, Circle 83 on the TSP Request Card.*

This invention is owned by NASA and a patent application has been filed. Inquiries concerning non-exclusive or exclusive license for its commercial development should be addressed to the Patent Counsel, Johnson Space Center [see page A8]. Refer to MSC-19535.

Solar Concentrator/Absorber

A dual concentrator and cylindrical counterflow absorber improve performance.

Marshall Space Flight Center, Alabama

A solar collector/energy converter, consisting of a dual-slope optical concentrator and a counterflow thermal-energy absorber, is attached to a multiaxis support structure. The concentrator/absorber is efficient over a wide range of illumination levels. Like other thermal-energy collectors, it may be used to generate high-temperature steam, may serve as a hot-air generator or solar-powered dryer, and can power an absorption-cycle cooler.

The concentrator consists of a primary and a secondary cone (see Figure 1). Concentration factors are from 10 to several hundred, depending on the ratio of the aperture area of the cone to the absorber surface area.

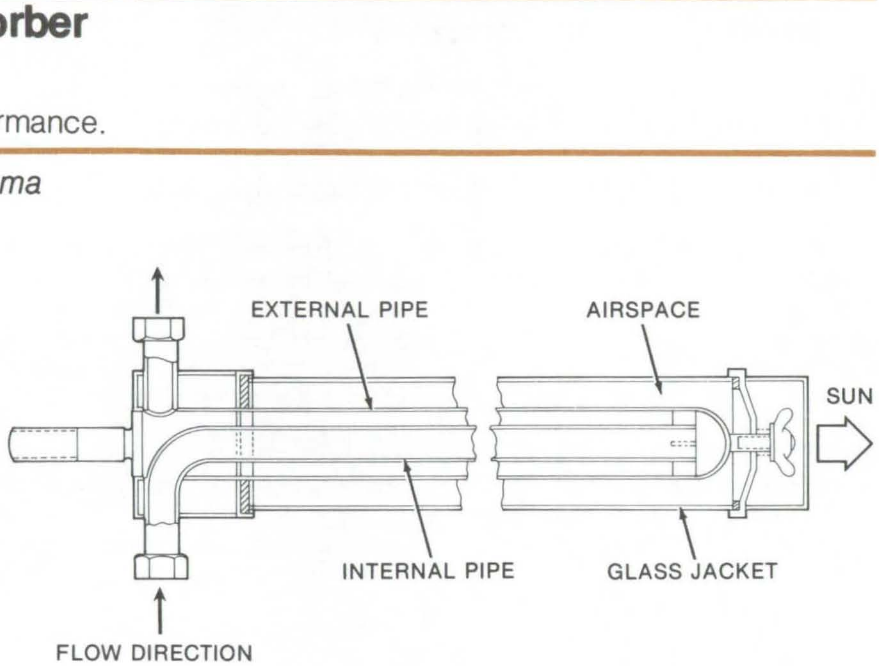

Figure 2. The **Counterflow Absorber** piping is copper tubing coated with a black oxide surface, but other high-temperature (600° C) materials and coatings are suitable.

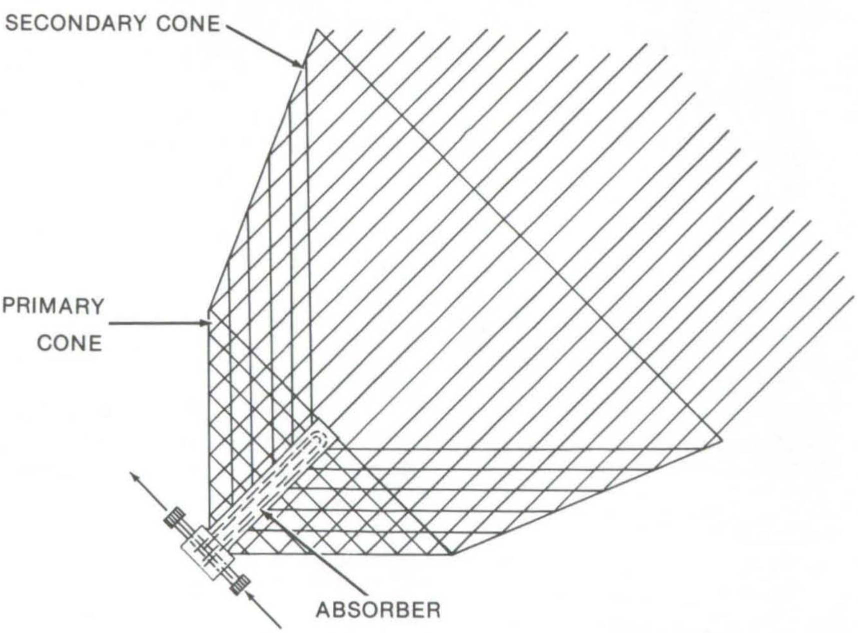

Figure 1. The **Dual-Slope Concentrator,** when aimed at the Sun, reflects solar rays into the center region of the primary cone. Theoretically, the secondary cone can increase the concentration factor of the primary cone by over 70 percent.

The absorber comprises two concentric pipes; the external pipe is closed at one end, as seen in Figure 2. A fluid inlet connection is located at the other end. The internal pipe is open at both ends and has a fluid connection at one end. The heat-transport fluid enters through the internal pipe and exits via the external pipe. Internal flow is preheated by the hot flow returning through the external pipe. In transferring from the internal to the external flow, the fluid contacts the hottest area of the absorber. The most efficient transfer of heat is thus provided through a maximum temperature difference.

A glass jacket surrounds the absorber to suppress convection. The space between the absorber and the tube is under low pressure after initial thermal expansion of the trapped air and expulsion through the spring-loaded top gasket.

This work was done by Georg F. von Tiesenhausen of **Marshall Space Flight Center.** *For further information, Circle 84 on the TSP Request Card.*

Inquiries concerning rights for the commercial use of this invention should be addressed to the Patent Counsel, Marshall Space Flight Center [see page A8] Refer to MFS-23428.

Proposed Low-Temperature Solar Engine

Thermal expansion and contraction of a metal rod is directly converted to rotary motion.

Marshall Space Flight Center, Alabama

A potentially economical way of utilizing solar energy is directly, or nearly directly, to convert the Sun's heat to motion, thereby avoiding the need for heat pumps and associated equipment. An engine proposed for this purpose converts the thermal expansion and contraction of a metal rod into rotary motion.

An aluminum rod is alternately cooled and heated, using hot water from a solar flat plate or concentrator. Translational motion is converted to rotational motion by the mechanical configuration of the rod and by its attachment to a modified "Chinese" windlass. A linear displacement of 0.076 cm in the rod will exert sufficient force to drive pumps, generators, and compressors.

Ideally, continuous rotation of the windlass is desired as the rod undergoes displacement. Linear motion is converted to rotational motion, using the mechanical configuration in the figure: One windlass pushes, and a second windlass pulls. Therefore one windlass rotates the load through angle $\Delta\Theta$, while the other reverses rotation through the same angle without carrying the load. Then the operation is reversed. A key feature of the windlass is the combination of requisite strength with moderate dimensions and great mechanical power.

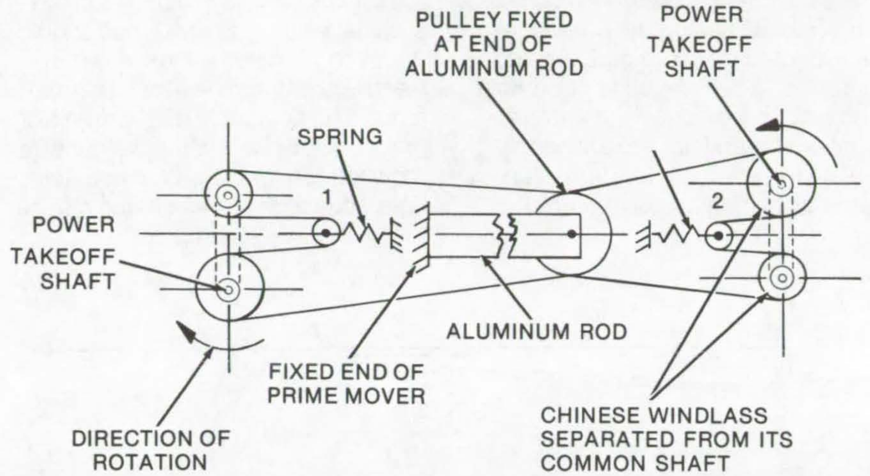

The Solar Engine uses the expansion and contraction of an aluminum rod to drive two out-of-phase windlasses. As shown, the rod is contracting, and the power takeoff shaft on windlass 2 applies a load to the system output shaft; the power takeoff shaft of windlass 1 applies no load. (The takeoff shafts connect to the system output shaft.) The process reverses upon expansion of the rod.

This work was done by Jerry A. Peoples and George B. Kearns of **Marshall Space Flight Center.** *For further information, Circle 85 on the TSP Request Card.*

Inquiries concerning rights for the commercial use of this invention should be addressed to the Patent Counsel, Marshall Space Flight Center [see page A8]. Refer to MFS-23403.

Conical Diffuser for Fuel Cells

A compact manifold has improved flow distribution and reduced pressure loss.

Lyndon B. Johnson Space Center, Houston, Texas

The space-saving fuel-cell conical diffuser shown in Figure 1 reduces the expected pressure gradient and the resulting cell-to-cell temperature gradient. This diffuser is inserted into the inlet manifold, producing a smooth transition of flow from pipe diameter to manifold diameter.

The included angle between the conical walls of the manifold should be 7° to 10° for the most effective recovery of the pipe dynamic pressure. The coolant is discharged from the diffuser insert some distance downstream of the actual manifold inlet, due to the length of the diffuser and space limitations. The length of the diffuser insert causes the effluent flow initially to bypass several cells near the manifold inlet.

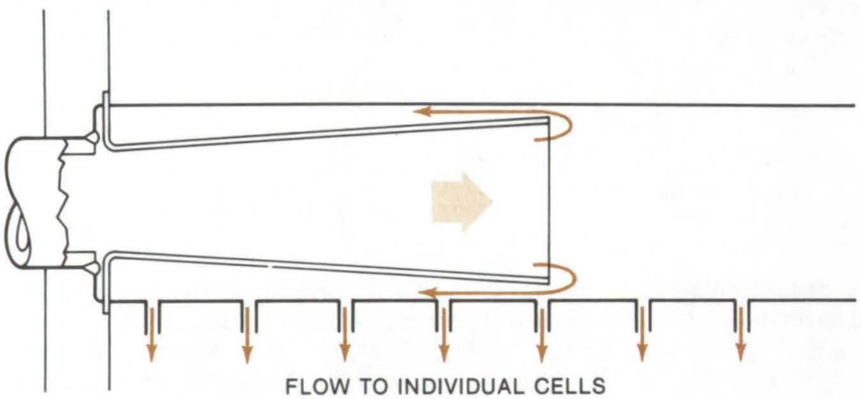

Figure 1. **Inlet Manifold** used in the conical diffuser for fuel cells reduces inlet losses and improves cell-to-cell flow distribution.

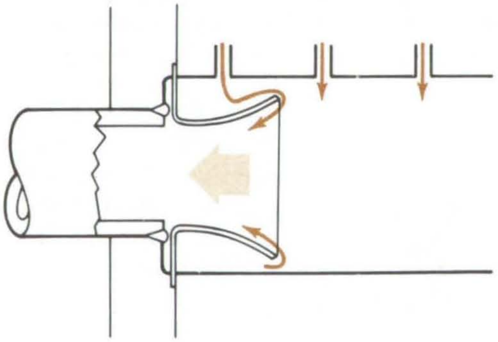

Figure 2. The **Outlet Manifold** has a nozzle insert that reduces exit losses.

This deficiency is overcome by allowing adequate clearance between the outlet of the diffuser insert and the internal diameter of the manifold, thus permitting coolant to flow into the first several cells without a significant pressure loss through the clearance area. The clearance allowance between the outlet of the diffuser insert and the manifold internal diameter does not reduce significantly the pressure recovery produced by the diffuser insert.

Although the abrupt change in flow area between the outlet manifold and the outlet piping has a minor effect on flow distribution, a nozzle insert used in the outlet manifold will further reduce overall system pressure losses. The nozzle insert which is shown in Figure 2 may be shorter than the diffuser insert, but there must be a clearance between the nozzle inlet and the inside diameter of the manifold to allow for coolant flow from the one or more cells near the manifold outlet. The nozzle insert reduces the system pressure loss by approximately 37 percent of the mean dynamic pressure in the connecting piping.

This work was done by D. W. Craft of General Electric Co. for **Johnson Space Center.** *No further documentation is available.*
MSC-14026

Horizontally-Mounted Solar Collector

Tracking solar collectors are size limited to reduce loading. Lightweight tracking vanes allow larger, more efficient collectors.

Marshall Space Flight Center, Alabama

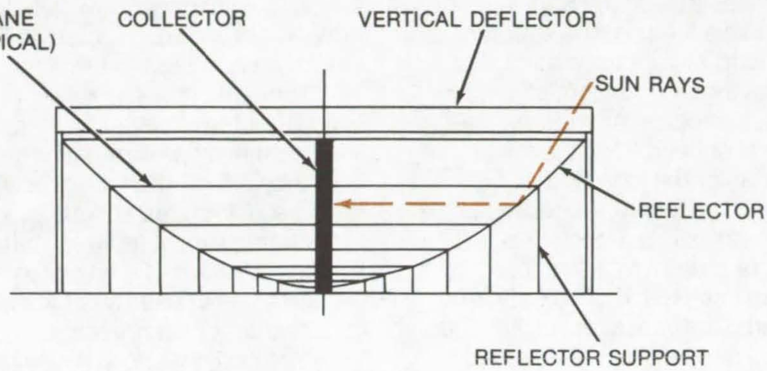

Figure 1. The **Vertical Deflector Structure,** which consists of a series of flat, horizontally-mounted vanes, is rotated to direct the incoming solar energy toward the collector.

A horizontally-mounted optical reflector is used to direct incoming solar energy, regardless of its angle of incidence, to a predetermined focus point or collection center in a solar collector. Consisting of three major components — a vertical solar-energy deflector assembly, a stationary reflector, and a motor-driven solar tracking mechanism, this collector may lower the cost of generating solar energy since its collection area may be made considerably larger than existing stationary or tracking solar collectors. The deflector assembly

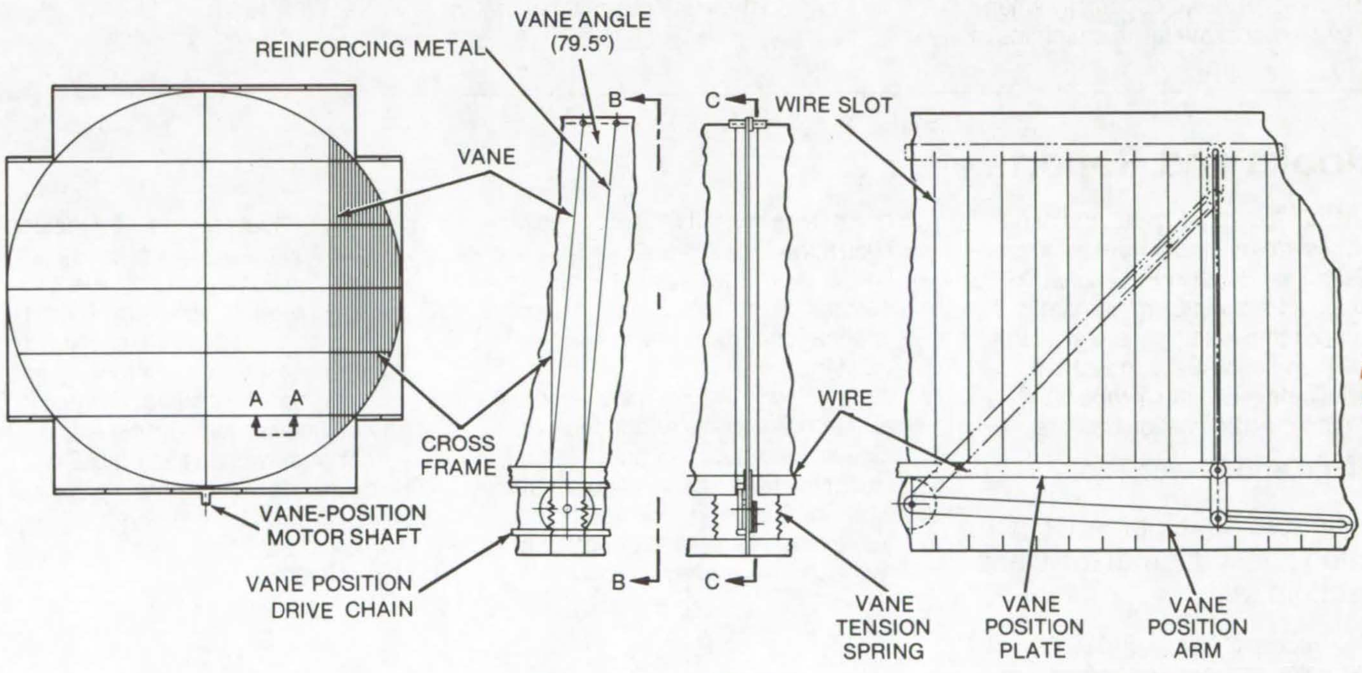

Figure 2. **Vane Angle** is changed by control wires driven by a motor via a position drive chain (View A-A). Each vane consists of a flexible, reflective material which is reinforced at the top and bottom by a thin metal strip (Views B-B and C-C). The vanes are kept under tension with springs and are adjusted using bolts (View D-D) located along one side.

(continued next page)

directs incident incoming solar energy to a vertical direction, using a series of tracking vanes. The energy is then redirected via a stationary reflector to a fixed collector which absorbs the solar energy as heat.

Many of the solar collection schemes either built as prototypes or as conceptualized models include collectors that are pointed at the Sun via a motorized assembly. While these collectors may be more efficient by virtue of their sophisticated tracking mechanisms, they are limited to some practical (usually small) size to reduce strain on the tracking drive motors. To offset the increased number of collectors needed to equal the collection efficiency of a much larger tracking collector, a greater number of solar collectors is required. This increases the total cost of the solar collecting array and also is a less efficient scheme, especially when used to generate large quantities of energy such as at a commercial electrical generating plant.

The new vertical deflector consists of a flat, horizontally mounted structure with vanes which change the direction of incoming solar energy. This structure, illustrated in Figure 1, is rotated to aline the deflector with the Sun. To maintain alinement the structure is able to rotate approximately 180° across the sky. At nightfall the tracking mechanism returns the vertical deflector back to the starting position for the following day.

As the structure rotates the angle of the vanes is matched to direct the solar rays down to the reflector. Approximately 75° of rotation are built into the vanes for tracking Sun angles ranging from 5° to almost 80°. The vane angle is changed by control wires, one wire per row of vanes. A wire for each row of vanes is rotated through slots in the cross frames and the vane position plates.

The vane consists of a flexible reflective material which is reinforced at the top and bottom via a thin metal strip. The strip is held to the nonreflective side of the vane. All vanes extend from one cross frame to another and are kept under tension with springs. The wires are held in adjustment with bolts located along one side of the outside flat surface (see view D-D in Figure 2).

The reflector assembly is constructed of several plates, each measuring approximately 4 by 8 ft (1.2 by 2.5 m), located on a support frame. The plates are attached to the frame with bolts which permit focus adjustment. The plates are conical; solar energy is focused at the center of the reflector.

This work was done by Dolphus H. Black of **Marshall Space Flight Center.** *For further information, including additional drawings, Circle 86 on the TSP Request Card.*
MFS-23349

Books and Reports

These reports, studies, and handbooks are available from NASA as Technical Support Packages (TSP's) when a Request Card number is cited; otherwise they are available from one of NASA's Industrial Application Centers or the National Technical Information Service.

Hand and Power Tools

Selected developments in shop and industrial tools and techniques

A recent NASA Compilation, SP-5976(06), entitled "Hand and Power Tools," describes 25 tools and tooling advancements developed for industrial and small machine shop adaptation. This Compilation is one of a series of NASA Technology Utilization Publications which, like NASA Tech Briefs, make available aerospace technology that may have application in commerce and industry.

"Hand and Power Tools" contains articles on shop tools and techniques, including a concept for universal pliers, an allen-head speed wrench, improved techniques for tool cleaning, and a description of a hydraulic valve-lifter remover. Articles on tools for industry include descriptions of a wrench for B-nuts, a cable tensiometer attachment for a torque wrench, spray tips formed from heat-shrinkable tubing, and an eccentric-pin alinement tool. Metal-working tools for milling, debrazing, and drilling are also described.

This work was done for **NASA Headquarters.** *To obtain a copy of SP-5976[06], Circle 87 on the TSP Request Card.*
HQN-10892

Fabrication Technology

RF Shaping of Silicon Ribbon

An RF coil generates magnetic forces within silicon melt and shapes it into a flat ribbon.

Marshall Space Flight Center, Alabama

Because of the high reactivity of the molten crystal, conventional methods of shaping molten silicon result in crystal contamination and die erosion. To overcome contact contamination, electromagnetic force, generated by a radio-frequency (RF) coil, has been used to shape molten silicon. Initial efforts were only moderately successful. Since the shape and position of the RF coil are crucial in applying maximum force to the melt, Marshall Space Flight Center has sponsored research to improve RF shaping-coil designs.

The improved design was directed at application in a low-gravity environment, as much of the applied shaping force is normally needed to overcome the effects of gravity. However, developments in the positioning and contouring of the coil have been sufficiently successful that the system may have application in normal environments.

The shaping sequence and simplified shaping concept is shown in Figure 1. For a ribbon 7.6 by 0.04 cm the RF coil requires 880 watts of power. The frequency, chosen so that the penetration (skin depth) is equal to the ribbon thickness, is slightly over 1 MHz. The copper shaping coil requires a mechanism for thermal control, such as a heat pipe, to maintain its electrical and mechanical properties. In addition, a thin layer of silver is deposited over the coil to reduce possible silicon contamination by such sublimated copper.

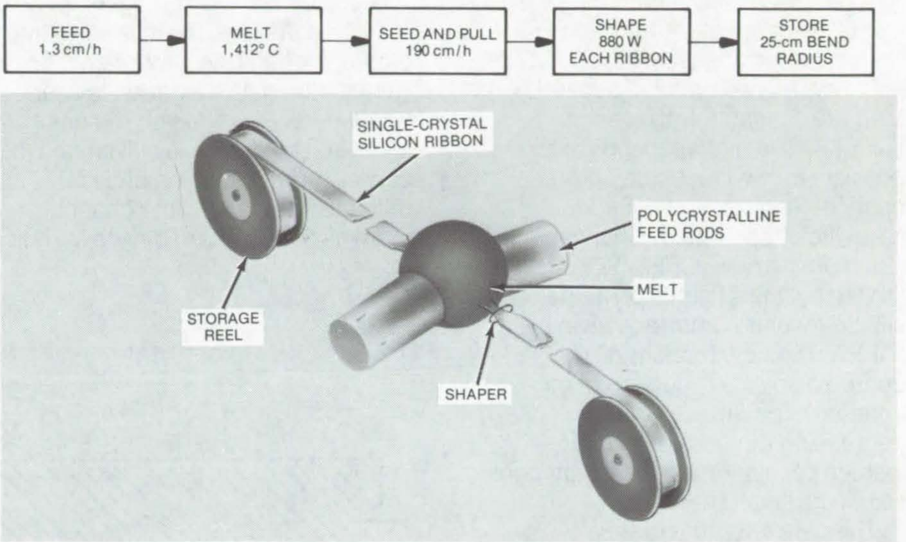

Figure 1. The **Silicon-Ribbon Fabrication Technique** RF electromagnetic forces to apply the pressure necessary to shape the melt. The shaping coil (see Figure 2) surrounds the melt near the solid-liquid interface and induces current in a surface region of the melt nearly equal to but opposite the coil current.

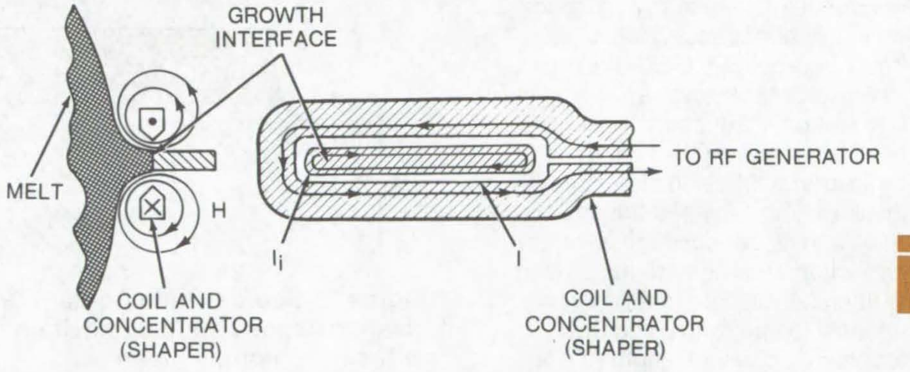

Figure 2. The arrows surrounding the **RF Shaping Coil** are for one instant only, as the current oscillates. The coil and the induced current generate an **H** field where the magnetic force (**IH**) acts in a direction to compress the liquid.

Figure 2 is a more detailed representation of the shaping process. The dimensions of the coil depend on the width and thickness of the ribbon. For an even amount distribution over the ribbon surface, the coil should be kept well away from the ribbon edges. The length of the coil (L_s) is approximately

$$L_s = 2w + 2\pi r_b + 2L_t$$

where w is the ribbon width,
r_b is the radius of coil bend, and
L_t is the distance from the ribbon to the cable connection where the coil is terminated.

The radial forces generated by a coil, as determined experimentally, decline exponentially as the distance from the coil increases. For an efficient system, 0.05 cm (0.02 in.) has been designated as the maximum coil-to-ribbon gap.

This work was done by Daniel A. Pelhank, Ross D. Rochat, and William Marx of McDonnell Douglas Corp. for **Marshall Space Flight Center.** *For further information, including coil dimensions and a discussion of the system, Circle 88 on the TSP Request Card.*
MFS-23424

IGFET/SOI Fabrication Method

Shorter channel length reduces parasitic capacitance. Switching speed, that one-time IGFET weak link, is considerably enhanced.

Marshall Space Flight Center, Alabama

A new method of fabricating the insulated-gate field-effect silicon-on-insulator transistor (IGFET/SOI) achieves higher switching speeds than are available with present IGFET's. The higher speeds are possible for two reasons: shorter channel length and reduced parasitic capacitance. Channel length in the new IGFET/SOI's is not limited by lateral diffusion at the silicon-insulator interface as in the IGFET. The new fabrication procedure also aids reduction of gate-channel capacitance, thereby decreasing the possibility of unwanted oscillation and resultant poor switching speeds.

The gate structure of the IGFET/SOI is pseudo-self-alined; e.g., it has very small dimensions compared to the conventional IGFET. The gate fabrication method, which is described in the figures, also results in virtually no gate overlap, resulting in minimum gate-to-channel capacitance. The implanted-gate FET/SOI has two main advantages over a conventional diffused enchancement-mode FET: (1) a rapid lateral diffusion along the Si-insulator interface of diffused impurities and (2) reduced Miller-effect capacitance. Lateral diffusion is a limiting factor in decreasing the channel length; and using this technique, channel length (the N region) can be reduced to the limits of the masking technology used to define the gate area — a factor of 5 or more reduction from the conventional FET.

The second advantage of the implanted-gate SOI transistor, its greatly reduced gate-to-channel capacitance (especially gate-to-drain Miller-effect capacitance), is achieved by using a self-alined polycrystalline Si gate. There is virtually no gate overlap (over source or drain) as the gate electrode is used to define the P+ diffusion regions. However, the device is still limited in source-to-drain spacing and is limited to about the same channel length as the standard devices. Thus its transconductance (g_m) is limited to about the same range of values as standard devices. The transistor also has about the same gate-channel capacitance, minus the overlap capacitance.

A third type of device employs a technique to overcome the limitation imposed by lateral diffusion. The

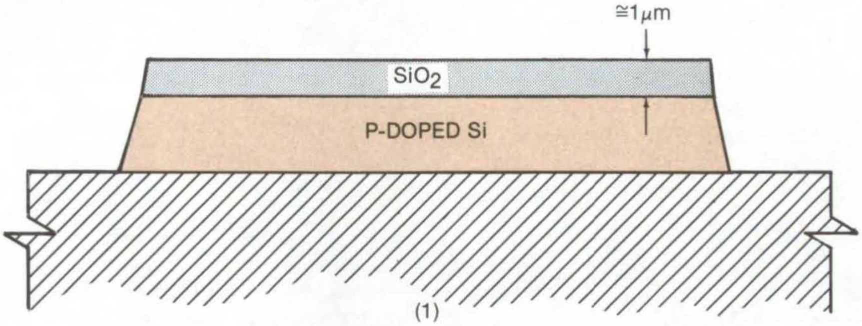

Figure 1. **Si Island Definition:** Si islands are defined to isolate transistors from one another using standard techniques.

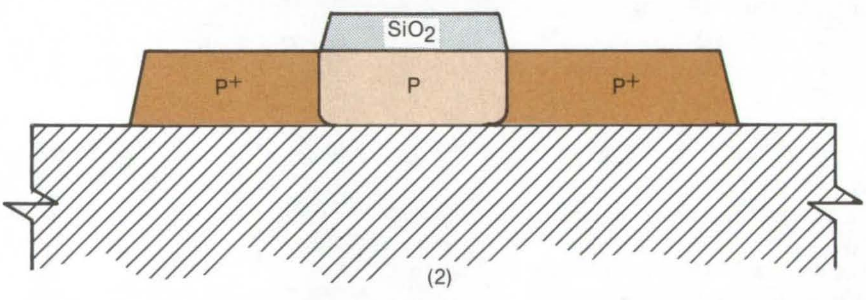

Figrue 2. **Source-Drain Contact Diffusions:** SiO_2 is selectively etched away to expose source and drain contact areas. These areas are then diffused by normal means.

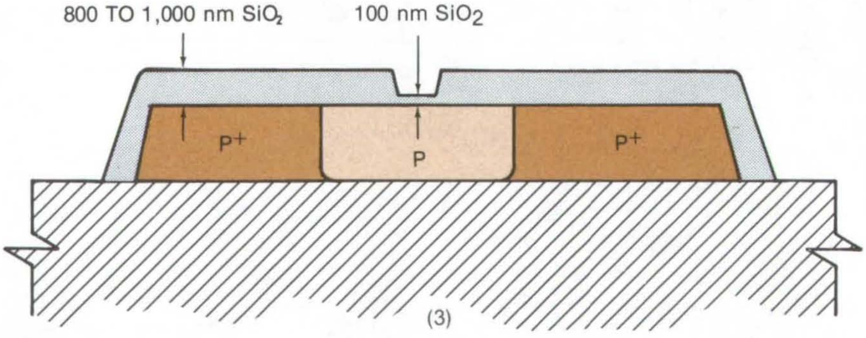

Figure 3. **Preparation for Gate Implantation:** Remaining SiO_2 is removed; then more SiO_2 is grown. The gate area is defined, and a 100-nm SiO_2 layer is grown.

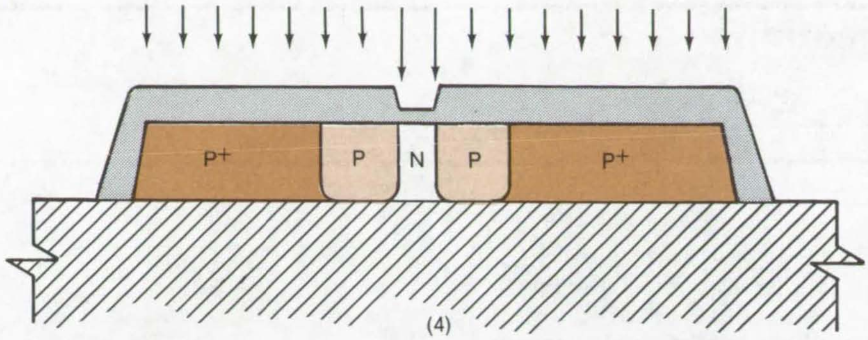

Figure 4. **Gate Implanted With N-Type Ions:** Wafer is subjected to N-type ion bombardment. Thick SiO_2 stops ions, while thin (100-nm) SiO_2 transmits ions as in normal ion implantation. Dosage is two times P-type concentration.

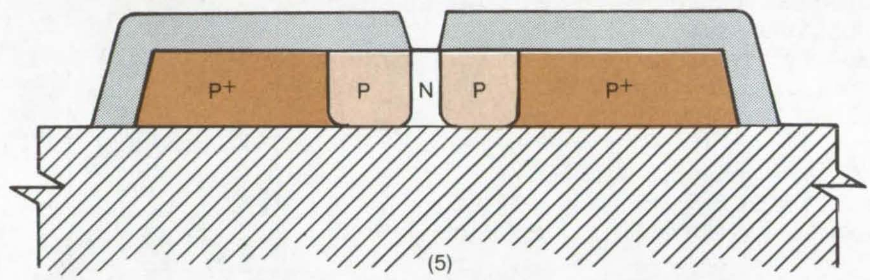

Figure 5. **Etch Away 100-nm SiO_2 Over Gate Area:** 100-nm transparent SiO_2 is etched away, and the wafer is cleaned for gate SiO_2.

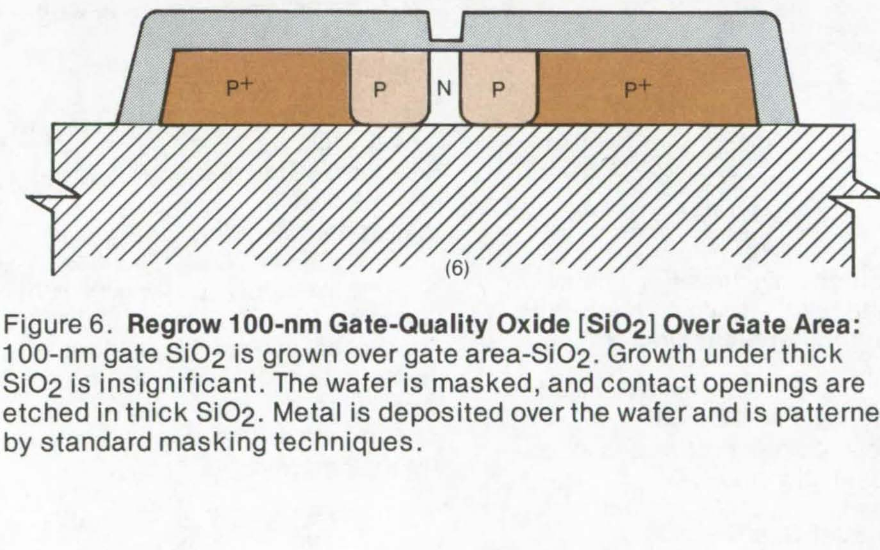

Figure 6. **Regrow 100-nm Gate-Quality Oxide [SiO_2] Over Gate Area:** 100-nm gate SiO_2 is grown over gate area-SiO_2. Growth under thick SiO_2 is insignificant. The wafer is masked, and contact openings are etched in thick SiO_2. Metal is deposited over the wafer and is patterned by standard masking techniques.

P+ regions are defined in a normal manner at a convenient spacing. Next the gate electrode is made as small as possible (limited by the ability to define the metal electrode). Finally the entire device is bombarded with P ions, thus doping the P+ gate gap as shown in Figure 4. The gate electrode protects the channel area from being doped. One disadvantage of this geometry is that the sharp doping profile of the implanted region might result in a low-voltage breakdown of the device due to high electric-field intensities in this region.

The double-diffused metal-oxide semiconductor (or DMOS) has been proposed as a very-high-speed IGFET/SOI. It is constructed by first independently doping the drain N and proceeding as with a standard self-alined gate device by P+ doping into the source, gate, and drain electrodes. The difference is that the channel is P doped instead of N. This geometry results in an extremely-short effective channel, supposedly giving high device speed and gain. Although this device may have very fast rise and fall times (in response to a pulse input), it may also have significant signal-propagation delay.

The new IGFET has the same electrical symbol as the conventional insulated-gate field-effect transistor. Note that, in the figures depicting stages of wafer growth, the P and N symbols may be reversed, thus forming complementary devices.

This work was done by William R. Feltner of **Marshall Space Flight Center.** *For further information, Circle 89 on the TSP Request Card.*

Inquiries concerning rights for the commercial use of this invention should be addressed to the Patent Counsel, Marshall Space Flight Center [see page A8]. Refer to MFS-23312.

Solar Cell Electrical Connections

A study of practical bonding techniques including thermo-compression bonding, parallel-gap welding, and ultrasonic welding.

Lewis Research Center, Cleveland, Ohio

A recent study was conducted to investigate solderless methods of electrically connecting solar cells intended to be encapsulated with Teflon FEP*. Results indicate that three bonding methods show promise as potential mass-production techniques for obtaining reliable, long-lasting electrical interconnects with silicon solar cells. These are: (1) thermocompression bonding, (2) parallel-gap welding, and (3) ultrasonic welding.

Numerous bonding and welding techniques have evolved over the years in the metalworking industry. However, the creation of solar cell technology with its attendant needs for establishing reliable, lightweight, flexible electrical connections between very thin, somewhat brittle, silicon solar cells has eliminated most of the traditional bonding methods. In addition, the electrical connections must withstand the 573 K (572° F) encapsulating-process temperature.

This study was conducted to find the best methods of attaching pure silver and silver-plated Kovar** interconnect ribbons to silicon solar cells with titanium-silver solderless contacts. Tests were conducted using 25 and 50 μm (0.001 and 0.002 in.) thick silver and 25 μm (0.001 in.) thick Kovar ribbons, 1.4 mm (0.055 in.) wide, and 10 mm (0.4 in.) long. The Kovar ribbons were plated with silver approximately 10 μm (0.0004 in.)thick. The solar cells were 0.4 to 0.6 mm (0.016 to 0.024 in.) thick with their titanium-silver contacts typically 3 μm (0.0001 in.) thick.

Thermocompression Bonding

This method consists of applying heat and pressure to the interconnect assembly by means of a press with separately controlled, electrically heated electrodes. Heating both electrodes instead of one produced better bonds with lower overall solar cell temperature. This technique also resulted in less cell breakage during bonding and less surface oxidation of the cells. The dark area of Figure 1 shows the combinations of weld force and duration which will produce acceptable bonds, e.g., 20 newtons (4.5 pounds) and 100 seconds, respectively. Minimum bonding temperatures were between 547 and 573 K (525° and 570° F), but the best bonds were obtained at 673 K (750° F).

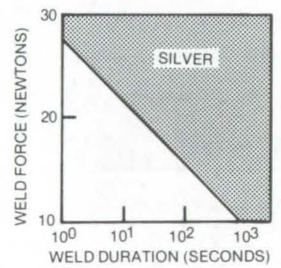

Figure 1. Domains in which good bonds could be made with **Thermocompression Bonding**

Although this method worked very well with the silver interconnects, it would not produce acceptable interconnects with the Kovar material.

Parallel-Gap Welding

A commercially available, parallel-gap, constant voltage welder with molybdenum electrodes was used for this part of the investigation. Good bonds were obtained for both the Kovar and the silver interconnect materials over a wide range of weld time, pressure, and voltage (Figure 2). The only disadvantage to this method was a degradation of electrical output in the maximum power region of the cell when excessive weld energy was applied to the cell N-contact.

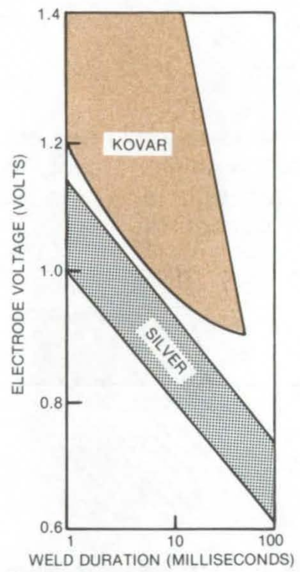

Figure 2. Domains in which good bonds could be made with **Parallel-Gap Resistance Welding**

Ultrasonic Welding

Both a 40-watt and a 75-watt commercially available bonder were used for ultrasonic welding of the interconnect ribbons. The applicable combinations of weld time and force are shown in Figure 3. Of the three methods evaluated, this method was least successful.

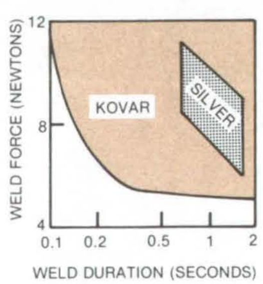

Figure 3. Domains in which good bonds could be made with **Ultrasonic Bonding**

*Trademark of DuPont, E.I. de Nemours & Co., Inc.

**Trademark of Carpenter Technology Corp.

A comparison of the three methods in responding to a "peel" test is shown in Figure 4.

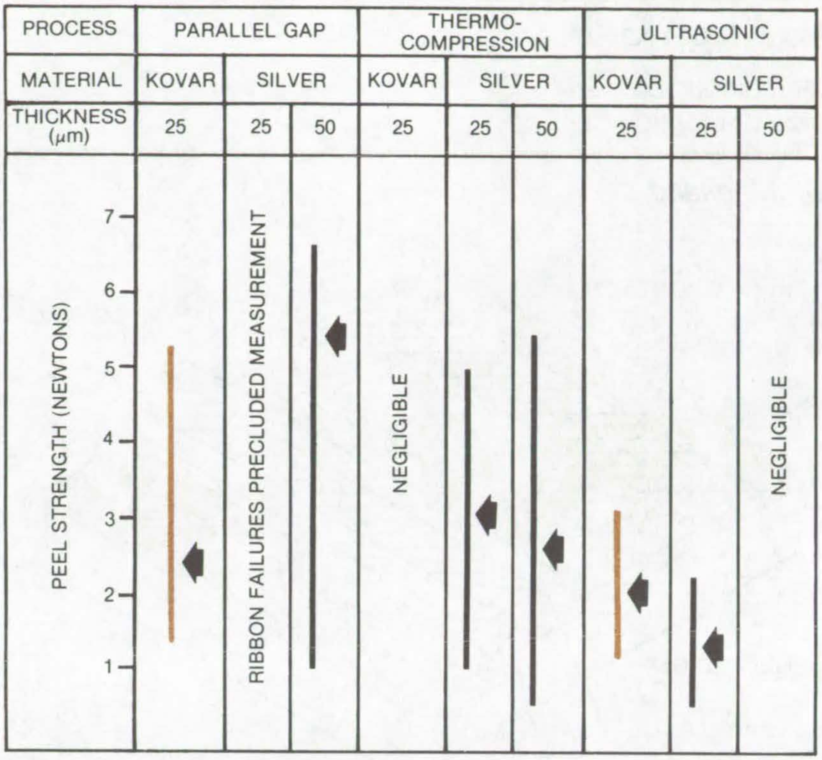

Figure 4. Comparison of **45° Peel Strength** obtained with three bonding methods: Line indicates range; arrow points to average.

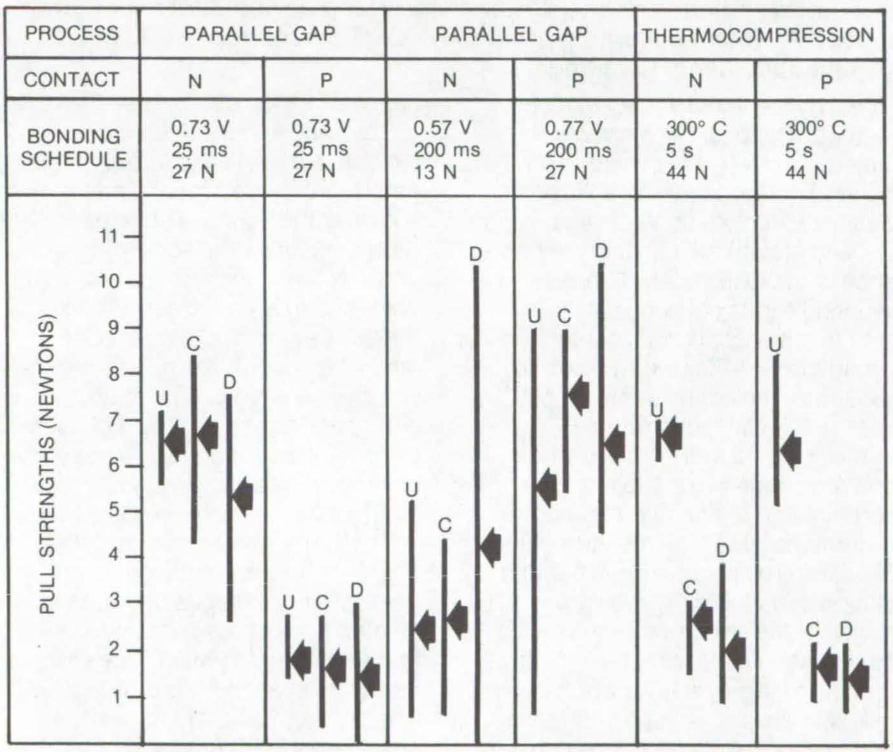

Figure 5. **Bonding Through Silane Layer** with two different parallel-gap processes and one thermocompression process. U = Untreated Cells, C = Treated With Concentrate Silane Solution, and D = Treated With Dilute Silane Solution.

Prior to encapsulating silicon solar cells with Teflon FEP, a silaning treatment is applied to the surface of the cells to promote adhesion of the encapsulant. In terms of the total module fabrication process, the most economical way to bond the interconnect is through the thin (one or more molecules thick) silane layer directly. Figure 5 shows that the bond strength of only the thermocompression bonding technique was adversely affected by bonding through the silane layer.

This work was done by Hans S. Rauschenbach and Hans G. Mesch of TRW, Inc., for **Lewis Research Center.** *Further information may be found in IEEE Order No. 74CH08011, "FEP Teflon-Covered Solar Cell Array Advancements," a copy of which may be obtained at cost [$25] from the IEEE Service Center, Department PB, 445 Hoes Lane, Piscataway, New Jersey 08854.*
LEW-12293

Epitaxial Growth of $Ga_{1-x}Al_xAs$ on GaP

A technique for the growth of light-emitting diodes on GaP substrates is suitable for monolithic device fabrication methods.

Goddard Space Flight Center, Greenbelt, Maryland

Recently there has been interest in the development of high-efficiency infrared light-emitting diodes (LED's) as pumping sources for Nd: YAG lasers. The $Ga_{1-x}Al_xAs$ mixed crystal system is very attractive for this purpose, since it has been shown to be superior for fabricating improved injection laser devices and for making efficient LED's by growing the crystals on GaAs substrates with the liquid-phase epitaxial (LPE) method. Further improvements in efficiency have been obtained recently by growing thick layers of $Ga_{1-x}Al_xAs$ on GaAs, removing the light-absorbing substrates, and forming the LED structures into a hemispherical geometry. A new technique permits the growth of efficient GaAlAs LED structures on transparent GaP substrates by the LPE method, thus obviating both the need for growing thick layers and for removing the substrates.

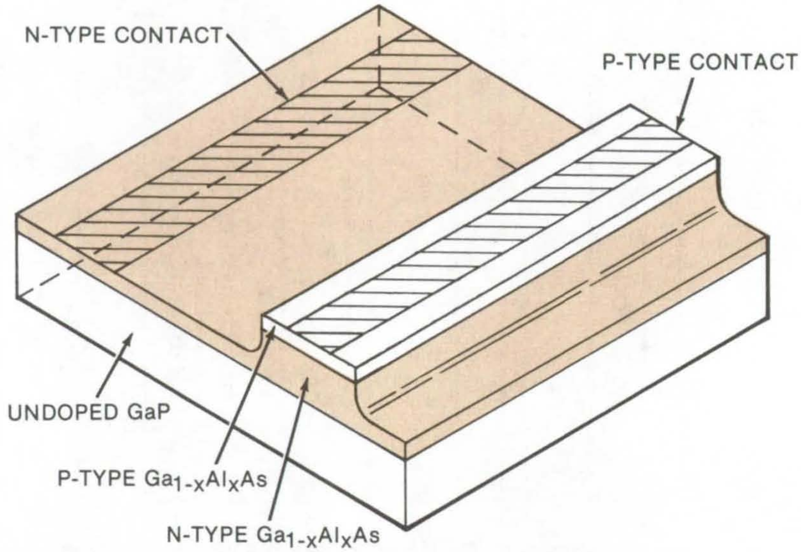

The **$Ga_{1-x}Al_xAs$ Mesa Diode on GaP Substrate:** Both contacts of the graded-layer diode are on the same side of the device. Light is emitted at 8500 Å, and the quantum efficiency is 1.2 percent up to 500 mA, without special heat sinking.

Two types of LED structures have been studied. The first was a GaAlAs n-type Te-doped layer which was counterdoped with Zn at one stage during growth to form the p-n junction. The layers were nearly linearly graded in composition along the growth direction, with the highest Al concentration occurring at the $GaP\text{-}Ga_{1-x}Al_xAs$ interface. The other type of layer, called the minimum-band-gap (MBG) structure, was such that the material with the smallest optical band gap was the material in which radiative recombination occurred. As a consequence of this structure, light leaving the generation region traveled into material with a very low absorption constant for the energy of the emitted light. Thus, with suitable geometries such as dome-shaped emitters, large external quantum efficiencies should be realized.

The growth experiments were performed on (111), $(\bar{1}\bar{1}\bar{1})$, (031), and (100) GaP surfaces. The GaP substrates were cut from crystals grown by the liquid encapsulation method. The best results were obtained with the $(\bar{1}\bar{1}\bar{1})$ surfaces. In order to achieve smooth epitaxy it was necessary to upheat a saturated GaAlAs growth melt 5° C in the presence of the GaP substrate before initiating expitaxial deposition. This resulted in phosphorous contamination in the GaAlAs layer next to the substrate, indicating some etch back of the GaP substrate.

It was found that phosphorous contamination in the radiative recombination region of the structure is detrimental to high quantum efficiencies. The phosphorous contamination can be greatly reduced in this region of the structure if, before the continuation of growth, the substrate and the first-grown layer are moved into subsequent $Ga_{1-x}Al_xAs$ melts that are free of phosphorous contamination. The growth temperatures studied were between 825° and 885° C, and the melt cooling rates were between 0.1° and 0.17° C/min. The melt compositions were based on 5g Ga and Excess GaAs.

Test diodes have been made using both types of structures. An example of a graded-layer diode is shown in the figure: a schematic representation of a diode structure which is mesa etched to allow both contacts to be on the same side of the device. The width of the GaP face is about 0.073 cm. This particular device emitted light at 8500 Å and operated at a quantum efficiency of 1.2 percent up to 500 mA without special heat sinking. The resistance of the device was about 0.5 Ω.

The same type of layer with the GaP substrate formed into roughly hemispherical shapes operated at an efficiency of 5.5 percent. The first results on the MBG-type structure were even more promising. Efficiencies of 3 percent for a peak emission of 8000 Å have been measured for mesa-etched structures, when the measuring cell collected only the light that was emitted through the GaP face.

There are currently several problems which need to be solved before large-scale device fabrication can be accomplished. There is evidence that a large amount of strain is generated at the GaP-$Ga_{1-x}Al_xAs$ interface because of the difference in both the lattice constants and the thermal-expansion coefficients. The $Ga_{1-x}Al_xAs$ layers will crack if the layers are over 20 μm thick. Cracking will also occur if the $Ga_{1-x}Al_xAs$ layer next to the GaP substrate is not graded in phosphorus in a manner which decreases from substrate to surface of the first layer at about the 0.1-0.01 weight fraction level.

In addition to cracking, there is evidence of other metallurgical imperfections in the layers. Currently, it is possible to fabricate single test units that are free of cracks. It is anticipated that growth conditions will be found to produce layers which are suitable for monolithic device fabrication methods.

This work was done by J. M. Woodall and G. I. Farmer of IBM Corp. for **Goddard Space Flight Center.** *For further information, see J. M. Woodall, R. M. Potemski, and S. E. Blum, $Ga_{1-x}Al_xAs$ LED Structures Grown on GaP Substrates, Appl. Phys. Letters, vol. 20, no. 10, 15 May 1975.*
GSC-11826

Method of Removing Drilling Chips

A special chuck and a fluid line are used to flush out chips during drilling.

Marshall Space Flight Center, Alabama

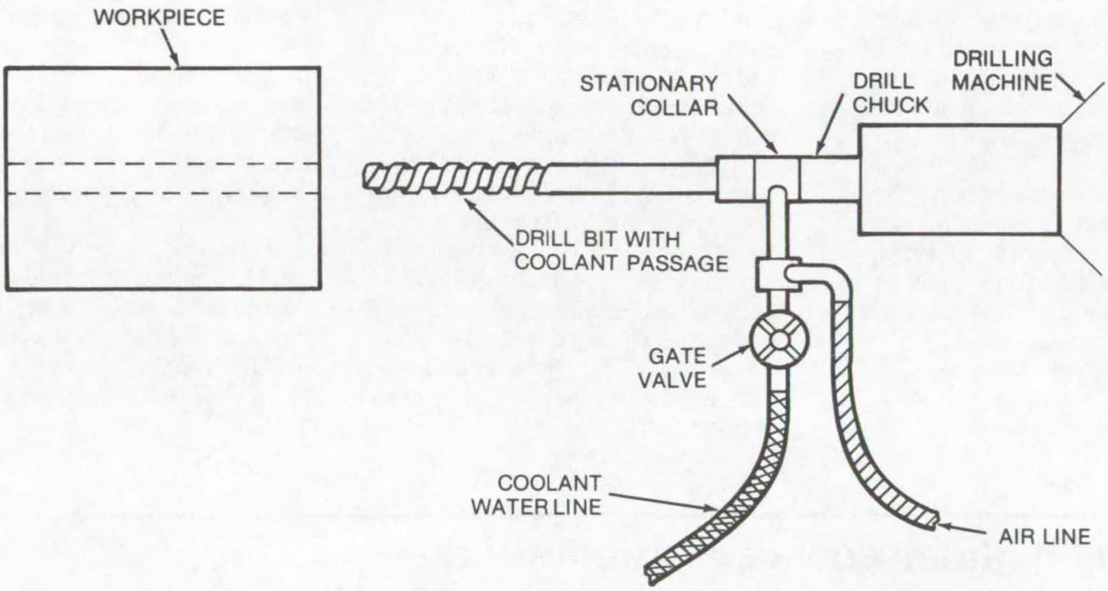

The **Drill Chuck with Axial Coolant** forces a mixture of air and coolant through the drill bit to flush out long holes as they are drilled.

It is difficult to remove drilling chips during the boring of long, large-diameter holes, for example in gun barrels. A new technique simplifies this operation. A special chuck (see figure) has been designed to receive a mixture of water and pressurized air during operation and to direct this mixture into a coolant passage within the drill bit. In operation, the water and air flush the hole being bored in the workpiece, thereby removing the chips.

This work was done by Francis E. Ransom of Rockwell International Corp. for the **Marshall Space Flight Center.** *For further information Circle 90 on the TSP Request Card.*
MFS-19235

Polishing Gold and Gold-Alloy Crystals

Surface damage is reduced when polishing cross-section samples of single crystals.

Marshall Space Flight Center, Alabama

In order to evaluate imperfections in gold-copper alloy single crystals, it is necessary to have a cross-sectional slice with a polished undamaged surface. Conventional means of polishing the surface after cutting cause even further damage, making evaluation impossible. Conventional cutting, grinding with 14-micron grit, and 0.05-micron grit polishing cause surface damage that extends much further into the crystal than is predicted by analytical means. When a grit-polished surface is etched to a depth below this surface damage, the etchant further damages the surface beyond evaluation. Chemical bath polishing produces results similar to those of conventional grit polishing.

A new polishing technique circumvents these problems. A single crystal of gold-copper is cut slowly on a chemical string saw or a wire saw to keep deep surface damage to a minimum. The surface is then rough polished with 14-micron grit, keeping the pressure on the crystal as light as possible. After the saw marks have been completely polished away, the polishing grit is changed to 0.05 micron, and the polishing pressure is maintained at a minimum level. The surface is polished until it has a smooth or almost smooth appearance. If the slice is polished too long, then gaulding will occur which produces deep scratches. When a smooth appearance is attained, the surface is then chemically polished by hand in a dust-free room.

A Corfam, or equivalent, polishing pad is cleaned, washed thoroughly, and rinsed with distilled water. A gold etchant, a mixture of 10 percent KCN and 10 percent $(NH_4)_2S_2O_8$, is used as the chemical polishing agent. This solution is poured onto the Corfam pad until a small pool is formed. Using surgical rubber gloves, the crystal is hand polished with a light, brisk, circular, or figure eight motion. Most importantly, the solution must be changed whenever a small amount of drag is noticed on the crystal.

If the polishing motion is halted during chemical solution change, then the surface must be rinsed off with distilled water immediately after motion stops. A continual flow of fresh chemical over the pad is ideal, and the flow rate should be such that a minimum of drag on the crystal is experienced at all times. (During the experimental development period, the surface was examined after every 15 to 20 minutes of polishing.) After a total of 12 to 14 hours of hand polishing, the damaged surface begins to be chemically eroded through, and the undamaged crystal begins to appear. Beyond this point the crystal surface can be etched by standard methods, and crystal defects which are not caused by the cutting and polishing can be observed.

This work was done by J. P. Doty of Eagle-Picher Industries, Inc. for **Marshall Space Flight Center.** *For further information, Circle 91 on the TSP Request Card.*
MFS-22800

Soldering High-Impedance Nichrome Wire

A nickel wire segment allows Nichrome wire to be soldered without changing its electrical characteristics.

Marshall Space Flight Center, Alabama

A Nichrome wire can neither be brazed nor soldered by ordinary means without changing its electrical properties. In a new technique, a nickel wire segment is attached to the Nichrome wire. The nickel may then be silver soldered, for example, to a coaxial cable connector.

The cable is first prepared for assembly. The Nichrome wire (see figure) is trimmed to 0.09 in. (0.23 cm). A nickel wire 0.051 in. (0.13 cm) in diameter is bonded to the conductor, as shown, by percussive arc welding. The exposed conductor is trimmed to 0.22 in. (0.56 cm), and the assembly is then completed as required.

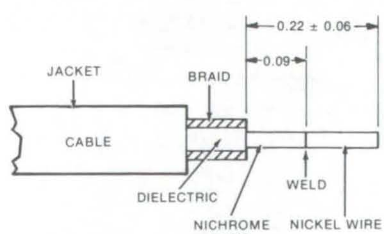

A **Solder Termination** for Nichrome wire consists of a short section of nickel wire.

This work was done by M. Spruill and P. R. Callen of Rockwell International Corp. for **Marshall Space Flight Center.** *For further information, Circle 92 on the TSP Request Card.*
MFS-1457

Diffusion Brazing Nickel-Plated Stainless Steel

Nickel-plated stainless steel can be brazed to aluminum at one-tenth the conventional pressure.

Lyndon B. Johnson Space Center, Houston, Texas

Conventional diffusion bonding of stainless steel to aluminum is accomplished by first placing chrome-over-nickel plating on the stainless steel. The aluminum and stainless steel parts are then subjected to a platen pressure of 2000 psi (1.4×10^6 N/m^2) at 850° F (455° C) for 4 hours. Such high pressure for such a long period of time may cause the aluminum to deform.

A modified process has been developed which requires only 10 minutes and a pressure of 200 psi (1.4×10^6 N/m^2). The lower pressure reduces the chance of aluminum deformation, and the reduced time requirement promises to make this process more economical than the conventional method. The process has been used to bond a stainless steel part to an aluminum cold plate as shown in the illustration.

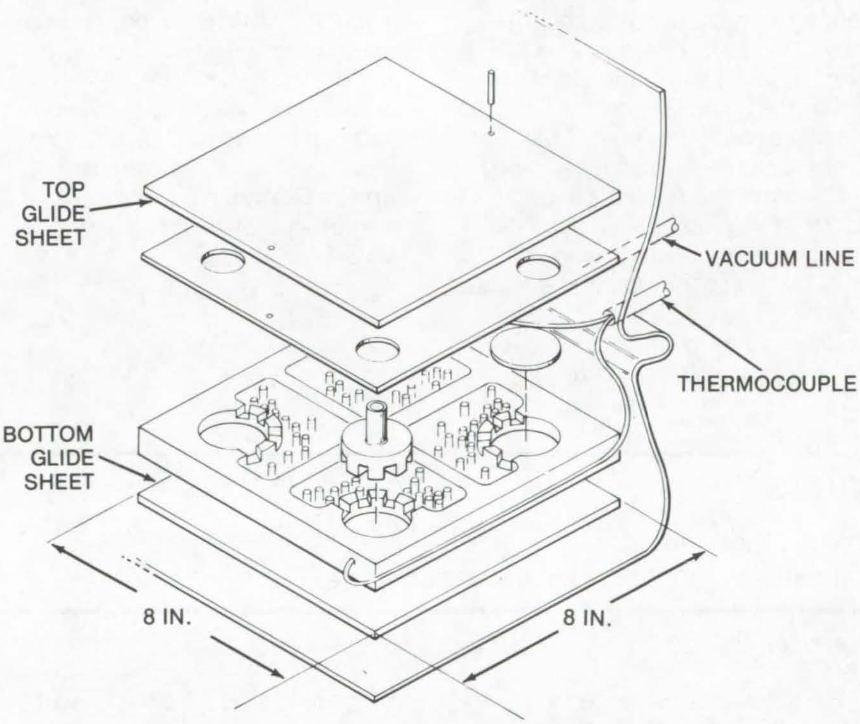

The **Diffusion Bonding Process** as developed for a stainless steel/aluminum heat exchanger requires only 10 minutes at 200 psi to reduce the deformation of the aluminum parts. The stainless steel/aluminum sandwich is placed between a bottom and top glide sheet that is placed in a stainless steel retort where the assembly is bonded at 580 °C.

To bond the parts, a sandwich assembly is made up of the aluminum core, an aluminum face sheet with a brazing-alloy interface, and the stainless steel part which has been nickel plated. The core and the face sheet are cleaned chemically prior to assembly. The stainless steel part is chemically cleaned and plated with 100 μin. (2.5 μm) of nickel.

The sandwich assembly is placed between two stainless steel glide sheets which in turn are placed in a stainless steel retort. The retort is sealed, evacuated, and placed in a heated platen press. The assembly is bonded at approximately 1075° F (580° C) and 200 psi for 10 minutes. The nickel-plated stainless steel bonds to the aluminum core, and the aluminum face sheet is brazed over the entire assembly.

This work was done by C. S. Beuyukian and M. J. Mitchell of Rockwell International Corp. for **Johnson Space Center.** *For further information, Circle 93 on the TSP Request Card.*
MSC-19322

Ultra-lightweight Pressure Vessels

A tank fabricated from two composite overwrapped metal sphere halves is 66 percent lighter than a similar all-metal vessel.

Lyndon B. Johnson Space Center, Houston, Texas

Ultra-lightweight pressure vessels formed from a metal liner and a composite overwrap have, to date, been utilized in applications where weight-saving materials are of prime importance. A metal tank liner having a spherical diameter of 12.5 in. (31.8 cm) with a composite [Kelvar/epoxy (or equivalent) resin] overwrap, for instance, weighs only 66 percent of a similar Inconel vessel. However, composite tanks fabricated from two metal spheres which are pressure welded and then wrapped with a plastic composite offer advantages other than light weight. The failure characteristics of the tanks differ from the all-metal versions: The new tanks offer improved worker safety since, in the event of tank failure, the overwrap minimizes shrapnel effects. The overwrap also tends to shift the failure mode to that of cyclic leakage.

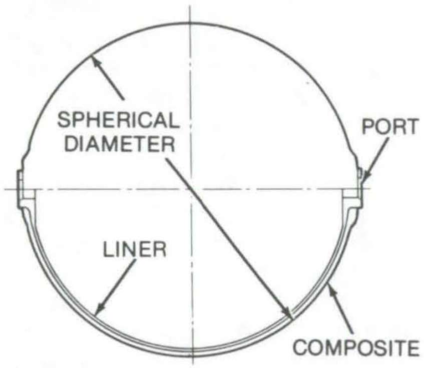

The Pressure Vessel has a spherical diameter of 12.5 in. (31.8 cm). A vessel 25 in. (63.5 cm) in diameter also is fabricated by using ultra-lightweight alloy metals with a composite overwrap.

The composite wall thickness is able to withstand minimum burst pressure, without considering the load-carrying capability of the metal liner. The composite is applied in multiple planar wrap patterns such that the thickness and materials orientation is essentially constant in all directions. Additional patterns are applied adjacent to polar openings for local reinforcement of blowout loads.

Liner assemblies are fabricated with matching hemispheres, machined from forgings with integral polar bosses and joined at the center girth using conventional metal pressure vessel technology. The liner serves as a winding mandrel and is pressurized during assembly when added rigidity is required. The completed vessel is finally proof-pressured nondestructively.

This work was done by Wayne W. Schmidt and Russell O. Hawkins of Brunswick Corp. for **Johnson Space Center.** *No further documentation is available.*
MSC-14983

Stripper for Silicone Polymers

Potassium hydroxide in an ethyl alcohol solution can strip away coatings, adhesives, and encapsulants without damaging the substrate.

Lyndon B. Johnson Space Center, Houston, Texas

An ethyl alcohol solution of potassium hydroxide (KOH), after aging a few weeks, becomes an effective stripper for silicone polymers, such as coatings, adhesives, encapsulants, oils, greases, and potting compounds. Strippers of this type are usually either acids that often corrode carbon steel or abrasives that tend to damage the substrate. The hydroxide solution removes silicone without these damaging characteristics. However, precautions for handling the hydroxide solution must be observed due to its hazardous properties.

The solution is prepared by dissolving 100 grams (3.5 oz) of KOH in 3 liters (3.2 qt) of denatured ethyl alcohol; the KOH is added slowly to prevent excessive heating. The solution is stored in a polyethylene container until the solution has acquired a deep red color. Polymers are stripped by immersing the part in the KOH solution at room temperature for 30 to 40 minutes and scrubbing it occasionally with a stiff brush. The part is then rinsed under running warm water using a stiff brush to assist in the removal of residue.

The solution is known to be effective on RTV-560 adhesive within a few days after adhesive application. It has little effect on RTV-566 adhesive and appears to have reduced effectiveness on aged RTV-560.

This work was done by Billy B. Williams of Rockwell International Corp. for **Johnson Space Center.** *No further documentation is available.*
MSC-19380

Improved Photochemical Etching of Stainless Steel

Machining jobs previously requiring electrical-discharge machining can be done by photochemical etching.

Lyndon B. Johnson Space Center, Houston, Texas

An improved photochemical-etch machining process combines conventional materials and techniques in a new way to produce a tougher and more-adherent photoresist coating on stainless steel. The coating withstands longer exposure to acid etch spray without cracking or flaking. It permits etching to a depth of 0.050 in. (0.127 cm) where it was previously restricted to 0.010 in. (0.025 cm).

The step-by-step procedures as developed to machine cold plates made from 347 CRES stainless steel are as follows:

Surface Treatment (of the 347 CRES stainless-steel base material)

1. Degrease in a vapor degreaser (trichloroethylene).
2. Vapor-hone the material on both sides.
3. Alkaline-scrub clean, and follow with a double water rinse.

Conversion Coating

4. Immerse the base material for 20 minutes in a 20-percent solution of nitric acid and water (concentrated nitric acid, 20 percent by volume) at 155° F (67° C).
5. Rinse in running water at room temperature.
6. Remove the water with oil-free compressed air.

Photoresist

7. Immerse the base material in Dynchem liquid resist No. DCR 3118HP (or equivalent).
8. Air-dry in a lighttight cabinet; follow with a heat cure at 180° F (82° C) for 20 to 30 minutes.
9. While the base material is still hot [150° F (65° C)] apply Dynchem dry-film photoresist (or equivalent) to both sides, using a roller applicator.
10. Allow the coated material to cool to room temperature.
11. Apply the photo artwork film to both sides, and expose it to a mercury-vapor light source (3,500 angstroms).
12. Remove the artwork film.
13. Develop a vapor degreaser (trichloroethylene) developer.
14. Inspect.
15. Touch up with Dynchem liquid touchup, DCR 5000TU (or equivalent), if required, and oven-dry at 130° F (55° C) for 30 minutes.

Etching

16. Etch in a solution of ferric chloride 36° to 43° Bé in a Chemcut No. 547 (or equivalent) spray etching machine at 130° F.
17. Etch both sides up to a depth of 0.050 in. Check the depth each second pass through the machine.
18. Strip. Remove the photoresist from the completed part, using Dynchem stripper No. SMR-5000 (or equivalent).
19. Alkaline-clean, and dry with oil-free air.
20. Inspect and package.

This work was done by Gene E. Lotgering of Rockwell International Corp. for **Johnson Space Center.** *No further documentation is available.*

Inquiries concerning rights to the commercial use of this invention should be addressed to the Patent Counsel, Johnson Space Center [see page A8]. Refer to MSC-19728.

Electron-Beam Welder Alinement

Parts can be easily and quickly positioned in an electron-beam welding vacuum chamber with the use of an inexpensive thin metal-foil plate.

Lyndon B. Johnson Space Center, Houston, Texas

An inexpensive method of quickly positioning parts in an electron-beam welding chamber can also be used in electron-beam machining. It consists of placing a piece of thin [0.005 in. (0.012 cm)] stainless-steel foil under the focus-coil housing of the welder, using vacuum grease. A pulse of the electron beam is used to pierce a pinhole in the foil. The light emitted by the filament when the welder is in the filament-only operating condition is then used to indicate the position of the electron beam on the piece to be welded. This method is much faster and easier to use than the standard crosshair optical or mechanical pointer systems, which also require frequent cleaning.

This work was done by Edwin L. Whiffen of Rockwell International Corp. for **Johnson Space Center.** *No further documentation is available.*
MSC-19642

Overhead Tray for Cable Test System

An overhead slotted tray housing a set
of adapter cables reduces test cable hookup time.

Lyndon B. Johnson Space Center, Houston, Texas

A major element of cost for electrical-cable checkout is the time required to run special test cables from the console to the cable assembly area. A new system reduces hookup time and also reduces the cost of fabricating and storing the test cables. The system consists of an overhead slotted tray, a series of compatible adapter cables, and an automatic cable test set which consists of a control console and a cable-switching console. The connector system can be used in the construction and testing of multiple-wire cable runs where considerable redundancy of cables is experienced.

The overhead slotted-tray cable support provides out-of-the-way runs of standardized test cables from the test consoles to convenient dropthrough points above each harness assembly station. Short easily-handled adapter cables permit quick-test plug-in. The photograph shows one implementation of the connector system. Floor-type test connector cables are used with short special adapters to reduce cable cost and to speed up test connections.

The overhead slotted tray is equipped with locking wheels that save time when moving the checkout station to different locations. Cable tiedowns are used to fasten down the test cables hanging between the slots, and they also speed up the rearrangement process of the standard cables when locating the system at other cable

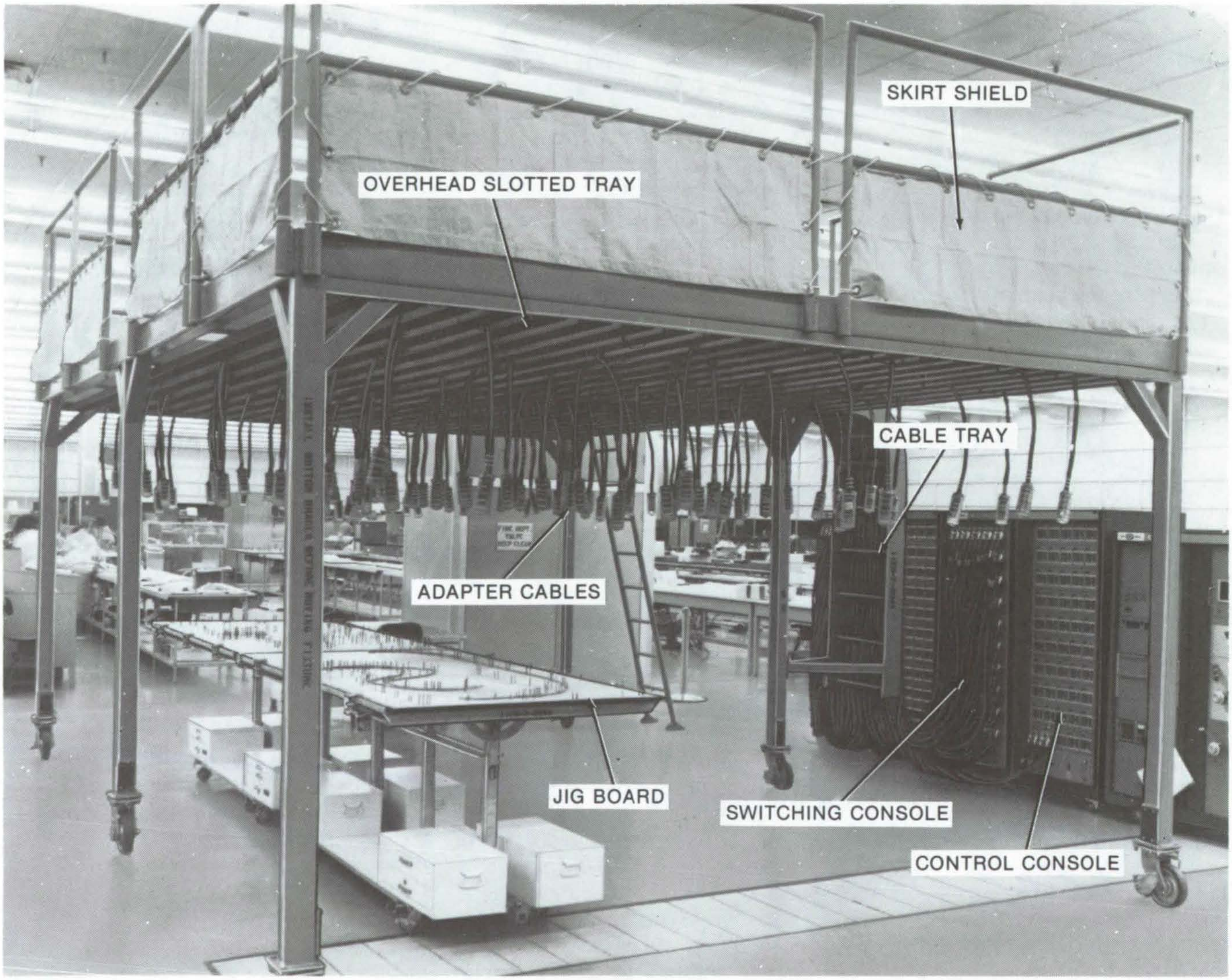

Overhead Tray for Cable Test System secures the test cables. It may be wheeled from one test site to another. Cable tiedowns speed the cable rearrangement process at the sites.

fabrication sites. The equipment in the overhead tray is made more secure by using the tiedowns, and cabinets are provided to store the short adapters for the various test sets.

This work was done by Kenneth T. Saltz of Rockwell International Corp. for **Johnson Space Center.** *No further documentation is available.* *MSC-19488*

3-D Foam Adhesive Deposition

A method for bonding 3-D foam is applicable to thermal insulation, acoustical barriers, and consumer goods.

Marshall Space Flight Center, Alabama

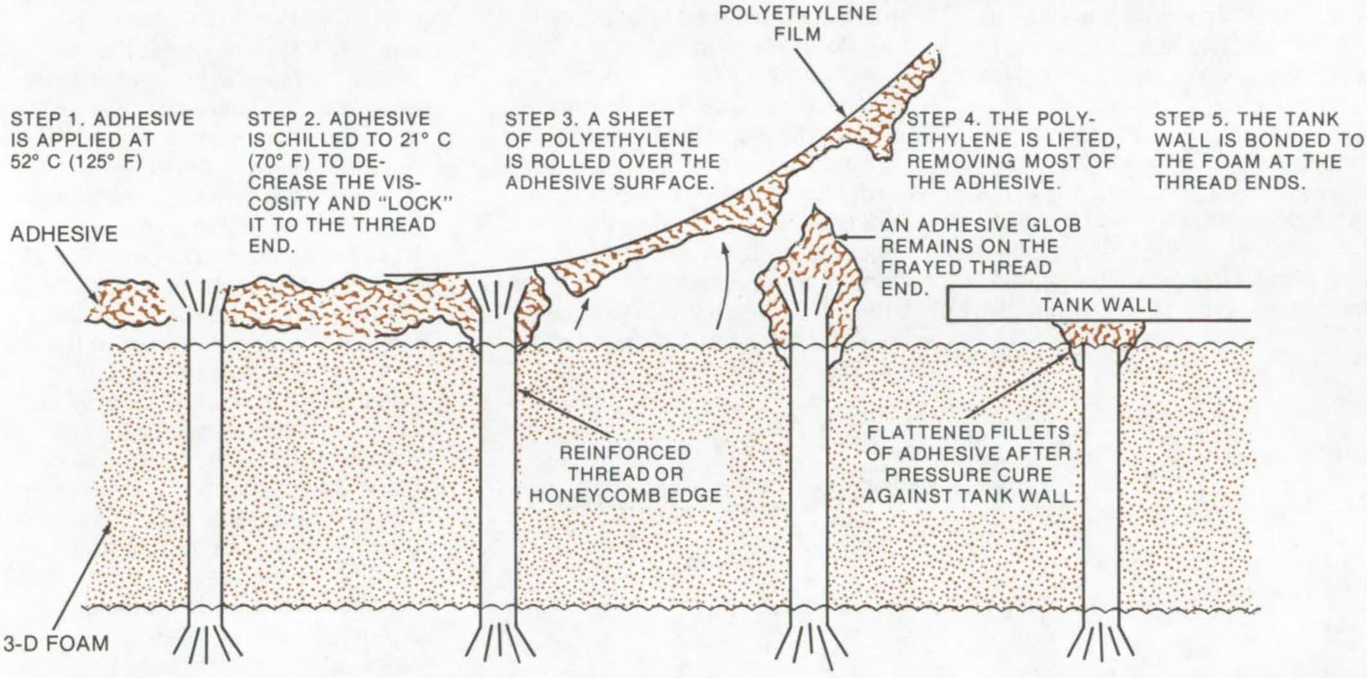

For **Adhesive Deposition Technique** of a foam core to a tank wall only the protruding ends of the threads are covered with adhesive. This reduces weight, but still results in a strong bond.

A new method for bonding 3-D foam reduces the amount and weight of the adhesive. The method is applicable to 3-D foam and foam-filled honeycomb-sandwich constructions. The novel features of the process (illustrated in the figure) are:

- A temperature-viscosity control that provides fiber-wetting and locking actions around thread ends and
- The removal of excess adhesive by transfer to cellophane film.

The reduction in adhesive weight that is possible using this method is dependent on the control of adhesive temperatures during critical operations. Tests have shown the method to be reliable in reducing the adhesive weight to less than one-half the normal amount, although greater reductions are possible.

The adhesive is applied at an elevated temperature in order to saturate the supporting threads. The system is then chilled, and excess adhesive is removed with an inexpensive cellophane roller. The net result is that only the protruding ends of the threads are covered with adhesive, reducing weight while at the same time providing adequate bonding properties. Industrial applications include acoustical barriers, thermal insulaton in public buildings, and the fabrication of decorative consumer goods.

This work was done by Carl R. Lemons and Omar K. Salmassy of McDonnell Douglas Co. for **Marshall Space Flight Center.** *For further information, Circle 94 on the TSP Request Card.* *MFS-22739*

Synchronized Backside-Weld Follower

An infrared sensor for sensing the backside hot spot is particularly useful with ferrous materials.

Marshall Space Flight Center, Alabama

Previous machine welding techniques using penetration control based on infrared sensing of the backside weld hotspot temperature require mechanical linkage between the weld power input side and the dropthrough side. To circumvent this problem, a magnetic tracking system has proved satisfactory for nonferrous materials. Materials which are ferrous, magnetic, or both, can be accommodated by a new infrared system.

For curved-path tracking with respect to the power input side, the new system employs two sets of infrared detectors on the dropthrough side for sensing. The first set functions with a closed-loop motor control system in the azimuthal direction (see figure), and the second set with its closed-loop motor control system positions the elevation. The systems locate the spot of highest temperature on the dropthrough side and track this moving spot throughout the weld length. Because the azimuth and elevation control systems are identical circuits, only the azimuth control circuit is illustrated.

The two sensors shown in the figure are incorporated into a bridge circuit. The signal is input to these sensors by a combination of lenses and mirrors. A balance of the bridge is achieved when the two sensors are positioned on either side of and equidistant from the spot of highest temperature. The output signal from the bridge circuit is passed to a differential amplifier, which in turn feeds the emitter follower stages. The emitter follower outputs are in turn fed into a wideband operational amplifier which, finally, is connected to the tracking motor.

Mechanically linked to the motor is a multiturned potentiometer which is electrically connected to a meter that indicates motor position. A slew control for setting the motor initial position is also included. The sensors in the bridge circuit will produce equal signals when the unit is centered on the spot of highest temperature. An unbalanced sensor output will result in the closed-loop motor system making a correction to lock onto and track the desired spot.

Another infrared sensor (not shown) may be added so that the programed distance between it and the weld hotspot is held constant. Together with a closed-loop current control system, it insures that the welding equipment maintains a constant weld penetration. The system can also be programed to control the offset for delayed opposed arc welding. The new system is currently more expensive than previous systems, which use oscillating scanners, but offers faster response and higher reliability.

This work was done by William F. Iceland and William M. Beaupre of Rockwell International Corp. for **Marshall Space Flight Center.** *For further information, Circle 95 on the TSP Request Card.*
MFS-24454

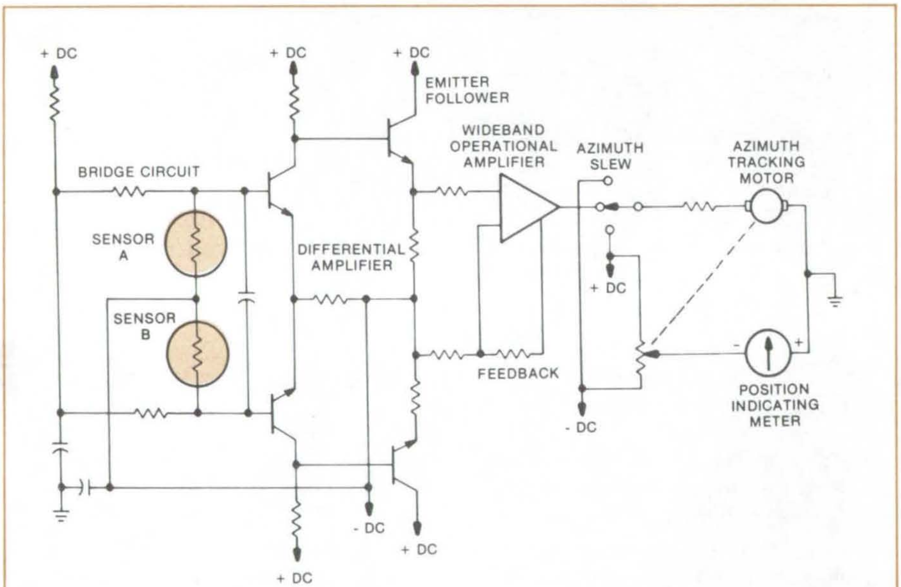

The **Infrared Azimuth Motor Control System** has two sensors incorporated into a bridge circuit. The signal is fed into these sensors by a combination of mirrors and lenses.

Ablative-Filled Honeycomb Composites

Two techniques reduce fabrication cost and complexity.

Langley Research Center, Hampton, Virginia

Two new techniques have been developed to simplify and reduce the expense of fabricating ablative-filled honeycomb composite structures. One technique, called net surface molding, permits ablative insulators with sculptured tapers to be produced over a substrate having unpredictable irregularities. Thickness may easily be controlled with a precision of $\pm$ 0.010 in. ($\pm$ 0.025 cm). Previous methods, which were very costly and not very reproducible, required a final machining of the entire outer surface after curing the ablative to an oversize thickness. This required that the depth of the molded material, to the substrate, be measured, followed by a rough machining and a final hand finishing to produce a tapered surface of precise thickness.

The second technique, called subsurface molding, results in an ablative surface below the honeycomb face. Then the composite is machined using the honeycomb face as a tooling reference surface. The method may also be used to fabricate composites having thin strata of different densities throughout their core thicknesses. This makes it possible to tailor the heat-char and ablation rates to satisfy varying requirements and to produce localized islands of high or low density without costly premolding or multiple-cure processing.

The steps of the processing sequences for both techniques are similar.

1. The core is machined in detail to final thickness using simple plane-surface machining methods, and the core thickness is verified. The core may be tapered as desired at that time.
2. The core details are hot formed and are bonded together. Alternatively, this may be done prior to machining.
3. The substrate and all details are cleaned.
4. The core is bonded to the substrate. Simple depth measurement techniques may be applied then to verify the core thickness.
5. The core is primed, and a base coat is applied.
6. The preweighed quantities of the desired filler are loaded to given surface areas using loading frames, a slipsheet, and a leveler bar.

At this stage the two techniques differ. If the first process is being used, proceed directly to step 10.; if the second process or a variable density core filler is desired, then:

7. Uncured silicon gum-rubber sheets are positioned over the surface to be molded and serve to drive the filler into the core, producing controlled depressions.
8. The filler is cured under a vacuum bag in a convection oven.

This completes the subsurface molding process. For a variable density filler that completely fills the honeycomb core, the steps are:

9. The gum rubber is then stripped away, and step 6. is repeated, using a filler of a different density.
10. The last of the filler is pressed into the cells which are then covered with a flexible pressure membrane. A controlled pressure is applied over the membrane, assuring uniform cell filling and the control of the filler densities.
11. The flexible pressure membrane is removed, and the excess filler extending beyond the core surface is removed using flexible strips of metal shim stock as scrapers.
12. Rigid caul sheets are positioned over the surface to be molded and serve to bridge over the core cell width. This prevents the core pressure membrane from pulling into the cells, thus precluding the possibility of an uneven filler thickness occurring across the open cell faces.
13. The filler is finally cured under a vacuum bag in a convection oven.

The resultant ablative net thickness has a molded finish which requires no additional machining.

This work was done by H. L. Linebarier of Martin Marietta Corp. for **Langley Research Center.** *No further documentation is available.*

Inquiries concerning rights for the commercial use of this invention should be addressed to the Patent Counsel, Langley Research Center [see page A8]Refer to LAR-11180.

Compound Solder Joints

A technique for joining pipes under sterile conditions can be used to join dissimilar-metal tubes.

Langley Research Center, Hampton, Virginia

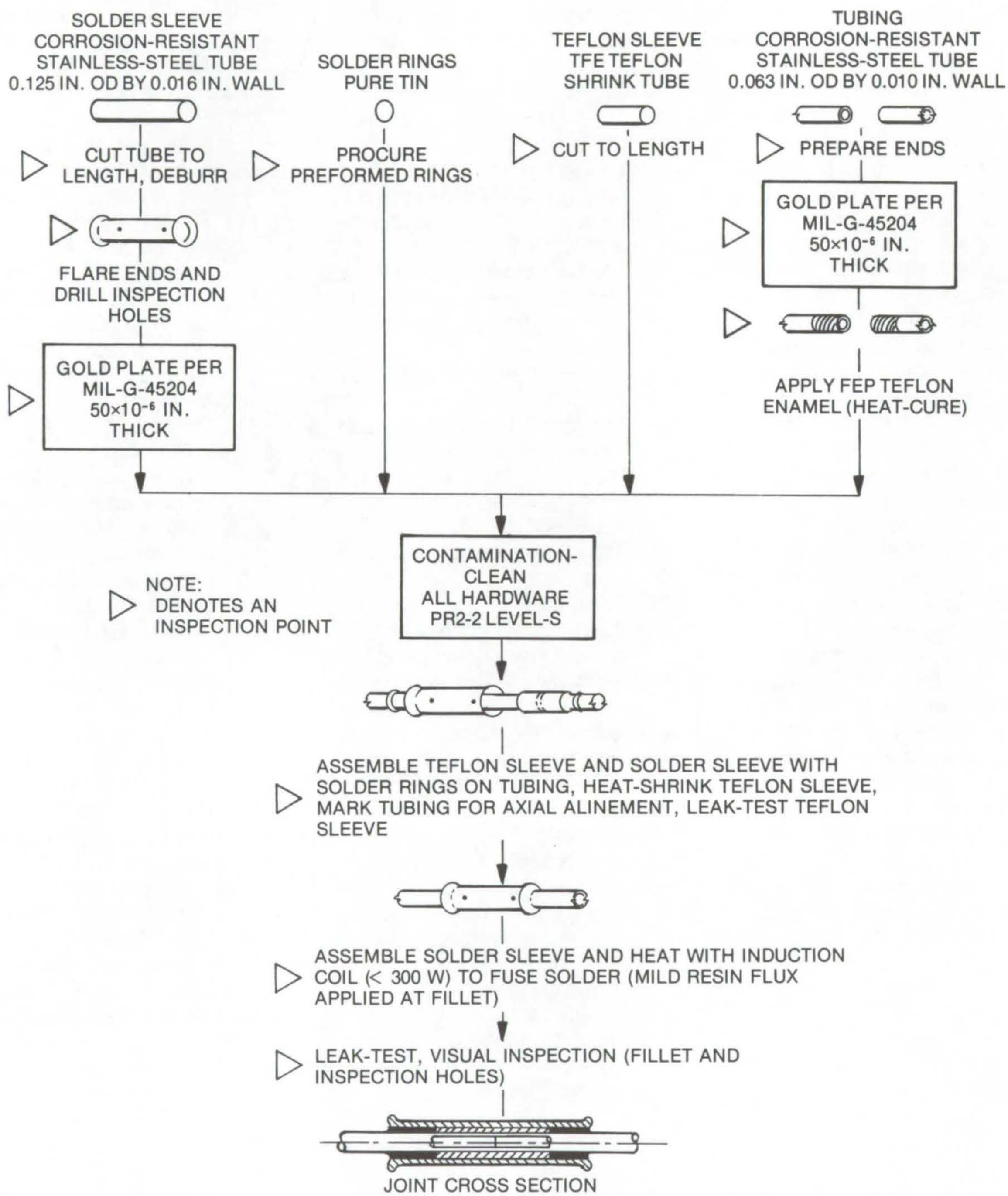

Flow Chart For Compound Solder Joint Technique shows butt ends of tubes to be joined are held in place by a pair of concentric sleeves. The outer sleeve is stainless steel and the inner sleeve is Teflon.

The techniques for joining pipe or tubing under ordinary circumstances are well defined. When ultrasterile conditions must be preserved, however, special precautions must be taken to prevent flux or solder from flowing into a tube and contaminating a whole system. Thus, existing procedures need modification.

A new joining technique has been developed. The new technique not only prevents contamination but also may be used to join dissimilar metal tubes (thus avoiding couples). It minimizes fluid and gas entrapment, expedites repairs and can yield joints having leakage rates less than 10^{-6} standard cm^3 He/min. As shown in the figure, the butt ends of the tubes to be joined are held in place by a pair of concentric sleeves. The outer sleeve is stainless steel, and the inner sleeve is Teflon. Thus, the components of the joint are a solder sleeve, two solder rings, a Teflon sleeve, and the tubing to be joined.

The solder sleeve is usually stainless steel. Its diameter is slightly greater than the O.D. of the tubing, and its length is determined by the position and location of the joint. After deburring, the ends of the sleeve are flared, inspection holes are drilled, and the unit is given a gold plate 1.3×10^{-3} mm (50×10^{-6} in.) thick. The solder rings are shaped to slip over the tubing and nestle inside the flared ends of the solder sleeve. They may be pure tin or any other suitable solder compound. The Teflon sleeve is TFE shrink tube cut to about half the length of the stainless sleeve.

The ends of the tubes to be joined are prepared and also given a gold plate 1.3×10^{-3} mm thick. Then FEP Teflon enamel is applied and heat cured; this improves the chances of a solid bond with the Teflon sleeve. Before final assembly, all parts are cleaned thoroughly. The parts are then assembled on the tubing in sequence: one solder ring, the solder sleeve, the Teflon sleeve, and the second solder ring. The Teflon sleeve is positioned over the butt joint and is heat shrunk (leakage through the Teflon sleeve may then be tested). Keeping the tubing axially alined, the solder sleeve is moved over the butt joint, and the solder rings are snubbed into the flared ends. A 300-W induction coil is sufficient to fuse the solder and complete the joint. A mild resin flux may be applied to the fillet to help solder flow. Finally, the completed joint is leak tested according to specifications.

This work was done by Roy I. Batista and Robert B. Simonson of TRW, Inc. for **Langley Research Center.** *No further documentation is available.*
LAR-11444

Cleaning Carbon Steel

A fast cleaning method for carbon steel results in a more protective passive coating.

John F. Kennedy Space Center, Florida

Chemical cleaning of carbon steel bottles and vessels, using a citric acid solution, requires considerable time. A new method reduces the time required in the citrosolve process and provides a more protective passive coating.

The new method employs an increased concentration of citric acid. In the old method a 3-percent acid solution was used as higher concentrations increase the etch rate. Tests have revealed, however, that an increased etch rate using 8 percent citric acid actually reduces the total amount of material etched away by eliminating the reprocessing that was frequently required, using the 3-percent citric acid concentration, in order to meet cleaning specifications. The average time required to clean and validate a carbon steel vessel, using the old method was about 20 hours. By using a more concentrated acid solution, the time required is reduced to approximately 5 hours.

The improved citrosolve process has two steps: (1) degreasing and (2) derusting and cleaning. The degreasing procedure consists of heating the vessel or part for 0.5 to 2 hours in an aqueous solution of sodium hydroxide (10 to 20 percent by weight) containing 0.01 percent by weight of detergent. Drying is not required following this process. For derusting, the article is heated for approximately 3 hours in an aqueous solution of citric acid (8±0.5 percent by weight), ammonium hydroxide (approximately 3 percent by volume) to stabilize the pH at 3.5±0.5 percent, small amounts of ammonium bifluoride, and an inhibitor.

During the heating, citric acid is added as required to maintain the pH below 4.0. When the ferric ion content has stabilized, the solution temperature is allowed to fall to 145±5° F (63±3° C). Citric acid (0.4 percent by weight) is added, and the pH is readjusted to 9.5±0.5 with ammonium hydroxide. Sodium nitrite (0.5±0.05 percent by weight) is added, and the solution is aerated with nitrogen. The temperature is maintained at 140±5° F (60±3° C) for approximately 2 hours until the ferric ion content has again stabilized. The article is flushed and purged with nitrogen until it is dry.

This work was done by Vadis Maynard of The Bendix Corp. for **Kennedy Space Center.** *No further documentation is available.*
KSC-10689

Repair of Fused Silica Platens

Refill/leveling of platens used in retort brazing extends their service life fivefold.

Lyndon B. Johnson Space Center, Houston, Texas

Silica platens used in 2,000° F (1,107° C) retort brazing processes normally have very short service lives, on the order of 5 to 10 cycles before platen replacement is required. The platens, a sample of which is shown in Figure 1, measure 34 by 60 in. (86 by 152 cm) and are supplied in densities optimized to minimize brittleness and thus wear longer. As they are used, however, the platens tend to develop surface cracks and depressions in the loading area (Figure 2), hastening their replacement.

A refill/leveling technique now can extend the service life of the platen up to 5 times (50 production cycles between maintenance downtime). The cost of the technique is only $700 per repair as compared to the replacement cost of the platen which is valued at $17,000. A slurry refill material supplied by the platen manufacturer is repeatedly applied to the affected areas. Several in-place applications of the refill material gradually increase density in the affected area and extend platen lifespan.

After the refill is applied and leveled in the press, it is allowed to harden. An abrasive-paper-covered tool is drawn over the refilled surface to sand it to within ±0.003 in. (0.007 cm) of flat.

Figure 1. A **Silica Platen** used in retort brazing normally has a 5-to-10 cycle service life. The repair technique extends platen service life fivefold at a cost of $700 per repair.

The temperature and pressure (200 psi) of the brazing process cause the internal cast-in heater openings to close off gradually. As a final maintenance procedure the holes are resized to their original diameters. To resize, the heaters are removed, and carbide extension drills are used to bore the holes. After boring, the heaters are replaced, and the platen is returned to service.

This work was done by Robert M. Heisman and Charles S. Beuyukian of Rockwell International Corp. for **Johnson Space Center.** *No further documentation is available.*
MSC-19713

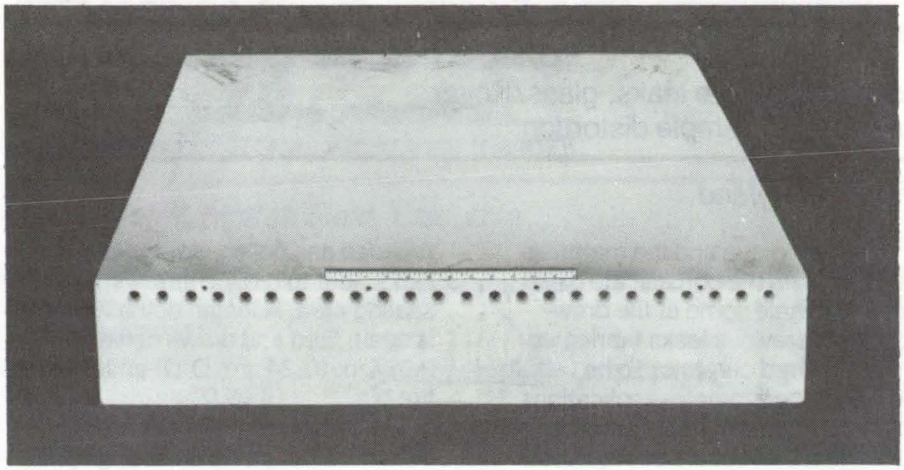

Figure 2. The **Silica Platen After Use** develops surface cracks and depressions in the loading area. The refill/leveling repair technique consists of spreading slurry refill material to the affected areas and then sanding until the surfaces are flat.

Flexible Fitting for Fluid Lines

A stainless-steel tubular coupling permits axial and/or rotational motion.

Lyndon B. Johnson Space Center, Houston, Texas

The tube fitting, shown in the illustration, provides a flexible joint that allows axial and rotational motion. The fitting consists of a movable tubular section containing two spring-pressure Teflon-actuated low-friction seals, two standard connectors, and two hexagonal retaining nuts. The sizes range from ¼ to 2 in. (0.6 to 5 cm), but can be manufactured in larger dimensions. All parts, except the seals, are of stainless steel.

The fitting is pressure-balanced, bidirectional, and has straight-through flow for easy cleaning. It is compatible with most liquids and gases, and ideal for high pressures requiring a low-pressure drop and zero leakage. The fitting is operational from 16 to 505 K (-430 to 450° F).

Manufacturers of tube fittings, especially where contraction and expansion points are needed, could use this innovation in place of bellows fittings.

This work was done by S. L. Barajas of Rockwell International Corp. for **Johnson Space Center.** *No further documentation is available.*
MSC-17780

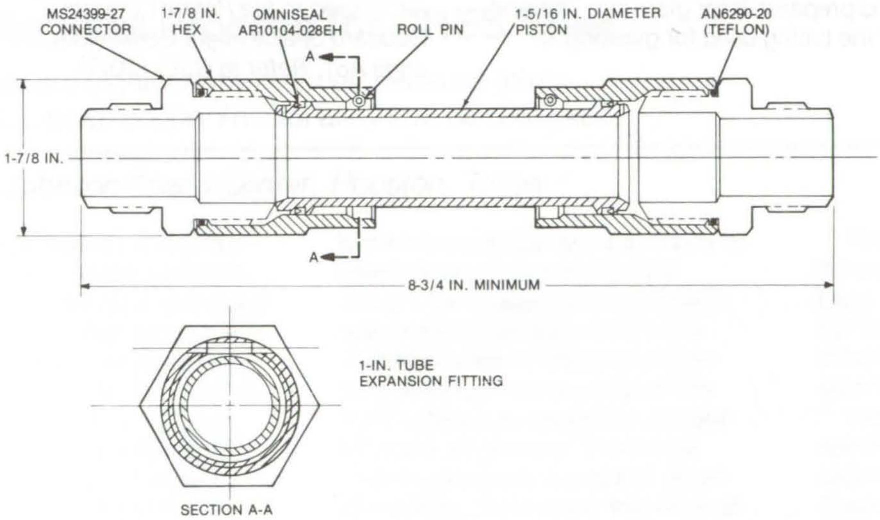

The **Flexible Tube Fitting** includes low-friction seals, two standard connectors, a pair of hex retaining nuts, and a tubular stainless-steel section. The fitting is leak-free over the temperature range of from 16 to 505 K.

Borosilicate Glass-to-Kovar Tube Bonding

When compared to prior materials used to fabricate leaks, glass/Kovar leaks used in mass spectrometry minimize gas sample distortion.

Goddard Space Flight Center, Greenbelt, Maryland

A 2-micron-diameter inlet leak is fabricated from a tube of borosilicate glass. The glass tube is fired and drawn down to the inner diameter of a Kovar metal tube, which is prepared to receive the glass by rounding the Kovar edges and then oxidizing them. The glass is inserted and then bonded to the oxide film; it is heated and drawn again until the interior diameter reaches the desired leak size. When fabricated in this fashion, the inlet leak is suitable for operation in high-temperature [475° C (887° F)], high-pressure [1,500 psi (103.5×10^5 N/m^2)] mass-spectrometry applications.

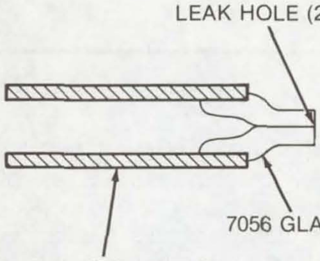

The **Borosilicate Glass Leak** is drawn under a microscope; Corning-type 7056 borosilicate glass is reduced to 2 micrometers diameter. Prior to drawing, the glass is bonded to Kovar tubing, first oxidized to implement a glass-to-metal seal.

The technique and the materials used to form the borosilicate glass leak eliminate some of the drawbacks of previous leaks fabricated from sintered ceramic. To be useful in mass-spectrometry applications, the leak must minimize gas sample distortion that occurs between the sample and the leak, must be easily joined to the spectrometer inlet system, and must withstand unusual gas pressures or temperatures. The large internal surface area of the sintered leak, under certain conditions, modifies the gas constituents under analysis by adsorbing some of the gas on the walls of the porous material. The adsorbed gas can later be released from the ceramic walls and cause sample distortions. The minute openings of the ceramic are also susceptible to blockage; instrument calibration thus is not long-term stable.

The leak is fabricated by wet-hydrogen firing a length of tubing, 0.125 in. (0.32 cm) O.D., 900° to 1,000° C (1,652° to 1,832° F) for 30 minutes. This oxidizes the tubing and prepares it for glassing. The end of the tubing used for glassing is rounded and polished with 600-grit sandpaper to reduce strain in the sealing area. A length of the tubing is again fired and drawn down to 0.094 in. (0.24 cm) O.D. and then is fire cut.

The lesser diameter tubing is sealed inside the Kovar tubing by using a torch having a flame temperature of about 1,115° C (1,259° F). After the seal is made, the borosilicate glass is slowly heated with a hand torch. The inside diameter of the glass is reduced while viewed under a microscope to the correct diameter. After testing, the excess glass is cut off to expose the leak hole.

This work was done by Robert F. Harris of **Goddard Space Flight Center.** *For further information, including bonding-process data and the test configuration, Circle 97 on the TSP Request Card.*

This invention is owned by NASA, and a patent application has been filed. Inquiries concerning non-exclusive or exclusive license for its commercial development should be addressed to the Patent Counsel, Goddard Space Flight Center [see page A8]. Refer to GSC-12077.

Technique for Joining Metal Tubing

A shaped insert is used to achieve uniform wall thickness and improved heat transfer across the joint.

Ames Research Center, Moffett Field, California

Uniform wall thickness and uninterrupted heat transfer in metal tubing joints can be achieved by using a shaped insert as wall material for the joint. The insert acts as a support during brazing, after which excess material is ground away to bring the joint to the original tubing size. The short, hollow insert is formed from the same material as the tubing to be joined. Its bore size is the same as the internal diameter of the tubing.

The outer surfaces of the insert are shaped to fit between flared ends of the tubing lengths to be joined, as shown in the diagram. The angles of the flares and the surfaces of the insert must be accurate to within a few degrees. A compatible braze material, without flux, is laid in the gap as indicated in the upper part of the diagram. Then the junction is slipped into a short length of glass tubing that is large enough to permit packing glass wool around the metal tube so as to form sealed sleeves.

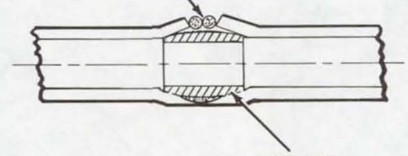

In the **Joining Technique** for metal tubing, a machined insert has outer surfaces matching the angle of the flared tube ends. The upper half of the drawing shows the joint before brazing, and the lower half, after brazing and filing.

A seal is made by induction brazing in an argon atmosphere. The tube assembly is purged externally with argon, while the inside of the tube is evacuated with a vacuum pump. When the dewpoint is less than -73° C (about 30 minutes), the seal is consummated.

The joint is barely visible when its periphery has been filed down to the external diameter of the tubing. Lengths up to 60 meters have been made from several lengths of 1.6-mm, 316 stainless-steel tubing (nickel-gold braze). When wound on a 2.5-cm mandrel and pressurized at 69×10^6 N/m^2 (10,000 psi), no joints ruptured. Measurements after the pressure test indicated leakage rates of less than 5×10^{-10} scc/s helium at 0.69×10^6 N/m^2 (100 psi).

This work was done by Harvey W. Wright of TRW, Inc., for **Ames Research Center.** *For further information, Circle 98 on the TSP Request Card.*
ARC-10946

Braze/Rebraze Process for CRES Steel

Repair costs are significantly reduced because joints brazed with a gold/copper/nickel alloy can be reworked.

Lyndon B. Johnson Space Center, Houston, Texas

Tubing made from 21-6-9 CRES steel (a high-manganese stainless steel) is finding wide application due to its high strength that allows thin lightweight tubes to replace those made of heavier steels. Using an induction brazing process, joints in this tubing can be reworked up to seven times, thus significantly reducing the cost of fabrication, repair, and part replacement.

An 8.5-Au/16.5-Cu/2.0-Ni braze alloy is used. This alloy has better wettability than the industry standard of 82 Au/18 Ni, and it may be cycled to the braze temperature as many as seven times. It was previously thought that copper was unacceptable in the braze alloy for 21-6-9 CRES because of intergranular attack. Although the success of this Au/Cu/Ni braze cannot be attributed to any single step, the overall process produces a braze of excellent quality. Tests show that even after seven heat cycles the alloy intrusion is less than 0.003 in. (0.075 mm), a negligible amount on tubes 0.016 in. (0.4 mm) thick.

This work was done by Clinton E. Silverman of Rockwell International Corp. for **Johnson Space Center.** *For further information, including detailed brazing procedures, Circle 99 on the TSP Request Card.*

Inquiries concerning rights for the commercial use of this invention should be addressed to the Patent Counsel, Johnson Space Center [see page A8]. Refer to MSC-19600.

Age-Forming Aluminum Panels

Contoured-stiffened 2124 aluminum alloy panels are machined in-the-flat using combination check and forming fixtures.

Lyndon B. Johnson Space Center, Houston, Texas

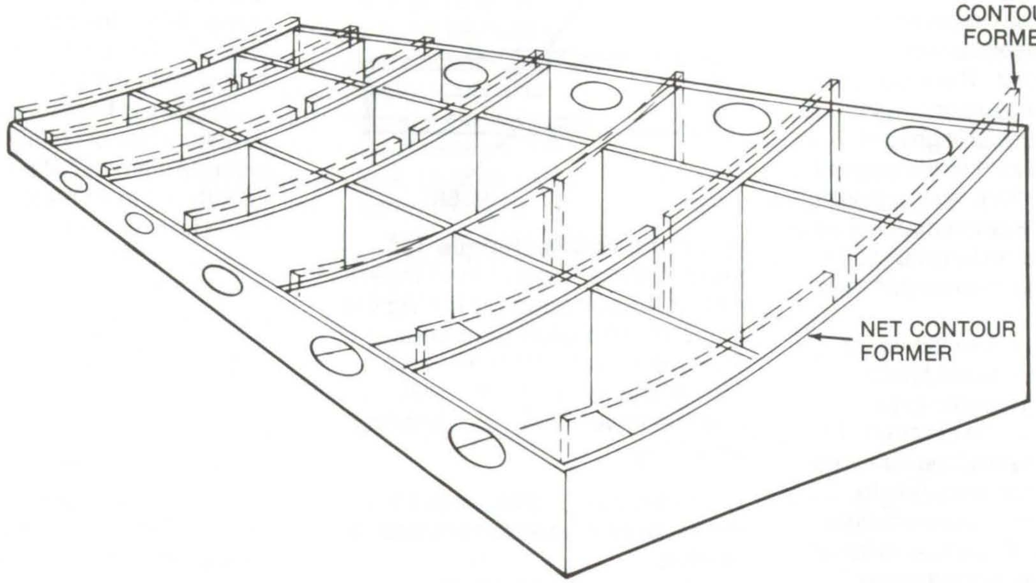

Figure 1. **Aging Fixture,** showing net contour and overbowing contour, has an eggcrate-like structure for use in forming and checking the integrally-stiffened panels. The fixture includes net contour formers made from lofted contour templates.

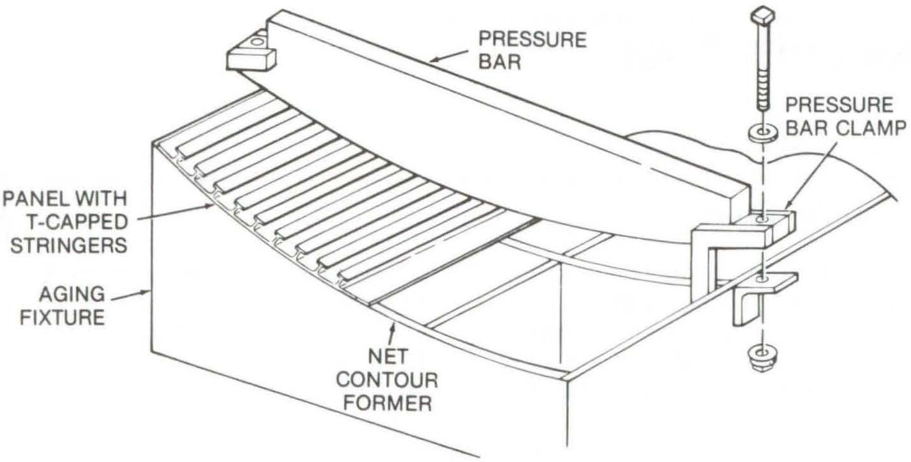

Figure 2. To **Compensate for Springback Effect,** sliding formers are bolted through slotted holes to net contour formers. Pressure bars, made to match the overbowed contour, are used to convert from a check fixture to an age-forming fixture.

An improved technique has been developed for forming contoured-stiffened aluminum panels. The panels, 63 by 337 in. (1.6 by 8.6 m), are machined in-the-flat to make integral, tapered T-capped stringers, parallel with the longitudinal centerline. The stringers vary in height from about 2.0 to 2.5 in. (5.1 to 6.5 cm). The selected material is 2124 aluminum alloy. The finished panels are in a twisted compound-curve configuration. This configuration introduces difficulty in forming due to the inherent stiffness of this type of panel, in either the T351 condition or in the finish (T851) temper.

Most of the common forming techniques, including stretch, explosive, shot peen, and creep forming, were investigated for use in this application, and were rejected as inadequate, insufficiently developed, or too expensive. The method selected, age forming, is analogous to creep forming.

Combination check (contour) and forming fixtures (Figure 1) have been built for use in forming and checking the integrally stiffened panels. These age forming fixtures are made as an eggcrate-like structure and include net contour (structural inner mold line) formers made from lofted contour templates which, after assembly into the eggcrate structure, become a check form for inspection of the inner mold line of a panel. They also support it while the structural outer mold lines are checked with the lofted contour templates. During panel forming, it is necessary to compensate for the springback effect. To accomplish this, the fixture includes sliding, mated formers which are bolted, through slotted holes, to the net contour formers. These mated formers can be raised (from the net contour) and secured in the raised position for use as an overbowing device to convert the check fixture to an age-forming fixture. Pressure bars, made to match the overbowed contour, are used on the panel surface to clamp the panel over the overbowing formers (Figure 2).

The panel is fully clamped into the age-forming fixture which then is placed in an electric heat treatment furnace where the panel is aged at 375° F (464 K) for 12 hours to make the T851 temper. Upon cooling, the panel is unclamped and removed from the fixture. The overbow formers are then lowered out of the net contour, exposing fixed net contour (inner mold line) formers. The age-formed panel is then relocated on the fixture, and the fit to the inner mold line (the stiffeners) is checked.

The contour templates for the skin surface then are positioned across the panel surface, and the outer mold line is checked at each butt line. In addition, station line contours are checked, with templates, along each edge and midway between the stations. If the panel deviates slightly from the correct contour, hand pressure at the butt lines and/or the station lines may be enough to correct it. If hand pressure cannot correct the contour, the overbow formers are adjusted for refinement on the next panel.

This work was done by G. I. Baxter of General Dynamics Corp. for **Johnson Space Center.** *For further information, Circle 100 on the TSP Request Card.*
MSC-12648

Books and Reports

These reports, studies, and handbooks are available from NASA as Technical Support Packages (TSP's) when a Request Card number is cited; otherwise they are available from one of NASA's Industrial Application Centers or the National Technical Information Service.

Fracture Mechanics for Weld Acceptance

A new set of weld acceptance criteria reduces the number of weld repairs required.

A set of acceptance criteria for welds for the Space Shuttle external tank (2219 Aluminum) has been developed by the application of fracture mechanics technology. These criteria are generally applicable to the fabrication of welded pressure vessels and other similar structures. Although conservative, they are less stringent than previous weld specifications and result in a significantly smaller number of weld repairs.

The criteria include specifications for allowable cracklike defect lengths, undercut, underfill, suckback, mismatch, and peaking in butt welds; and for root penetration, weld bead dimensions, lap joint dimensions, and acceptable defect sizes and densities for double and single fillet welds. Also included are specifications for welding operations and quality assurance testing, including tensile tests, bend tests, metallographic sections, and visual, radiographic, and penetrant inspections.

This work was done by C. A. Bolstad and L. W. Loechel of Martin Marietta Corp. for **Marshall Space Flight Center.** *To obtain a copy of the criteria, Circle 101 on the TSP Request Card.*
MFS-23360

Machining Titanium Alloys

A study suggests ways of reducing chatte, increasing productivity, and reducing tool wear.

A recent report on the machining of titanium and titanium alloys will be of interest to organizations setting up titanium machining programs. The low thermal conductivity of titanium, the low contact area between tool and chips, and the high chip velocity cause high tool-tip temperatures and accelerated tool wear. To avoid these problems, machining speeds are usually reduced considerably, resulting in productivity loss. To restore productivity, the feed and the depth of cut can be increased; however, this leads to another problem: tool instability or chatter.

The report describes a thorough investigation of titanium-machining problems. Static and dynamic cutting tests are described. Static cutting tests indicate that both tool-nose forces and components of the cutting force that deflect the cutting tool can cause poor machining tolerances. It is shown that the cutting-force components can be reduced by a proper tool-rake angle and that tool-nose forces can be reduced by lapping the tool after grinding it.

The dynamic tests show that the dynamic cutting force in the thrust direction is a stabilizing force. The workpiece material affects only the magnitude of the stabilizing force. Simple tool-grinding procedures can, therefore, increase productivity by reducing chatter problems.

Tool materials and finishes are also discussed. Tool-finish tests show that an improved finish reduces tolerances and increases

(continued next page)

tool life. Optimum machining conditions are reported for both lapped and as-ground tools. The effects of a proper coolant are also found to be important. The most effective cooling is achieved with a spray-mist coolant at 100 psi (6.9×10^5 N/m^2). Tool life is then three times greater than when no coolant is used.

This work was done by Ian A. Sutherland of **Marshall Space Flight Center.** *To obtain a copy of the report, Circle 102 on the TSP Request Card.*
MFS-23006

Annealing Strained Alloy 718

Tensile tests and metallographic examinations of grain size.

Zone cracking (microfissuring), produced by weld heating, has recently been encountered in several parts fabricated from Alloy 718. The components had been hydrosized and annealed prior to welding, and the hydrosizing may have imparted a critical amount of strain to the material, which in turn could cause severe grain coarsening during the annealing. It has been shown that grain coarsening in Alloy 718 can result in a greatly reduced resistance to weld-heat-produced zone fissuring, especially when the final grain size is ASTM #2 or coarser. A report is now available detailing the influence of annealing time-temperature parameters on the grain size of critically strained Alloy 718. Tensile tests and the metallographic examination of bend test specimens provide the necessary data.

The Alloy 718 stock tested was 0.133 in. (0.338 cm) thick and was in the cold-rolled condition. A total of 26 bend-test specimens, each measuring 0.25 by 0.133 by 2.00 in. (0.64 by 0.338 by 5.08 cm), and 12 tensile strips, each measuring 9 by 0.50 in. (22.86 by 1.27 cm), were cut from the plate transverse to the rolling direction. All pieces were solution annealed at 1900° F (1310 K) for one-half hour to duplicate the standard as-received material condition. The bend specimens, excepting a single control piece, were bent through an angle of greater than 135° around a mandrel 0.125 in. (0.318 cm) in diameter.

An examination of the grain size data for the critically strained areas of the bend test specimens shows that annealing temperatures of 1700° F (1200 K) and 1750° F (1227 K) with times up to 2 hours do not cause any measurable amount of grain coarsening. At 1800° F (1255 K) for 10 minutes, the first evidence of grain coarsening is observed, and grain size increases significantly with increasing time. This is the initial sign of the grain coarsening which could degrade Alloy 718 weld-microfissure resistance and is the result of the presence of critical strain prior to grain size formation. As higher temperatures and longer times are employed, the grain size in the area of critical strain continues to coarsen. Temperatures above 1900° F (1310 K) for 10 minutes or any time at 1950° F (1339 K) result in severe grain coarsening, with areas of grain size ASTM #2 or #1. Alloy 718 with such areas has been shown to have a reduced weld-fissure resistance.

The tensile testing of the rectangular 9-in. by 0.50-in. (22.86-cm by 1.27-cm) strips was employed to determine if detrimental effects on the yield strength and ductility of Alloy 718 would result from a lower temperature annealing than is normally used. An appreciable increase in the yield strength of Alloy 718 and a decrease in its tensile ductility, due to such annealing, might preclude the use of such a process where good material formability is necessary. The data, however, reveal that even a low-temperature, 1900° F (1227 K) anneal restores virtually full ductility and removes the cold work from Alloy 718. The low-temperature anneal can therefore be used without any loss in alloy formability. After welding, a 1900° F (1310 K), or higher, solution treatment followed by a 1400° F/1200° F (1035 K/920 K) aging should be used to obtain full material properties.

In conclusion, any Alloy 718 component which is thought to have a critical amount of strain (between 0 and 15 percent) in an area to be welded should not be annealed at a temperature above 1800° F (1255 K), and preferably not above 1767° F (1230 K) if times exceeding one-half hour at temperature are expected. The use of a solution-annealing temperature of from 1255 K to 1230 K, in place of the standard 1310 K anneal for Alloy 718 components, should not impair ductility and formability to an extent where production problems could arise.

This work was done by Thomas J. Morrison of Rockwell International Corp. for **Marshall Space Flight Center.** *To obtain a copy of the report, Circle 103 on the TSP Request Card.*
MFS-19242

Mathematics and Information Sciences

Relative Humidity from Psychrometric Data

An analytical expression for relative humidity includes the effects of pressure.

Dryden Flight Research Center, Edwards, California

The determination of relative humidity from measurements of wet and dry bulb temperature has long been a tedious table look-up task. In addition to depending on wet and dry bulb temperatures, the relative humidity depends on the ambient atmospheric pressure. Tables of relative humidity as a function of dry bulb temperature, wet bulb temperature, and atmospheric pressure are not widely available.

An analytical equation for computing relative humidity as a function of wet bulb temperature, dry bulb temperature, and atmospheric pressure has been developed which is suitable for use with a calculator or computer. The precise definition of relative humidity was taken from the Smithsonian Meterological Tables as shown in Equation 1.

Using analytical expressions for e and e_S, Equation 1 can be expressed as a function of the psychrometric variables and atmospheric pressure. The result is shown in Equation 2, which is valid for wet bulb temperatures 32° F and greater and for dry bulb temperatures less than 120° F.

In addition to this expression, additional equations relating relative humidity, absolute humidity, dew point, dry and wet bulb temperatures, and atmospheric pressure in U.S. and metric units are being developed. These analytical expressions may also be useful for chemical process control systems and building environmental control systems.

This work was done by Terrill W. Putnam of **Dryden Flight Research Center.** *For further information, Circle 104 on the TSP Request Card.*
FRC-10108

$$\text{Relative Humidity} = RH = 100\left(\frac{e}{e_S}\right)$$

Where e is the Vapor Pressure of Water Vapor in Moist Air, and e_S is the Saturation Vapor Pressure

Equation 1: The precise definition of relative humidity

$$RH = 100\left\{\frac{10^{B} - 0.001243P(T_d - T_w)\left[1 + \left(\frac{T_d - 32}{1571}\right)\right]}{10^{A}}\right\}$$

Where A and B are:

$$A = \frac{-2937.4}{\frac{5}{9}(T_d + 459.4)} - 4.9283\log_{10}\left[\frac{5}{9}(T_d + 459.4)\right] + 22.5518$$

$$B = \frac{-2937.4}{\frac{5}{9}(T_w + 459.4)} - 4.9283\log_{10}\left[\frac{5}{9}(T_w + 459.4)\right] + 22.5518$$

and,

T_w = Wet Bulb Temperature in Degrees Fahrenheit
T_d = Dry Bulb Temperature in Degrees Fahrenheit
P = Atmospheric Pressure in Inches of Mercury

Equation 2: An analytical expression for RH as a function of pressure.

Bit-Error Rates in Optical Communications

Optimal threshold detection reduces bit errors caused by atmospheric scintillation

Marshall Space Flight Center, Alabama

A statistical model for optical communications over atmospheric channels has been derived. The effects of atmospheric scintillation are considered more closely than in previous models. As a result a more reliable output is obtained. The model, which consists of an on/off binary system, assumes a Poisson detection process and log-normal atmospheric scintillation. Based upon the detection process and atmospheric ionization, a piecewise-linear model for an adaptive threshold system is developed. The optimum receiver threshold for binary on/off keying is predicted through semiempirical methods.

In a pulse-code-modulated (PCM) optical communications channel, atmospheric scintillation not only increases the bit-error probability but also influences the decision level for optimum threshold detection. The latter effect is of considerable practical importance to the design of efficient PCM optical communications systems whether fixed or adaptive threshold detection is used. Prior studies of bit-error rates in an optical communications channel assumed Gaussian or Poisson detection statistics, approximations which are valid only for large and small numbers of signal photons, respectively.

In an on/off binary optical communications channel, a laser may transmit either a "1", which corresponds to a transmitted pulse, or a "0" (no pulse). A threshold detection system in the receiver interprets the received signal as either a "1" or a "0", depending on whether the total number of received photoelectrons is greater or less than some threshold level T. In the new model the optimum detection threshold is developed as a function of the number of received photons and the strength of scintillation.

The bit-error probability has been evaluated by numerical integration on a UNIVAC 1108 computer. An iterative procedure was used to minimize the error probability and to determine the optimum threshold in the presence of scintillation. In addition, simultaneously, the effect of suboptimum threshold levels on the error rates was studied.

This work was done by W. E. Webb of the University of Alabama for **Marshall Space Flight Center.** *For further information, Circle 105 on the TSP Request Card.*
MFS-23340

Books and Reports

These reports, studies, and handbooks are available from NASA as Technical Support Packages (TSP's) when a Request Card number is cited; otherwise they are available from one of NASA's Industrial Application Centers or the National Technical Information Service.

Learning/Cost-Improvement Curves

A clear view of, and reference tool for, an important aspect of cost estimation.

A review, "Guidelines for Application of Learning/Cost-Improvement Curves," has been published as an aid to the manager or engineer who must determine production costs for components, systems, or services. The approach combines two factors: increased skill achieved through the repetition of assembly or clerical operations (learning curve) and improvements in methods, design, tooling, and processes (cost-improvement curve).

A learning/improvement curve is generally drawn with time or number of units on the horizontal axis (abscissa). The ordinate units are cost per unit in man-hours or dollars for the Crawford system and the cumulative average cost per unit in the Wright system. Both systems are discussed in the "Guidelines," although a survey is reported showing that 93 percent of manufacturers currently use the Crawford, or unit cost, system.

Methods are described by which manufacturers may use historical data, task characteristics, and current cost data to estimate unit prices as a function of the number of units to be produced. Curve slopes are cited for various industries and task types. Several sample problems are included, such as how to determine the cost of a given number of items when the slope of the improvement curve is unknown.

The volume contains tables and formulas that make it a handy reference for cost estimation. Cost projections for complex tasks are discussed and explained, and present practices and future trends in cost estimation are also discussed.

This report was prepared by Leon M. Delionback of **Marshall Space Flight Center.** *To learn how to obtain a copy of the Guidelines, Circle 106 on the TSP Request Card.*
MFS-23429

Computer Programs

These programs may be obtained at very reasonable cost from COSMIC, a facility sponsored by NASA to make new programs available to the public. For information on program price, size, and availability, circle the reference letter on the COSMIC Request Card in this issue.

Multivariate Normal Integration

A Monte Carlo evaluation of integrals over rectangular and elliptical regions

A Monte Carlo program evaluates multivariate normal integrals over rectangular regions for dimensions less than six and over elliptical regions in the bivariate case. Integration over rectangular areas is performed by generating the product of independent uniform distributions and a random vector. The program gives the positive definite symmetric variance/covariance matrix factorization, and it calculates the reciprocal of a lower triangular matrix and the product of the diagonal elements of the triangular matrix. This procedure converges slowly in most cases, and an effort was made to increase the precision and speed of convergence. This was done by expanding an exponential expression into a Taylor's series.

Integration over elliptical regions, a requirement common in meteorological problems, is similar to the case for rectangular areas. Just as in the rectangular-area case, a series of random vectors are generated in the region being integrated. The procedure is to assume the ellipse is in standard position, to obtain a random point in the ellipse, and to rotate and/or translate it to the prescribed area. The random point is obtained by generating to uniform numbers. Once translated or rotated to the prescribed area, the method of rectangular areas applies.

The program inputs permit considerable flexibility in the elliptical parameters required. Specifically, there are two options:

1. Inputs include x,y axis lengths, rotation angle, and center after rotation; or
2. Inputs are five points on the locus of an ellipse (the program determines the ellipse and puts it in standard form).

FORTRAN
UNIVAC, EXEC VIII

This program was written by Lee W. Falls of **Marshall Space Flight Center** *and M. C. Carter of Appalachian State University. For further information, Circle H on the COSMIC Request Card.*
MFS-22867

DORCA II

Dynamic Operations Requirements and Cost Analysis Program

DORCA II was written to handle the logistics of acquisition and transport of personnel, equipment, and services. It determines costs, transport schedules, acquisition schedules, and fuel requirements of cargo transport.

Functionally the DORCA II program has four main features:

1. **Cargo loading** encompasses procedures and computations associated with the assignment of cargo/vehicle combinations. Cargo item numbers, weights, and lengths are accumulated as the loading operation progresses and are compared to vehicle capabilities and other loading restrictions to assure that vehicles are not overloaded and applicable restrictions are not violated.
2. **Propellant computation** permits the summing of fuel requirements. This summing can be done in one of two ways at the option of the user. With the first method, fully loaded tanks are assumed; in the second method the fuel required is computed based on the load weight being transported.
3. **Vehicle traffic/fleet computation** is used to assign to individual vehicles all runs generated by the cargo-loading process. Within this feature all of the bookkeeping is performed related to transport time and history of individual vehicles. The number of transports of a given vehicle in a given year and the total number of vehicles required in that year are determined. In addition, vehicles are retired at their assigned ends-of-life, and new vehicles are acquired as dictated by yearly requirements.
4. **Cost computation** — Once vehicle loading and scheduling have been accomplished and traffic rates and fleet acquisition have been determined, the costs are determined. The cost report contains cost subtotals for: (a) vehicle costs, (b) payload costs, and (c) operations costs.

FORTRAN
CDC 6000/UNIVAC 1100 Series

This program was written by The Aerospace Corp. for **NASA Headquarters.** *For further information, Circle J on the COSMIC Request Card.*
HQN-10834

SUBJECT INDEX

☆ U.S. GOVERNMENT PRINTING OFFICE : 1976 O—215-330

National Aeronautics and
Space Administration

Washington, D.C.
20546

Official Business
Penalty for Private Use, $300

SPECIAL FOURTH CLASS MAIL
BOOK

Postage and Fees Paid
National Aeronautics and
Space Administration
NASA-451

NASA

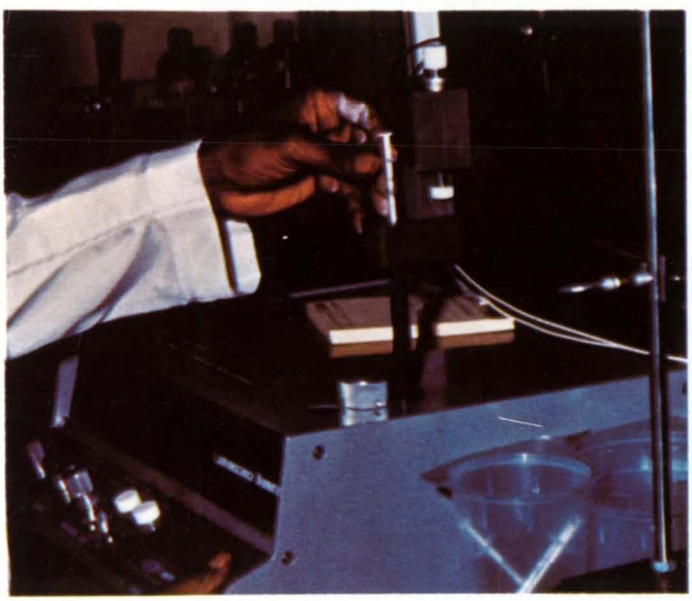

Bacteria counts are made in a fraction of the time previously required, with luciferase [an enzyme derived from fireflies] to measure ATP in cells.

Rubber developed for a small Moon tire that remains pliable in extreme cold was used for a winter radial that grips ice without metal studs.